

## Novel crystallization techniques for separation in multi-component systems

Li, Weiwei

**DOI**

[10.4233/uuid:436c4e79-7b47-40b7-ade0-fc24b8a5e5c2](https://doi.org/10.4233/uuid:436c4e79-7b47-40b7-ade0-fc24b8a5e5c2)

**Publication date**

2018

**Document Version**

Final published version

**Citation (APA)**

Li, W. (2018). *Novel crystallization techniques for separation in multi-component systems*. [Dissertation (TU Delft), Delft University of Technology]. <https://doi.org/10.4233/uuid:436c4e79-7b47-40b7-ade0-fc24b8a5e5c2>

**Important note**

To cite this publication, please use the final published version (if applicable).  
Please check the document version above.

**Copyright**

Other than for strictly personal use, it is not permitted to download, forward or distribute the text or part of it, without the consent of the author(s) and/or copyright holder(s), unless the work is under an open content license such as Creative Commons.

**Takedown policy**

Please contact us and provide details if you believe this document breaches copyrights.  
We will remove access to the work immediately and investigate your claim.

# **Novel Crystallization Techniques for Separation in Multi-component Systems**

**Proefschrift**

**ter verkrijging van de graad van doctor  
aan de Technische Universiteit Delft,  
op gezag van de Rector Magnificus, Prof. dr. ir. T. H. J. J. van der Hagen,  
voorzitter van het College voor Promoties,  
in het openbaar te verdedigen op  
woensdag 14 november 2018  
om 12:30 uur**

**door**

**Weiwei LI**

**Ingenieur in Biochemical Engineering,  
Technische Universiteit Delft, Nederland  
geboren te Shanghai, China**

**Dit proefschrift is goedgekeurd door de promotoren**

**Prof. dr. ir. A. I. Stankiewicz**

**Prof. dr. ir. J. H. ter Horst**

**Samenstelling promotiecommissie bestaat uit:**

<b>Rector Magnificus,</b>	<b>voorzitter</b>
<b>Prof. dr. ir. A. Stankiewicz</b>	<b>Technische Universiteit Delft, promotor</b>
<b>Prof. dr. ir. J. H. ter Horst</b>	<b>University of Strathclyde, the United Kingdom, promotor</b>
<b>Dr. ir. H. J. Kramer</b>	<b>Technische Universiteit Delft, copromotor</b>

**onafhankelijke leden:**

<b>Prof. dr. J. H. van Esch</b>	<b>Technische Universiteit Delft</b>
<b>Prof. dr. Ing. A. Seidel-Morgenstern</b>	<b>Max Planck Institute for Dynamics of Complex Technical Systems (Germany)</b>
<b>Prof. dr. D. Maes</b>	<b>Free University Brussels (Belgium)</b>
<b>Prof. dr. R. M. Kellogg</b>	<b>Syncom B.V.</b>
<b>Prof. dr. ir. W. de Jong</b>	<b>Technische Universiteit Delft, reservelid</b>

**Het onderzoek beschreven in dit proefschrift is uitgevoerd bij de afdeling Proces en Energie, faculteit Werktuigbouwkunde, Maritieme Techniek en Technische Materiaalwetenschappen, Technische Universiteit Delft, Nederland. Het onderzoek werd financieel ondersteund door de Nederlandse Organisatie voor Wetenschappelijk Onderzoek (NWO).**

**This thesis is printed by: Ridderprint BV | [www.ridderprint.nl](http://www.ridderprint.nl).**





# Table of Contents

<b>Summary/Samenvatting</b>	1
<b>Chapter 1:</b>	
Introduction	9
<b>Chapter 2:</b>	
Is the 10% rule valid for Co-crystals of Chiral Compounds?	19
<b>Chapter 3:</b>	
A Screening Approach for Resolution Opportunities in Complex Multicomponent Chiral Systems	45
<b>Chapter 4:</b>	
Chiral Resolution of a Racemic Compound via its Conglomerate Co-crystal	77
<b>Chapter 5:</b>	
Deracemization of a Racemic Compound via Its Conglomerate-forming Salt Using Temperature Cycling	103
<b>Chapter 6:</b>	
Concomitant Solid Separation through Electric Field Enhanced Crystallization	121
<b>Chapter 7:</b>	
Solid Separation From a Multi-component Mixture by Electric-Field-Enhanced Crystallization	139
<b>Chapter 8:</b>	
Conclusions	155
Curriculum Vitae	159
Publications and Conferences	161
Acknowledgement/Dankwoord	163



# Summary

Crystallization-based chiral resolution techniques was born when Pasteur discovered the chirality of tartaric acid and manually separated its two enantiopure crystals by his tweezers. Ever since then, these techniques have been in constant development, mainly due to the needs from the pharmaceutical and food industries. In the past decades, techniques such as preferential crystallization have been studied and some of them have already been applied at pilot scale. Deracemization is of more recent date and is actually the process that stirs up attention in chiral resolution the last few years. These techniques draw more and more attention from both academic world and the industries owing to one common feature: the potential to recover the desired enantiomer with unrivaled high product purity in a single process step.

Up till now, only the classical resolution technique, based on the formation of diastereomeric salts, has been used in an industrial scale. Other relatively younger chiral resolution techniques, such as preferential crystallization, are only studied in either lab or pilot scale. One of the main drawbacks of these techniques, especially deracemization, is that their applications are restricted to chiral molecules crystallizing as conglomerates, while more than 90% of the chiral chemicals form racemic compounds. Therefore, **the first objective of this dissertation is to expand the application range of crystallization based chiral resolution techniques to racemic compounds by converting them into conglomerate multi-component crystals (e.g., co-crystals).**

Racemic compounds can be converted into conglomerates via chemical modification, solvate formation and salt formation. Co-crystallization can also be used as an intermediate for the racemic-compound-to-conglomerate conversion. However, the formation of conglomerate co-crystals is seldom reported (up to now only two systems are published: Naproxen-Nicotinamide and Ibuprofen- trans-1-(2-pyridyl)-2-(4-pyridyl)-ethylene). **Chapter 2—4** of this dissertation describe our contribution in the development of the chiral separation of racemic compounds by the formation of co-crystal conglomerates while in **Chapter 5**, we introduce the application of a deracemization technique on a racemic compound by conglomerate salt formation.

The search for co-formers that change a target racemic compound into a conglomerate co-crystal consumes a lot of time and resources and has a low success rate. An important question in this respect is how many racemic compounds can be converted into conglomerate co-crystals. In other words “Is the 10% rule, i.e. only 10% of the chiral compounds form conglomerates, also valid for co-crystals from chiral compounds?” In **Chapter 2**, the answer of this question is given with a study

combining Cambridge Crystallography Data Center (CCDC) screening and experimental investigation. By home-made software, the data screening of CCDC identified 227 organic co-crystals composed of a chiral component, with a single chiral center, and an achiral co-former. All systems have known racemic compound co-crystals, while no conglomerate co-crystals are found. Moreover, a list of the enantiopure co-crystals was generated, which provide potential candidates for conglomerate co-crystals. From this list, 6 enantiopure co-crystal entries were selected for further experimental investigation. Out of these 6 enantiopure co-crystal systems, all form new racemic compound co-crystals from a racemic mixture, using the same conditions of which their corresponding enantiopure co-crystals are reported to be formed. This result shows that the formation condition of an enantiopure co-crystal is a good starting point to crystallize stable co-crystals from the corresponding racemic mixture and the co-former. Finally, a preliminary analysis of the data shows that the likelihood that the 10% rule holds for co-crystals from chiral compounds is only  $7.1 \cdot 10^{-9}$ , which makes this hypothesis invalid. This study provides a quick way of experimentally screening the potential conglomerate co-crystal list generated here, while giving an indication of the technical challenge of converting racemic compounds into conglomerate co-crystals.

After selecting the candidate co-formers for the target chiral compounds, the next question is three fold: what type of co-crystals are formed? what are the suitable chiral resolution techniques for these co-crystals? what are the optimal operation conditions? In **Chapter 3**, the development of a method is described to answer this question based on pseudo-binary phase diagrams. Such phase diagrams describe liquid-solid equilibria in mixtures with varying ratios between the two enantiomers.

Different co-crystal types from a racemic compound and a co-former (chiral or achiral) show distinguishable features in their pseudo-binary phase diagrams: a typical phase diagram of a diastereomerically related co-crystals, for instance from RS-Valine and S-Phenylalanine, contains one eutectic point which divides the diagram into two asymmetrical parts; a racemic compound co-crystal, such as from RS-Ibuprofen and 1,2-Bis(4-pyridyl)ethane, has a typical phase diagram of two symmetrically located eutectic points, which divide the diagram into three parts. The middle part represents the region where the racemic co-crystal is formed while the parts on the sides represent the enantiopure co-crystal regions; on the other hand the typical phase diagram of a conglomerate co-crystal, RS-Ibuprofen and trans-1-(2-pyridyl)-2-(4-pyridyl)-ethylene for example, has only one eutectic point, which divides the diagram into two symmetrical parts, each representing enantiopure co-crystals from either one of the enantiomers.

It is shown that using this procedure developed in this chapter, the type of co-crystals from the target racemic compound and the candidate co-former can be readily identified by their corresponding pseudo-binary phase diagrams. The identified types of co-crystals can in turn determine the suitable crystallization-based chiral resolution techniques. Moreover, the phase diagram of the target system provides information about the suitable operation conditions, for instance temperature and mixture compositions, for the chiral resolution process.

The identification of conglomerate co-crystals of racemic compounds offer potential for chiral resolution techniques such as preferential crystallization. In **Chapter 4**, the S-enantiomer of Ibuprofen (IBU), a racemic compound, was successfully recovered from a racemic suspension in Heptane by preferential crystallization, in the form of enantiopure co-crystals using the co-former trans-1-(2-pyridyl)-2-(4-pyridyl)-ethylene (BPE). A small amount of S-IBU-BPE co-crystals were introduced into the Heptane suspension to start the preferential crystallization by three different methods: A) direct seeding, B) auto-seeding and C) nucleation by seeding BPE. The obtained co-crystal products had an enantiomeric excess up to 95% and its mass was up to 50% more than the amount of seeds. This co-crystallization-mediated preferential crystallization process, which to our knowledge has never been reported, extend the application of chiral resolution techniques towards many racemic-compound-forming target molecules.

Another chiral resolution technique is temperature-cycling-mediated deracemization, which requires, in addition to conglomerate crystals, a solution phase racemization reaction for the target chiral compounds. In **Chapter 5**, the deracemization of the racemic compound Phenylalanine (Phe) was achieved via the formation of its conglomerate salt with 2,5-xylenesulfonic acid (XSA). Starting as an Acetic acid suspension containing RS-Phe and XSA, the racemic Phe-XSA salt crystals were fully converted into enantiopure ones after subjecting the suspension to repeating cycles of heating-cooling, coupled with a solution phase racemization reaction. This result confirms the feasibility of using conglomerate salts as intermediate for the purpose of deracemization.

In **Chapters 2—5**, we use multi-component crystallization as an intermediate for the application of chiral resolution techniques on racemic compounds. However, in many other occasions, the existence of a multi-component mixture hinders the application of direct crystallization, because a mixed solid phase is formed requiring additional steps for product purification. In these cases, the coupling between particle separation based on their chemical compositions and simultaneous crystallization of these particles is desired. Therefore, **the second aim of this dissertation is to explore the possibility of simultaneously separating multi-component systems by crystallization.**

In **Chapters 6 and 7**, we describe a novel technique, namely Electric-Field-Enhanced-Crystallization (EFEC), which can achieve the aforementioned simultaneous particle separation during crystallization in one or two steps. Such a technique is based on one phenomenon: an inhomogeneous electric field in an insulator solvent such as dioxane acts on any present particles, which subsequently circulate between the two electrodes generating the field and eventually accumulate on one of them. Onto which electrode crystals accumulate is dependent on the chemical composition of the crystals. For instance, Isonicotinamide (INA) crystals always accumulate on the anode surface.

We used this phenomenon to separate two solutes from each other from a complex multicomponent mixture: in **Chapter 6**, a DC electric field applied in a mixed dioxane suspension leads to the selective accumulation of the crystals of the two solutes, Phenazine (PHE) and Caffeine (CAF), on the cathode and the anode, respectively. A subsequent cooling step enables the growth and

immobilization of these crystals on the corresponding electrodes. At the end of the cooling step, CAF of a purity higher than 91% wt is collected from the anode while PHE of a purity as high as 97% wt is recovered from the cathode.

PHE and CAF are separated by EFEC because their crystals are attracted by different electrodes. However, there exist other systems, such as the mixture of CAF and INA, where the crystals of both solutes accumulate on the same electrode. In **Chapter 7**, we introduce a new operation strategy of EFEC for the separation of systems such as the CAF-INA mixture: in the mixed solution of CAF and INA, crystals of either solute is seeded into the mixed dioxane solution and EFEC immobilizes the crystals on the anode. Afterwards, the polarity of the electric field is reversed and crystals of the other solute are seeded into the system. Another step of EFEC immobilizes the new crystals on the new anode while the crystals of the first solute keep on growing on the old anode. Eventually, crystals containing either INA or CAF with purities higher than 91 % wt are recovered from different electrodes. The success in separate recovery of both solutes from two different mixture systems proves that EFEC can be potentially used to recover multiple solutes from a multi-component system in one to two steps.

This dissertation deals with the two sides of multi-component systems: on one hand, a systematic procedure is developed to screen, identify and use multi-component crystalline materials (e.g., conglomerate co-crystals) as intermediates for the application of chiral resolution techniques on racemic compounds. This part of the work can be potentially used as a standard to produce enantiopure product from target racemic compounds in industry. On the other hand, the effective separation of two solutes from their multi-component suspension by a newly developed technique is described, coupling electric-field-mediated-particle-separation with cooling crystallization. This EFEC technique can be further developed into a one-step tool for the purification of multiple solutes in a mixture.

# Samenvatting

Chirale resolutietechnieken gebaseerd op kristallisatie vonden hun bestaan toen L. Pasteur de chiraliteit ontdekte van wijnsteenzuur en handmatig de twee enantiomeerzuivere kristallen scheidde met zijn pincet. Sinds die tijd zijn deze technieken constant ontwikkeld, vooral door de behoefte van de farmaceutische en voedselindustrie. In de afgelopen tientallen jaren zijn technieken zoals selectieve kristallisatie bestudeerd en enkelen zijn al toegepast op pilot-schaal. Deracemisatie is een recenter voorbeeld en is het proces dat de aandacht trekt binnen de chirale resolutie in de afgelopen jaren. Deze technieken trekken steeds meer de aandacht van zowel de academische wereld als de industrieën dankzij één gezamenlijk kenmerk: de potentie om de gewenste enantiomeer te winnen met een ongeëvenaard hoge productzuiverheid in een enkele processtap.

Tot nu toe is alleen de klassieke resolutietechniek, gebaseerd op de vorming van diastereomere zouten, gebruikt op industriële schaal. Andere, relatief jongere, chirale resolutietechnieken, zoals selectieve kristallisatie, worden alleen nog bestudeerd op lab- of pilot-schaal. Een van de belangrijkste nadelen van deze technieken, met name deracemisatie, is dat de toepassing beperkt blijft tot chirale moleculen die kristalliseren als conglomeraten, terwijl meer dan 90% van de chirale chemicaliën racemische verbindingen vormen. Daarom is **het eerste doel van dit proefschrift om het toepassingsbereik van chirale resolutietechnieken gebaseerd op kristallisatie uit te breiden naar racemische verbindingen, door ze om te zetten naar multi-componentkristallen (bijv. co-kristallen) die conglomeraten vormen.**

Racemische verbindingen kunnen worden omgezet naar conglomeraten via chemische modificatie, solvaatvorming en zoutvorming. Co-kristallisatie kan ook worden gebruikt als een tussenvorm voor de racemische verbinding-naar-conglomeraat omzetting. Echter, de vorming van conglomerate co-kristallen is nog zelden gerapporteerd (tot nu toe zijn slechts twee systemen gepubliceerd: Naproxen-Nicotinamide en Ibuprofen-trans-1-(2-pyridyl)-2-(4-pyridyl)-etheen. **Hoofdstukken 2-4** van dit proefschrift beschrijven onze bijdrage aan de ontwikkeling van de chirale scheiding van racemische verbindingen door de vorming van conglomeraat co-kristallen, terwijl we in **Hoofdstuk 5** de toepassing van een deracemisatietechniek introduceren op een racemische verbinding door een zout te vormen dat zich als conglomeraat gedraagt.

De zoektocht naar co-vormers die een specifieke racemische verbinding in een conglomeraat co-kristal kunnen veranderen kost veel tijd en middelen en heeft een laag slagingspercentage. Een belangrijke vraag hierin is hoe veel racemische verbindingen omgezet kunnen worden in conglomerate

co-kristallen. Met andere woorden “is de 10% regel, i.e. slechts 10% van de chirale verbindingen kunnen conglomeraten vormen, ook waar voor co-kristallen van chirale verbindingen?”. In **Hoofdstuk 2** wordt het antwoord op deze vraag gegeven, tezamen met een studie die de Cambridge Crystallography Data Center (CCDC) screening combineert met experimenteel onderzoek. Door zelfgemaakte software werden in een data screening van het CCDC 227 organische co-kristallen geïdentificeerd met die bestaan uit een chirale component, met een enkel chiraal centrum en een achirale co-vormer. Alle systemen hebben bekende racemische co-kristallen, terwijl er geen conglomerate co-kristallen zijn gevonden. Bovendien was een lijst van enantiomeerzuivere co-kristallen gegenereerd, welke potentiële kandidaten voor conglomerate co-kristallen geeft. Uit deze lijst zijn 6 enantiomeerzuivere co-kristalitems geselecteerd voor verder experimenteel onderzoek. Van deze 6 enantiomeerzuivere co-kristalssystemen vormen allen nieuwe racemische co-kristallen uit een racemisch mengsel in dezelfde condities waarin werd gerapporteerd dat de bijbehorende enantiomeerzuivere co-kristallen waren gevormd. Dit resultaat laat zien dat de vormingscondities van een enantiomeerzuiver co-kristal een goed startpunt zijn voor de kristallisatie van stabiele co-kristallen uit het bijbehorende racemisch mengsel en de co-vormer. Tot slot laat een voorlopige analyse van data zien dat de waarschijnlijkheid dat de 10% regel ook stand houdt voor co-kristallen van chirale verbindingen slecht  $7.1 \cdot 10^{-9}$  is, wat de hypothese ongeldig maakt. Dit onderzoek geeft een snelle manier van het experimenteel screenen van de lijst met potentiële conglomerate co-kristallen die hier is gegenereerd, alsmede een indicatie van de technische uitdaging die het omzetten van racemische verbindingen in conglomerate co-kristallen met zich meebrengt.

Na de selectie van de kandidaat co-vormers voor de beoogde chirale verbindingen, komt de volgende vraag in drievoud: welk type co-kristallen worden gevormd? Wat zijn de passende chirale resolutietechnieken voor deze co-kristallen? Wat zijn de optimale operationele condities? In **Hoofdstuk 3** wordt de ontwikkeling van een methode omschreven om deze vraag te beantwoorden gebaseerd op pseudo-binaire fase-diagrammen. Dergelijke fase-diagrammen beschrijven vloeistof-vast evenwichten in mengsels met variërende ratio's tussen de twee enantiomeren.

Verschillende types co-kristallen van een racemische verbinding en een co-vormer (chiraal of achiraal) vertonen onderscheidbare kenmerken in hun pseudo-binaire fase-diagrammen: een typisch fase-diagram van een diastereomeerisch-gerelateerd co-kristal, bijvoorbeeld van RS-Valine en S-Phenylalanine, bevat één eutectisch punt dat het diagram in twee asymmetrische delen verdeelt; een racemisch co-kristal, zoals van RS-Ibuprofen en 1,2-Bis(4-pyridyl)ethaan, heeft een typisch fase-diagram van twee symmetrisch gelocaliseerde eutectische punten die het diagram in drie delen opdelen. Het middenstuk vertegenwoordigt de regio waar het racemische co-kristal wordt gevormd en de delen aan de zijanten zijn de enantiomeerzuivere co-kristalregio's; aan de andere kant heeft een typisch fase-diagram van een conglomeraat co-kristal, RS-Ibuprofen en trans-1-(2-pyridyl)-2-(4-pyridyl)-ethaan bijvoorbeeld, slechts één eutectisch punt dat het diagram in twee symmetrische delen opdeelt, welke elk de enantiomeerzuivere co-kristallen van een van de enantiomeren representeren.

Er wordt aangetoond dat met gebruik van de procedure ontwikkeld in dit hoofdstuk het type co-kristallen van een beoogde racemische verbinding en de kandidaat co-vormer gemakkelijk geïdentificeerd kan worden uit hun bijbehorende pseudo-binaire fase-diagram. De geïdentificeerde types co-kristallen kunnen op hun beurt de passende op kristallisatie gebaseerde chirale resolutietechnieken bepalen. Bovendien geeft het fase-diagram van het beoogde systeem informatie over passende operationele condities, zoals temperatuur en mengselcomposities, voor het chirale resolutieproces.

De identificatie van conglomerate co-kristallen van racemische verbindingen geeft potentie aan chirale resolutietechnieken zoals selectieve kristallisatie. In **Hoofdstuk 4** was de S-enantiomeer van Ibuprofen (IBU), een racemische verbinding, succesvol gewonnen van een racemische suspensie in Heptaan door middel van selectieve kristallisatie, in de vorm van enantiomeerzuivere co-kristallen met de co-vormer trans-1-(2-pyridyl)-2-(4-pyridyl)-etheen (BPE). Een kleine hoeveelheid S-IBU-BPE co-kristallen was toegevoegd in de Heptaansuspensie om de selectieve kristallisatie te starten door 3 methodes: A) direct enten, B) auto-enten en C) nucleatie door enten met BPE. De verkregen co-kristalproducten hadden een overmaat in één van de enantiomeren tot 95% en de massa was tot 50% meer dan de hoeveelheid entstof. Dit co-kristallisatie-gemedieerde selectieve kristallisatieproces, dat naar ons weten nog nooit is gerapporteerd, verbreedt de toepassing van chirale resolutietechnieken naar vele racemische verbinding-vormende moleculen.

Een andere chirale resolutietechniek is deracemisatie door het toepassen van temperatuurcycli. Dit vereist, naast conglomerate kristallen, een racemisatiereactie in de oplossing voor de beoogde chirale stof. In **Hoofdstuk 5** is de deracimisatie van Phenylalanine (Phe) gelukt door het vormen van zijn conglomerate zout met 2,5-xyleensulfonzuur (XSA). Beginnend als een Azijnzuur suspensie met RS-Phe en XSA werden de racemische Phe-XSA zoutkristallen volledig omgezet naar enantiomeerzuivere kristallen nadat de suspensie herhaaldelijk was onderworpen aan verwarming-koelingcycli, gekoppeld met een racemisatiereactie in oplossing. Dit resultaat bevestigt dat het mogelijk is om conglomerate zouten als tussenstoffen te gebruiken voor deracimisatie.

In **Hoofdstukken 2 – 5** gebruiken we multicomponentkristallisatie als een tussenstap voor de toepassing van chirale resolutietechnieken van racemische verbindingen. Echter, in veel andere gevallen hindert het bestaan van een multicomponentenmengsel de toepassing van directe kristallisatie, omdat een gemixte vaste fase wordt gevormd die verdere stappen vereist voor productzuivering. In deze gevallen is de koppeling tussen deeltjesscheiding gebaseerd op hun chemische samenstelling en simultaan de kristallisatie van deze deeltjes gewenst. Daarom **is het tweede doel van dit proefschrift om de mogelijkheden te verkennen van het simultaan scheiden van multicomponentsystemen door middel van kristallisatie.**

In **Hoofdstukken 6 en 7** beschrijven we een nieuwe techniek, namelijk Elektrisch Veld Versterkte Kristallisatie (EVVK), welke de hiervoor genoemde simultane deeltjesscheiding tijdens kristallisatie in één of twee stappen kan bewerkstelligen. Een dergelijke techniek is gebaseerd op één fenomeen: een inhomogeen elektrisch veld in een isolerend oplosmiddel zoals dioxaan beïnvloedt alle

aanwezige deeltjes, die daaropvolgend circuleren tussen de twee elektroden die het veld opwekken en uiteindelijk verzamelen op een daarvan. Op welke elektrode de kristallen verzamelen is afhankelijk van de chemische samenstelling van de kristallen. Bijvoorbeeld, Isonicotinamide (INA) kristallen verzamelen altijd op het oppervlak van de anode.

We hebben dit fenomeen gebruikt om twee opgeloste stoffen van elkaar te scheiden uit een complex multicomponentenmengsel: in **Hoofdstuk 6** leidt het toepassen van een gelijkstroom elektrisch veld in een gemengde suspensie in dioxaan tot de selectieve verzameling van de kristallen van de twee opgeloste stoffen, Phenazine (PHE) en Caffeïne (CAF), respectievelijk op de kathode en anode. Een daaropvolgende koelingstap maakt de groei en immobilisatie van deze kristallen op hun elektroden mogelijk. Aan het einde van de koelingstap worden CAF, met een zuiverheid van hoger dan 91% massa, en PHE, met een zuiverheid zo hoog als 97% massa, opgevangen van de anode en kathode.

PHE en CAF worden gescheiden door EVVK, omdat hun kristallen worden aangetrokken door verschillende elektroden. Echter, er bestaan ook andere systemen, zoals het mengsel van CAF en INA, waar de kristallen van beide opgeloste stoffen verzamelen op dezelfde elektrode. In **Hoofdstuk 7** introduceren we een nieuwe werkstrategie van EVVK voor het scheiden van systemen zoals het CAF-INA mengsel: in de gemengde oplossing van CAF en INA worden entkristallen van een van de opgeloste stoffen toegevoegd aan de gemixte dioxaanoplossing en EVVK immobiliseert de kristallen op de anode. Daarna wordt de polariteit van het elektrische veld omgedraaid en worden entkristallen van de andere opgeloste stof ingebracht in het systeem. Een tweede stap van EVVK immobiliseert de nieuwe kristallen op de nieuwe anode, terwijl de kristallen van de eerst gekristalliseerde stof door blijven groeien op de oude anode. Uiteindelijk worden kristallen van danwel INA of CAF met zuiverheden hoger dan 91 % massa opgevangen van de verschillende elektroden. Het succes van het gescheiden winnen van beide opgeloste stoffen van twee verschillende gemengde systemen bewijst dat EVVK potentieel gebruikt kan worden om meerdere opgeloste stoffen van multicomponentsystemen te winnen in één of twee stappen.

Dit proefschrift behandelt de twee kanten van multicomponentsystemen: aan de ene kant is een systematische procedure ontwikkeld om multicomponent kristallijne materialen (bijv. conglomerate co-kristallen) te onderzoeken, identificeren en gebruiken als tussenstoffen voor de toepassing van chirale resolutietechnieken op racemische verbindingen. Dit deel van het werk kan mogelijk in de industrie gebruikt worden als standaard voor het produceren van enantiomeerzuivere producten van beoogde racemische verbindingen. Aan de andere kant is de effectieve scheiding van twee opgeloste stoffen uit hun multicomponentsuspensie door een nieuw ontwikkelde techniek beschreven, die de elektrisch veld geassisteerde deeltjesscheiding koppelt aan koelkristallisatie. De EVVK techniek kan verder ontwikkeld worden naar een éénstapsproces voor de zuivering van meerdere opgeloste stoffen in een mengsel.

# Chapter 1. Introduction

Multi-component systems, in various physical phases, exist in almost every bio- or chemical process. The existence of these systems both imposes problems and provide opportunities to the relevant process and separation technologies. In the specific case of crystallization technology, multi-component systems are also challenges as well as chances: on one hand, a multi-component solution is usually where the target product is recovered by crystallization, which strives to minimize the contamination by the other compounds from the solution; on the other hand, the formation of multi-component crystalline materials, for instance co-crystals, from the target compound can alter the physical properties (e.g., solubility) of the product, which may in turn improve the product quality (e.g., dissolution kinetics).

In this thesis, we demonstrate our contribution in exploiting the chances and tackling the challenges of the multi-component systems: we systematically apply crystallization-based chiral resolution (CCR) techniques, especially deracemization, on racemic compounds, systems which are not suitable for many CCR techniques, via their corresponding multi-component conglomerate crystals (**Chapter 2—5**); we crystallize and separate two solute compounds, enhanced by a strong electric field, from their multi-component solutions so that neither solute is contaminated by the other (**Chapter 6 and 7**).

In this chapter, the background of the thesis topics is given, including the state-of-art CCR techniques and effects of electric field on crystalline particles. Afterwards, our objectives and the corresponding approaches are briefly introduced, followed by a brief summary of each chapter in the thesis.

## 1. BACKGROUND

### 1.1 CRYSTALLIZATION

Crystallization is one of the most commonly used separation techniques in industry and it enables the recovery of the target products in the form of crystalline phase of high purity. In fact, around 70% of the chemical products are in the form of crystalline materials, especially in the pharmaceutical, food and nutrition industries<sup>1</sup>. In this section, the fundamentals of crystallization is briefly introduced, which contain information relevant to the techniques used in this thesis.

The initial stage of crystallization is nucleation, which is the creation of new crystalline entities of solute molecules by a phase transformation from the liquid or vapor phase<sup>2</sup>. If the initial fluid is a clear liquid the nucleation process is referred as primary nucleation, while secondary nucleation refers to the case where the liquid already contains one or more crystals of the target compounds<sup>3-4</sup>. If the new phase formation is caused by solute entities clustering, the process is called homogeneous nucleation. In heterogeneous nucleation, on the other hand, nuclei are formed on the surface of foreign particles in the liquid<sup>5</sup>.

After nucleation, the formed nuclei experience growth<sup>6</sup>, agglomeration<sup>7</sup> and also breakage<sup>8</sup>, as a result of the supersaturation of the liquid phase and the thermal and hydrodynamic conditions in their surrounds<sup>4</sup>. The final crystalline products can be characterized by their size distribution<sup>4</sup>, purity, shape<sup>9</sup> as well as their morphology, which influence the physical properties of the crystals such as solubility and melting point<sup>10</sup>. The overall process of crystallization can be simulated via Population Balance Equations<sup>11</sup>, which describe the properties of the crystals spatially and temporally.

Crystals can contain more than one compounds in their lattice. Multicomponent crystals can be grouped into salts, solvates and co-crystals<sup>12</sup>. A salt crystal contains ions inside its lattice, while a solvate or a co-crystal only composes of neutral molecules or atoms<sup>12</sup>. The formation of multicomponent crystals from a target compound can change the physical properties of the final products such as solubility<sup>13</sup> and optical properties<sup>14-15</sup>. Therefore, the use of a suitable counter-ion, solvent or co-former is a common tool in crystal engineering.

One essential requirement for the design and operation of a crystallization process is the liquid-solid phase equilibrium information, often expressed in the form of phase diagrams<sup>16-19</sup>. A phase diagram can provide information such as solubility as well as theoretical recovery yield from a crystallization process<sup>19</sup>. Moreover, it can be used to identify the types of crystalline materials involved in a process or with a target compound<sup>20</sup>.

A phase diagram can be as simple as a solubility line of a single component<sup>21</sup> or as complicated as a multicomponent crystal from a mixture containing several co-formers or electrolytes<sup>21</sup>. Based on the purpose of the phase diagram, it can be simplified and yet maintain all the relevant information. For instance, in a co-crystal forming mixture which contains the target compound A, the co-former B and the solvent C, a pseudo-binary phase diagram describing the molar ratio between the A and B as a function of system temperature can be used to identify the composition region where the co-crystals are formed<sup>22</sup>. (Please see **Chapter 3** for detailed descriptions for phase diagrams.)

## 1.2 CRYSTALLIZATION-BASED CHIRAL RESOLUTION (CCR)

One special application of crystallization is to recover the target enantiomer of a chiral compound from its racemic mixture, a technique commonly referred to as crystallization-based chiral resolution (CCR). In the following paragraphs, the state-of-art CCR techniques are introduced.

Chiral molecules, those molecules that cannot be superimposed on their mirror images, play important roles in pharmaceutical, food and nutrition industries. For instance, around 56% of the drugs currently in use are chiral. Most biomolecules, such as proteins and sugars, are chiral which means that human body can react drastically differently to the two enantiomers of the same compounds. In most cases, the undesired enantiomer has a significantly lower pharmaceutical activity than the desired one (e.g., the almost 100 times activity difference between the S- and the R-Ibuprofen, where the S-enantiomer is the desired one). In some extreme cases, the undesired enantiomer (e.g., the S-enantiomer of Thalidomide) can cause severe side effects (e.g., deformation of the newly born infants). Therefore, it is beneficial for industries to manufacture the desired enantiomer while avoiding the opposite. However, up till now, the majority of the chiral medicines are marketed as racemates, mixtures containing equal amount of the two enantiomers<sup>23-24</sup>, due to the technical and economic difficulties in separating the two enantiomers from each other.

For decades, enormous amounts of studies and industrial applications have been conducted to obtain the desired enantiomers of target chiral compounds. The desired enantiomer can be selectively synthesized via Kinetic Resolution (KR), by enzymatic<sup>25-26</sup> or non-enzymatic<sup>27</sup> routes. Alternatively, separation techniques such as chromatography<sup>28</sup>, membrane<sup>29</sup> and extractions<sup>30</sup> are also used to recover the desired enantiomers from the corresponding racemic mixtures.

Ever since last century, crystallization-based chiral resolution (CCR) techniques have significantly contributed to the process of obtaining the desired enantiomers. The oldest and the most commonly used CCR technique is classic resolution, in which the two enantiomers of the target compound separately form diastereomeric salts with a chiral counter-ion. The resulting salt crystals from the two enantiomers, which have different solubilities, can be subsequently separated<sup>31</sup>. The derivative of the classic resolution, namely ‘Dutch Resolution’, utilizes a mixture of chiral agents to achieve more efficient resolution<sup>32</sup>.

Another commonly studied CCR technique is preferential crystallization (PC), which uses enantiopure crystal seeds to recover only the desired enantiomer from a racemic mixture<sup>33</sup>. During a PC process, the seeds recover the desired enantiomer from a racemic solution while increasing the supersaturation of the unseeded and undesired enantiomer. The process is stopped before the primary nucleation of the unseeded enantiomer takes place to avoid the contamination of the final product (see

schematic demonstration in Figure 1 (top)). Please see **Chapter 4** for detailed description of PC processes.

CCR techniques such as classical resolution and PC can theoretically recover all the desired enantiomer from a racemic mixture while recycling back the opposite one, thus achieving a yield of 50%. On the other hand, deracemization techniques such as Viedma Ripening and Temperature Cycling can theoretically achieve 100% yield. The deracemization is achieved by partial dissolution/recrystallization of the crystals in the suspension via either mechanical grinding of the solid phase or periodic cycles of heating and cooling, coupled with a solution phase racemization reaction<sup>34-36</sup> (see schematic demonstration in Figure 1 (bottom)). Please see **Chapter 5** for detailed description of temperature-cycling deracemization processes.

### Preferential Crystallization

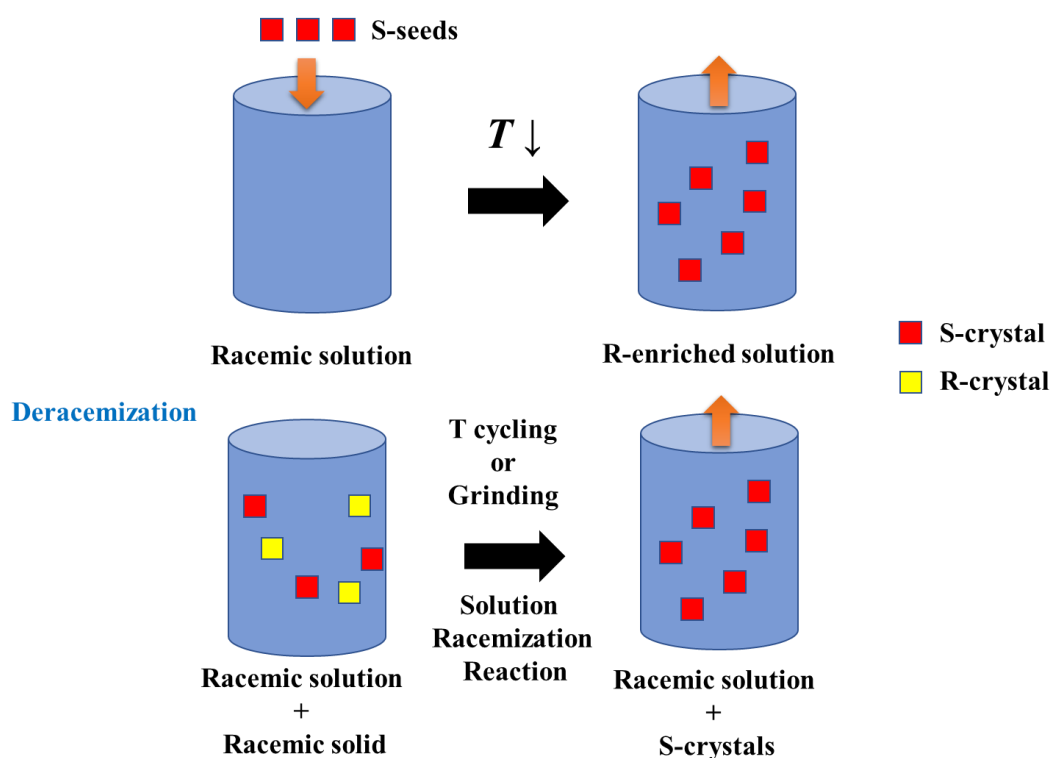


**Figure 1.** Schematic demonstrations of typical Preferential Crystallization (top) and deracemization (bottom) processes.

### 1.3 PROCESS INTENSIFICATION BY EXTERNAL FIELDS

In the past decades, various alternative energy sources have been used to improve crystallization processes: nucleation has been induced by laser<sup>37</sup> and ultrasound<sup>38</sup>; deracemization has

been achieved by ultrasound-induced attrition<sup>39</sup>; microwave has been used for Direct Nucleation Control (DNC)<sup>40</sup>, etc. In addition, electric field, either Alternative Current (AC) or Direct Current (DC), has been utilized in localizing protein nucleation<sup>41</sup> and controlling protein crystal size distribution<sup>42-44</sup>, as well as the polymorphism of pharmaceutical compounds<sup>45</sup>.

On the other hand, external field such as electric and magnetic fields have been studied to manipulate and eventually separate different particles. Magnetic levitation has been reported to separate different polymorphs<sup>46</sup> as well as co-former from co-crystals<sup>47</sup> based on their differences in particle densities. The application of an electric field can induce two different forces on a particle within: the electrophoretic force, which acts on charged particles<sup>48</sup>, and the dielectrophoretic force, which influences polarized neutral particles<sup>49</sup> (see Figure 2 for schematic demonstration of the two forces). It is shown that based on dielectrophoretic forces an electric field is capable to separate gold particles from an aqueous stream<sup>50</sup>, cancer cells from healthy ones<sup>51</sup>, nanoparticles of different sizes<sup>48, 52</sup> etc.

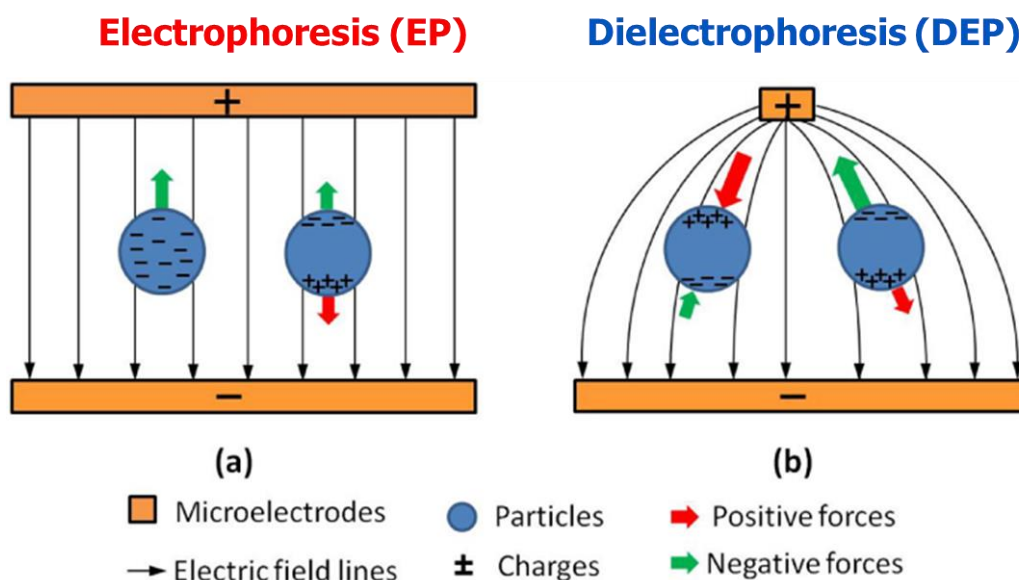


**Figure 2.** Schematic demonstrations of Electrophoresis (left) and Dielectrophoresis (right). Reprinted from Li M. et al.<sup>53</sup>

## 2. PROBLEM STATEMENTS

CCR techniques can effectively recover the desired enantiomer, in the form of pure crystalline materials, from a racemic mixture. However, the development of CCR is far from being complete with one drawback that needs to be tackled. The varying CCR techniques are crystallization processes which selectively retain the desired enantiomers in the crystalline phase and reject the opposite enantiomers. Therefore, the target compounds of a CCR technique needs to crystallize as a conglomerate, a physical

mixture of enantiopure crystals<sup>20</sup>. However, of all the reported chiral compounds, around 90% crystallize as racemic compounds, which are crystals containing equal amount of the two enantiomers in the lattice<sup>20</sup>, unsuitable for CCR techniques. **Therefore, the application of CCR techniques is severely limited due to the lack of conglomerate-forming chiral compounds.**

A racemic mixture is essentially a multi-component system requiring recovery and purification of the target compound, in this case the desired enantiomer, from an equal amount of impurity. Many other multi-component systems, for instance the product stream from a Multi-Component Reaction batch, also contain product with comparable amount of impurities. The application of direct crystallization on these systems usually leads to a mixed solid phase, which requires additional steps for product purification and inevitably results in extra cost and product loss. Therefore, **the second problem to be tackled in this thesis is the contamination of target product by the present of impurity crystals from a multi-component mixture after direct crystallization.**

### **3. OBJECTIVES**

This thesis aims to contribute to the solution of these drawbacks: one in CCR techniques and one in the direct crystallization of multi-component systems. This aim is specified into two main objectives:

- 1) To expand the application range of CCR techniques to racemic compounds by converting them into conglomerate multi-component crystals.**
- 2) To crystallize and separate target product from impurities in a multi-component solution, using the forces of an electric field on solid particles.**

### **4. THESIS OUTLINE**

The conversion of racemic compounds into conglomerates can in principle be achieved through the formation of multi-component crystals such as conglomerate salts<sup>54-56</sup>, solvates<sup>57</sup> and co-crystals<sup>15</sup>, provided that suitable counter-ions, solvent molecules and co-formers are found, (see Figure 3 for schematic demonstration). However, the search of suitable couples for multi-component crystallization is time-consuming and of low successful rates, especially in the case of conglomerate co-crystal, which has only been reported twice in literature<sup>15, 58</sup>. Therefore, a method combining computational database screening and experimental investigation is developed. This method is introduced in Chapter 2 and

describes the technical difficulties in converting racemic compounds into conglomerate co-crystals while providing a quick way of experimentally screening the co-crystal systems from racemic compounds;

When a suitable co-former is selected, the type of its corresponding co-crystal with the target racemic compound needs to be determined. Moreover, it is also desired to select a suitable CCR technique as well as its operation conditions based on the type of the co-crystals. In **Chapter 3**, a phase-diagram-based method is described, which is used to identify various co-crystal types from a racemic compound and to provide guidelines for the design of suitable chiral resolution processes.

The last step in achieving objective one is to provide the Proof of Principle that multi-component conglomerates are feasible to be used as intermediates for the application of CCR techniques on racemic compounds. In **Chapter 4**, the successful resolution is described of a commonly used racemic compound, Ibuprofen, via its conglomerate co-crystal with an achiral co-former, proving the possibility to use conglomerate co-crystals as an intermediate for the preferential crystallization of a racemic compound; Finally, the feasibility of racemic compound deracemization via its conglomerate salt is demonstrated in **Chapter 5** in which the deracemization of Phenylalanine is achieved by the temperature-cycling method, using the conglomerate salt with 2,5-xylenesulfonic acid as an intermediate.

For the second objective, we have explored the effect of an electric field on crystals in an insulator suspension and its application in separating target product from impurities in a multi-component system. In **Chapter 6**, we describe the observed selective accumulation of the crystals on one of the two electrodes, under the influence of an inhomogeneous electric field. Moreover, we describe how to use this phenomenon to simultaneously separate the crystals of Phenazine (PHE) and Caffeine (CAF) onto the cathode and the anode, respectively, while crystallizing them from a multi-component suspension.

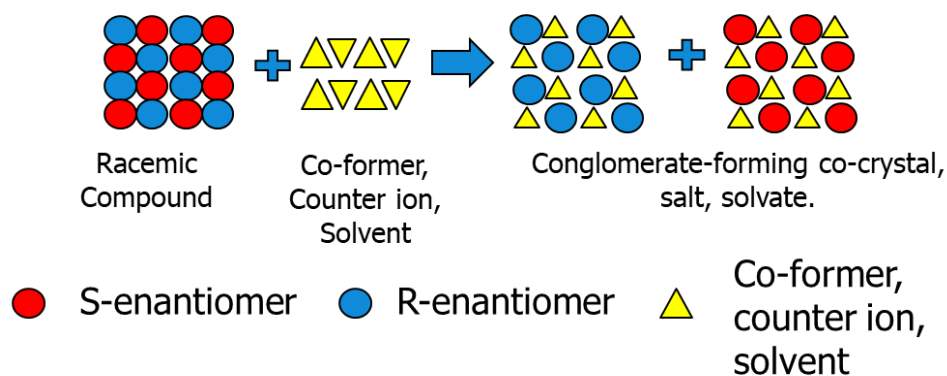


**Figure 3.** Schematic demonstration: racemic compounds to multi-component conglomerate.

In **Chapter 7**, we show that the separation of crystals by electric field can also be used for multi-component systems, in which the two solute crystals both accumulate on the same electrode. In this chapter, we describe a new strategy by which CAF and Isonicotinamide (INA) are separated from each other by a two-step crystallization, under the effect of the electric field.

## REFERENCES

1. Ter Horst, J. H.; Schmidt, C.; Ulrich, J., Fundamentals of industrial crystallization. In *Handbook of Crystal Growth*, 2015; Vol. II, pp 1317-1349.
2. Davey, R. J.; Schroeder, S. L. M.; ter Horst, J. H., Nucleation of Organic Crystals—A Molecular Perspective. *Angewandte Chemie International Edition* **2013**, *52* (8), 2166-2179.
3. Botsaris, G. D., Secondary Nucleation — A Review. In *Industrial Crystallization*, Mullin, J. W., Ed. Springer US: Boston, MA, 1976; pp 3-22.
4. Lewis, A.; Seckler, M.; Kramer, H.; van Rosmalen, G., *Industrial Crystallization: Fundamentals and Applications*. Cambridge University Press: 2015.
5. Liu, X. Y., Heterogeneous nucleation or homogeneous nucleation? *The Journal of Chemical Physics* **2000**, *112* (22), 9949-9955.
6. Andrea, C. L.; Miroslav, K., Theory and simulation of crystal growth. *Journal of Physics: Condensed Matter* **1997**, *9* (2), 299.
7. Brunsteiner, M.; Jones, A. G.; Pratola, F.; Price, S. L.; Simons, S. J. R., Toward a Molecular Understanding of Crystal Agglomeration. *Crystal Growth & Design* **2005**, *5* (1), 3-16.
8. Randolph, A. D., Effect of Crystal Breakage on Crystal Size Distribution in Mixed Suspension Crystallizer. *Industrial & Engineering Chemistry Fundamentals* **1969**, *8* (1), 58-63.
9. Lovette, M. A.; Browning, A. R.; Griffin, D. W.; Sizemore, J. P.; Snyder, R. C.; Doherty, M. F., Crystal Shape Engineering. *Industrial & Engineering Chemistry Research* **2008**, *47* (24), 9812-9833.
10. Mangin, D.; Puel, F.; Veesler, S., Polymorphism in Processes of Crystallization in Solution: A Practical Review. *Organic Process Research & Development* **2009**, *13* (6), 1241-1253.
11. Omar, H. M.; Rohani, S., Crystal Population Balance Formulation and Solution Methods: A Review. *Crystal Growth & Design* **2017**, *17* (7), 4028-4041.
12. Grothe, E.; Meekes, H.; Vlieg, E.; ter Horst, J. H.; de Gelder, R., Solvates, Salts, and Cocrystals: A Proposal for a Feasible Classification System. *Crystal Growth & Design* **2016**, *16* (6), 3237-3243.
13. Yadav, A. V.; Shete, A. S.; Dabke, A. P.; Kulkarni, P. V.; Sakhare, S. S., Co-Crystals: A Novel Approach to Modify Physicochemical Properties of Active Pharmaceutical Ingredients. *Indian Journal of Pharmaceutical Sciences* **2009**, *71* (4), 359-370.
14. Springuel, G.; Leyssens, T., Innovative Chiral Resolution Using Enantiospecific Co-Crystallization in Solution. *Crystal Growth & Design* **2012**, *12* (7), 3374-3378.
15. Neurohr, C.; Marchivie, M.; Lecomte, S.; Cartigny, Y.; Couvrat, N.; Sanselme, M.; Subra-Paternault, P., Naproxen–Nicotinamide Cocrystals: Racemic and Conglomerate Structures Generated by CO<sub>2</sub> Antisolvent Crystallization. *Crystal Growth & Design* **2015**, *15* (9), 4616-4626.
16. Chiarella, R. A.; Davey, R. J.; Peterson, M. L., Making Co-Crystals The Utility of Ternary Phase Diagrams. *Crystal Growth & Design* **2007**, *7* (7), 1223-1226.
17. Crocker, L. S.; Ge, Z.; Abraham, A.; Hartman, R.; Xu, J., An Etoricoxib Phase Diagram: Hemihydrate and Anhydrate. *Organic Process Research & Development* **2003**, *7* (6), 958-961.
18. Haas, C.; Drenth, J., Understanding protein crystallization on the basis of the phase diagram. *Journal of Crystal Growth* **1999**, *196* (2), 388-394.

19. Coquerel, G., Crystallization of molecular systems from solution: phase diagrams, supersaturation and other basic concepts. *Chemical Society Reviews* **2014**, *43* (7), 2286-2300.
20. Srisanga, S.; ter Horst, J. H., Racemic Compound, Conglomerate, or Solid Solution: Phase Diagram Screening of Chiral Compounds. *Crystal Growth & Design* **2010**, *10* (4), 1808-1812.
21. Reus, M. A.; van der Heijden, A. E. D. M.; ter Horst, J. H., Solubility Determination from Clear Points upon Solvent Addition. *Organic Process Research & Development* **2015**, *19* (8), 1004-1011.
22. ter Horst, J. H.; Deij, M. A.; Cains, P. W., Discovering New Co-Crystals. *Crystal Growth & Design* **2009**, *9* (3), 1531-1537.
23. Maher, T. J.; Johnson, D. A., Review of chirality and its importance in pharmacology. *Drug Development Research* **1991**, *24* (2), 149-156.
24. Nguyen, L. A.; He, H.; Pham-Huy, C., Chiral Drugs: An Overview. *International Journal of Biomedical Science : IJBS* **2006**, *2* (2), 85-100.
25. May, O.; Verseck, S.; Bommarius, A.; Drauz, K., Development of Dynamic Kinetic Resolution Processes for Biocatalytic Production of Natural and Nonnatural l-Amino Acids. *Organic Process Research & Development* **2002**, *6* (4), 452-457.
26. Pàmies, O.; Bäckvall, J.-E., Combination of Enzymes and Metal Catalysts. A Powerful Approach in Asymmetric Catalysis. *Chemical Reviews* **2003**, *103* (8), 3247-3262.
27. Vedejs, E.; Jure, M., Efficiency in Nonenzymatic Kinetic Resolution. *Angewandte Chemie International Edition* **2005**, *44* (26), 3974-4001.
28. Welch, C. J., Chiral Chromatography in Support of Pharmaceutical Process Research. In *Preparative Enantioselective Chromatography*, Blackwell Publishing Ltd: 2007; pp 1-18.
29. Armstrong, D. W.; Jin, H. L., Enrichment of enantiomers and other isomers with aqueous liquid membranes containing cyclodextrin carriers. *Analytical Chemistry* **1987**, *59* (18), 2237-2241.
30. Ren, Z.; Zeng, Y.; Hua, Y.; Cheng, Y.; Guo, Z., Enantioselective Liquid-Liquid Extraction of Racemic Ibuprofen by l-Tartaric Acid Derivatives. *Journal of Chemical & Engineering Data* **2014**, *59* (8), 2517-2522.
31. Collet, A., Resolution of Racemates: Did You Say "Classical"? *Angewandte Chemie International Edition* **1998**, *37* (23), 3239-3241.
32. Dalmolen, J.; Tiemersma-Wegman, T. D.; Nieuwenhuijzen, J. W.; van der Sluis, M.; van Echten, E.; Vries, T. R.; Kaptein, B.; Broxterman, Q. B.; Kellogg, R. M., The Dutch Resolution Variant of the Classical Resolution of Racemates by Formation of Diastereomeric Salts: Family Behaviour in Nucleation Inhibition. *Chemistry – A European Journal* **2005**, *11* (19), 5619-5624.
33. Coquerel, G., Preferential Crystallization. In *Novel Optical Resolution Technologies*, Sakai, K.; Hirayama, N.; Tamura, R., Eds. Springer Berlin Heidelberg: Berlin, Heidelberg, 2007; pp 1-51.
34. Sogutoglu, L.-C.; Steendam, R. R. E.; Meekes, H.; Vlieg, E.; Rutjes, F. P. J. T., Viedma ripening: a reliable crystallisation method to reach single chirality. *Chemical Society Reviews* **2015**, *44* (19), 6723-6732.
35. Spix, L.; Meekes, H.; Blaauw, R. H.; van Enkevort, W. J. P.; Vlieg, E., Complete Deracemization of Proteinogenic Glutamic Acid Using Viedma Ripening on a Metastable Conglomerate. *Crystal Growth & Design* **2012**, *12* (11), 5796-5799.
36. Suwannasang, K.; Flood, A. E.; Rougeot, C.; Coquerel, G., Using Programmed Heating-Cooling Cycles with Racemization in Solution for Complete Symmetry Breaking of a Conglomerate Forming System. *Crystal Growth & Design* **2013**, *13* (8), 3498-3504.
37. Soare, A.; Dijkink, R.; Pascual, M. R.; Sun, C.; Cains, P. W.; Lohse, D.; Stankiewicz, A. I.; Kramer, H. J. M., Crystal Nucleation by Laser-Induced Cavitation. *Crystal Growth & Design* **2011**, *11* (6), 2311-2316.
38. Luque de Castro, M. D.; Priego-Capote, F., Ultrasound-assisted crystallization (sonocrystallization). *Ultrasonics Sonochemistry* **2007**, *14* (6), 717-724.
39. Xiouras, C.; Van Aeken, J.; Panis, J.; Ter Horst, J. H.; Van Gerven, T.; Stefanidis, G. D., Attrition-Enhanced Deracemization of NaClO<sub>3</sub>: Comparison between Ultrasonic and Abrasive Grinding. *Crystal Growth & Design* **2015**, *15* (11), 5476-5484.

40. Kacker, R.; Salvador, P. M.; Sturm, G. S. J.; Stefanidis, G. D.; Lakerveld, R.; Nagy, Z. K.; Kramer, H. J. M., Microwave Assisted Direct Nucleation Control for Batch Crystallization: Crystal Size Control with Reduced Batch Time. *Crystal Growth & Design* **2016**, *16* (1), 440-446.
41. Taleb, M.; Didierjean, C.; Jelsch, C.; Mangeot, J. P.; Capelle, B.; Aubry, A., Crystallization of proteins under an external electric field. *Journal of Crystal Growth* **1999**, *200* (3), 575-582.
42. Yan, J. Y.; Patey, G. N., Heterogeneous Ice Nucleation Induced by Electric Fields. *The Journal of Physical Chemistry Letters* **2011**, *2* (20), 2555-2559.
43. Kashchiev, D., Nucleation in external electric field. *Journal of Crystal Growth* **1972**, *13*, 128-130.
44. Hammadi, Z.; Veessler, S., New approaches on crystallization under electric fields. *Progress in Biophysics and Molecular Biology* **2009**, *101* (1), 38-44.
45. Parks, C.; Koswara, A.; Tung, H.-H.; Nere, N.; Bordawekar, S.; Nagy, Z. K.; Ramkrishna, D., Molecular Dynamics Electric Field Crystallization Simulations of Paracetamol Produce a New Polymorph. *Crystal Growth & Design* **2017**, *17* (7), 3751-3765.
46. Atkinson, M. B. J.; Bwambok, D. K.; Chen, J.; Chopade, P. D.; Thuo, M. M.; Mace, C. R.; Mirica, K. A.; Kumar, A. A.; Myerson, A. S.; Whitesides, G. M., Using Magnetic Levitation to Separate Mixtures of Crystal Polymorphs. *Angewandte Chemie International Edition* **2013**, *52* (39), 10208-10211.
47. Matheys, C.; Tumanova, N.; Leyssens, T.; Myerson, A. S., Magnetic Levitation as a Tool for Separation: Separating Cocrystals from Crystalline Phases of Individual Compounds. *Crystal Growth & Design* **2016**, *16* (9), 5549-5553.
48. Velev, O. D.; Bhatt, K. H., On-chip micromanipulation and assembly of colloidal particles by electric fields. *Soft Matter* **2006**, *2* (9), 738-750.
49. Pethig, R., Review Article—Dielectrophoresis: Status of the theory, technology, and applications. *Biomicrofluidics* **2010**, *4* (2), 022811.
50. Dash, S.; Mohanty, S.; Pradhan, S.; Mishra, B. K., CFD design of a microfluidic device for continuous dielectrophoretic separation of charged gold nanoparticles. *Journal of the Taiwan Institute of Chemical Engineers* **2016**, *58*, 39-48.
51. Moon, H.-S.; Kwon, K.; Kim, S.-I.; Han, H.; Sohn, J.; Lee, S.; Jung, H.-I., Continuous separation of breast cancer cells from blood samples using multi-orifice flow fractionation (MOFF) and dielectrophoresis (DEP). *Lab on a Chip* **2011**, *11* (6), 1118-1125.
52. Gascoyne, P. R. C.; Vykoukal, J., Particle separation by dielectrophoresis. *ELECTROPHORESIS* **2002**, *23* (13), 1973-1983.
53. Li, M.; Li, W. H.; Zhang, J.; Alici, G.; Wen, W., A review of microfabrication techniques and dielectrophoretic microdevices for particle manipulation and separation. *Journal of Physics D: Applied Physics* **2014**, *47* (6), 063001.
54. Li, W. W.; Spix, L.; de Reus, S. C. A.; Meekes, H.; Kramer, H. J. M.; Vlieg, E.; ter Horst, J. H., Deracemization of a Racemic Compound via Its Conglomerate-Forming Salt Using Temperature Cycling. *Crystal Growth & Design* **2016**, *16* (9), 5563-5570.
55. Spix, L.; Alfring, A.; Meekes, H.; van Enckevort, W. J. P.; Vlieg, E., Formation of a Salt Enables Complete Deracemization of a Racemic Compound through Viedma Ripening. *Crystal Growth & Design* **2014**, *14* (4), 1744-1748.
56. Wermester, N.; Aubin, E.; Pauchet, M.; Coste, S.; Coquerel, G., Preferential crystallization in an unusual case of conglomerate with partial solid solutions. *Tetrahedron: Asymmetry* **2007**, *18* (7), 821-831.
57. Würges, K.; Petruševska-Seebach, K.; Elsner, M. P.; Lütz, S., Enzyme-assisted physicochemical enantioseparation processes—Part III: Overcoming yield limitations by dynamic kinetic resolution of asparagine via preferential crystallization and enzymatic racemization. *Biotechnology and Bioengineering* **2009**, *104* (6), 1235-1239.
58. Elacqua, E. Supramolecular chemistry of molecular concepts:tautomers, chirality, protecting groups, trisubstituted olefins, cyclophanes, and their impact on the organic solid state. University of Iowa, 2012.

# Chapter 2. Is the 10% rule valid for Co-crystals of Chiral Compounds?

**Key Words:** Chiral Compounds, Chiral Resolution, Conglomerate Co-crystal, CCDC Screening

**Abstract:** Crystallization-mediated chiral resolution techniques usually require their target compounds to crystallize as conglomerates. Only around 10% of the reported chiral compounds form conglomerates, which is sometimes referred to as the 10% rule; almost all other chiral compounds crystallize as racemic compounds. In principle, racemic compounds can be converted into conglomerate co-crystals via co-crystallization, although the number of examples is rather limited. In this study, we investigate the validity of the 10% rule for co-crystals of chiral compounds via a preliminary analysis on data collected by an automated screening in the Cambridge Crystallography Data Center (CCDC). Out of 227 organic co-crystals composed of a chiral component, having a molecule with a single chiral center, and an achiral co-former, 227 systems have known racemic compound co-crystals, while no conglomerate co-crystals are found. A separately generated list of systems, for which only enantiopure co-crystals are reported, contains potential conglomerate co-crystal candidates. From this list, 6 systems were selected for experimental investigation. Using the reported preparation procedure of the enantiopure co-crystals applied to the racemic system, all systems formed co-crystals from the corresponding racemic mixtures and the co-formers. However, none of these co-crystals appeared to be conglomerates. Nevertheless, this list of co-crystals from chiral compounds can be used to investigate the crystal structures on the scientific principles behind co-crystal formation. The preliminary analysis of the data shows that the likelihood that the 10% rule holds for co-crystals from chiral compounds is only  $7.1 \cdot 10^{-9}$ , which makes this hypothesis invalid. Our study demonstrates the technical difficulty in converting racemic compounds into conglomerate co-crystals, while providing a list of potential candidates for conglomerate co-crystal screening.

## 1. INTRODUCTION

The strict regulation on the enantiopurity of chiral products, especially pharmaceutical, due to the difference in bioactivity of the enantiomers<sup>1-2</sup>, triggers the development of chiral resolution techniques. When enantioselective synthesis becomes too difficult or costly, chiral resolution through crystallization can offer an alternative for the recovery of enantiopure products. Crystallization-mediated chiral resolution techniques have been known and used since the discovery of enantiomorphous crystals by Pasteur<sup>3</sup>. More recently also deracemization methods have been developed, for which the resolution is combined with a racemization reaction leading to a 100% conversion of the solids into a single enantiomer.

For all these resolution and deracemization techniques a prerequisite is that the chiral compound of interest forms a conglomerate, a physical mixture of crystals each containing a single enantiomer. It is generally found that only 10% of the chiral compounds form a racemic conglomerate<sup>4</sup> and the other 90% being covered mainly by racemic compounds, crystals containing both enantiomers of even amounts in a regularly structured array<sup>2</sup>. A small fraction of the chiral compounds forms a solid solution of the two enantiomers.

In order to apply chiral resolution techniques on molecules crystallizing as racemic compounds, it is important to find conditions or other ways to force these molecules to form racemic conglomerates. For that, one can exploit the limited lifetime of metastable conglomerate phases<sup>5</sup>. One can also screen for conglomerate forming salts or solvates of the compound of interest<sup>6-7</sup>. An alternative approach towards conglomerate systems is the formation of conglomerate co-crystals from racemic compounds. In order to estimate the challenges in changing a racemic compound to a conglomerate co-crystal, we aim to investigate whether the 10% rule is valid for co-crystals formed from chiral compounds, the majority of which are racemic compounds.

To do this we use a recently reported search method for co-crystals on the basis of data mining, using the Cambridge Crystallography Data Center (CCDC)<sup>8-9</sup>, as well as a method to search the database for structures involving chiral compounds. This new method enables the fast and specific search of all the co-crystal structures reported for chiral compounds. Within this list we determine the number of conglomerate and racemic compound co-crystals. In addition, we experimentally test the existence of conglomerate co-crystals from a limited number of selected potential candidates. This combination allows us to make an educated estimation of the validity of the 10% rule for chiral co-crystals.

## 2. MATERIALS AND METHODS

**Data Screening.** ConQuest was used to access the CCDC version 1.19 and to export all organic entries which had 3D-coordinates, no disorder, no errors, no polymers. For entries with identical

refcodes the highest sequential number was chosen. The exported data was analyzed with ChiChi, an algorithm for identifying chiral carbon atoms and thereby chiral molecules/ions. An overall list (List 1) was generated containing all the systems from CCDC that:

- Contains one chiral compound, with only one chiral carbon, and an achiral co-former;
- Are not salts, solvates or solid solutions;

Entries within List 1 were further divided into three sub-lists: systems with both enantiopure and racemic compound co-crystals reported (List 2.1), with only racemic compound co-crystals (List 2.2) and with only enantiopure co-crystals (List 2.3).

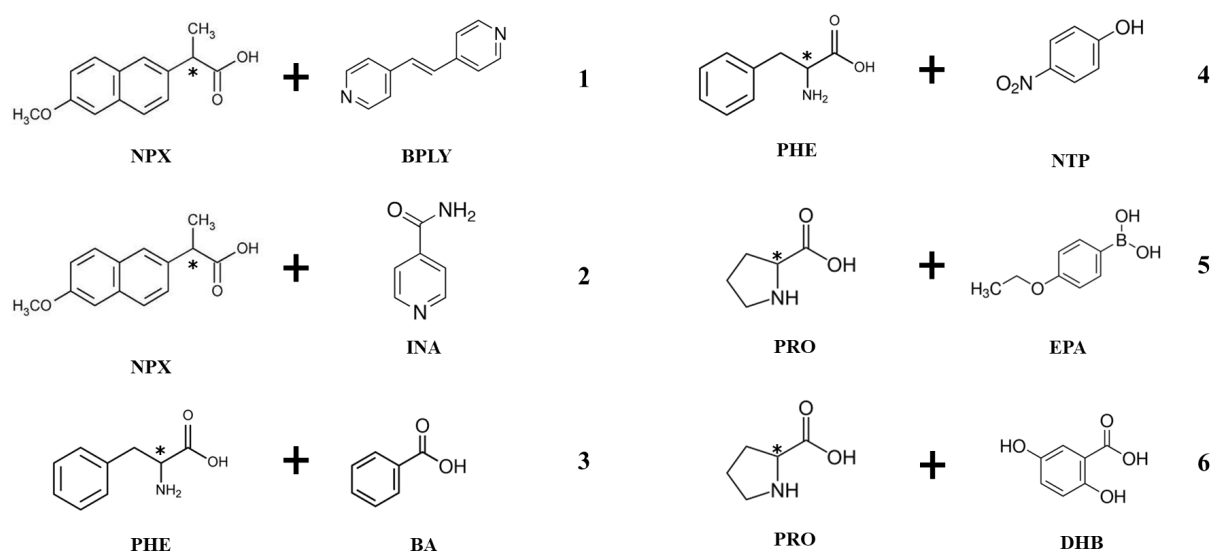


**Figure 1.** Molecular structures of racemic compounds and co-formers experimentally investigated in this study. The chiral carbons are indicated by asterisk.

**Materials.** 1,2-Di(4-pyridyl)ethylene (BPLY), L- and DL-Proline (PRO), L- and DL-Phenylalanine (PHE), Benzoic acid (BA), 4-ethoxyphenylboronic acid (EPA), 4-nitrophenol (NTP), 2,5-Dihydroxybenzoic acid (DHB), S-Naproxen (NPX), Isonicotinamide (INA), Ethanol (EtOH) and Methanol (MeOH) were purchased from Sigma Aldrich. RS-Naproxen was purchased from LKT Laboratories. All chemicals were used as received. The structures of combinations experimentally investigated are shown in Figure 1.

## 2.1 EXPERIMENTAL PROCEDURES

### **NPX + BPLY (system 1)**

80 mg NPX (either S- or RS-) was mixed with 32 mg BPE in 2 ml EtOH/MeOH (50/50 vol/vol). The mixture was held at 40°C for 2 hours and all solids were fully dissolved. The mixture was then slowly evaporated at room temperature. Crystals formed were collected and sent for analysis by X-ray Powder Diffraction (XRPD).

### **NPX + INA (system 2)**

107 mg RS-NPX and 110 mg INA were dissolved in 1 ml EtOH at 65°C. The solution was linearly cooled down to room temperature (0.3°C/min), in a Crystalline workstation (Technobis B.V. The Netherlands), for recrystallization. The solid phase was separated from the solution by filtration and analyzed by XRPD.

### **PHE + BA (system 3)**

6.75 mg PHE (either L- or DL-) was mixed with 5 mg BA and fully dissolved in 2 ml water at 80°C. The mixture was then linearly cooled down slowly (0.03°C/min), in a Crystalline workstation (Technobis B.V. The Netherlands) to room temperature after which the water was allowed to slowly evaporate in 2 weeks. The resulting crystals were collected and analysed by XRPD.

In a separate experiment, 40.8 mg DL-PHE and 30 mg BA were fully dissolved in 20 ml water at 80°C. The mixture was distributed in 20 plastic tube (0.3 ml each) for slow evaporation at room temperature in 2 weeks. Some good quality single crystals were formed in a number of tubes and subsequently collected for single crystal X-ray diffraction.

A single crystal was coated with high viscosity oil, mounted on a Mitagen Microloop and shock frozen to 208K using liquid nitrogen. Intensity data were collected at 208K. The measurement was performed on a Nonius Kappa CCD,  $\varphi$  and  $\omega$  scans, using monochromated Mo K  $\alpha$  radiation. The structure was solved using CRUNCH<sup>10</sup> and was refined with standard methods using SHELXL<sup>11</sup>. All non-hydrogen atoms were refined with anisotropic temperature factors. The positions of the hydrogen atoms could initially be determined using a difference Fourier map. Hydrogens were subsequently, if possible, replaced by hydrogens at calculated positions and refined riding on the parent atoms.

### **PHE + NTP (system 4)**

At 50°C, 30 mg DL-PHE was dissolved in 1 ml water and 25 mg NTP was dissolved in 2.2 ml MeOH. The two solutions were then mixed and linearly cooled down (0.03°C/min) to room temperature. The solution was slowly evaporated and the resulting crystals were collected for XRPD.

### **PRO + EPA (system 5)**

138 mg DL-PRO and 199.2 mg EXO were fully dissolved in 6 ml EtOH at room temperature. The solution was slowly evaporated at room temperature for 1 week and the crystals formed were analyzed by XRPD.

### **PRO + DHB (system 6)**

69 mg DL-PRO and 92.4 mg DHB were mixed in 6 ml MeOH and fully dissolved at room temperature. The solution was slowly evaporated and the resulting crystals were collected for XRPD.

**X-ray Powder Diffraction (XRPD) to Identify the Crystalline Phase Composition.** The analysis by XRPD was carried out using a Bruker D2 Phaser (Bruker AXS GmbH, Karlsruhe, Germany). Data collection was done using monochromatic Cu K  $\alpha$ 1 radiation ( $\lambda = 0.154060$  nm) in the  $2\theta$  region between  $8^\circ$  and  $50^\circ$ , with a  $2\theta$  step size of  $0.022^\circ$ . Data evaluation was done with the Bruker program EVA.

The XRPD measurement of NPX:INA co-crystals were performed using a Bruker D8 AXS Advance X-ray Diffractometer (Bruker AXS GmbH, Karlsruhe, Germany). The data was collected in reflection geometry using monochromatic Cu K  $\alpha$ 1 radiation ( $\lambda = 0.154060$  nm). The samples were scanned in a  $2\theta$  range from  $2^\circ$  to  $50^\circ$ , with  $0.01^\circ$  step size and a counting time of 10 s per step.

## **3. RESULTS**

**Data Screening.** From all organic entries in the CCDC, 757 co-crystal systems are identified, containing a chiral compound with a single chiral center and an achiral co-former. These systems, collected in List 1 (see the full list in the Appendix), are further divided into three sub-lists (see figure 2):

1. In List 2.1, systems with a pair of enantiopure and racemic co-crystal structures are reported (31). In this case the system can usually be classified as a racemic co-crystal system. List 2.1 contains 31 racemic co-crystal systems.

2. In List 2.2, systems with only a racemic co-crystal are reported. If only a racemic co-crystal is reported the enantiopure co-crystal does not exist or its structure has not yet been determined. In this case the system can also be classified as a racemic co-crystal system. List 2.2 contains 196 racemic co-crystal systems.

3. In List 2.3, systems with only an enantiopure co-crystal are reported. List 2.3 contains 530 co-crystal systems. If only an enantiopure co-crystal is reported this does not necessarily mean that the system are conglomerate co-crystal system, as the reported enantiopure co-crystal can be formed from an enantiopure rather than a racemic mixture. Moreover, many entries from CCDC lack the information whether the co-crystals reported are formed from the enantiomer or the racemic mixture. Such lack of information makes the automatic identification of a conglomerate co-crystal from List 2.3 difficult. In this case there are two opposite scenarios: a) the racemic compound co-crystal does exist but is not yet determined, which means that this system should be identified as a racemic co-crystal system. b) the racemic co-crystal does not exist. In case (b) the system should be identified as a conglomerate co-crystal system. The number of such systems in List 2.3 is given a

symbol of  $i$ , as at this moment the actual number is unclear from the database. Therefore, potential conglomerate co-crystals, if they exist, are included in this list 2.3. We thus have identified 530 chiral systems that potentially are conglomerate co-crystals.

To experimentally identify what systems in List 2.3 form conglomerate co-crystals is challenging, as it is difficult and tedious to find the right condition to form stable co-crystals from the racemic mixtures and the co-formers. In the next section, we provide a schematic demonstration of possible outcomes from an experimental screening of co-crystal systems from racemic compounds.

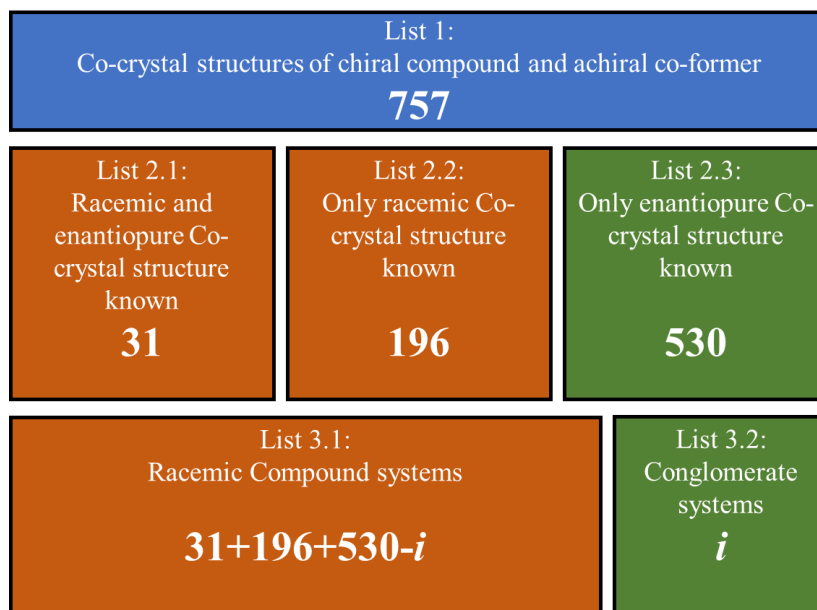


**Figure 2.** Schematic overview of co-crystal lists identified through an automated data screening in CCDC. List 1 contains all organic co-crystals from a chiral compound and an achiral co-former; Systems in List 1 is divided into three sub-lists: systems with both enantiopure and racemic compound co-crystals reported (List 2.1), with only racemic compound co-crystals reported (List 2.2) and with only enantiopure co-crystal co-crystals (List 2.3). All the systems are grouped into either racemic compound co-crystals List 3.1 or conglomerate co-crystals list 3.2. The symbol  $i$  is the number of conglomerate co-crystal systems in List 2.3, as the actual number is unclear from the information of the database.

**Possible outcomes from screening of co-crystals from chiral compounds.** At constant pressure and temperature, in order to describe a system containing solvent, the two enantiomers of the chiral compound and the co-former, a quaternary phase diagram. In such a phase diagram, to screen for a suitable condition to form co-crystals from a racemic mixture and a co-former, there are two degrees of freedom of the system: the molar fractions of the chiral compound and the co-former. It is difficult and tedious to determine the exact location in the phase diagram to screen for co-crystals of the chiral compounds of interest. From a particular screening condition, several possible outcomes can be expected from a co-crystal-forming system of a chiral compound. In Scheme 1 we demonstrate these

possible outcomes if the chiral compound is a racemic compound on a simplified isothermal 2D phase diagram.

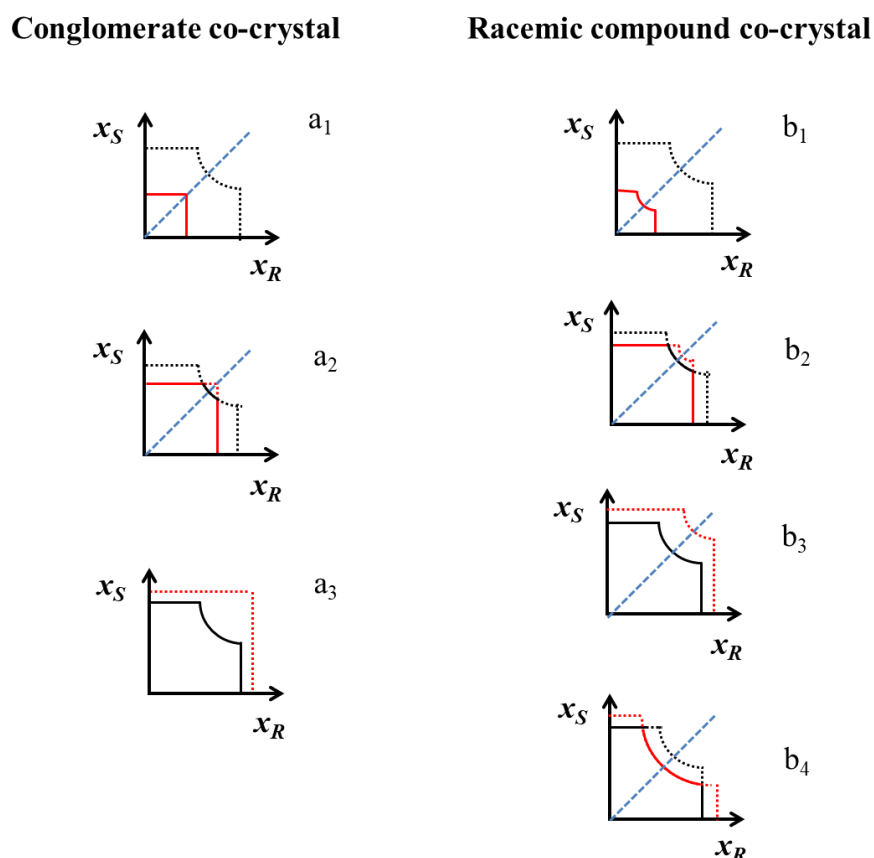
In the isothermal phase diagrams, the black lines show the solubility lines in a racemic compound system A in absence of co-former B: the horizontal and vertical lines represent the equilibrium solution composition in case of a liquid-solid equilibrium between the solution and pure S and R crystals, respectively. The curved line shows the equilibrium solution composition in case of a liquid-solid equilibrium between the solution and the racemic compound crystals. The intercept between the two straight lines and the curved line indicates the eutectic composition at which a three phase equilibrium exists between the solution, the racemic crystal and the enantiopure crystal R or S. The red lines show the solubility lines of the same system in the presence of a constant amount of B: the red solid lines indicate more stable solids and the red dashed lines indicate less stable solids than those in absence of B.

When an achiral co-former is used, the co-crystals formed are either conglomerates or racemic compounds, with the rare exception of solid solution. Phase diagrams  $a_1$ — $a_3$  show the phase behavior in case the system behaves as conglomerate co-crystals. The phase diagram  $a_1$  describes the situation in which the enantiopure co-crystals are more stable than the pure RS crystals. Therefore, the co-crystal solubilities (red solid lines) are lower than those of the enantiopure and racemic compound. If the screening takes place at this condition, the obtained co-crystals from the racemic mixture have the same XRPD patterns as those from the enantiopure mixture. In  $a_2$ , the RS crystals are still more stable than the enantiopure co-crystals in the region close to the racemic composition. Although the phase diagram in the presence of the co-former B (solid lines) is similar to the pure component phase diagram, the parts on the two sides of the eutectic points (solid red lines) show the solubilities of the enantiopure co-crystals. Normally, the enantiopure co-crystals need to be more stable in order to be formed at the racemic composition. In  $a_3$ , the co-crystals are less stable than the pure component crystals. Therefore, the phase diagram in the presence of the co-former B is the same as that without.

Phase diagrams  $b_1$ — $b_4$  describe the phase behaviors of racemic compound co-crystals RS:B. In  $b_1$ , both the racemic co-crystals RS:B and the enantiopure co-crystals R:B and S:B are more stable than the pure component crystals. The phase diagram (solid red lines) suggests the solubilities of the co-crystals. If the screening takes place at this condition, the recovered co-crystals from the eutectic composition have different XRPD patterns from those of enantiopure co-crystals. In  $b_2$ , the enantiopure co-crystals are more stable than the S or R crystals but the RS crystals are still more stable than the co-crystals in the region close to the racemic composition. Therefore, the parts of the phase diagram on the two sides of the eutectic points (solid red lines) show the solubilities of co-crystals R: or S:B while the region close to the middle indicates the RS crystals solubility. In  $b_3$ , the co-crystals are less stable than the pure component crystals and the phase diagram with the co-former B is the same as that without. In  $b_4$ , the RS:B co-crystals are more stable than the corresponding pure component crystals RS but the enantiopure R:B or S:B co-crystals are less stable than either R or S crystals. Therefore, the section

between the eutectic points represents the solubility of the RS:B co-crystals while the two sides indicate that of the enantiopure pure component crystals R and S.

In the experimental screening of systems in List 2.3, the possible outcomes are a<sub>1</sub>, a<sub>2</sub>, b<sub>1</sub> or b<sub>2</sub>, as the enantiopure co-crystals have already been identified. In the following section, we introduce a quick experimental screening method for systems in List 2.3, based on the reported condition for the corresponding enantiopure co-crystal formation.



**Scheme 1.** Schematic isothermal phase diagrams of a racemic compound RS system with or without co-former B in various concentrations below its pure component solubility. All black lines show the solubility lines for a racemic compound system in absence of co-former B: the horizontal and vertical lines represent the equilibrium solution composition in case of a liquid-solid equilibrium between the solution and pure S and R crystals, respectively. The curved line shows the equilibrium solution composition in case of a liquid-solid equilibrium between the solution and the racemic compound crystals. The intercept between the two straight line and curved line indicates the eutectic composition at which a three phase equilibrium exists between the solution, the racemic crystal and the enantiopure crystal R or S. All red lines show the solubility lines of the same systems in the presence of a certain concentration of B: the red solid lines indicate more stable solids and the red dashed lines indicate less stable solids than

those in absence of B. The blue dashed lines in all figures indicate the eutectic composition of the two enantiomers.

**Experimental Investigation.** From the articles reporting the crystal structures in the CCDC it was found that a large number of the systems in List 2.3 were prepared from enantiopure rather than racemic solutions. We assumed that these reported preparation procedures were a good starting point to determine whether or not the corresponding chemical systems form conglomerate co-crystals. Therefore, we selected 6 systems from List 2.3 of the common racemic compounds Naproxen, Phenylalanine and Proline, for experimental investigation. We used the reported experimental procedures to prepare co-crystals from the corresponding racemic mixtures and the achiral co-formers. The obtained co-crystals are analyzed by XRPD and the patterns are compared with those of the corresponding enantiopure co-crystals, either from CCDC or experimentally obtained. If the XRPD patterns of the two co-crystals are the same, we assume that the co-crystals are conglomerates. Otherwise, we assume the co-crystals are racemic compounds. The results of the systems tested are shown in the coming sections.

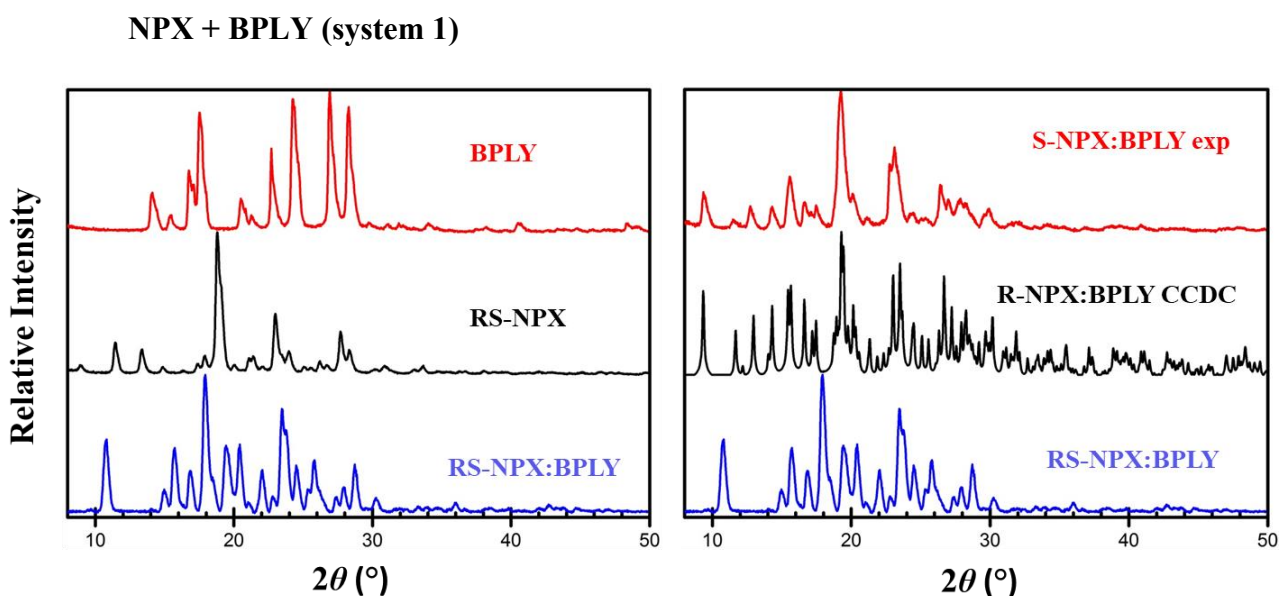


**Figure 3.** Left: Powder pattern of crystals from RS-NPX + BPLY mixture (blue), compared with those from BPLY (red) and RS-NPX (black), shows that co-crystals NPX:BPLY are formed. Right: Powder pattern of RS-NPX:BPLY co-crystals (blue), compared with those of enantiopure co-crystals from this study (red) and literature (black)<sup>12</sup>, shows that NPX+BPLY is not a conglomerate co-crystal system.

Following the reported enantiopure R-NPX:BPLY co-crystal preparation procedure for the racemic system using RS-NPX<sup>12</sup>, small crystals were formed after slowly evaporating the ethanol/methanol solution of RS-NPX+BPLY mixture. No suitable single crystal was formed for

structure analysis. However, the distinctly different powder pattern of the obtained crystals from those of BPLY and RS-NPX indicate that the crystals collected were co-crystals (Figure 3, left). Moreover, the powder pattern of the recovered crystals was compared with the enantiopure NPX:BPLY co-crystals (CCDC deposition 730422)<sup>12</sup>. Peaks from the collected crystals (e.g., at  $2\theta = 10.8^\circ$  and  $18.3^\circ$ ) were different from those of enantiopure co-crystal from this study and the reference. Therefore, it is concluded that a new co-crystal, most likely a racemic compound co-crystal (type  $b_1$  from Scheme 1), was formed between RS-NPX and BPLY.

### NPX + INA (system 2)

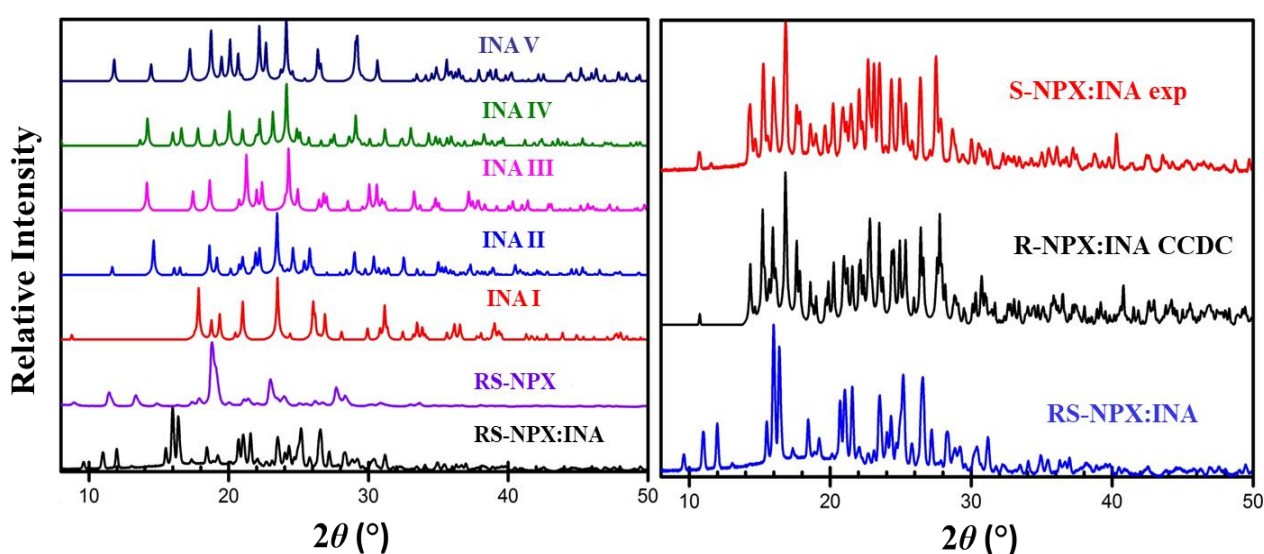


**Figure 4.** XRPD pattern of RS-NPX:INA co-crystals compared with RS-NPX and INA from CCDC (deposition form I: 199977, form II: 215254, form III: 794755, form IV: 844552 and form V: 844553) (left) and enantiopure co-crystal NPX:INA (right).

In literature, co-crystals R-NPX:INA are formed by mechanically grinding a 1:1 mixture of the two compounds in ethanol. In this study, crystals were formed by linearly cooling an EtOH solution of equimolar RS-NPX and INA from  $65^\circ\text{C}$  to room temperature, as automated mill was not available. The powder pattern of the collected crystals was compared with that of RS-NPX and the polymorphs of INA from CCDC. The comparison shows (Figure 4, left) that the crystals formed are co-crystals. Moreover, the comparison of the powder pattern of R-NPX:INA co-crystals (CCDC deposition: 815241)<sup>13</sup> and the collected co-crystals show several different peaks (see Figure 4, right), indicating that a new racemic compound co-crystal RS-NPX:INA (type  $b_1$  in Scheme 1) has been identified.

### PHE + BA (system 3)

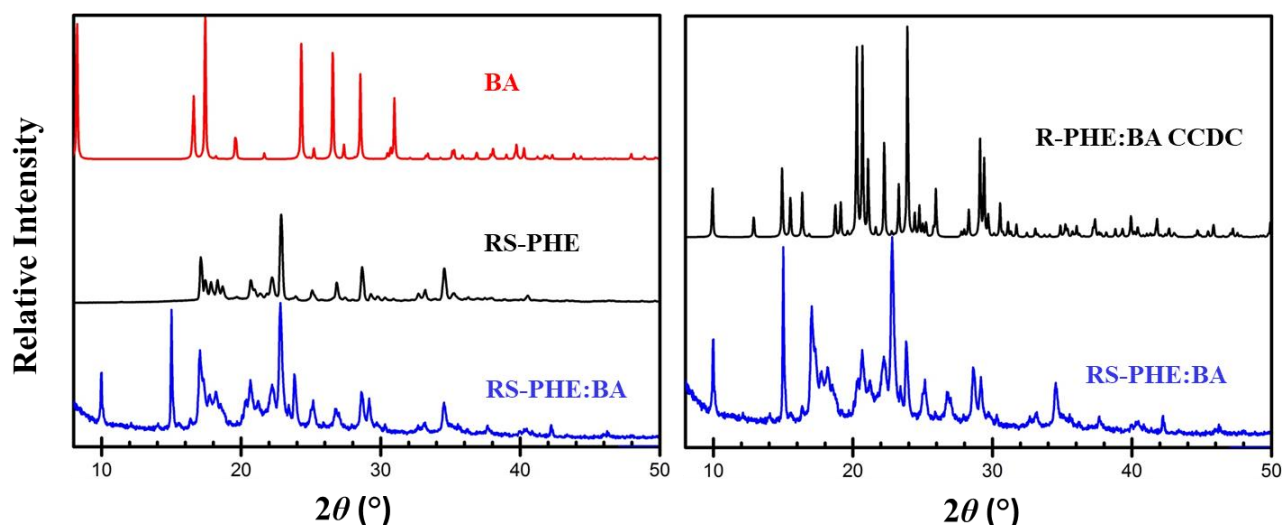


**Figure 5.** Left: Powder pattern of crystals from RS-PHE + BA mixture (blue), compared with those from BA (red) and RS-PHE (black), shows that co-crystals PHE:BA are formed. Right: Powder pattern of RS-PHE:BA co-crystals (blue), compared with those of enantiopure co-crystals R-PHE:BA from the literature (black)<sup>14</sup>.

After evaporating an aqueous solution of racemic PHE and BA, small crystals were collected from the bottom of the vial and analyzed by XRPD. In Figure 5, the powder pattern of the recovered crystals was compared with that of RS-PHE and BA. Additional peaks (e.g.,  $2\theta = 10^\circ$  and  $15^\circ$ ) can be seen. Also, peaks apparently corresponding to RS-PHE were found in the powder pattern of the collected crystals, indicating that they might be a physical mixture of co-crystals and the RS-PHE. The recovered co-crystals were then compared with the enantiopure PHE:BA co-crystals (CCDC deposition 289626)<sup>14</sup> which did not show a good match (see Figure 6, bottom for the unit cell structure).

Since the powder pattern is inconclusive in deciding whether it is a conglomerate or a racemic compound co-crystal, a single-crystal XRD analysis was performed on the collected transparent needle-like crystals. The structure of PHE:BA was refined to  $R1 = 0.0532$  for 3558 reflections with  $I_o > 2.0 \sigma(I_o)$ . Crystal data:  $C_{16}H_{17}NO_4$ , monoclinic, space group  $P2_1/c$  (#14),  $a = 5.390(2) \text{ \AA}$ ,  $b = 7.375(2) \text{ \AA}$ ,  $c = 35.235(7) \text{ \AA}$ ,  $\beta = 93.17(3)^\circ$ ,  $V = 1398.5(7) \text{ \AA}^3$  and  $Z = 4$ . (see structure in Figure 6, bottom). The structure of the enantiopure co-crystal R-PHE:BA, with space group  $P2_1$ , is similar to the racemic one<sup>14</sup> (see Figure 6, top). The stoichiometric ratio of PHE and BA is also 1:1 in the enantiopure co-crystal. A comparison between the structures of both racemic and enantiopure co-crystals show that the hydrogen bonds involved in both cases are similar: the PHE molecules are bonded between the amine group and the carboxyl group while the PHE and BA are interacted via both carboxyl groups.

The asymmetric unit contains one molecule of PHE and one molecule of BA, leading to a 1:1 ratio for PHE and BA. The positions of the hydrogen atoms could be determined independently using a difference Fourier map showing clearly that no hydrogen atoms are attached to the carboxylate group of the zwitterionic PHE molecule and that the BA molecule is present in its neutral form having a hydrogen attached to one of the oxygen atoms of the carboxylic acid group. Since no proton transfer has taken place in the complex of PHE and BA it is indeed a co-crystal and not a salt. An intermolecular hydrogen bond is formed between the hydroxyl group of the BA molecule and one of the oxygen atoms of the carboxylate group of the PHE molecule.

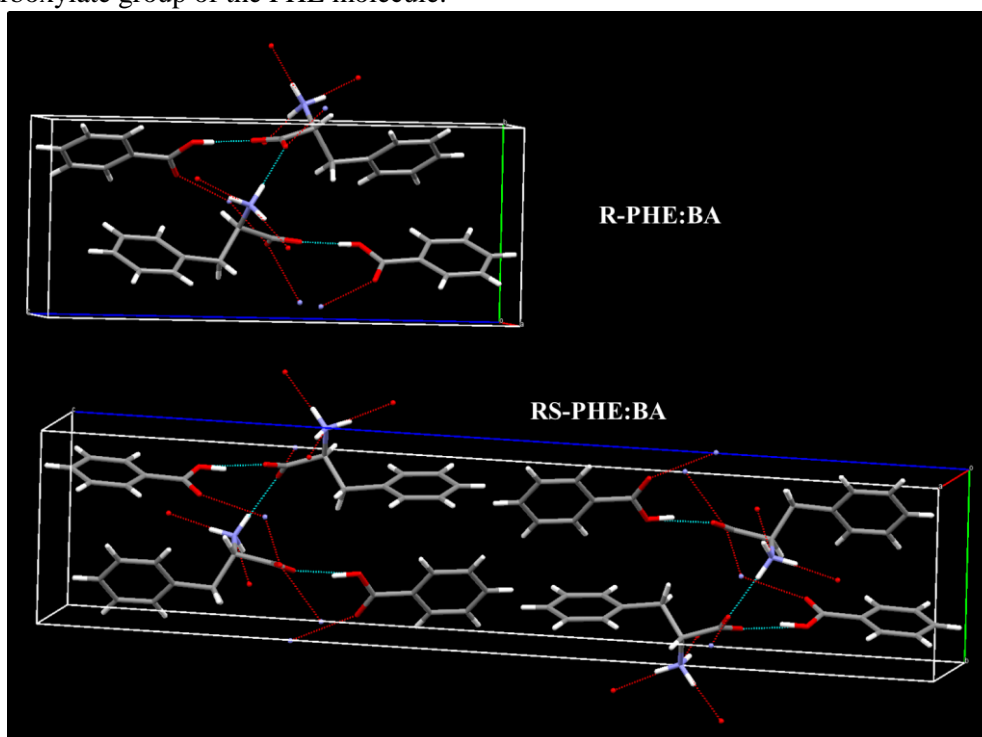


**Figure 6.** Molecular structure of one unit cell in co-crystal  $R\text{-PHE:BA}^{14}$  (top) and  $RS\text{-PHE:BA}$  (bottom) For easy vision, the hydrogen bonds with molecules outside the unit cells are represented only by red dash lines.

Since the space group  $P21/c$  is centrosymmetric, the crystal structure shows that we indeed have a racemic compound co-crystal of BA with racemic PHE. It is therefore concluded that the co-crystal system of  $RS\text{-PHE}$  and BA is racemic (type  $b_1$  in Scheme 1).

## PHE + NTP (system 4)

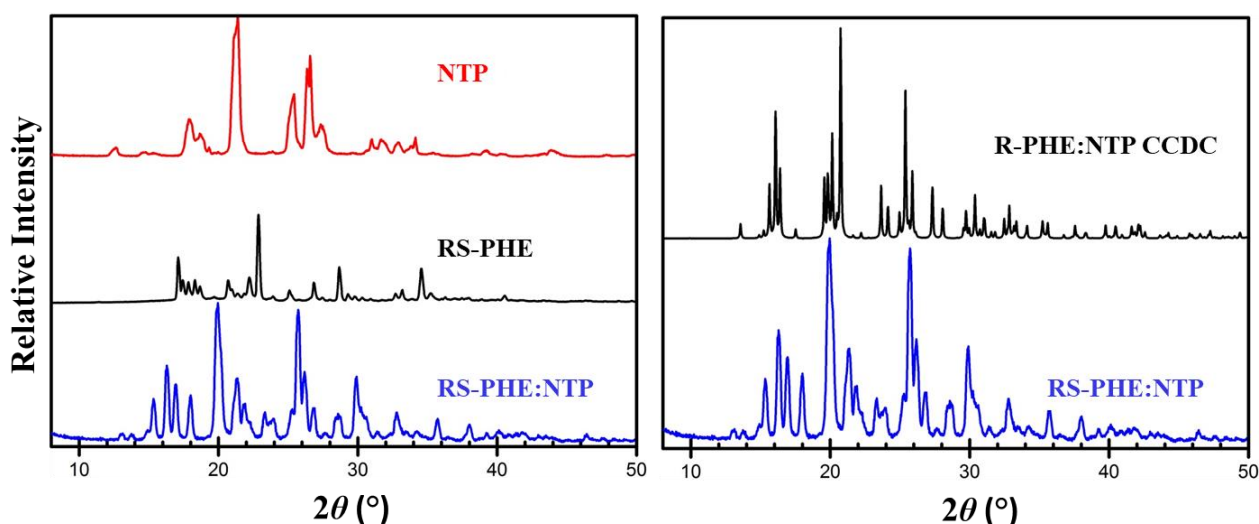


**Figure 7.** Left: Powder pattern of crystals from RS-PHE + NTP mixture (blue), compared with those from NTP (red) and RS-PHE (black), shows that co-crystals PHE:NTP are formed. Right: Powder pattern of RS-PHE:NTP co-crystals (blue), compared with those of enantiopure co-crystals R-PHE:NTP from the literature (black)<sup>15</sup>.

Using the reported preparation procedure of R-PHE:NTP co-crystals using the racemic RS-PHE and NTP, small crystals were collected from evaporated MeOH:Water (1:1 molar ratio) solution of racemic PHE and NTP. In Figure 7, the powder pattern of the newly made crystals shows that they were not the physical mixture of crystals RS-PHE and NTP. Moreover, the powder pattern was distinctly different (e.g., at  $2\theta = 18.5^\circ$  and  $13.3^\circ$ ) from that of the enantiopure PHE:NTP co-crystals (CCDC deposition: 632941). It is therefore highly likely that a new racemic compound co-crystal RS-PHE:NTP (type  $b_1$  in Scheme 1) was identified.

## PRO + EPA (system 5)

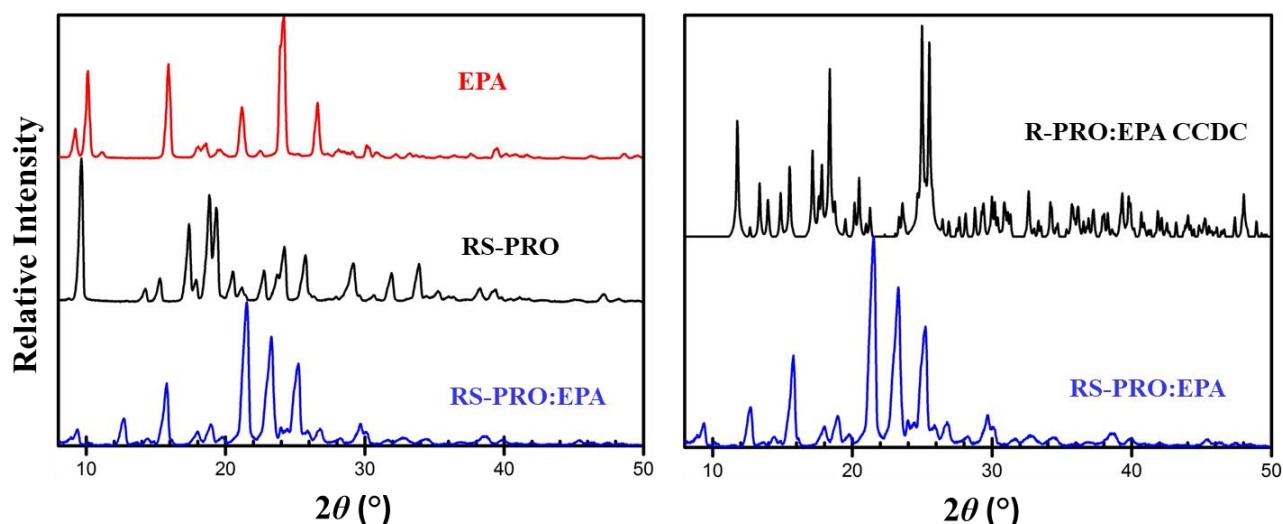


**Figure 8.** Left: Powder pattern of crystals from RS-PRO + EPA mixture (blue), compared with that from EPA (red) and RS-PRO (black), shows that co-crystals are formed. Right: Powder pattern of RS-PRO:EPA co-crystals (blue), compared with that of enantiopure co-crystals R-PRO:EPA from the literature (black)<sup>16</sup>.

Replacing RS-PRO with R-PRO in the reported preparation method for R-PRO:EPA co-crystals<sup>16</sup> resulted in small crystals. In Figure 8, the XRPD pattern of the collected crystals shows that they were not the physical mixture of crystals RS-PRO and EPA. Furthermore, several additional peaks were found in the powder pattern of another distinct crystalline material (e.g., at  $2\theta = 21.5^\circ$  and  $23.1^\circ$ ), when compared with that of the enantiopure PRO:EPA co-crystals (CCDC deposition 277519)<sup>16</sup>. Therefore, the newly identified RS-PRO:EPA co-crystal is racemic (type b<sub>1</sub> in Scheme 1).

## PRO + DHB (system 6)

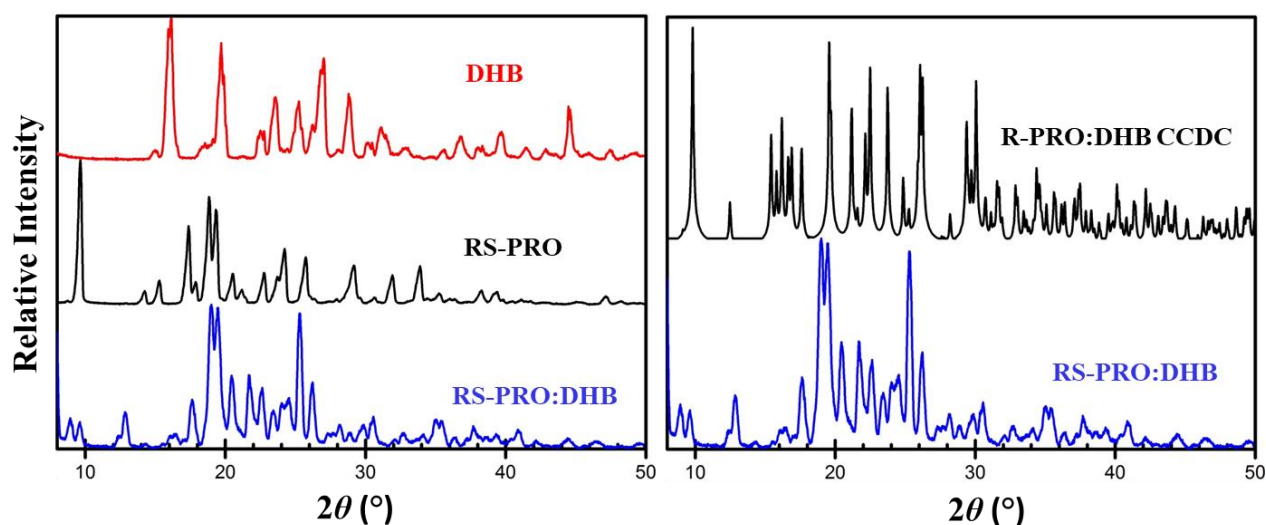


**Figure 9.** Left: Powder pattern of crystals from RS-PRO + DHB mixture (blue), compared with those from DHB (red) and RS-PRO (black), shows that co-crystals PRO:DHB are formed. Right: Powder pattern of RS-PRO:DHB co-crystals (blue), compared with those of enantiopure co-crystals R-PRO:DHB from the literature (black)<sup>17</sup>.

Crystals were formed by evaporating a MeOH solution of RS-PRO and DHB and collected for XRPD following the preparation procedure of R-PRO:DHB<sup>17</sup>. From a powder pattern comparison of the collected crystals and RS-PRO and DHB (see Figure 9, left), additional peaks (e.g.,  $2\theta = 12.3^\circ$ ) were found in the new crystals. Compared with the enantiopure co-crystal R-PRO:DHB (CCDC deposition: 1311858) in Figure 9 (right), the powder pattern of the new crystals was also different at several  $2\theta$ , for instance at  $8.1^\circ$ . It was concluded that the PRO:DHB co-crystal is very likely to be a racemic compound (type  $b_1$  in Scheme 1)<sup>17</sup>.

## 4. DISCUSSION

In this study, from the list generated from CCDC, no confirmed conglomerate co-crystals have been identified using our criteria. However, this does not mean that there are no conglomerate co-crystals found. A conglomerate co-crystal system from Ibuprofen (IBU) and trans-1-(2-pyridyl)-2-(4-pyridyl)-ethylene (BPE) has not been included in the CCDC but reported in literature<sup>18</sup>. The authors identified a monoclinic co-crystal of P21 space group from a racemic mixture of IBU and BPE.

Moreover, even within the list generated in this study, there is a special case which might be a conglomerate co-crystal system. In List 2.1, the system Naproxen (NPX) and Nicotinamide (NA) form both racemic compound and conglomerate co-crystals from the racemic mixture and the co-former<sup>19</sup>. As the racemic compound co-crystal of NPX and NA is known here, our data screening identifies this

system as racemic compound. However, it is unclear which co-crystal is more stable one. Therefore, the NPX-NA system is assumed to be a conglomerate co-crystal system in the following preliminary analysis.

Probability theory<sup>20</sup> enables us to determine the probability  $P(i)$  of the random variable  $j$ , the particular number of co-crystal conglomerates in a list of chiral co-crystals. We can describe  $P(j)$  as a binomial distribution if we assume that: 1. each co-crystallizing system has only two possible outcomes: conglomerate or not conglomerate; 2. the co-crystal conglomerate probability  $p$  is constant and equal for all chiral compound – co-former combinations; and 3. the experiments are independent. If  $p=0.1$  is the probability that a co-crystal conglomerate is formed, the probability  $q$  that no conglomerate is formed is  $q=1 - p$ . For  $N$  identical samples with identical co-crystal conglomerate probability  $p$  the discrete probability distribution  $P(j)$  that  $j$  samples have crystallized as co-crystal conglomerate is:

$$P(j) = \frac{N!}{j! (N - j)!} * p^j q^{N-j} \quad \text{Equation 1.}$$

where the exclamation mark indicates the faculty operator.

The null hypothesis  $H_0$  to be tested is  $p = 0.1$ . The alternative hypothesis  $H_1$  is then  $p < 0.1$ . If we find  $j$  conglomerate systems in a total of  $N$  systems, and the probability of that, assuming  $p=0.1$  (the 10% rule is valid), is less than 5%, we reject the null hypothesis (the 10% rule is not valid). For  $N$  samples this effectively means we need to find a minimum number  $j_{\min}$  in a sample size of  $N$  for the 10% rule to be valid. The value  $j_{\min}$  is the smallest  $j$  for which  $P(x \leq j) = \sum_0^j P(x) > 0.05$  and 0.05 is the significant level of 5% set in this study. The number of independent systems  $N$  is the sum of system numbers in List 2.1 (31) and List 2.2 (196) (see Figure 2), plus the 6 new co-crystals discovered in this study. Additionally, the conglomerate co-crystal system IBU-BPE, which is not recorded in the CCDC, is included in this analysis as well which consequently brings  $N$  to 234.

For the value of  $N = 234$ , the minimum value  $j_{\min}$  for which the 10% rule holds is determined to be  $j_{\min} = 16$ . Including the systems of IBU-BPE and NPX-NA (from List 2.1) the actual number of conglomerate co-crystals  $j$  is 2. This number  $j = 2 < j_{\min}$  is substantially smaller than the minimum number  $j_{\min}$  for which the 10% rule would hold. The calculated  $P(x \leq 2)$  is  $7.1 \cdot 10^{-9}$ , which is much smaller than the preset significance threshold 0.05. Therefore, we have to reject our null hypothesis: it is highly unlikely that 10% of the co-crystals from chiral compounds are conglomerate systems.

Our preliminary analysis contains several assumptions, which can be biased to some extent. First of all, it is assumed that any system which has a confirmed racemic compound co-crystal reported is not a conglomerate co-crystal system. The existence of NPX-NA system shows that this assumption has exceptions. Moreover, it is significantly more difficult to identify a conglomerate co-crystal system using our data screening method, as enantiopure co-crystals need to be reported from both the enantiomer and the racemic mixtures. These information is usually missing from CCDC and, therefore,

we leave out the entire List 2.3 from the analysis, as we are not sure which systems within are conglomerates. These are the improvements both CCDC and our method can make in the future investigation.

The main discovery from this study is that the 10% rule is probably not valid for co-crystals from chiral compounds. However, this statement can be reversed if more conglomerate co-crystals are found from the list of potential conglomerate systems (List 2.3). Except for the 6 systems experimentally determined as racemic compound co-crystals in this study, two extreme scenarios exist from List 2.3: all are either racemic compound co-crystals or conglomerate co-crystals. In the first scenario, the total number of conglomerate co-crystal systems remain as 2 but the total co-crystal systems determined now include the whole List 2.3. Therefore,  $N$  in Equation 1 is now 758 instead 234. In this case, the likelihood that the 10% rule is valid here is even lower:  $7.51 \cdot 10^{-32}$ . In the second scenario where all are conglomerate co-crystals, unlikely as no conglomerate co-crystals have been found from our experimental investigation, the number of confirmed conglomerate co-crystals is  $2 + 524$  (the number of systems untested in List 2.3) = 526. In this scenario, the null hypothesis ( $p = 0.1$ ) is rejected if  $P(x \geq 526) = 1 - P(x \leq 526 - 1) \leq 0.05$ . The total systems confirmed  $N$  is 758 and the likelihood that the 10% rule is valid ( $P(x \geq 526)$ ) is now infinitely close to 0, meaning this rule is also not valid.

Furthermore, in order to validate the null hypothesis that  $p = 0.1$ , the number of confirmed conglomerate co-crystals from list 2.3 need to be in a certain range. If the lower and higher limits of this range are  $x_L$  and  $x_H$ , respectively, they fulfill the conditions that:

$$P(x \leq x_L + 2) \geq 0.05 \quad \text{Equation 2}$$

$$P(x \geq x_H + 2) \geq 0.05 \quad \text{Equation 3}$$

Here both  $x_L$  and  $x_H$  are summed with 2, as the total conglomerate co-crystals are the two confirmed systems in this study (NPX-NA and IBU-BPE) plus the number of systems found from List 2.3.

Using Equation 2 and 3, the lower and higher limits of numbers of conglomerate co-crystals are calculated to be 61 ( $x_L$ ) and 87 ( $x_H$ ). Therefore, when all the systems in List 2.3 are screened, if between 61—87 of them are confirmed as conglomerate co-crystals, it is probable that the 10% rule is valid for co-crystals from chiral molecules.

From the analysis results, it can be clearly seen that we need further confirmation in order to either reject or accept the 10% rule. A highly potential route towards this is to investigate the list 2.3 of potential conglomerate systems and either confirm or reject conglomerate formation for all these systems. Furthermore, such investigation can start with the reported conditions of enantiopure co-crystal formation of each entry in the list. In our experimental investigation, new racemic compound co-crystals (type  $b_1$  in Scheme 1) have been identified in all tested systems under the same or similar conditions where enantiopure co-crystals are formed from one of the enantiomer and the co-former. Our results

strongly indicate that these conditions are also suitable to form stable co-crystals from the corresponding racemic mixtures and co-formers.

When the identities of all the systems from List 2.3 are determined, i.e. all the systems are either confirmed or rejected conglomerate formation. The overall List 1 is complete, which can be then used for the study of co-crystal formation from chiral compounds. The crystal structures from the pure chiral compounds and their corresponding co-crystals from List 1 can be compared to investigate the scientific principle behind the racemic compound and conglomerate co-crystal formation.

## 5. CONCLUSIONS

Our statistical study, based on an automated data screening in the CCDC, shows that it is very unlikely 10% co-crystals from chiral compounds are conglomerates, which is the fraction of pure component conglomerates in all the reported chiral compounds. Moreover, our experimental investigation suggests that the reported procedures for enantiopure co-crystal formation between an enantiomer and a co-former can be used as the starting conditions for the co-crystallization between the corresponding racemic mixtures and the co-formers, thus facilitating the screening for conglomerate co-crystals. Our results identify a technical challenge in converting racemic compounds, the most common chiral compounds, into conglomerate co-crystals, while providing a list of potential conglomerate co-crystals, which also contains good starting points for the fast screening of them.

## REFERENCES

1. Nguyen, L. A.; He, H.; Pham-Huy, C., Chiral Drugs: An Overview. *International Journal of Biomedical Science : IJBS* **2006**, *2* (2), 85-100.
2. Srisanga, S.; ter Horst, J. H., Racemic Compound, Conglomerate, or Solid Solution: Phase Diagram Screening of Chiral Compounds. *Crystal Growth & Design* **2010**, *10* (4), 1808-1812.
3. Gal, J., The discovery of biological enantioselectivity: Louis Pasteur and the fermentation of tartaric acid, 1857—A review and analysis 150 yr later. *Chirality* **2008**, *20* (1), 5-19.
4. Jacques, J.; Collet, A.; Wilen, S. H., *Enantiomers, racemates, and resolutions*. Krieger Pub. Co.: 1994.
5. Spix, L.; Meekes, H.; Blaauw, R. H.; van Enkevort, W. J. P.; Vlieg, E., Complete Deracemization of Proteinogenic Glutamic Acid Using Viedma Ripening on a Metastable Conglomerate. *Crystal Growth & Design* **2012**, *12* (11), 5796-5799.
6. Spix, L.; Alfring, A.; Meekes, H.; van Enkevort, W. J. P.; Vlieg, E., Formation of a Salt Enables Complete Deracemization of a Racemic Compound through Viedma Ripening. *Crystal Growth & Design* **2014**, *14* (4), 1744-1748.
7. Li, W. W.; Spix, L.; de Reus, S. C. A.; Meekes, H.; Kramer, H. J. M.; Vlieg, E.; ter Horst, J. H., Deracemization of a Racemic Compound via Its Conglomerate-Forming Salt Using Temperature Cycling. *Crystal Growth & Design* **2016**, *16* (9), 5563-5570.
8. Grothe, E.; Meekes, H.; Vlieg, E.; ter Horst, J. H.; de Gelder, R., Solvates, Salts, and Cocrystals: A Proposal for a Feasible Classification System. *Crystal Growth & Design* **2016**, *16* (6), 3237-3243.

9. Grothe, E.; Meekes, H.; de Gelder, R., Searching for stereoisomerism in crystallographic databases: algorithm, analysis and chiral curiosities. *Acta Crystallographica Section B* **2017**, *73* (3), 453-465.
10. de Gelder, R.; de Graaff, R. A. G.; Schenk, H., Automatic determination of crystal structures using Karle-Hauptman matrices. *Acta Crystallographica Section A* **1993**, *49* (2), 287-293.
11. Sheldrick, G., SHELXT - Integrated space-group and crystal-structure determination. *Acta Crystallographica Section A* **2015**, *71* (1), 3-8.
12. Weyna, D. R.; Shattock, T.; Vishweshwar, P.; Zaworotko, M. J., Synthesis and Structural Characterization of Cocrystals and Pharmaceutical Cocrystals: Mechanochemistry vs Slow Evaporation from Solution. *Crystal Growth & Design* **2009**, *9* (2), 1106-1123.
13. E. Castro, R. A.; Ribeiro, J. D. B.; Maria, T. M. R.; Ramos Silva, M.; Yuste-Vivas, C.; Canotilho, J.; Eusébio, M. E. S., Naproxen Cocrystals with Pyridinecarboxamide Isomers. *Crystal Growth & Design* **2011**, *11* (12), 5396-5404.
14. Suresh, J.; Krishnakumar, R. V.; Natarajan, S., l-Phenylalanine-benzoic acid (1/1). *Acta Crystallographica Section E* **2005**, *61* (11), o3625-o3627.
15. Prakash, M.; Lydia Caroline, M.; Geetha, D., Growth, structural, spectral, optical, and thermal studies on amino acid based new NLO single crystal: l-phenylalanine-4-nitrophenol. *Spectrochimica Acta Part A: Molecular and Biomolecular Spectroscopy* **2013**, *108* (Supplement C), 32-37.
16. Rogowska, P.; Cyrański, M. K.; Sporzyński, A.; Ciesielski, A., Evidence for strong heterodimeric interactions of phenylboronic acids with amino acids. *Tetrahedron Letters* **2006**, *47* (9), 1389-1393.
17. Aakeroy, C. B.; Bahra, G. S.; Brown, C. R.; Hitchcock, P. B.; Patell, Y.; Seddon, K. R., L-Proline 2,-Dihydroxybenzoic acid (1/1): A Zwitterion Co-crystal. *Acta Chemica Scandinavica* **1995**, *49*.
18. Elacqua, E. Supramolecular chemistry of molecular concepts:tautomers, chirality, protecting groups, trisubstituted olefins, cyclophanes, and their impact on the organic solid state. University of Iowa, 2012.
19. Neurohr, C.; Marchivie, M.; Lecomte, S.; Cartigny, Y.; Couvrat, N.; Sanselme, M.; Subra-Paternault, P., Naproxen–Nicotinamide Cocrystals: Racemic and Conglomerate Structures Generated by CO<sub>2</sub> Antisolvent Crystallization. *Crystal Growth & Design* **2015**, *15* (9), 4616-4626.
20. Skellam, J. G., A Probability Distribution Derived from the Binomial Distribution by Regarding the Probability of Success as Variable Between the Sets of Trials. *Journal of the Royal Statistical Society. Series B (Methodological)* **1948**, *10* (2), 257-261.

# Appendix Chapter 2

## Table of Contents

1. List 2.1 Systems for which both enantiopure and racemate crystals exist in the CCDC (1)
2. List 2.2. Refcodes of systems for which only a racemate crystal is known (2)
3. List 2.3 Refcodes of systems for which only an enantiopure crystal is known (3)

## Co-crystal systems containing one chiral compound, with one chiral centre, and one achiral co-former.

### 2.1. Systems for which both enantiopure and racemate crystals exist in the CCDC

Refcodes in our dataset, per system			COMMENT
ANOLIZ	ANOLUL	ANOLOF	ANOLOF different stoichiometry
CIZTAH	CODCOO		
GERWEF10	GERWIJ10		
HAGYEU	VIKLUX		
HUPPAJ	IJJAN		
NUJCEC	NUJCAY		
ROLFUU	RONDEE	RONDII	
RUWHEX	RUWHIB		
SADDUW	SEWWIA		
SADFEI	SEWWUM		
SODDIZ01	SOGLAC		
UHACIQ	UHAFEP		
UYOTAE	UYOTEI		
UYOTIM	UYOTOS		
UYOTUY	UYOVAG		
VAWLEK	VAWLAG		
VIKLOR	OJEPEY		
XOGMIR	XOGMOX		
XOGMUD	YASGAC01		
XOGNEO	XOGNIS		
XOGNOY	XOGNUE		
ZEBXUB	ZEBXOV		
	JULJEH		see enantiopure HEGGAD*
RONDAA			see racemate ROLFOO*
SEWWOG			see racemate SADFAE*
TOBMAA			see racemate TOBLUT*
TOBMII			see racemate TOBMEE*
UYOSUX			see racemate UYOVEK*
XOZSOV			see racemate RUCFIF*
ZEBXEL			see racemate ZEBXIP*
ZIZZAL			see racemate ZIZZEP*

## 2.2. Refcodes of systems for which only a racemate crystal is known

ACESAE	EQUMOU	JAFHUT	OQEDIZ	TEVLOW	EQOPUV
ACETEJ	EVACAH	JAWVIN	OVUFUH	TILLUX	
ANOLOF	EVAMIX	JESCAL	OWIGEH	UHOXAR	
AVIWEH01	EYASUT	JOJGUK	PEHGIT	UHOXEV	
AWABUW	FAKQUF01	JOJVAF	PESHIG	UMIBEY	
BADCOY10	FAKRAM	JUCYAH	QACPAM	UWEMUG	
BICMUX	FANJAG	JURGIM	QAKRIF	VEKKIF	
BIJFUW	FAYPOL	KIHZIL	QUGWAQ	VISBOP	
BIJGAD	FEGPOW	KIHZOR	QUKJIP	VIXHEQ	
BIJYEY	FEKQOC	KOWJOV	QUWWAI	WARQAI	
BIRQUO	FEVQAZ	LATRAB	RAFZEF	WEDLUN	
BOLSOK	FIHSUL	LERVEK	RAWXOC	WEXCIM	
BOWCIB01	FIKHAJ	LITSOX	REDJAM	WOBPIN	
BRCPDG	FOFZEH01	LODKUM	REGCIR	WUNNUP	
BUMGUL	FOFZIL	LODLIB	REPCOF	WUSTEL	
CENHEI	FOGBOT	LOFHAQ	RIHDIV	XACXEH	
COBBAW	FONXEN	LOGBUG	ROKQIR	XAWFIK	
CONYAF10	FUHRAC	LUDCES	RUMFOV	XISDEK	
COSZOB	GACZEQ	LUDCOC	RUXYOZ	XOBGIF	
CRQZMC	GEGTUJ	LUNPAL	SACJOW	XOBHEC	
CUBBEH	GEPTIG	LUSXAA	SADHAI	XODPIR	
DANLAG	GIRBOY	LUSXUU	SEFXAC	XODPOX	
DEPOAM01	HAZVIO	MILSOP	SIDVOS	XOWVEK	
DILSOI	HEPMIY	MOKQUZ	SIQLOU	XUGGIQ	
DIMSUP	HIBGII	NEBFUV	SOWDEP	XUTWUG	
DIRVAD	HIBHEF	NIWKIN	SOXVEH	YACXIJ	
DOMHAQ	HIVHIE	NIZQES	SOYFIV	YAFJUK	
DOMHEU	HOTZEW	NOLJUT	SUFFOO10	YASKEJ	
DOSJIE	HOZPOD	NUHBAV	SUFFUU10	YEBJEW	
DOSKAX	HUKPIM	ODEJIR	SUMMOE	YEFNAA	
DOWTAL	HUVGAI	ODOSIJ	SUZNUY	YEFNOO	
DOWTAM	ICOGOW	ODOSUV	TABYAW	YINWAV	
DOXDUR	IFUYUD	OFOKEA	TAGXEH	YINWID	
DOXFAZ	IQAMAP	OHAXEA	TANCAO	YISZUV	
DOXFED	IQOMIM20	OJIDIV	TARWAL	YOJBAC	
EMONAW	ISUNAN	OJIDOB	TAWSOB	YORJOF	
EMUKEE	IVUJUE	OJUNEO	TELBUJ	YUHTAY	
EMUKII	IWOLIQ	OKEGOC	TELCAQ01	JACZAO	
EQOPAB	IZAXIQ	ONODAY02	TELDIZ	ZUFQAU	

### 2.3. Refcodes of systems for which only an enantiopure crystal is known

ADOSBU01	AVES0J	BIHJEJ	BUPDEV	CAMPIP
ADOXAS	AVIPEA	BOBPEN	BUYSET10	CAQPAL
ADRBFT10	BCYTGA	BOBQUG	CABTEG	CATGAG
ANDTRD	BEFHOJ	BOBRAN	CABTIK	CATGIP
ANIREV	BEHKAB	BOHWUQ	CABTOQ	CATGOV
ANIROF	BEVJUJ	BOLVUT	CABTUW	CATGUB
ANOPUP	BEYLOG	BONKIZ	CABVAE	CAXBAF
APUTIP01	BEYPEA	BUDKEQ	CACQED	CDEXTI10
CEWYOT	EVODIC	GUJHOJ	JILZOU01	MUYVAE
CIGLAG	EVUZOK	GUJHUP	JOKLEC	NAJCIM
CIJVEY	EWACAG01	GUNKUV	JOKPII	NAJJAK
CIWHUM	EYUJEO	GUNLAC	JOQHEC	NASDUG
CIYLUT	EYULUG	GUNLEG	JOQHIG	NASFAO
COHZII	EZAVOQ	GUNLIK	JUGZOA	NAYKED
COWTAK	FAFGOI	GUNMIL	JUMYOF	NECPUG
COYTOZ	FALRAM	GUNMOR	JUMYUL	NEHPIZ01
COZyas	FALROA	GUNMUX	JUPVIZ	NIFXIJ
CUSYOF	FAZBOY	GUNNAE	JUPVOF	NIHGOB
CUSYUL	FAZBUE	GUNNEI	KABNAC	NIHMOH01
CUSZAS	FAZCAL	GUNNIM	KABNEG	NIHNIC
CUSZEW	FEFPUC	GUNNOS	KABNIK	NILQUV
CUSZIA	FEFQAJ	GUNNUY	KAFFUS10	NISVOA01
CUSZOG	FEHPAK	GUNPOU	KECJIM	NODVOT
CUSZUM	FEHPEO	GUNPUA	KEQBUF	NOGPAC
CUTBAV	FEMMAM	HADKAZ	KERSAB	NOTKIQ
CUTBEZ	FEMMEQ	HAHVES	KICTEV10	NOTQUK
CUTBID	FICCUR	HAHVIW	KITMOR	NOTSEU
CUTBOJ	FICDAY	HAKWOF	KIXVES	NOTSIY
DABFIV	FINTAZ03	HAMHOS	KONVEO	NUKBEA
DABQOM	FINTIH	HOGGOB	KOXPIW	NUKGAB
DAMFUS	FOGWIH	HOPHAX	KUDZUE	NUKGEF
DANFUT	FUMKAB	HORNAE	KULMOU	NUTPOJ
DASZIH	FUMKIJ	HORNEI	LABJIH	NUWKEX
DCANBD	FUVZUS	HOTEST10	LAQXIM	NUYBOY01
DEBTIN	GELKEN10	HOVFIJ	LASZUC	OKIRAB
DETPOI	GEPROI	HOVFOP01	LATBAL	OKOZAQ
DEWCOY	GEYYUE	HUCVOQ	LATBEP	OKOZEU
DEXQIG	GEYZAL	HUPWAR	LEJM0E	OKOZIY
DICVUH	GIHBOQ	HURNUD	LIMREE	OMIFUL

DIFFOO	GIHBUE	HURPEP	LOCQIF	OWEHII
DITSEE	GIHCAD	HUSWIB	LOWHUA	OZIDIL
DITSOO	GIHCEH	HUZVUT	LOXCOS	PALCIP
DITSUU	GIHCIL	IBALAZ	LOXHAI01	PAMQAX
DOKCAJ	GIKZAB	IBILAG	LOXHR	PASHEX
DOPPIH	GIMKES	IBOWAX	LUMFIK	PAVPUX
DUXSAR	GIMKIW	IDEBOJ	MAPHES	PAXNOR
EBIBEW	GIPQOL	IFALOQ	MEGXIF	PAZYIA
EJEPOA	GIPQUR	IHAWOD	MEGXOL	PAZYOG
EJEPUG	GLUCUR20	IHUMAZ	MEGYAY	PAZYUM
EJEQAN	GOJHAQ	IMENIX	MEGYEC	PAZZAT
EJEQER	GOVQAJ	IRACAH	MEWFUP	PEGNUK
EJEQIV	GOVQOX	ISOJAB	MIRHIF	PEHQIC
EJEQOB	GOVRAK	ITYRMA10	MOXXAZ	PEHYOR
EJEQUH	GOYHEH	IYAXIQ	MPPYRL	PEHYUX
EJERES	GUCSAY	JAQHIT	MULREQ	PEHZAE
ERAUAU	GUHTOS	JAXZIS	MUPNEQ01	PEHZIM
ERIKUL	GUHTOT	JEFRER	MUXHIX	PEHZOS
ESOURE11	GUHTUZ	JENTOL01	MUYTEG	PEJBAI
PEJBEM	QOVYOP	TALCOA	VIZPAW	WUSFOG
PEJBIQ	QOVYUV	TALCUG	VIZPEA	WUWREM
PEJBOW	QOVZIK	TANCOC	VIZPIE	WUWRIQ
PEMRIJ	QOXMAS	TANCUI	VIZPUQ	XASDIE
PEMZAI02	QQQDFA01	TANDET	VIZQAX	XEJQIM
PEPQIL	QUJNAM	TAZQAM	VIZQEB	XEJQOS
PEQKIH	QUSREC01	TEMWOX	VIZQIF	XEMCIB
PIGPAX	RABJUV	TEPCEY	VIZQOL	XETLEO
PIGQAY	RABKAC	TESBRP	VIZQUR	XETLIS
PINNAD	RABKEG	TIJTIQ	VIZROM	XICSAF
PIWKIP	RAVVUF	TIRMUE	VIZED	XIDBAO
PIWKUB	RAXKIL	TUBVOB	VOCTEN	XIMFII
PIWLEM02	REGKUK	TUGJOW	VOCTIR	XOGYEY
POGWUE	RELCUH	TUHWAW	VOCTUD	XUWFIG
POHDAR	RERNUZ	TUWWEO	VOCVAL	YARXAS
POKHAY10	RESBIB	TUXBUK	VOCVIT	YAZTIC01
POPJOT	REWBIE	UBIXUA	VONPET	YERBOM
POQSUK	RIGPED	UBIYAH	VOPCOU	YETMUF
POSMUF	RIKKUR	UBIYEL	VOPCUA	YIFLAB
POWMET	ROKNAH*	UBIYIP	VOQKOB	YIHJUJ
POZPUP	RUCDUP	UBIYOV	VOQKUH	YIQBUX

POZQAW	RUFYIC	UBIYUB	VOQLAO	YOCZUL
PRORES	RUFYOI	UBODIA	VOQLES	YODYAR
PUWREE	RUGYEZ	UCEXAB	VOQLIW	YOFWIA
PUWROO	RUGYID	UCEXIJ	VOTBEL	YONDAH
QAHPAQ	RUPFOY	UCEXUV	VOYNUS	YONVAY
QAYVES	RUWDUJ	UDIGET	VUYGUT	YOTSIJ
QAYVIW	RUWFAR01	ULUFIS	WACBEK	YUJDAI
QAYWET	RUWFEV	ULUZIM	WALNED	YUNYOV01
QAYWIX	SABJEK	ULUZOS	WALNIH	YUNZAI
QAYXUK	SAGKIV	UMABAL	WALNON	YUQQOS
QAYYIZ	SALCYS	UMABAN	WALNUT	YUYFON
QAYYUL	SAMWOT	UNEJUJ	WEFGIZ	YUYFUT
QAYZAS	SAMWUZ	UPULEX	WIBSEH	YUYFUU
QAYZIA	SAMXAG	UPUWEI	WILTOB	YUYWUK
QAZGEE	SAPLAW	VADGOW	WIRXEA	ZEDJOH
QAZGII	SEPKON	VAKQIK	WOHLOU	ZEDJUN
QAZGUU	SEPVEP	VECLIY	WOMGOV	ZESTIA
QAZHIJ	SEQRAJ	VEFZEM	WOMGUB	ZEZHIV
QAZYEV	SIBSIG	VEQTES	WOMHAI	ZIPZIH
QENTOT	SITCUU	VEQTIW	WOTZAG01	ZIZYUE
QERDEW	SUKGUC	VIMLOU	WOTZEK	ZUWQEN
QERDIA	SURLAS	VIMMEL	WOTZOU	ZUZDIH
QIRNUC	SUTVIO	VISWAX	WOTZUA	ZUZDON
QIZMIW	SUVFUL	VIWFEN	WOVBEO	ZUZDUT
QODKIF	SUVGAS	VIWFIR	WUCHAD01	ZUZFAB
QODKUR	SUVNEC01	VIZNUO	WUKLAP	QQQBIJ
SUVPUU				
QQQFAD	TAFDIN			
QOTNIW	TAFDOT			

\*Conquest states that BOWKAA is the racemate of ROKNAH, but BOWKAA has meso-tartaric acid.



# Chapter 3. A Screening Approach for Resolution Opportunities in Complex Multicomponent Chiral Systems

**Key words:** Phase Diagram, Chiral Separation, Co-crystals, Chiral Molecules

**Abstract:** Co-crystallization of racemic-compound-forming chiral molecules can generate other types of crystalline products, such as co-crystal conglomerates and diastereomerically related co-crystals, which enable the application of chiral separation techniques such as preferential crystallization and classic resolution. Here, a systematic method to identify the types and phase diagrams of co-crystals formed by chiral target compounds and candidate co-formers in a particular solvent system is developed. The method is based on clear point temperature measurements of specific solution compositions containing both chiral molecules and a co-former. For racemic Phenylalanine (Phe) in water/ethanol mixtures one of the enantiomers selectively co-crystallizes with the opposite chirality enantiomer of Valine (Val), forming the more stable diastereomerically related co-crystals. The racemic compound Ibuprofen crystallizes with the non-chiral co-former 1,2-Bis(4-pyridyl)ethane (BPN) as racemic compound co-crystals. More interestingly, when combined with trans-1-(2-pyridyl)-2-(4-pyridyl)-ethylene (BPE), the racemic compound Ibuprofen co-crystallizes as a conglomerate, which enables the application of preferential crystallization of this racemic compound. The systematic method shows the benefit of using pseudo-binary phase diagrams. Such pseudo-binary phase diagrams depict the clear point temperature on a very specific route through the quaternary phase diagram, allowing the identification of various co-crystal types as well as the corresponding co-crystallization conditions. The systematic method can be used to identify a suitable solid phase for chiral separation and the obtained phase diagram information enables to perform a crystallization-mediated chiral resolution process design. Such guideline for chiral resolution process design has never been reported for conglomerate co-crystal systems such as IBU:BPE in this study.

## 1. INTRODUCTION

Enantiomers of chiral products possess both pharmacological and toxicological differences. The awareness of such differences has driven the development towards new chiral separation techniques.<sup>1-2</sup> Chiral separation techniques such as preferential crystallization and Viedma ripening are now effective and efficient in achieving high enantiopurity for specific scientific examples of chiral product.<sup>1, 3-5</sup> The general industrial application of these techniques requires the target compounds to form crystals which contain only a single enantiomer. However, in the substantial majority of the cases the two enantiomers of a chiral compound together form a solid (racemic compound) which significantly limits the application of chiral separation techniques.<sup>6</sup>

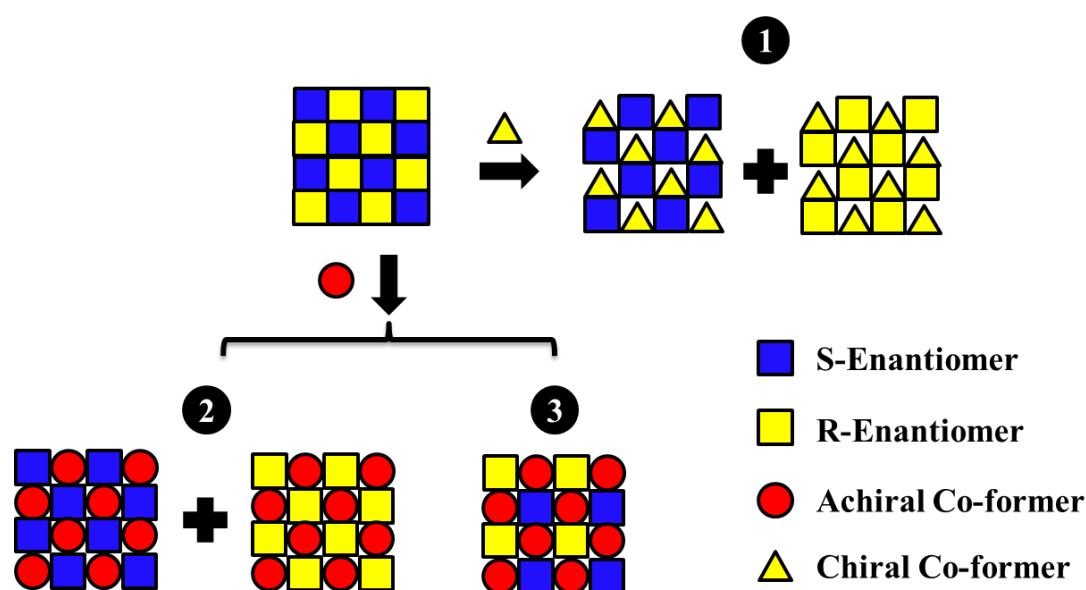
To overcome this drawback, various approaches can be followed to enable chiral separation through a solid state conversion. A racemic compound-forming chiral compound can be chemically modified into derivatives that crystallize as conglomerates. For instance, Naproxen has been successfully deracemized via its conglomerate ester derivatives.<sup>7</sup> Salt and solvate formation, for instance the ethanolamine salt of Mandelic acid and the monohydrate of Asparagine, can also provide the opportunity to convert a racemic compound to a conglomerate.<sup>8-10</sup> Alternatively, co-crystallization can modify the solid phase of the chiral compounds for the application of chiral separation techniques, for instance by converting racemic compounds into conglomerate co-crystals. Up till now, the conglomerate co-crystal systems of Naproxen (NPX):Nicotinamide (NA) and Ibuprofen (IBU): trans-1-(2-pyridyl)-2-(4-pyridyl)-ethylene (BPE) are the only two reported in literature<sup>11-12</sup>.

Various co-crystal types can be formed when combining a racemic compound and a co-former into co-crystals. Co-crystals are crystals containing two or more non-solvent molecular components in the same crystal lattice.<sup>13</sup> Successful chiral co-formers form two diastereomerically related co-crystals with the enantiomers (see co-crystal type 1 in Scheme 1). The two enantiomers could be separated based on solubility differences between diastereomeric co-crystals or between the co-crystals and the pure component crystals.<sup>14-15</sup> On the other hand, an achiral co-former can co-crystallize with a racemic compound into either conglomerate or racemic compound co-crystals (see co-crystal type 2 and 3 in Scheme 1, respectively), and the former type paves a path to the application of chiral separation techniques such as preferential crystallization on racemic compound via co-crystallization.<sup>11, 16</sup> In much rarer cases, solid solution co-crystals are formed between an achiral co-former and a racemic compound, which contain random amounts of the two enantiomers in the lattice<sup>17</sup>. In the present study, the solid solution co-crystals are not discussed due to their rarity. A systematic screening method to identify the various co-crystal types in these complex multicomponent chiral systems benefits the selection and design of a suitable chiral separation process.

The phase diagram of a multi-component system provides information about the compositions in the various phases. However, a complete phase diagram for a quaternary system containing both enantiomers, a co-former and a solvent, which also includes temperature as a variable, exists only in a

four-dimensional space. The construction of such a quaternary phase diagram requires large amount of measurements, slowing down the efficient screening of suitable co-formers for the target compound.<sup>18</sup> A projection of the interesting part of such phase diagram on a two-dimensional plane, a pseudo-binary phase diagram, can identify co-crystal formation as well as co-crystal type with significantly less measurements, thus suitable as a screening tool.

In this study, a systematic method using pseudo-binary phase diagrams is developed in order to identify the co-crystal types formed using a racemic compound and a candidate co-former. The method is experimentally verified as a useful screening procedure prior to the design and operation of a co-crystallization-mediated chiral separation process.



**Scheme 1.** Schematic demonstration of co-crystal types using a racemic compound (square) and a chiral (triangle) or achiral (circle) co-former: (1) diastereomerically related co-crystals; (2) conglomerate co-crystals and (3) racemic compound co-crystals. For convenience we ignored formation of relatively rare solid solutions.

## 2. EXPERIMENTAL

**Materials.** Racemic Ibuprofen (RS-IBU, 99%) and trans-1-(2-pyridyl)-2-(4-pyridyl)-ethylene (BPE, 98%) were obtained from Santa Cruz Biotechnology. S-Ibuprofen (S-IBU, 99%), 1,2-Bis(4-pyridyl)ethane (BPN, 99%), Heptane (99%), S-Phenylalanine (S-Phe,  $\geq 99.0\%$ ), R-Phenylalanine (R-Phe,  $\geq 98.0\%$ ), RS-Phenylalanine (RS-Phe,  $\geq 99.0\%$ ), R-Valine (R-Val,  $\geq 98.0\%$ ), S-Valine (S-Val,  $\geq 98.0\%$ ), RS-Valine (DL-Val,  $\geq 99.0\%$ ) and ethanol were supplied by Sigma Aldrich. All chemicals were used without further purification. Molecular structures of Val, Phe, IBU, BPN and BPE are shown in Figure 1. From this point onwards we will adopt the RS notation for the amino acids, meaning that

D-Phe corresponds to R-Phe and D-Val corresponds to R-Val. This is done for consistency in notation throughout the paper.

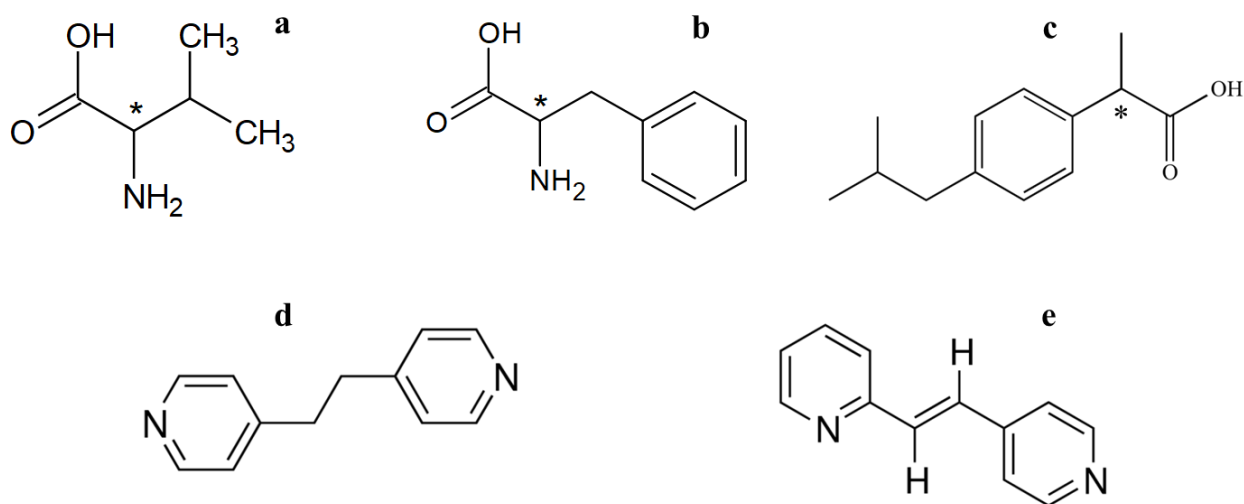


**Figure 1.** Molecular structures of Val (a), Phe (b), IBU (c), BPN (d) and BPE (e). Asterisks in a–c show the locations of the chiral centers.

**Solubility Measurement.** Crystal16 equipment (Technobis B.V.) was used for all saturation temperature measurement in this study, following a method developed by ter Horst et al<sup>19</sup>. A suspension of a known composition  $x$  was prepared from the pure components and the corresponding solvent. The suspension was linearly heated (0.3°C/min) until full dissolution (clear point) and then linearly cooled down (-0.3°C/min) for recrystallization. The clear point temperature was noted as the saturation temperature  $T_s$  of the corresponding composition. The heating-cooling cycle was repeated for three times and the average  $T_s$  was taken to represent the saturation temperature of the sample composition.

**Saturation temperature of mixed compositions.** A series of mixed samples were prepared containing the target compound (either its racemic form or the enantiopure form) and the co-former in order to determine co-crystal existence. The compositions of the target compound (A) and the co-former (B) in the mixed samples were their equilibrium molar fractions  $x_A^*(T_r)$  and  $x_B^*(T_r)$  in the corresponding pure component solutions at various reference temperatures  $T_r$ , estimated from van 't Hoff equation (Equation 2). The measured  $T_s(x_A^*(T_r), x_B^*(T_r))$  of the mixed samples were compared with  $T_r$ . Positive temperature differences  $\Delta T = T_s - T_r$  indicate the appearance of a solid different from either pure compound A or B. Due to the possibility of non-ideal solutions we assigned an arbitrarily chosen  $\Delta T > 10^\circ\text{C}$  to indicate the existence of a stable co-crystal consisting of compound A and B.<sup>19</sup>

**Type-I Phase Diagram.** In a Type-I phase diagram, the sample composition ( $x_A, x_B$ ) of the target compound A (either its racemic form or enantiopure form) and the co-former B is described by the following equation:

$$\frac{x_B}{x_B^*(T_r)} = 1 - \frac{x_A}{x_A^*(T_r)} \quad \text{Equation 1}$$

where  $x_A$  and  $x_B$  are the molar fractions of the target compound (A) and the co-former (B), while  $x_A^*$  and  $x_B^*$  are the equilibrium molar fractions of A and B at a chosen temperature  $T_r$  in their corresponding pure component solution. The saturation temperatures  $T_s$  of such a series of samples was measured and plotted against the solvent-excluded molar fraction  $y_B = x_B/(x_A + x_B)$ , as a type I pseudo-binary phase diagram.

**Type-II Phase Diagram.** In order to identify racemic compound or conglomerate behavior of the co-crystals a Type-II phase diagram was determined. In the samples of a Type-II phase diagram, the total molar fraction of both enantiomers  $x = x_R + x_S$  is chosen constant, as well as the molar fractions  $x_B$  and  $1 - x - x_B$  of co-former and solvent, respectively. This leaves the enantiomer fraction  $y_S = x_S/(x_S + x_R)$  as a variable in the sample compositions. The measured saturation temperatures  $T_s$  for these samples with varying  $y_S$  but constant  $x_B$  and  $x$  were plotted against the molar fraction  $y_S$  of S-enantiomer in both enantiomers of the corresponding samples. The sample compositions used in all type II phase diagrams in the present study are shown in Table. 1.

**Table 1.** Molar compositions of samples for each Type-II pseudo-binary phase diagram. A = Target Compound, B = Co-former, Val = Valine, Phe = Phenylalanine, IBU = Ibuprofen, BPE = *trans*-1-(2-pyridyl)-2-(4-pyridyl)-ethylene and BPN = 1,2-Bis(4-pyridyl)ethane. Ethanol/H<sub>2</sub>O solvent composition: 20/80 %v/v.

Experiment Nr.	Target Compound (A)	Co-former (B)	Solvent	$x_A$ [mmol/mol]	$x_B$ [mmol/mol]
1	RS-Val	-	Ethanol/H <sub>2</sub> O	7.6	0
2	RS-Phe	-	Ethanol/H <sub>2</sub> O	2.3	0
3	RS-Val	S-Phe	Ethanol/H <sub>2</sub> O	7.6	2.3
4	RS-Phe	S-Val	Ethanol/H <sub>2</sub> O	2.3	4.4
5	IBU	-	Heptane	114	0
6	IBU	BPE	Heptane	114	28
7	IBU	BPN	Heptane	114	28

**X-ray powder diffraction (XRPD) to identify the crystalline phase composition.** After recrystallization, samples were filtered at room temperature and the obtained solid was analyzed by XRPD, carried out in a Bruker D2 Phaser (Bruker AXS GmbH, Karlsruhe, Germany). Data collection was done using monochromatic Cu K  $\alpha$  1 radiation ( $\lambda = 0.154060$  nm) in the  $2\theta$  region between  $8^\circ$  and  $50^\circ$ , with a  $2\theta$  step size of  $0.022^\circ$ . Data evaluation was done with the Bruker program EVA.

**Construction of theoretical solubility lines in the Type-I and Type-II pseudo-binary phase diagrams.** In order to estimate the theoretical solubility in the various phase diagrams used, a modified Van 't Hoff equation was used:

$$\sum_i^N \ln x_i = -\frac{\Delta H}{R} \left( \frac{1}{T_s} - \frac{1}{T_0} \right) \quad \text{Equation 2}$$

where  $x_i$  are the molar fraction of the component(s)  $i$ , forming the solid phase,  $N$  is the total number of components  $i$ , including enantiomers, in the co-crystals,  $T_s$  [K] is the saturation temperature and  $\Delta H$  and  $T_0$  [K] are parameters specific for each solubility line and phase diagram, estimated from corresponding experiment data. As an example, the Van 't Hoff parameters of the S-IBU:BPE co-crystal were estimated from the experimental  $T_s$  and the corresponding molar fraction product  $x_{S-IBU} \cdot x_{BPE}$  ( $N=2$  here as R-IBU is not in the enantiopure co-crystal). In the case of the co-crystal of RS-IBU:BPN, on the other hand, the molar fractions of both R- and S-IBU and of BPN were taken into account. Therefore,  $\Delta H$  and  $T_0$  of RS-IBU:BPN were estimated from experimental  $T_s$  and  $x_{R-IBU} \cdot x_{S-IBU} \cdot x_{BPN}$  ( $N=3$  here as both enantiomers and the co-former are in the co-crystals). The parameters of the Van 't Hoff equation were used to interpolate or extrapolate solubility of the target component at other temperatures, as well as to construct theoretical phase diagrams.

**Single-crystal X-ray diffraction (XRD) of co-crystals.** Crystals of IBU:BPE suitable for X-ray diffraction were prepared by slowly evaporating an ethanol solution containing 510.3 mg/ml RS-IBU and 232.0 mg/ml BPE at 40°C. For single-crystal X-ray diffraction a crystal was coated with high viscosity oil, mounted on a Mitagen Microloop and shock frozen to 208 K using liquid nitrogen. Intensity data were collected at 208 K. The measurement was performed on a Nonius KappaCCD,  $\phi$  and  $\omega$  scans, using monochromated MoK $\alpha$  radiation.

Crystals of S-IBU:BPN suitable for X-ray diffraction were prepared by slowly evaporating an ethanol solution containing 19.9 mg/ml S-IBU and 17.9 mg/ml BPN at room temperature. For single-crystal X ray diffraction, a crystal was coated with high viscosity oil, mounted on a Mitagen Microloop and shock frozen to 150 K using liquid nitrogen. Intensity data were collected at 150 K. The measurement was performed on a Bruker D8 Quest,  $\phi$  scans, using monochromated MoK $\alpha$  radiation.

The structures were solved using CRUNCH<sup>20</sup> (IBU-BPE) and SHELXT<sup>21</sup> (S-IBU:BPN) and were refined with standard methods using SHELXL.<sup>22</sup> All non-hydrogen atoms were refined with anisotropic temperature factors. The positions of the hydrogen atoms could initially be determined using a difference Fourier map. Hydrogens were subsequently, when possible, replaced by hydrogens at calculated positions and refined riding on the parent atoms.

**Table 2.** Values of the van 't Hoff parameters in Equation 2 for each crystalline materials introduced in this study. Val = Valine, Phe = Phenylalanine, IBU = Ibuprofen, BPE = *trans*-1-(2-pyridyl)-2-(4-pyridyl)-ethylene and BPN = 1,2-Bis(4-pyridyl)ethane. The errors of the two parameters are standard deviations from fitting experimental data in the van 't Hoff equation.

Crystal Composition	Exp. Nr.	$\Delta H$ [KJ/mol]	$T_0$ [K]
S-Val	1	$21.5 \pm 1.7$	$792 \pm 177$
S-Phe	2	$19.7 \pm 0.8$	$1314 \pm 237$
RS-Val	1	$29.2 \pm 1.1$	$363 \pm 104$
RS-Phe	2	$46.8 \pm 0.9$	$927 \pm 85$
R-Val:S-Phe or S-Val:R-Phe	3 and 4	$43.4 \pm 0.8$	$1209 \pm 86$
RS-IBU	5	$134.7 \pm 4.0$	$351 \pm 18$
S-IBU	5	$58.4 \pm 0.5$	$311 \pm 4$
S-IBU:BPE	6	$55.3 \pm 1.6$	$487 \pm 28$
RS-IBU:BPN	7	$57.7 \pm 3.4$	$576 \pm 78$
S-IBU:BPN	7	$22.1 \pm 2.4$	$1102 \pm 430$

### 3. RESULTS AND DISCUSSIONS

#### 3.1 Diastereomerically Related Co-crystals using Chiral Co-formers

Phenylalanine (Phe) and Valine (Val) are amino acids with a single chiral center. Both amino acids are reported to crystallize as racemic compounds from racemic solutions. Interestingly, it has also been reported that S-Phe and R-Val can form a 1:1 co-crystal while there are to our knowledge no reports on co-crystal formation of the diastereomerically related co-crystal with the same enantiomers of Phe and Val.<sup>23</sup> Therefore, it was chosen to investigate the effect of the S-Val co-former for the RS-Phe system and the S-Phe co-former for the RS-Val system.

**Pure Component Solubilities.** Firstly, the solubilities of the pure components S-Val, RS-Val, S-Phe and RS-Phe in an 20/80 % v/v ethanol/water mixture were measured. The solubility is plotted as a function of temperature in Figure 2 (left) along with the corresponding Van 't Hoff plots in Figure 2 (right). While the data points of the other compounds gave a good fit to Equation 2, the solubility curve of S-Val showed a discontinuity near 42 mg/ml, which is a possible result of S-Val polymorphism<sup>24</sup>. Since pure component polymorphism is not the focus of the study we did not further look into this. RS-Val shows a higher solubility than the enantiopure S-Val. For example, at 50°C, the solubility of S-Val is 44.5 mg/ml, which is more than half of the solubility of RS-Val at the same temperature (58.7 mg/ml),

indicating that RS-Val is a racemic compound. On the other hand, RS-Phe shows a much lower solubility than S-Phe, which indicates that RS-Phe is a highly stable racemic compound. For example, at 40°C, the solubility of S-Phe is 25.7 mg/ml ( $x_{S-Phe}^*(40^\circ\text{C}) = 3.3$  mmol/mol) and the solubility of RS-Phe is 13.3 mg/ml ( $x_{RS-Phe}^*(40^\circ\text{C}) = 1.7$  mmol/mol). The experimental pure component solubilities were fitted to Equation 2 in order to determine the Van 't Hoff parameters, which were used to construct theoretical phase diagrams of the model systems.

**Saturation Temperatures of Co-crystal Systems.** During a solution co-crystal screening, the composition with the highest possibility of forming a new co-crystalline material is not determined by the expected co-crystal stoichiometry but by the pure component solubilities<sup>19</sup>. Specifically, a system containing the target compound A and the co-former B of the composition  $[x_A^*(T_r), x_B^*(T_r)]$  has the highest possibility of forming co-crystals A:B, where  $x_A^*$  and  $x_B^*$  are the equilibrium molar fraction of respectively A and B at a reference temperature  $T_r$ <sup>19</sup>. If a more stable co-crystal forms, the measured saturation temperature  $T_s > T_r$  of such a composition is usually substantially higher than the reference temperature  $T_r$ , since the saturation temperature  $T_s$  is that of the more stable co-crystal rather than the pure component crystals<sup>19</sup>.

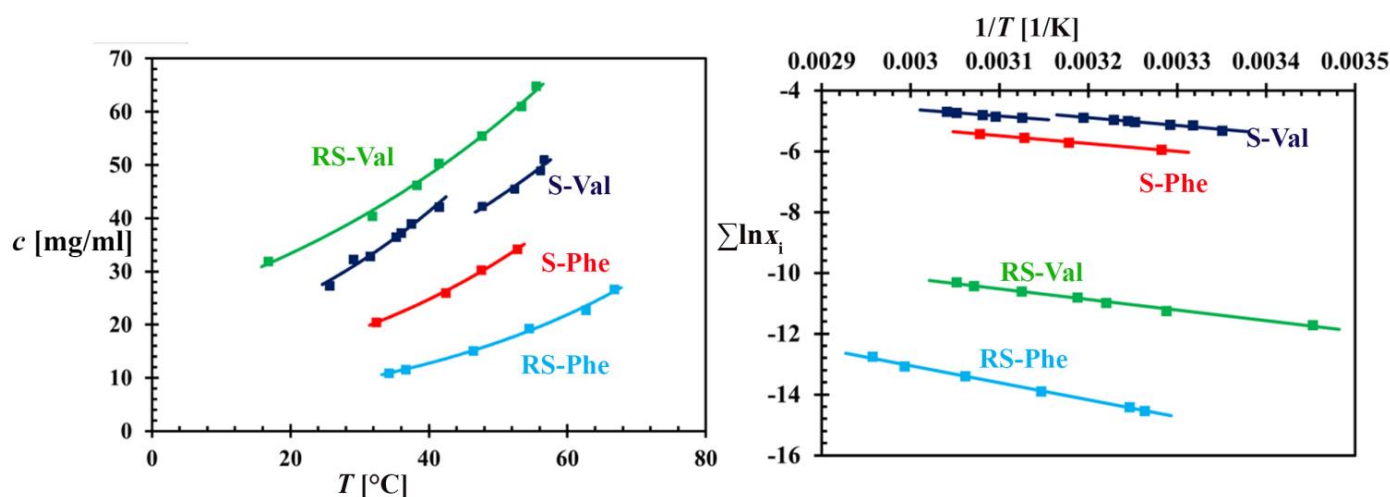


**Figure 2.** Left: Solubility of RS-Val, S-Val, RS-Phe and S-Phe in 20/80 % v/v ethanol/water (left) as a function of temperature. Right: The experimental data fitted to equation 2. The solid lines in both figures are theoretical solubilities estimated from Equation 2.

Therefore, by measuring the temperature difference  $T_s - T_r$  new co-crystal materials constructed of the target molecule and the co-former can be identified<sup>19</sup>. Here the saturation temperatures of a series of mixtures of S-Phe, as the chiral co-former, and either S- or R-Val, as the target molecule, were measured. In Figure 3, the determined temperature difference  $T_s - T_r$  is plotted against the chosen reference temperature  $T_r$ . The saturation temperatures  $T_s$  of the R-Val + S-Phe system are substantially higher than the corresponding reference temperatures  $T_r$ , strongly indicating the existence of R-Val:S-Phe co-crystals. On the contrary, the saturation temperatures of the S-Val + S-Phe were slightly lower

than the corresponding reference temperatures, suggesting that no co-crystallization took place between the two compounds.

**Type-I Pseudo-binary Phase Diagrams.** Chiral co-formers interact differently with the opposite enantiomers of the same chiral compound. The results in Figure 3 suggest that Phe only co-crystallizes with Val of the opposite chirality and vice versa. For further verification, two Type-I pseudo-binary phase diagrams were constructed from the three component mixtures of S-Val, as the chiral co-former, with either S- or R-Phe, as the target molecule, in 20/80 % v/v ethanol/water.

Figure 4 shows the type I pseudo-binary phase diagram of S-Val and R-Phe in 20/80 %v/v ethanol/water mixture and the schematic procedure of the construction of this type of phase diagrams, from a quaternary phase diagram. A Type-I pseudo-binary phase diagram describes the solubility of a mixture containing the chiral compound, racemic or enantiopure, and the candidate co-former. In it, the molar ratio between the chiral compound and the co-former in the mixture is varied in order to identify the existence of stable co-crystal regions.<sup>19</sup>

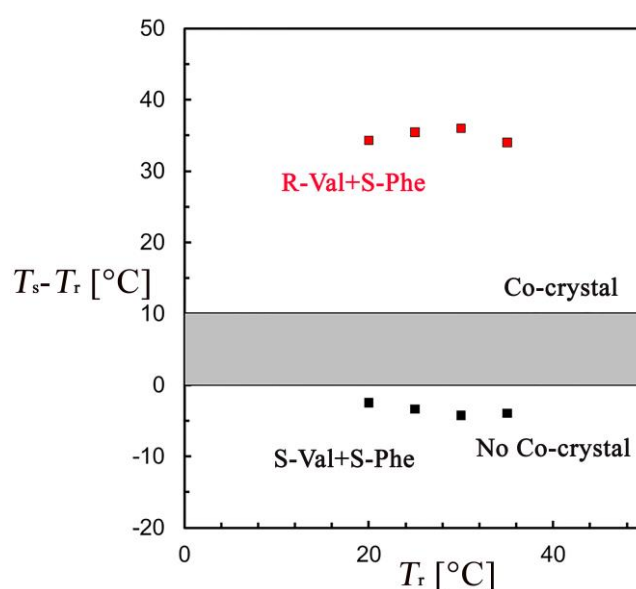


**Figure 3.** Difference  $T_s - T_r$  between saturation temperature  $T_s$  and reference temperature  $T_r$  of R-Val + S-Phe (red) and S-Val + S-Phe compositions (black) in 20/80 %v/v Ethanol/Water. The large positive difference indicates the existence of a stable co-crystalline phase for R-Val:S-Phe while there is no indication for a stable co-crystal from S-Val and S-Phe.

In the top of Figure 4, an isothermal quaternary phase diagram, at a reference  $T_r$ , is given for the co-crystal system from the target racemic compound A (Phe), the co-former B (S-Val) and the solvent H (20/80 v/v % ethanol/water). The two planes (red and green) describe compositions of mixtures containing H, B and only one of the enantiomers of A. From each of these two planes, a line is drawn to demonstrate the compositions of the type-I pseudo-binary phase diagrams below. For instance, two points on the sides of the red plane, which contains the solvent, S-Phe and S-Val, are

connected by a solid line. The two points represent the solubilities of S-Val ( $x_B^*(T_r)$ ) and S-Phe ( $x_S^*(T_r)$ ) at  $T_r$  in their corresponding pure-component solutions. Therefore, any point on the red solid line represents a composition ( $x_S, x_B$ ) from Equation 1.

In Figure 4 (left), the phase diagram of S-Val+R-Phe is divided into three parts by two eutectic points. The two parts on the sides indicate the solubilities of R-Phe and S-Val, the theoretical solubilities of which are represented by the red and the black solid lines, respectively. The middle part ( $0.3 < y_{\text{Val}} < 0.9$ ), which is significantly deviating from the theoretical saturation temperatures of the pure components, shows the composition region of a more stable co-crystal S-Val:R-Phe. The XRPD diffractogram of the collected crystals is distinctly different from those of both S-Val and R-Phe crystals. On the other hand, the powder patterns of the collected crystals and the reported<sup>25</sup> R-Val:S-Phe co-crystals are quite similar but not exactly the same, indicating strong preferential orientation (see details in Appendix). Therefore, the solid phase of the samples is indeed the co-crystal S-Val:R-Phe.

Figure 4 (right) shows that for the S-Val+S-Phe system no co-crystal region exists. Moreover, the left part of the phase diagram indicates the solubility of S-Phe, whose theoretical solubility is represented by a red line. When  $y_{\text{Val}} > 0.7$ , where S-Val is theoretically the more stable solid phase, no saturation temperature could be measured since none of the samples recrystallized. It seems that S-Phe substantially inhibits the crystallization of S-Val, whereas S-Phe crystallizes within the time frame of the saturation temperature measurement. The comparison between the two phase diagrams in Figure 4, along with the results of the XRPD analysis, proves that Phe and Val can only form stable co-crystals with each other if they possess opposite chiralities.

**Type-II Pseudo-binary Phase Diagram.** A Type-II pseudo-binary phase diagram illustrates the change in solubility in a three or four component mixture in which only the ratio between the two enantiomers of the chiral compound is varied. The shape of the phase diagram, especially the number and the location of its eutectic point(s), provides information about the types of the corresponding co-crystals.<sup>6</sup>

In Figure 5 (top), an isothermal quaternary phase diagram is given and the plane HRS contains only the solvent H (20/80 v/v % ethanol/water) and the two enantiomers of the target racemic compound A (Phe). The black line across the HRS plane represents the compositions of a constant total molar fraction of A and a varying R/S ratio.  $T_s$  of each point is plotted against its  $y_S$  as the type-II pseudo-binary phase diagram of the target compound A in H, without the co-former. Similarly, the red dashed line represents the compositions of all the points on a type-II pseudo-binary phase diagram of A in H, with the co-former B. Both black and red lines have the same total molar fraction of A.

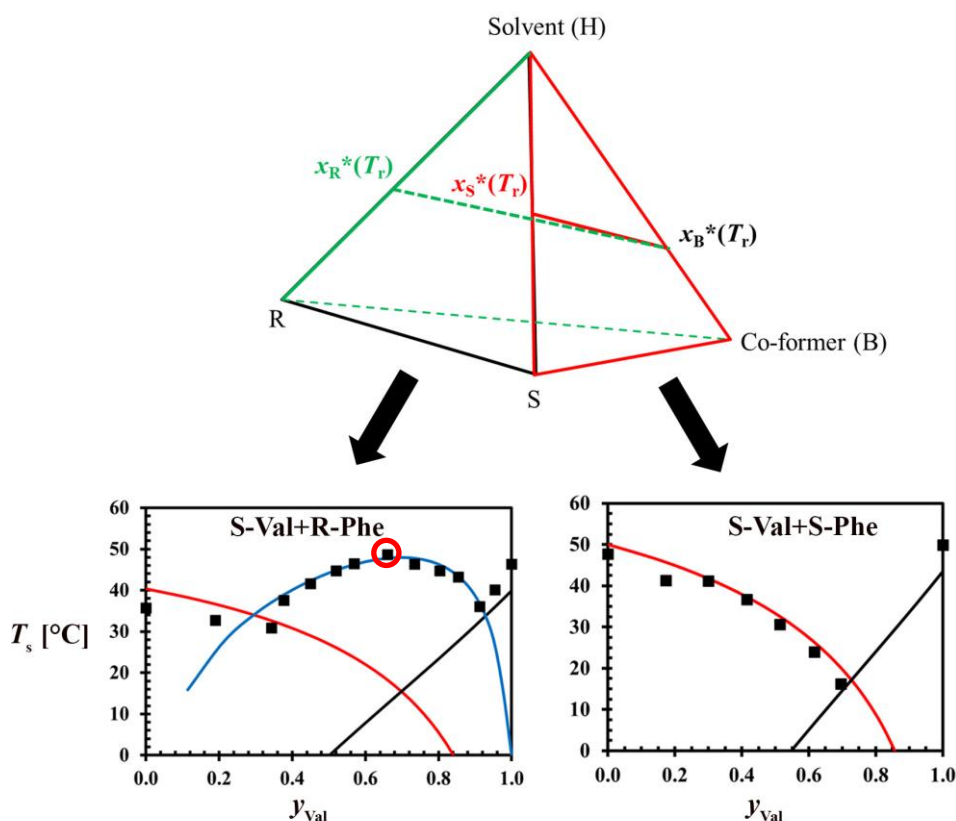


**Figure 4.** Top: Schematic demonstration of an isothermal quaternary phase diagram of the target racemic compound A, the co-former B and the solvent H. The lines (either solid or dashed) crossing the two colored planes (red and green) represent the compositions of the type-I pseudo-binary phase diagrams from H, B and one enantiomer of A. Bottom: Type I pseudo-binary phase diagrams for the system S-Val with R-Phe at a pure component reference temperature of 40°C (left) and the system S-Val with S-Phe at a pure component reference temperature of 50°C (right), both in a 20/80 %v/v ethanol/water mixture. The saturation temperature  $T_s$  is measured as a function of solvent-excluded molar fraction  $y_{Val}$  ( $y_{Val} = x_{Val} / (x_{Val} + x_{Phe})$ ). The molar compositions  $x_{Val}$  and  $x_{Phe}$  (for either S- or R-Phe) followed Equation 1. Solid lines are theoretical saturation temperature of pure S-Val (black) and either S- or R-Phe (red) estimated from Equation 1. The blue solid line is theoretical saturation temperature of co-crystal S-Val:R-Phe estimated from Equation 2. The solid phase of the circled sample in the left phase diagram was recovered at room temperature and analyzed by XRPD.

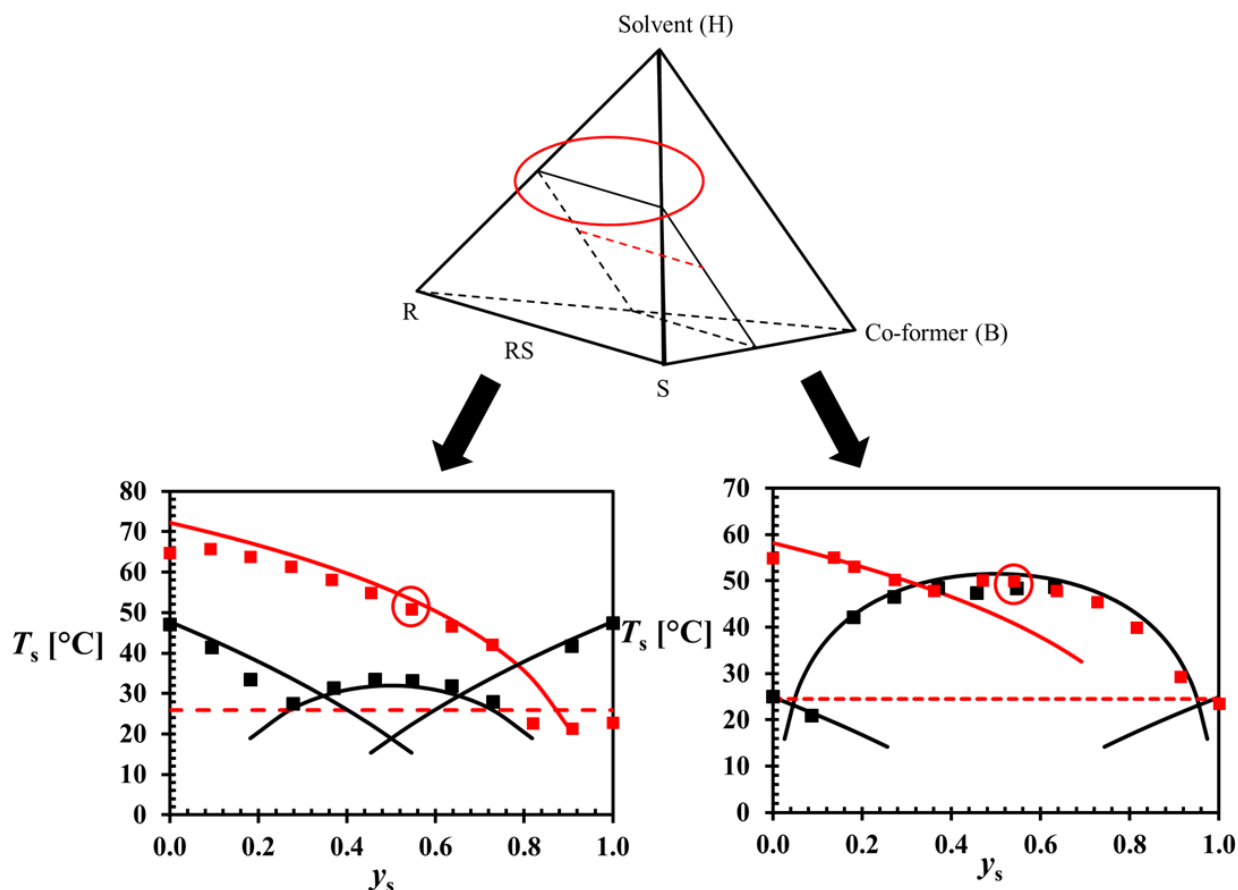


**Figure 5.** Top: Schematic demonstration of an isothermal quaternary phase diagram of the target racemic compound A (both R and S enantiomers), the co-former B and the solvent H. The black line crossing the HRS plane and the red dashed line represent the compositions in type-II pseudo-binary phase diagrams of A in H, without and with the co-former B, respectively. Bottom: Type-II pseudo-binary phase diagrams of RS-Val showing  $T_s$  versus  $y_s$  at  $x_{Val} = 7.6$  mmol/mol without (left, black) and with co-former S-Phe ( $x_{Phe} = 2.3$  mmol/mol) (left, red) and RS-Phe ( $x_{Phe} = 2.3$  mmol/mol) without (right, black) and with co-former S-Val ( $x_{Val} = 4.4$  mmol/mol) (right, red) in a 20/80 %v/v ethanol/water mixture. The dashed lines indicate the saturation temperature of the co-formers. The black solid lines are theoretical saturation temperatures  $T_s$  of Val (left) and Phe (right), estimated from Equation 2. The red solid lines are theoretical  $T_s$  of co-crystal S-Phe:R-Val (left) and S-Val:R-Phe (right) estimated from Equation 2.

**RS-Val+S-Phe System.** The type II pseudo-binary phase diagrams of RS-Val without the co-former in 20/80 v/v % ethanol/water is shown in Figure 5 (left, black lines). Two symmetrical eutectic points are located at  $y_s = 0.3$  and  $0.7$ , respectively. In the phase diagram region between the two eutectic points the racemic compound RS-Val is the more stable crystalline phase. Outside of this region, the

saturation temperature of the mixture is determined by either the R- ( $y_S < 0.3$ ) or the S-Val ( $y_S > 0.7$ ) solid phase.

By adding the co-former S-Phe (2.3 mmol/mol), an asymmetrical type II pseudo-binary phase diagram is obtained in Figure 5 (left, red). This is because S-Phe only co-crystallizes with R-Val and not with S-Val. The elevated sample saturation temperatures in the presence of co-former compared to those without the co-former indicate that in a large region ( $0 < y_S < 0.8$ ) of the phase diagram the co-crystal R-Val:S-Phe is more stable than both the RS-Val and R-Val crystal phase.

Additionally, the solid phase of the sample circled in red was recovered at room temperature and analyzed by XRPD. The powder pattern (see Appendix) of the crystalline sample obtained from the circled point in Figure 5 indicates the presence of the co-crystal S-Val:R-Phe. For high  $y_S > 0.8$ , the saturation temperature of roughly 25°C indicates that instead of S-Val, S-Phe crystallized in the samples despite it being slightly less stable than S-Val.

**RS-Phe+S-Val System.** Similar to that of Val, the type II pseudo binary phase diagram of Phe in Figure 5 (right, black lines) also contains two symmetrical eutectic points. Noticeably, since the solubility of RS-Phe is significantly lower than that of the pure enantiomer, the racemic Phe is the stable crystalline phase in a larger region in the phase diagram ( $0.1 < y_S < 0.9$ ) compared to racemic Val.

In the presence of the co-former S-Val (4.4 mmol/mol) in the Phe system (Figure 5, right, red lines), the co-crystal R-Phe:S-Val is the most stable compound from  $y_S = 0$  to 0.35. At higher  $y_S$ , RS-Phe is the most stable compound. The powder pattern of the solid phase of the circled sample at room temperature indicates the presence of pure RS-Phe and co-crystal R-Phe:S-Val (see Appendix).

### 3.2 Co-crystals using Achiral Co-formers.

Ibuprofen (IBU) is a commonly used nonsteroidal anti-inflammatory drug (NSAID) and is marketed in its racemic form, although S-IBU is over 100-fold more bioactive than the R-enantiomer.<sup>26-</sup><sup>27</sup> RS-IBU crystallizes as a stable racemic compound and Figure 6 shows that the solubility of the racemic IBU is significantly lower than its pure enantiomer in Heptane. To investigate co-crystal

formation of RS-IBU, two achiral co-formers, BPN and BPE, were screened to identify their co-crystal types.

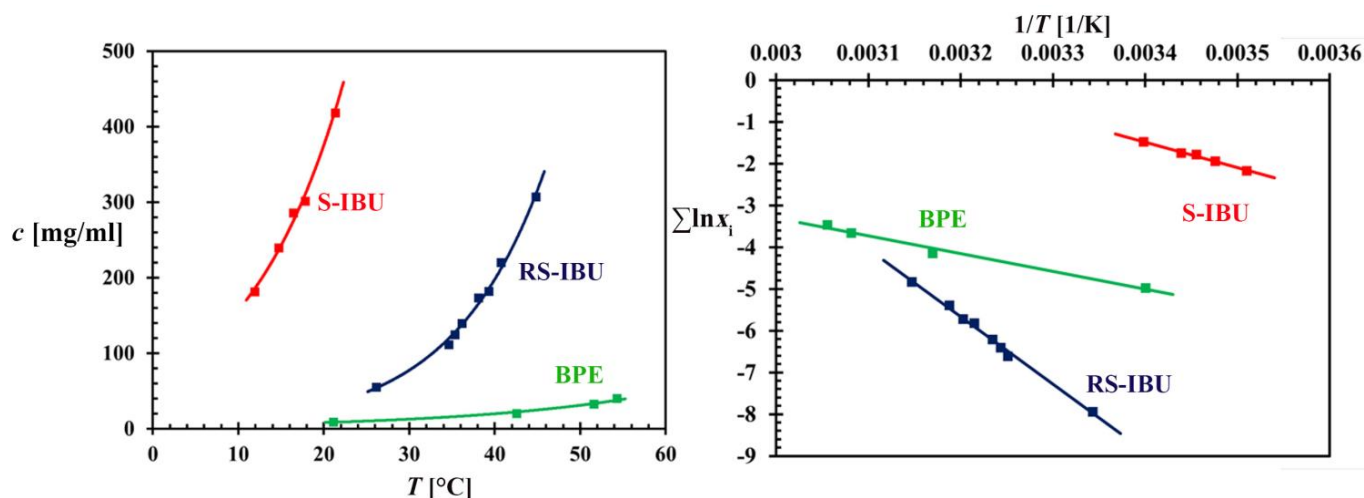


**Figure 6.** Left: Solubility of RS-IBU, S-IBU and BPE in Heptane (left) as a function of temperature. Right: The summations of natural logarithms of equilibrium molar fractions  $x_i$  of each compound  $i$  are linear functions of the inverse of temperature  $T$ . The solid lines are a linear regression of the experimental data points.

### IBU-BPN Co-crystal

Solubility data of the achiral co-former BPN in Heptane could not be reproducibly obtained from clear point temperature measurements because of the severe fluctuation of laser transmission signals, probably from the crystals floating on the liquid-gas interface in the Crystal16 vials. However, a rough estimation of the co-former BPN solubility was obtained to be less than 5 mg/ml at room temperature.

As a reliable solubility data of the co-former is not available, a short-cut approach was employed to quickly determine the type of co-crystals formed from IBU and BPN. In this short-cut approach, two Heptane mixtures were prepared, one from RS-IBU + BPN and the other from S-IBU + BPN. In both mixtures, the concentrations of RS-IBU and S-IBU were the same (180 mg/ml) and the BPN concentration was also constant (40 mg/ml). The saturation temperature of the RS-IBU + BPN mixture is around 49°C and that of S-IBU + BPN is approximately 40°C. The saturation temperatures of RS-IBU and S-IBU of 180 mg/ml are around 36°C and 12°C, respectively. Therefore, the  $T_s$  of the mixtures from RS- and S-IBU are 13°C and 28°C higher than those of the pure IBU. Moreover, although the solubility of BPN is unknown, the different  $T_s$  of the two mixture, which contain equal concentration of the co-former, indicates that these  $T_s$  are not of the pure component BPN. Therefore, it is likely that the solid phases from these two mixtures contain co-crystals from IBU and BPN.

This assumption is confirmed from an XRPD analysis of the solid phases recovered from the two mixtures at room temperatures (see details in Appendix). The XRPD patterns of the solid phases

from both mixtures are different from those of the pure component IBU and BPN, indicating that the solid phases are co-crystals. Additionally, the two XRPD patterns of the co-crystals are different from each other, suggesting that the co-crystals are racemic compounds.

BPN and RS-IBU are reported to co-crystallize as racemic compounds, as also is expected from our short-cut approach.<sup>28</sup> We also obtained single co-crystals of S-IBU:BPN for single crystal XRD analysis. The co-crystal structure with formula  $C_{38}H_{48}N_2O_4$ , refined to  $R1 = 0.0403$  for 6486 reflections with  $I_o > 2.0 \sigma(I_o)$ , is monoclinic with the space group  $C2$  (#5) and unit cell parameters  $a = 18.2165(12)$  Å,  $b = 5.5960(4)$  Å,  $c = 33.393(2)$  Å,  $\beta = 92.075(2)^\circ$ ,  $V = 3401.8(4)$  Å<sup>3</sup> and with  $Z=4$  asymmetric units in the cell. The asymmetric unit contains one molecule of BPN and two IBU molecules of S-IBU, leading to a 1:2 ratio for the two compounds BPN and S-IBU. An intermolecular hydrogen bond is formed between the hydroxyl groups of the IBU molecules and both Nitrogen atoms at the pyridine groups of BPN (see structure in Figure 7, top). The generated powder patterns from the racemic and enantiopure co-crystal structure data match those measured in the short-cut approach, indicating that the measured  $T_s$  correspond to the solubilities of the co-crystals (see Figure SIII in Appendix).

In a short-cut approach, the screening procedure stops when the single-crystal structure is obtained. However, one of the goals of this study is to demonstrate that the Type-II pseudo-binary phase diagrams of different types of co-crystals are different, thus being feasible as a screening tool. Therefore, the Type-II pseudo-binary phase diagram of the IBU:BPN system is constructed and shown in Figure 8. The phase diagram in absence of the co-former (black) was constructed with a constant total concentration of 180 mg/ml IBU ( $x_{IBU} = 111$  mmol/mol) and a varying solvent-excluded molar fraction  $y_s$  of the S-enantiomer. Figure 8 demonstrates that the model compound IBU in Heptane is a racemic compound system and the racemic form is significantly more stable than the pure enantiomer solid phase: The saturation temperature  $T_s$  of the racemic composition is approximately 30°C higher than that of pure R- or S-enantiomer.

The saturation temperatures in between the two symmetric eutectic points,  $y_s = 0.05$  and  $0.95$ , are for the racemic compound RS-IBU. Therefore, enantiopure S- or R-IBU crystals can only be recovered from a system where more than 95% of the IBU is composed of the corresponding enantiomer. Theoretical solubility lines of racemic IBU and the two enantiomers are shown as black solid lines in Figure 8 as well. Since the solubility of RS-IBU is significantly lower than that of either enantiomer, the racemic IBU is theoretically the dominant solid phase across the whole phase diagram. However, the measured phase diagram shows an increase of RS-IBU solubility due to the presence of the S-enantiomer. This leads to a deviation of the measured RS-IBU solubility line from the theoretical one towards higher and lower  $y_s$  fractions.

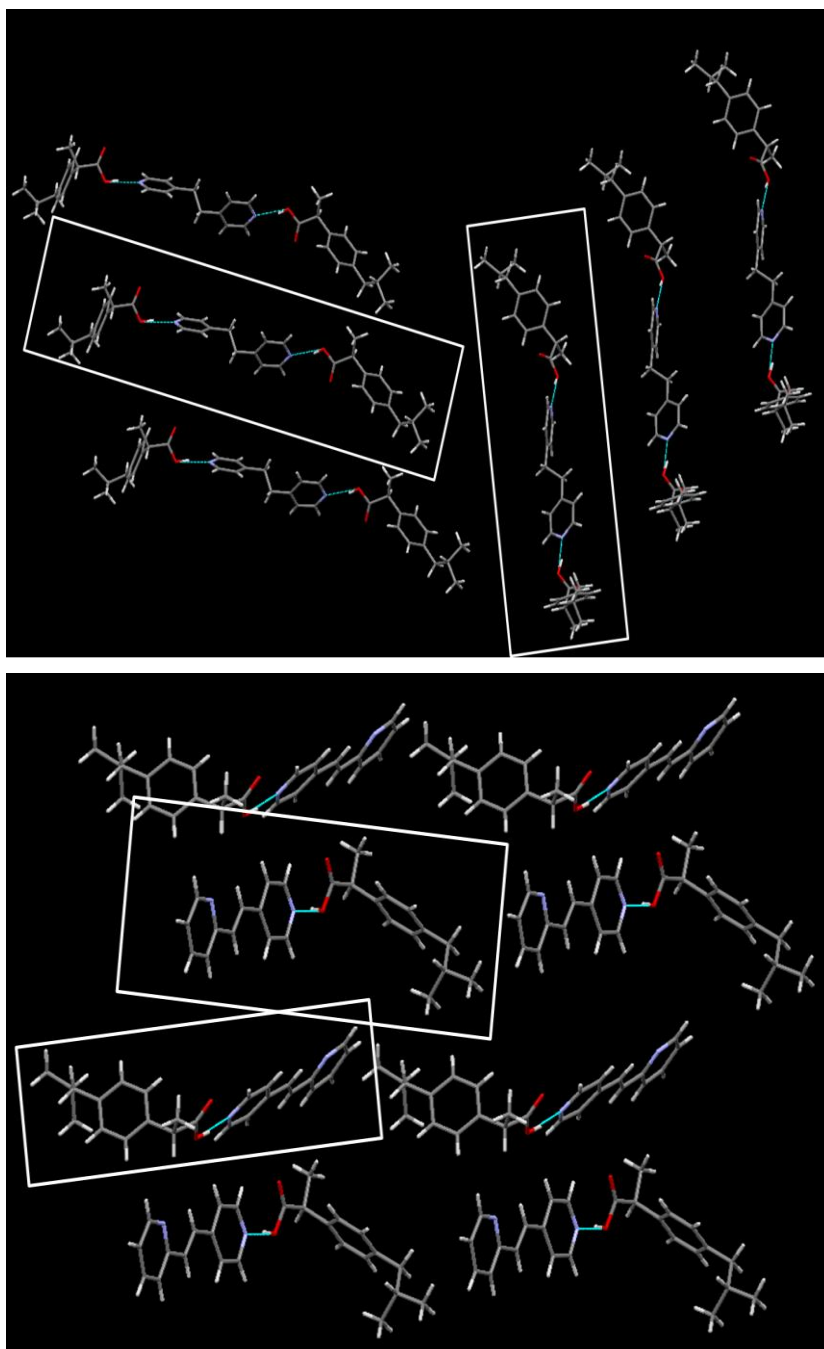


**Figure 7.** Structure of co-crystals *S*-IBU:BPN (top) and enantiopure IBU:BPE (bottom).

Figure 8 also shows the type II pseudo-binary phase diagram of 180 mg/ml (114 mmol/mol) IBU in the presence of a constant BPN co-former concentration of 40 mg/ml ( $x_{\text{BPN}} = 28$  mmol/mol). The saturation temperature  $T_s$  at the racemic composition increased by approximately 15°C while that of the enantiopure form increased by more than 30°C. Although the racemic form is still more stable within a large  $y_s$  range, the eutectic points moved closer towards the middle (from  $y_s = 0.05$  and 0.95 to  $y_s = 0.1$  and 0.9).

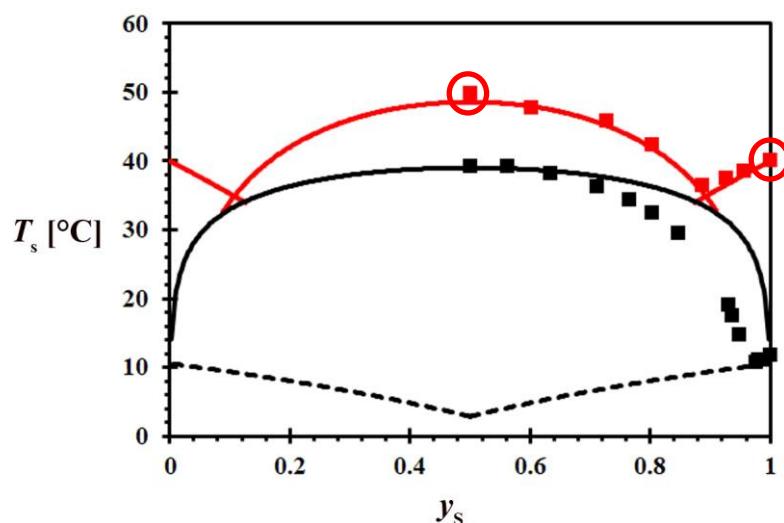


**Figure 8.** Type-II pseudo-binary  $T_s, y_s$  phase diagrams of IBU (black) and IBU-BPN (red) in Heptane. In both phase diagrams the total concentrations of IBU were 180 mg/ml ( $x_{IBU} = 114$  mmol/mol). In the IBU-BPN phase diagram (red) the concentration of the co-former BPN was 40 mg/ml ( $x_{BPN} = 28$  mmol/mol). The points are saturation temperature measurements and the lines are theoretical phase diagrams of pure RS-IBU crystals (black solid), pure S- or R-IBU (black dashed) as well as of co-crystals (red solid) using Equation 2. The two points circled are of the same compositions of the mixtures used in the short-cut approach.

### IBU-BPE Co-crystal

The co-crystal of IBU and BPE is one of the only two conglomerate co-crystals reported so far<sup>12</sup>. The solubilities of the second achiral co-former trans-1-(2-pyridyl)-2-(4-pyridyl)-ethylene (BPE) is significantly lower than those of IBU. As can be seen from Figure 6 (left), at the same temperature, the solubility of BPE is at least 5 times lower than that RS-IBU, let alone the more soluble S-IBU. Such large solubility difference between the target compound and the co-former B can lead to a Type-I pseudo-binary phase diagram with an eutectic point very close to one side.

In order to verify co-crystal formation between IBU and BPE, saturation temperatures  $T_s$  of mixed RS-IBU and BPE samples in Heptane were measured and Type-I pseudo-binary phase diagram of RS-IBU+BPE was also constructed. In Figure 9 (left), the temperature differences  $T_s - T_r$  of mixtures of RS-IBU and BPE in Heptane were all substantial, which indicates the existence of a stable co-crystal IBU:BPE. The powder pattern (see Appendix) of the solid phases of the circled samples in Figure 9 (left) indicate a solid phase different from IBU and BPE. It is noticeable in Figure 9 (left) that the temperature difference  $T_s - T_r$  decreases as the reference temperature  $T_r$  increases. It can be seen from Figure 6 that BPE's solubility is significantly less sensitive to the temperature compared with IBU, which means that the increase of  $T_r$  in Figure 9 (left) is accompanied with the change of the

stoichiometry between the two compounds. Therefore, the decrease of  $T_s - T_r$ , along with the increasing IBU/BPE ratio, indicates an influence of the presence of IBU on the solubility of the co-crystals.

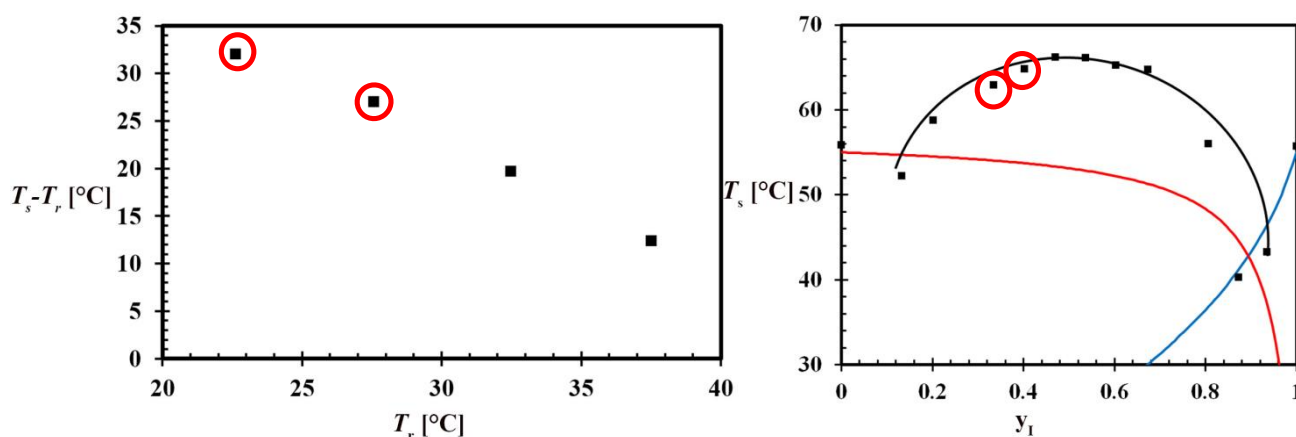


**Figure 9.** Left: The temperature difference ( $T_s - T_r$ ) of samples with composition ( $x_{RS-IBU}^*(T_r)$ ,  $x_{BPE}^*(T_r)$ ) versus the reference temperature  $T_r$ . Right: Type I pseudo-binary phase diagram plots measured saturation temperature  $T_s$  as a function of solvent-excluded molar fraction of RS-IBU  $y_I$  ( $y_I = x_{IBU}/(x_{IBU} + x_{BPE})$ ) from RS-IBU-BPE mixtures in Heptane. The molar composition of  $x_{RS-IBU}$  and  $x_{BPE}$  follow Equation 2. The solid lines are theoretical saturation temperature of pure RS-IBU (blue) and BPE (red) estimated from Equation 2. The black solid line is a guide to the eye.

Furthermore, a Type-I pseudo-binary phase diagram is constructed from RS-IBU and BPE in Heptane (Figure 9, right). The measured saturation temperatures  $T_s$  of mixtures of RS-IBU and BPE in Heptane are plotted as a function of the solvent-excluded molar fraction of RS-IBU  $y_{IBU}$ . The increased saturation temperature  $T_s$  between  $0.2 < y_{IBU} < 0.8$  indicates the existence of a co-crystal region. Further evidence for co-crystal formation is provided by the XRPD patterns from the circled samples in the phase diagram (see Appendix), which indicate different solid phases than the pure component crystals. Interestingly, the maximum  $T_s$  of the co-crystal is not at the theoretical eutectic point of RS-IBU and BPE ( $y_I = 0.9$  in Figure 9, right), instead is at around the middle of the phase diagram. This observation is in line with that from Figure 9 (left), which suggests that the presence of IBU significantly increase the solubility of the co-crystals.

Subsequently, a Type-II pseudo-binary phase diagram is constructed following the confirmation of co-crystal formation between IBU and BPE, in order to identify the co-crystal type. Constant concentrations of total IBU of 180 mg/ml ( $x_{IBU} = 114$  mmol/mol) and BPE of 40 mg/ml ( $x_{BPE} = 28$  mmol/mol) are used in the phase diagram (red) in Figure 10, with a varying molar ratio between S- and R-IBU. The phase diagram (black) of only IBU of the same total concentration is also shown in Figure 10 as comparison.

In Figure 10, the Type-II pseudo-binary phase diagram of IBU and BPE in Heptane demonstrates a typical feature of conglomerates: only one eutectic point can be found at the racemic

composition in the middle of the phase diagram. When the system is enriched with either enantiomer, the saturation temperature  $T_s$  is elevated. The estimated phase diagram (red solid line) also indicates the solubility of the enantiopure co-crystal. Two samples were taken at room temperature from the samples circled in Figure 10. XRPD results suggest that the crystalline phases from these two samples were a mixture of the same co-crystals with either the racemic or the enantiopure IBU (see Figure SV in Appendix). Based on the results of the Type-II pseudo-binary phase diagram screening, there are very strong indications that IBU and BPE co-crystallize as conglomerates. Additionally, this conglomerate co-crystal system is special as the racemic IBU is significantly more stable than its enantiomer but its enantiopure co-crystal is more stable. As a last step, single crystals were formed from racemic IBU and BPE in ethanol for co-crystal structure determination.

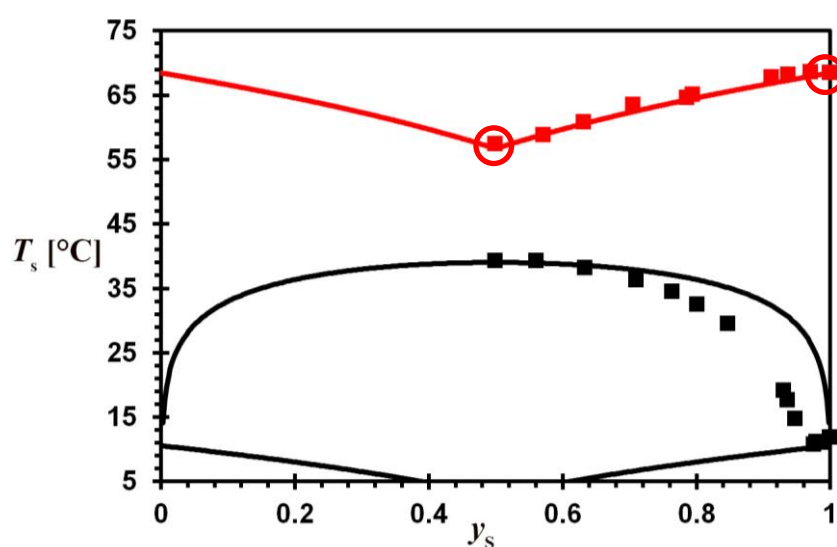


**Figure 10.** Type II pseudo-binary phase diagrams of IBU ( $x_{IBU} = 114$  mmol/mol, black) and IBU-BPE ( $x_{IBU} = 114$  mmol/mol and  $x_{BPE} = 28$  mmol/mol, red) in Heptane. The graph shows the saturated temperature  $T_s$  as a function of  $y_s$ , the molar fraction of the *S*-enantiomer in total IBU. The red solid lines indicate the solubility of the enantiopure co-crystal *R*- or *S*-IBU:BPE, estimated from Equation 2. The black solid lines are theoretical phase diagrams of pure component IBU crystals.

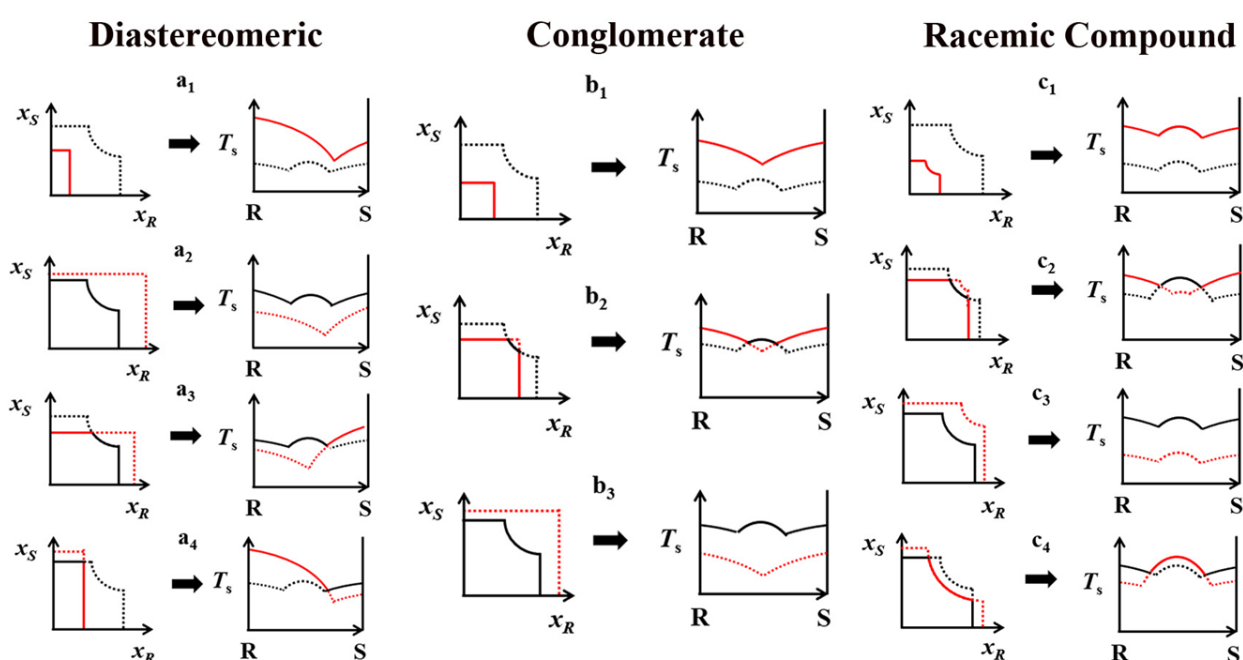
The structure of the co-crystals formed from RS-IBU and BPE was refined to  $R1 = 0.0397$  for 5602 reflections with  $I_o > 2.0 \sigma(I_o)$ . Crystal data:  $C_{25}H_{28}N_2O_2$ , monoclinic, space group P21 (#4),  $a = 6.4896(2)\text{\AA}$ ,  $b = 9.5675(6)\text{\AA}$ ,  $c = 17.5232(10)\text{\AA}$ ,  $\beta = 99.892(4)^\circ$ ,  $V = 1071.83(10)\text{\AA}^3$  and  $Z = 2$  (see crystal structure in Figure 7, bottom). This structure is the same as the one reported in literature<sup>12</sup>.

The asymmetric unit contains one molecule of BPE and one molecule of enantiopure IBU, leading to a 1:1 ratio for IBU and BPE. An intermolecular hydrogen bond is formed between the hydroxyl group of the carboxylic acid of the IBU molecule and the pyridine nitrogen at the four position

of BPE. The co-crystals from the racemic IBU and BPE contain only one of the two enantiomers, thus being conglomerate co-crystals.

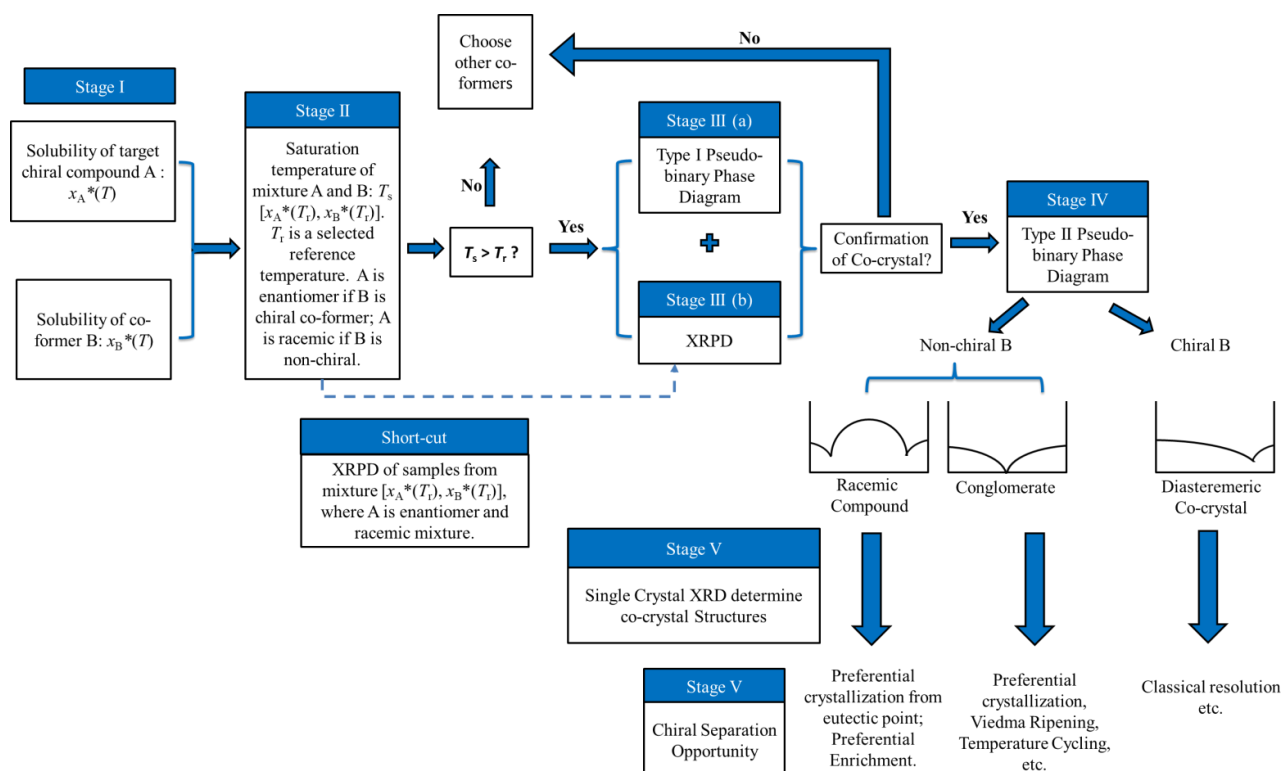
Moreover, IBU has a  $pK_a=4.91$  while that of BPE can be estimated to be  $pK_a=5.5$ , assuming a  $pK_a$  value equal to that of its structural isomer, *trans*-1,2-bis(4-pyridyl)ethylene<sup>29</sup>, indicates that co-crystals rather than salts are formed between the two compounds.

The calculated diffractogram of the conglomerate co-crystals is compared with those from the samples circled in Figure 10. The results of the comparison suggest that the solid phase of the sample at  $y_s=0.5$  is a mixture of the conglomerate co-crystals and RS-IBU. The other solid phase is composed of S-IBU:BPE co-crystals and S-IBU (see Appendix).



**Scheme 2.** Schematic isothermal phase diagrams of a racemic compound RS system with or without co-former B (either chiral C or achiral N) in various conditions. All black lines show the solubility lines in a racemic compound system in absence of co-former B: the horizontal and vertical lines represent the equilibrium solution composition in case of a liquid-solid equilibrium between the solution and pure S and R crystals, respectively. The curved line shows the equilibrium solution composition in case of a liquid-solid equilibrium between the solution and the racemic compound crystals. The intercept between the two straight line and curved line indicates the eutectic composition at which a three phase equilibrium exists between the solution, the racemic crystal and the enantiopure crystal R or S. All red lines show the solubility lines of the same systems in the presence of a constant amount of B: the red solid lines indicate more stable solids and the red dashed lines indicate less stable

solids than those in absence of B. Next to each isothermal phase diagram is a corresponding Type-II pseudo-binary phase diagram. The black lines, solid or dashed, show the solubility of the target compounds, racemic or enantiopure, without the co-former B. In the presence of a co-former B of a constant molar fraction, a new liquid-solid equilibrium is established in the system, represented by a new phase diagram (red). The solid or dashed red lines indicate the solubility of crystals more or less stable than those without the co-former, respectively.



**Scheme 3.** The subsequent steps to screen the types of co-crystals from racemic-compound-forming molecules. The mole fractions  $x_A^*(T_r)$  and  $x_B^*(T_r)$  are the solubilities of the target chiral molecule A and the co-former B at a selected reference temperature  $T_r$ . In stage II and III, the target compound A is enantiomer if the co-former B is chiral and A is racemic if B is non-chiral. The Type-II Pseudo-binary phase diagrams shown in Stage IV are only some examples of possible phase diagrams of the co-crystals. For a complete list of possible phase diagrams, see Scheme 2. For quick screening, a short-cut approach can be used, which is indicated by the dashed arrows. Two mixtures are prepared, one from the racemic target compound and the co-former and the other from the enantiomer target compound and the co-former. Solid phases from the mixtures are analyzed by XRPD and the co-crystal types of interest will be further determined by single-crystal XRD analysis. If solubility data is not

*available, mixtures can also be prepared with equal concentrations of the racemic and enantiomer target compounds and a constant concentration of co-former.*

## DISCUSSIONS

In this study, we have identified three different co-crystal types, diastereomerically related, racemic compound and conglomerate, from a racemic compound and a co-former. Four Type-II pseudo-binary phase diagrams are constructed and three of them, in Figure 5 (left), 8 and 10, are of the compositions where the co-crystals are more stable than the pure component crystals. In the phase diagram in Figure 5 (right), the co-crystals S-Val:R-Phe is less stable than RS-Phe. For each type of co-crystal, more composition possibilities exist and the corresponding isothermal and Type-II pseudo-binary phase diagrams are schematically summarized in Scheme 2.

In the isothermal phase diagrams, the black lines show the solubility lines in a racemic compound system in absence of co-former B (either chiral or achiral): the horizontal and vertical lines represent the equilibrium solution composition in case of a liquid-solid equilibrium between the solution and pure S and R crystals, respectively. The curved line shows the equilibrium solution composition in case of a liquid-solid equilibrium between the solution and the racemic compound crystals. The intercept between the two straight lines and curved line indicates the eutectic composition at which a three phase equilibrium exists between the solution, the racemic crystal and the enantiopure crystal R or S. All red lines show the solubility lines of the same systems in the presence of a constant amount of B: the red solid lines indicate more stable solids and the red dashed lines indicate less stable solids than those in absence of B.

Similarly, in a Type-II pseudo-binary phase diagram, the black lines, solid or dashed, show the solubility of the target compounds, racemic or enantiopure, without the co-former B. In the presence of a co-former B of a constant molar fraction, a new liquid-solid equilibrium is established in the system, represented by a new phase diagram (red). The solid or dashed red lines indicate the solubility of crystals more or less stable than those without the co-former, respectively.

Phase diagrams  $a_1$ — $a_4$  demonstrate the equilibrium solution composition of diastereomerically related co-crystals R:B and S:B, such as the Phe-Val system. In  $a_1$ , both R:B and S:B co-crystals are more stable than the pure component crystals. Therefore, the red solid lines indicate the solubilities of the R:B and S:B co-crystals, which are different since the co-crystals are diastereomerically related. In  $a_2$ , both R:B and S:B co-crystals are less stable than the pure component crystals. The solubilities of the more stable pure component crystals are suggested by the black solid lines. In  $a_3$ , the S:B co-crystal is more stable than the S crystal but less stable than the RS crystal. Moreover, the R:B co-crystal is less stable than the pure component crystals. The mixture of RS-Phe+S-Val in Figure 5 (right) is an example of  $a_3$ . In  $a_4$ , the R:B co-crystal is more stable than both the RS and the R crystals but the co-crystals S:B are less stable than the S crystals. In this case, the phase diagram in the racemic or R-enantiomer

enriched region suggests the solubility of the R:B co-crystals while the rest of the phase diagram indicates the solubility of the S crystals. A typical  $a_4$  system is the RS-Val+S-Phe mixture in Figure 5 (left).

When an achiral co-former is used, the co-crystals formed are either conglomerates (Type 2 in Scheme 1) or racemic compounds (Type 3 in Scheme 1), with the rare exceptions of solid solution. Phase diagrams  $b_1$ — $b_3$  show the phase behavior of conglomerate co-crystals S:B and R:B (type 2 in Scheme 1). The phase diagram  $b_1$  describes the situation in which the enantiopure co-crystals are more stable than the pure RS crystals (such as in the case of RS-IBU+BPE system in Figure 10). Therefore, the phase diagram (red solid lines) suggest the solubilities of the two enantiopure co-crystals. In  $b_2$ , the RS crystals are still more stable than the enantiopure co-crystals in the region close to the racemic composition. Although the phase diagram with the co-former B (solid lines) is similar to the pure component phase diagram, the parts on the two sides of the eutectic points (solid red lines) show the solubilities of the enantiopure co-crystals. In  $b_3$ , the co-crystals are less stable than the pure component crystals. Therefore, the phase diagram with the presence of the co-former B is the same as that without

Phase diagrams  $c_1$ — $c_4$  describe the phase behaviors of racemic compound co-crystals RS:B (type 3 in Scheme 1). In  $c_1$ , both the racemic co-crystals RS:B and the enantiopure co-crystals R:B and S:B are more stable than the pure component crystals, for instance as in the case of RS-IBU+BPB system in Figure 8. The phase diagram (solid red lines) suggests the solubilities of the co-crystals. In  $c_2$ , the enantiopure co-crystals are more stable than the S or R crystals but the RS crystals are still more stable than the co-crystals in the region close to the racemic composition. Therefore, the parts of the phase diagram on the two sides of the eutectic points (solid red lines) show the solubilities of co-crystals R: or S:B while the region close to the middle indicates the RS crystals solubility. In  $c_3$ , the co-crystals are less stable than the pure component crystals and the phase diagram with the co-former B is the same as that without. In  $c_4$ , the RS:B co-crystals are more stable than the corresponding pure component crystals RS but the enantiopure R:B or S:B co-crystals are less stable than either R or S crystals. Therefore, the section between the eutectic points represents the solubility of the RS:B co-crystals while the two sides indicate that of the enantiopure pure component crystals R and S.

In addition to identifying co-crystal types, a Type-II pseudo-binary phase diagram also provides guidelines for the conceptual design of suitable chiral separation processes. Figure 5 gives suggestions on the chiral resolution of either Phe or Val. In absence of the chiral co-former, the recovery of enantiopure Val or Phe cannot be achieved from their racemic solutions due to racemic compound formation. By adding 18 mg/ml of the chiral co-former S-Phe, in a solution of Val ( $c_{\text{Val}} = 42$  mg/ml), R-Val can be recovered in the form of R-Val:S-Phe co-crystals, even when the original solution is racemic. The cooling crystallization of R-Val:S-Phe can be operated until around 30°C, which is the  $T_s$  of pure RS-Val. Below this temperature, the nucleation of RS-Val can contaminate the co-crystal product. In the case of Phe, without the co-former S-Val, R-Phe can be recovered by cooling

crystallization if the solution is enriched so that  $y_s < 0.1$ . By adding 24 mg/ml co-former S-Val, R-Phe can be recovered as R-Phe:S-Val co-crystals as long as the original solution has an enantiomeric excess  $E > 0.4$  (corresponding to  $y_s < 0.3$ ). It is estimated from Equation 2 that if the amount of S-Val increases to around 35 mg/ml S-Val, R-Phe:S-Val co-crystals can be recovered from a racemic Phe mixture.

The achiral co-former BPN co-crystallizes with IBU as racemic compounds, which is not ideal for chiral separation techniques. However, the change in the position of the eutectic points can still reduce the requirement for the application of chiral separation: for instance, without co-crystallization, preferential crystallization could be applied on the IBU system if the solution is enriched with 95% of S-enantiomer, for instance by chiral chromatography<sup>30</sup>. With the co-former BPN, the requirement of enrichment is decreased to only 90%. Therefore, with a racemic compound co-crystal, a relatively less demanding chiral separation process can be designed.

With the structural information from the single crystal, IBU is confirmed to co-crystallize as a conglomerate using the co-former BPE. The IBU:BPE co-crystal is, to our knowledge, the second co-crystal conglomerate structure reported from a racemic compound, after the system of Naproxen-Nicotinamide<sup>11</sup>. The conversion from the racemic compound IBU to the conglomerate-forming IBU:BPE co-crystal enables the application of chiral separation techniques such as preferential crystallization. For instance, if a Heptane solution of IBU, with total concentration of 180 mg/ml, contained an initial enantiomeric excess  $E$  (e.g.,  $E = 6\%$ ), a direct crystallization step cannot recover enantiopure solid phase as can be seen from the phase diagram (black) in Figure 10. However, by adding 40 mg/ml BPE into the system, the initial enantiomeric excess can all be recovered as enantiopure IBU:BPE co-crystals.

Co-crystallization provides opportunities for chiral separation of racemic-compound-forming molecules. Type-II pseudo-binary phase diagrams can be used to identify the types of co-crystals from racemic compounds, as has been proved by the three systems investigated in this study. Based on this result, a systematic screening method has been developed to search for suitable co-crystal combinations of the target compounds for chiral separation opportunities. A schematic demonstration of the newly developed screening method is shown in Scheme 3.

Stage I—III in the screening method is to identify the formation of co-crystals between the target chiral compound (A) and the selected co-former (B), as described by ter Horst *et al.* in a previous study on discovering new co-crystals.<sup>19</sup> The enantiomer of A is used if B is chiral and a racemic mixture of A is used if B is achiral.

In stage IV, a Type-II pseudo-binary phase diagram is constructed to determine the type of co-crystal between A and B (see co-crystal types in Scheme 1) and the corresponding co-crystal structures are identified by Single Crystal XRD (SCXRD) in Stage V. The Type-II pseudo-binary phase diagrams (see the complete list of possible phase diagrams in Scheme 2) are used in Stage VI to select a suitable chiral separation technique.

In the case of B being an achiral co-former, a short-cut approach can be employed for quick screening. Crystals can be formed from two solutions of compositions  $[x_A^*(T_r), x_B^*(T_r)]$ , where A is one enantiomer in one solution and is the racemic mixture in the other. The crystals from the two solutions are then analyzed by XRPD and the obtained powder patterns are first compared with those of pure component crystals to determine whether co-crystals are formed. If so, the two XRPD patterns are compared with each other to determine whether conglomerate co-crystals are formed, as the patterns are the same from a conglomerate co-crystal system. In the case where solubility data is not available, two mixtures containing equal concentrations of one enantiomer and the racemic mixture of the target compound can be used, as in the case of IBU + BPN system in this study. This short-cut procedure (see Scheme 3) determines whether or not the combination A-B forms desired co-crystal types without the two pseudo-binary phase diagrams. As a trade-off, relevant guidelines for chiral separation process design provided by Type-II pseudo-binary phase diagrams are not available from the short-cut step.

#### 4. CONCLUSIONS

A systematic phase-diagram-based screening method to identify the co-crystal types from racemic-compound-forming molecules has been developed and experimentally verified by studying 3 chiral systems. The system of Phe and Val in 20/80 % v/v ethanol/water mixtures form diastereomerically related co-crystals. The non-chiral co-former BPN forms racemic compound co-crystals with IBU. The racemic compound IBU is converted into a conglomerate co-crystal by using the non-chiral co-former BPE. These three chiral compound systems have different Type-II pseudo-binary phase diagrams, which can be used to identify their co-crystal types and co-crystallization conditions. Such pseudo-binary phase diagrams enable a structured exploration of co-crystal phase diagrams of chiral compounds and their chiral separation opportunities.

#### REFERENCES

1. Lorenz, H.; Seidel-Morgenstern, A., Processes To Separate Enantiomers. *Angewandte Chemie International Edition* **2014**, *53* (5), 1218-1250.
2. Rouhi, A. M., Chirality at work. *Chem. Eng. News* **2003**, *81* (18), 56-61.
3. Ward, T. J.; Ward, K. D., Chiral Separations: A Review of Current Topics and Trends. *Analytical Chemistry* **2012**, *84* (2), 626-635.
4. Coquerel, G., Preferential Crystallization. In *Novel Optical Resolution Technologies*, Sakai, K.; Hirayama, N.; Tamura, R., Eds. Springer Berlin Heidelberg: Berlin, Heidelberg, 2007; pp 1-51.
5. Sogutoglu, L.-C.; Steendam, R. R. E.; Meekes, H.; Vlieg, E.; Rutjes, F. P. J. T., Viedma ripening: a reliable crystallisation method to reach single chirality. *Chemical Society Reviews* **2015**, *44* (19), 6723-6732.

6. Srisanga, S.; ter Horst, J. H., Racemic Compound, Conglomerate, or Solid Solution: Phase Diagram Screening of Chiral Compounds. *Crystal Growth & Design* **2010**, *10* (4), 1808-1812.
7. Noorduyn, W. L.; Kaptein, B.; Meekes, H.; van Enkevort, W. J. P.; Kellogg, R. M.; Vlieg, E., Fast Attrition-Enhanced Deracemization of Naproxen by a Gradual In Situ Feed. *Angewandte Chemie International Edition* **2009**, *48* (25), 4581-4583.
8. Li, W. W.; Spix, L.; de Reus, S. C. A.; Meekes, H.; Kramer, H. J. M.; Vlieg, E.; ter Horst, J. H., Deracemization of a Racemic Compound via Its Conglomerate-Forming Salt Using Temperature Cycling. *Crystal Growth & Design* **2016**, *16* (9), 5563-5570.
9. Spix, L.; Alfring, A.; Meekes, H.; van Enkevort, W. J. P.; Vlieg, E., Formation of a Salt Enables Complete Deracemization of a Racemic Compound through Viedma Ripening. *Crystal Growth & Design* **2014**, *14* (4), 1744-1748.
10. Wermester, N.; Aubin, E.; Pauchet, M.; Coste, S.; Coquerel, G., Preferential crystallization in an unusual case of conglomerate with partial solid solutions. *Tetrahedron: Asymmetry* **2007**, *18* (7), 821-831.
11. Neurohr, C.; Marchivie, M.; Lecomte, S.; Cartigny, Y.; Couvrat, N.; Sanselme, M.; Subra-Paternault, P., Naproxen–Nicotinamide Cocrystals: Racemic and Conglomerate Structures Generated by CO<sub>2</sub> Antisolvent Crystallization. *Crystal Growth & Design* **2015**, *15* (9), 4616-4626.
12. Elacqua, E. Supramolecular chemistry of molecular concepts:tautomers, chirality, protecting groups, trisubstituted olefins, cyclophanes, and their impact on the organic solid state. University of Iowa, 2012.
13. Grothe, E.; Meekes, H.; Vlieg, E.; ter Horst, J. H.; de Gelder, R., Solvates, Salts, and Cocrystals: A Proposal for a Feasible Classification System. *Crystal Growth & Design* **2016**, *16* (6), 3237-3243.
14. Springuel, G.; Robeyns, K.; Norberg, B.; Wouters, J.; Leyssens, T., Cocrystal Formation between Chiral Compounds: How Cocrystals Differ from Salts. *Crystal Growth & Design* **2014**, *14* (8), 3996-4004.
15. Sánchez-Guadarrama, O.; Mendoza-Navarro, F.; Cedillo-Cruz, A.; Jung-Cook, H.; Arenas-García, J. I.; Delgado-Díaz, A.; Herrera-Ruiz, D.; Morales-Rojas, H.; Höpfl, H., Chiral Resolution of RS-Praziquantel via Diastereomeric Co-Crystal Pair Formation with l-Malic Acid. *Crystal Growth & Design* **2016**, *16* (1), 307-314.
16. Berry, D. J.; Seaton, C. C.; Clegg, W.; Harrington, R. W.; Coles, S. J.; Horton, P. N.; Hursthouse, M. B.; Storey, R.; Jones, W.; Frišćić, T.; Blagden, N., Applying Hot-Stage Microscopy to Co-Crystal Screening: A Study of Nicotinamide with Seven Active Pharmaceutical Ingredients. *Crystal Growth & Design* **2008**, *8* (5), 1697-1712.
17. Chen, S.; Xi, H.; Henry, R. F.; Marsden, I.; Zhang, G. G. Z., Chiral co-crystal solid solution: structures, melting point phase diagram, and chiral enrichment of (ibuprofen)<sub>2</sub>(4,4-dipyridyl). *CrystEngComm* **2010**, *12* (5), 1485-1493.
18. Reus, M. A.; van der Heijden, A. E. D. M.; ter Horst, J. H., Solubility Determination from Clear Points upon Solvent Addition. *Organic Process Research & Development* **2015**, *19* (8), 1004-1011.
19. ter Horst, J. H.; Deij, M. A.; Cains, P. W., Discovering New Co-Crystals. *Crystal Growth & Design* **2009**, *9* (3), 1531-1537.
20. de Gelder, R.; de Graaff, R. A. G.; Schenk, H., Automatic determination of crystal structures using Karle-Hauptman matrices. *Acta Crystallographica Section A* **1993**, *49* (2), 287-293.
21. Sheldrick, G., SHELXT - Integrated space-group and crystal-structure determination. *Acta Crystallographica Section A* **2015**, *71* (1), 3-8.

22. Sheldrick, G., Crystal structure refinement with SHELXL. *Acta Crystallographica Section C* **2015**, 71 (1), 3-8.
23. Prasad, G. S.; Vijayan, M., X-ray studies on crystalline complexes involving amino acids and peptides. XXI. Structure of a (1:1) complex between l-phenylalanine and d-valine. *Acta Crystallographica Section C* **1991**, 47 (12), 2603-2606.
24. Moitra, S.; Kar, T., Growth and characterization of L-valine - a nonlinear optical crystal. *Crystal Research and Technology* **2010**, 45 (1), 70-74.
25. Shiraiwa, T.; Ikawa, A.; Sakaguchi, K.; Kurokawa, H., Optical resolution of dl-amino acids with aliphatic side chain by using l-phenylalanine. *Chemistry Letters* **1984**, 13 (1), 113-114.
26. Nguyen, L. A.; He, H.; Pham-Huy, C., Chiral Drugs: An Overview. *International Journal of Biomedical Science : IJBS* **2006**, 2 (2), 85-100.
27. Chen, C. Y.; Chen, C. S., Stereoselective disposition of ibuprofen in patients with compromised renal haemodynamics. *British Journal of Clinical Pharmacology* **1995**, 40 (1), 67-72.
28. Alshahateet, S. F., Synthesis and Supramolecularity of Hydrogen-Bonded Cocrystals of Pharmaceutical Model Rac-Ibuprofen with Pyridine Derivatives. *Molecular Crystals and Liquid Crystals* **2010**, 533 (1), 152-161.
29. R Shattock, T., *Crystal engineering of co-crystals and their relevance to pharmaceutical forms*. 2017.
30. Welch, C. J., Chiral Chromatography in Support of Pharmaceutical Process Research. In *Preparative Enantioselective Chromatography*, Blackwell Publishing Ltd: 2007;pp 1-18.

# Appendix Chapter 3

## Table of Contents

1. X-ray Powder Diffraction (XRPD) for crystal composition identification (1)

## X-ray Powder Diffraction (XRPD) for crystal composition identification

XRPD diffractograms of samples taken from phase diagrams are shown here, in comparison with those calculated from single co-crystals as well as from relevant pure component crystals, in order to identify the compositions of the solid phases.

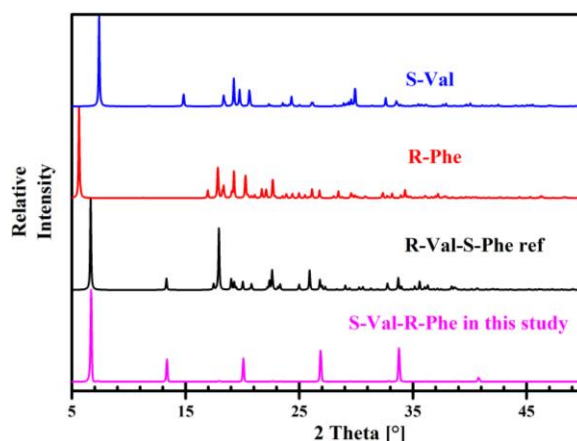


**Figure SI.** XRPD comparison between crystals collected from a sample circled in Figure 5 (right) and S-Val, R-Phe as well as R-Val-S-Phe co-crystal from literature<sup>1</sup>.

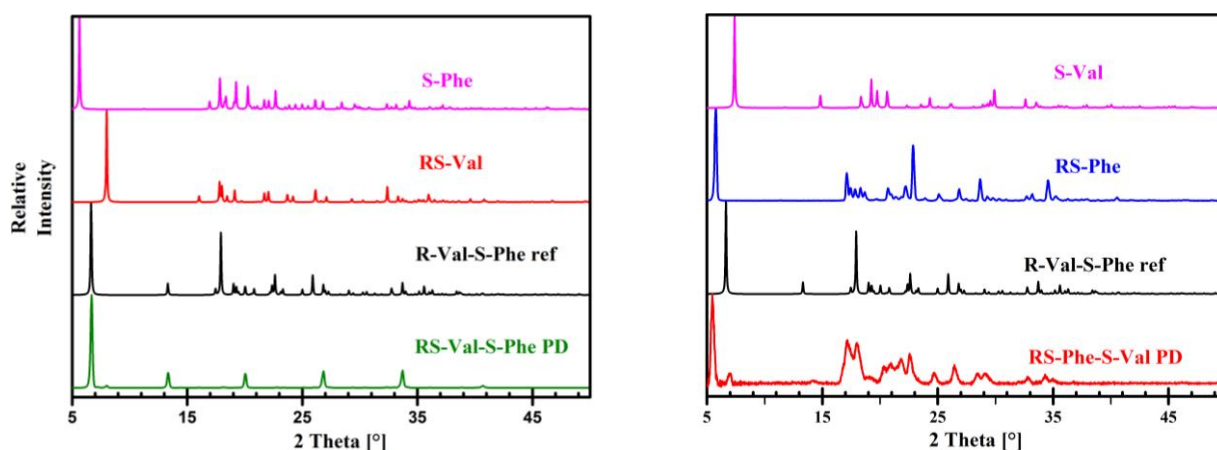


**Figure SII.** XRPD diffractograms of crystals collected at room temperature from 20/80 v/v Ethanol/Water suspensions of 42.5 mg/ml RS-Val and 18 mg/ml S-Phe (left) and of 17.5 mg/ml RS-Phe and 24.5 mg/ml S-Val (right). The diffractograms of the collected crystals were compared with those from the relevant pure components as well as the reference co-crystal R-Val-S-Phe from literature<sup>1</sup>.

In Figure SI and SII (left) the diffractograms of the collected crystals show severe preferred orientation. Only the 00l reflections are visible, which is not uncommon for powder patterns of hydrophobic amino acids and cocrystals of hydrophobic amino acids due to the layered structures of these compounds. The usual morphology of these compounds consists of very thin platelets in which the smallest dimension corresponds to the c-direction (the direction perpendicular to the layers in the crystal structure). This leads to severe preferred orientation when powder patterns are collected in reflection mode. However, the unique positions of the 00l reflections, especially the 001 and 002 reflections, make it possible to distinguish the pattern of the collected crystals from the pure S-Val and R-Phe patterns while at the same time they show a clear match with the corresponding reflections in the reference pattern for R-Val-S-Phe.

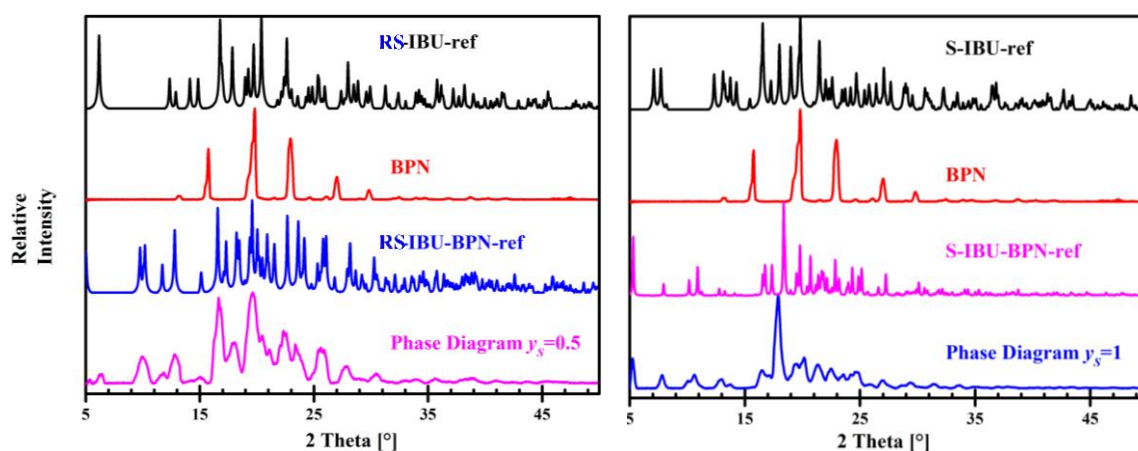


**Figure SIII.** XRPD diffractograms of crystals collected at room temperature from Heptane suspensions of 180 mg/ml RS-IBU and 40 mg/ml BPN (left) and of 180 mg/ml S-IBU and 40 mg/ml BPN (right). The diffractograms of the collected crystals were compared with those from the relevant pure components as well as the reference co-crystal RS-IBU-BPN from literature<sup>2</sup> and S-IBU-BPN from this study.

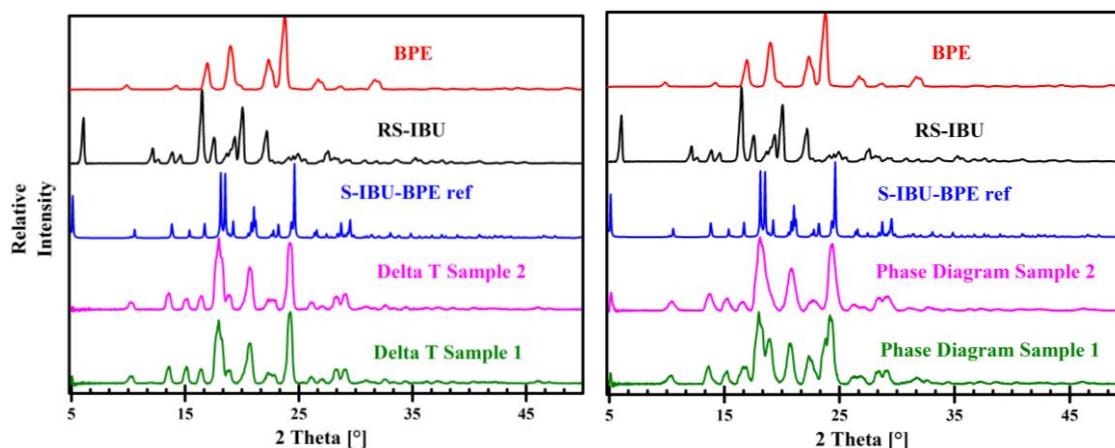


**Figure SIV.** Left: XRPD diffractograms of crystals collected from samples in temperature difference experiments of RS-IBU and BPE, as circled in Figure 7 (left). Right: XRPD diffractograms from samples in Type-I pseudo-binary phase diagram, as circled in Figure 7 (right). The diffractograms of the collected crystals were compared with those from the relevant pure components as well as the reference co-crystal S-IBU-BPE from this study.

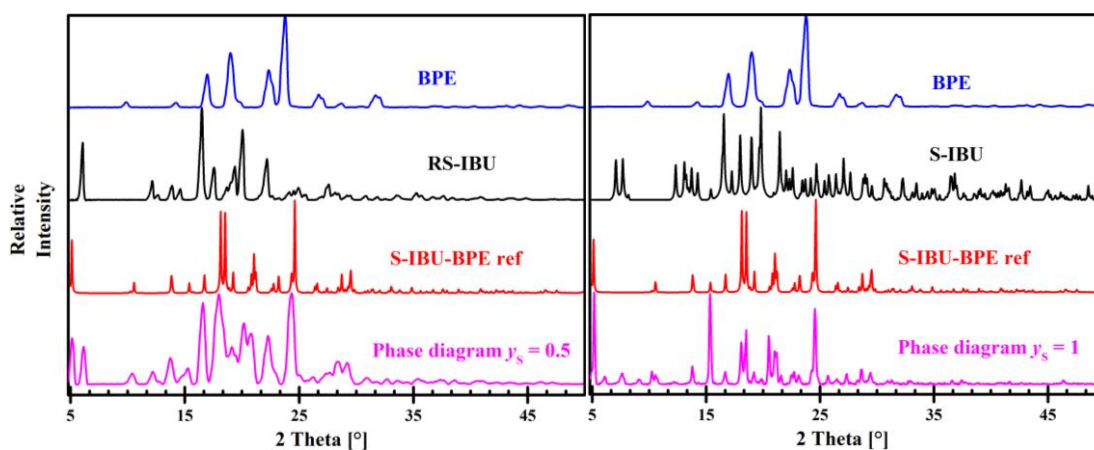


**Figure SV.** XRPD diffractograms of crystals collected at room temperature from Heptane suspensions of 180 mg/ml RS-IBU and 40 mg/ml BPE (left) and of 180 mg/ml S-IBU and 40 mg/ml BPE (right). The diffractograms of the collected crystals were compared with those from the relevant pure components as well as the reference co-crystal S-IBU-BPE from this study.

## References

- (1) Shiraiwa, T.; Ikawa, A.; Sakaguchi, K.; Kurokawa, H., OPTICAL RESOLUTION OF DL-AMINO ACIDS WITH ALIPHATIC SIDE CHAIN BY USING L-PHENYLALANINE. *Chemistry Letters* **1984**, 13, (1), 113-114.

- (2) Alshahateet, S. F., Synthesis and Supramolecularity of Hydrogen-Bonded Cocrystals of Pharmaceutical Model Rac-Ibuprofen with Pyridine Derivatives. *Molecular Crystals and Liquid Crystals* **2010**, 533, (1), 152-161.

# Chapter 4. Chiral Resolution of a Racemic Compound via its Conglomerate Co-crystal

**Keywords:** Chiral resolution, Racemic Compound, Conglomerate Co-crystal

**Abstract:** Chiral resolution techniques such as preferential crystallization are limited to chiral molecules that crystallize as conglomerate, which is the case in only roughly 10% of the reported chiral molecules. Co-crystallization provides the possibility to convert the racemic compounds, crystals formed by the majority of the chiral molecules, into conglomerates. In this study, a preferential crystallization process is developed, which is based on the conversion of the target racemic compound Ibuprofen (IBU) to its conglomerate co-crystal using the achiral co-former trans-1-(2-pyridyl)-2-(4-pyridyl)-ethylene (BPE). In the process, by three different methods, a small amount of S-IBU:BPE co-crystals is introduced into a solution of RS-IBU and BPE in Heptane to set the initial conditions for the preferential crystallization: A) direct seeding of enantiopure co-crystal, B) auto-seeding by suspension equilibration and C) enantiopure co-crystal nucleation by seeding a slightly enriched solution with BPE. Subsequently, the equilibrated suspension is cooled down and S-IBU:BPE co-crystals can be collected as product. The obtained co-crystal product, under the operation conditions tested, reaches a maximum enantiomeric excess of 95%. The enantiopurity of the final product is significantly influenced by two factors in the process: the process time and the final temperature. If the suspension does not have sufficient time to equilibrate at the starting temperature, a larger amount of the counter enantiomer co-crystal compound R-IBU:BPE contaminates the final product, presumably because the R-co-crystals are not fully dissolved before the cooling step. If the final temperature is lowered, significant crystallization of R-IBU:BPE takes place and the product is contaminated. This co-crystallization-mediated preferential crystallization process, which, to our knowledge, has not been reported before, opens a new process route to recover enantiopure products of a racemic-compound-forming chiral target molecules.

## 1. INTRODUCTION

Enantiomers often have drastic pharmacological and toxicological differences and this has stimulated the development of chiral resolution techniques.<sup>1-2</sup> Crystallization-based chiral resolution techniques have proven to be effective in achieving high enantiopurity in the final product by essentially one step, thanks to the unrivaled high selectivity of chiral crystal structures of enantiopure compounds for only one of the enantiomers.<sup>1, 3</sup> One intrinsic drawback of techniques such as preferential crystallization<sup>4</sup> is that the target compound has to form a conglomerate, a racemic physical mixture of enantiopure crystals, from racemic solutions. However, only 10% of the reported chiral molecules crystallize as conglomerates. Most chiral compounds form racemic compounds, crystals in which both enantiomers are evenly distributed in the lattice<sup>5</sup>, which are not ideal, if not impossible, for the application of crystallization-based chiral resolution techniques.

Various approaches have been developed to change the solid state of a racemic compound towards conglomerate behavior to enable crystallization-based chiral resolution techniques. The target molecules can be chemically modified into a derivative, which then potentially crystallize as a conglomerate.<sup>6</sup> Salt formation is another approach to convert a racemic compound to a corresponding conglomerate with often improved work-up towards the enantiopure enantiomer, such as the conglomerate salts of Mandelic acid and Phenylalanine<sup>7-9</sup>. Moreover, preferential crystallization has been successfully applied on racemic compounds via their conglomerate solvate, for instance the monohydrate of Asparagine<sup>10</sup>.

Co-crystallization<sup>11-12</sup> provides an additional approach in forming suitable crystalline structures for chiral resolution using either chiral or achiral co-formers. Co-crystals are defined as crystals of one target compound plus either one neutral co-former or at least two ions<sup>13</sup> and in this paper we focus on the former case. On the one hand chiral co-formers could selectively co-crystallize with only one of the enantiomers and such enantiospecific co-crystallization has been developed as an effective chiral resolution techniques for racemic compounds. For instance, (RS)-2-(2-oxopyrrolidin-1-yl)butanamide has been successfully resolved via a selective co-crystallization with the chiral co-former S-Mandelic acid in Acetonitrile<sup>14</sup>. On the other hand, achiral co-formers can co-crystallize with a racemic compound forming system into its conglomerate co-crystals, for instance the co-crystals from RS-Naproxen and Nicotinamide, which are then suitable for crystallization-based chiral resolution techniques such as preferential crystallization<sup>15</sup>. In this study, we experimentally verify the feasibility of a conglomerate co-crystal mediated preferential crystallization of a racemic compound, which, to the best of our knowledge, has never been reported.

Ibuprofen (IBU) is one of the top ten drugs sold worldwide and is currently marketed as a racemate, although only its S-enantiomer contains the desired bioactivity<sup>16-17</sup>. Chiral resolution is difficult to be directly applied on IBU due to its racemic compound solid state. An achiral co-former trans-1-(2-pyridyl)-2-(4-pyridyl)-ethylene (BPE) has been reported to convert the racemic compound

IBU into its conglomerate co-crystal<sup>18</sup>. In this study, three different operation procedures of the developed chiral resolution method are introduced as well as the product characterization technique combining <sup>1</sup>H-NMR and Polarimetry measurement. Additionally, the effects of various operation parameters on the enantiopurity of the crystalline product from this chiral resolution method are investigated.

## 2. EXPERIMENTAL

**Materials.** Racemic Ibuprofen (RS-IBU, 99%) and trans-1-(2-pyridyl)-2-(4-pyridyl)-ethylene (BPE, 98%) were obtained from Santa Cruz Biotechnology. S-Ibuprofen (S-IBU, 99%), Heptane (99%) and ethanol absolute (99.5%) were supplied by Sigma Aldrich. Methanol-d4 (water <0.03%) was purchased from Eurosi-top. All chemicals were used without further purification.

**Phase Diagram Construction.** The Cyrstal16 (Technobis B.V.) equipment was used for the construction of all phase diagrams. A suspension with a known composition was prepared using a physical mixture of the enantiopure and the racemic IBU, with or without the co-former BPE, in 1 mL Heptane. The suspension was linearly heated (0.3°C/min) until full dissolution, followed by a cooling step (-0.3°C/min) during which recrystallization took place. The heating-cooling cycle was repeated for three times. The transmission of light through the samples was automatically recorded as a function of temperature and time. The temperature at which a transmission of 100% was reached was taken as the clear point temperature of the measured sample composition. The clear point temperatures were assumed to be equal to the saturation temperature  $T_s$ , the temperature at which a solution with the sample composition would be in equilibrium with the solids that were dissolved. A series of samples was prepared in which the total molar fraction  $x=x_S+x_R$  of both S- and R-IBU was constant, as well as the molar fractions of Heptane and the co-former BPE so that only the enantiomeric excess in the samples series varied through the solvent and co-former free molar fraction  $y_S = x_S/(x_R+x_S)$  of S-IBU. The measured saturation temperature of the series of samples then was plotted against this molar fraction  $y_S$  of S-IBU.

Theoretical phase diagrams of the enantiopure IBU:BPE co-crystals were constructed based on the modified Van 't Hoff equation using the enantiopure co-crystal solubility product  $x_i \cdot x_{BPE}$ :

$$\ln(x_i \cdot x_{BPE}) = -\frac{\Delta H}{R} \left( \frac{1}{T_s} - \frac{1}{T_0} \right) \quad \text{Equation 1}$$

Here  $x$  is the molar fraction of the IBU and the BPE; the subscription  $i$  stands for either R- or S-IBU;  $T_s$  (K) is the saturation temperature;  $\Delta H$  (J/mol) and  $T_0$  (K) are used as fitting parameters to the experimentally measured saturation temperature  $T_s$  of the samples with known composition ( $x_i, x_{BPE}$ ). The effect of the counter enantiomer on the solubility is therefore assumed negligible.

**Analytical Method.** The ratios between IBU and BPE of the chiral resolution product were measured by <sup>1</sup>H-NMR. A sample of *ca.* 30 mg was dissolved in 1 mL Methanol D4 and was analyzed in Agilent Direct Drive 400 MHz NMR, with a relaxation time of 40 s and scan number of 16. Peaks

between the chemical shifts of 7.32-9.04 ppm belong to BPE and amount to 10 protons while the peak at 3.10-3.42 ppm represents IBU and amounts to 1 proton. The weighed ratio between the integrations of these two regions was used as the molar ratio of BPE and IBU in the sample.

The enantiomeric excess  $E$  of the crystalline samples was determined based on the optical rotation of their ethanol solution. A calibration sample series of 2 ml ethanol solution mixture of RS-, S-IBU and BPE (in total *ca.* 50 mg) with known enantiomeric excess were prepared and the optical rotation of the mixtures were measured by Polarimeter MCP 500 (Anton Paar), at 20°C with a wavelength of 589 nm. The specific optical rotation  $\alpha_{589}^{20}$  of each mixture was calculated as follows:

$$\alpha_{589}^{20} = \frac{\alpha}{l * c_{IBU}} \quad \text{Equation 2}$$

Here  $\alpha$  (°) is the optical rotation of the ethanol solution measured by the polarimeter;  $c_{IBU}$  (g/ml) is the concentration of IBU in the solution;  $l=1$  dm is the length of the pathway of light through the solution sample. A calibration line was established by plotting the specific rotation  $\alpha_{589}^{20}$  of each calibration sample series against the enantiomeric excess  $E$ . The calibration line in Figure 1 was used to determine the enantiomeric excess of the chiral resolution products.

The crystalline product from the model system can contain all three solute compounds, which are S- and R-IBU as well as the co-former BPE. Therefore, a method combining  $H^1$ -NMR and Polarimetry has been developed to analyze the composition of the products from the chiral resolution processes. First, the NMR determines the molar ratio  $p_{IB}$  between the total IBU (both S- and R-enantiomers) and BPE. Subsequently, the optical rotation of the samples were measured by the polarimeter. Using equation 3, the enantiopurity of each product was calculated.

$$E = \frac{\alpha}{c_{sam}} \left( \frac{1 + \frac{Mw_B}{p_{IB} Mw_I}}{57.4} \right) \quad \text{Equation 3.}$$

Here  $c_{sam}$  is the concentration of the ethanol solution from each product,  $p_{IB}$  is the molar ratio IBU/BPE measured by NMR,  $Mw$  is the molar weight of BPE (B) and IBU (I). Constants 57.4 were obtained from the linear relationship between  $E$  and  $\alpha_{589}^{20}$  in the calibration line in Figure 1 (left).

In order to determine the accuracy of this analytical method, a series of verification experiments were conducted. First, three 1 ml Methanol- $d_4$  solutions containing various compositions of IBU and BPE were prepared and analyzed by  $H^1$ -NMR using either S- or R-enantiomer or a mixture of both. The measured molar ratios IBU/BPE were compared with the actual values in Table 1. The comparison between the measured and the actual IBU/BPE molar ratios shows the accuracy of the NMR measurement: The largest relative error of the three measurements was 1.6%. This was taken as the error in the chiral resolution results.

**Table 1.** Accuracy in measuring molar ratio between IBU and BPE in Methanol-*d*4 solvent by NMR. *c* (mg/ml) are concentration of RS-IBU (*RS*), S-IBU (*S*) and BPE (*B*) in the test solutions.

Exp.	<i>c</i> <sub>RS</sub> (mg/ml)	<i>c</i> <sub>S</sub> (mg/ml)	<i>c</i> <sub>B</sub> (mg/ml)	IBU/BPE Actual	IBU/BPE NMR	Error
1	11.2	5.9	13.7	1.101	1.116	1.30%
2	23.8	0	6.6	3.181	3.164	0.60%
3	0	8.2	20.5	0.353	0.347	1.60%

The calibration line using the polarimeter does not account for the effects of the co-former BPE on the optical rotation. Therefore, the effect of BPE concentrations on the specific optical rotations of S-IBU-BPE mixtures was tested and the result (see Figure 1, right) indicates an average relative error of 1.3%. This relative error, along with the standard deviation of the linear correlation in Figure 1 (left), was included in estimating the results of preferential crystallization processes.

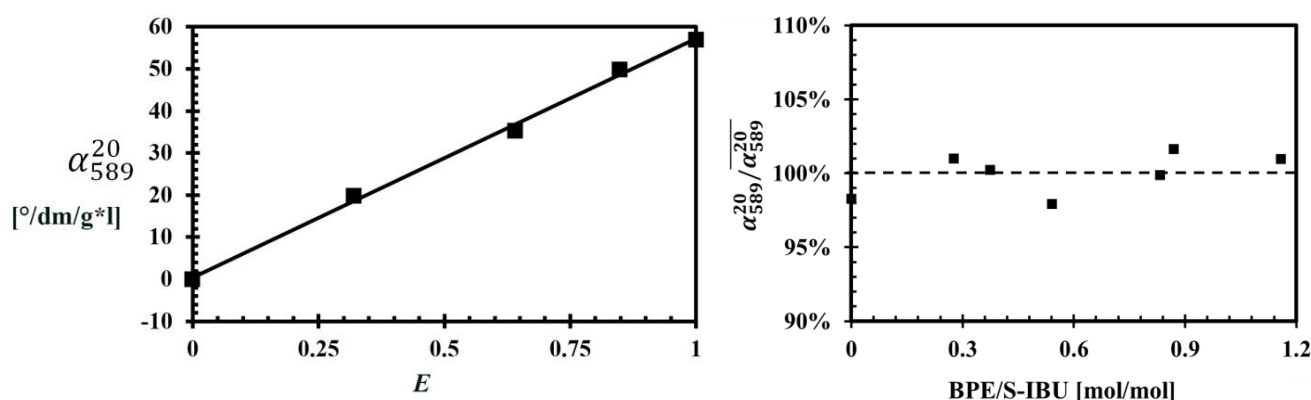


**Figure 1.** Left: Linear correlation between specific optical rotation  $\alpha_{589}^{20}$  and enantiomeric excess *E* of IBU-BPE mixtures. Right: Effect of BPE/IBU molar ratios on the deviation of  $\alpha_{589}^{20}$  of BPE-S-IBU mixtures from the average value  $\overline{\alpha_{589}^{20}}$ , indicated by the dashed line.

**Preferential Crystallization Experiments.** The conditions of the preferential crystallization (PC) experiments are shown in Table 2. Experiments R<sub>1</sub>, R<sub>2</sub> and 1-8 were conducted in 8 ml glass vials in a Crystalline (Technobis B.V.). The larger scale experiment 9 was performed in a 50 ml glass vessel in an Easymax workbench (Mettler Toledo B.V.).

Three seeding methods A, B and C were used. In method A (direct seeding), a Heptane suspension was prepared from both BPE (40 mg/ml) and RS-IBU (180 mg/ml). The suspension was then linearly heated up to its saturation temperature  $T_H$  (1°C/min) and S-IBU:BPE co-crystals (20 mg/ml, *ca.* 95 wt% co-crystal purity) were seeded into the solution. In method B (auto-seeding), the initial Heptane suspension was prepared with S-IBU (11 mg/ml) and RS-IBU (180 mg/ml) and BPE (50 mg/ml) and the suspension was heated to  $T_H$ . In the third method C (nucleation by seeding BPE), the initial suspension contained only RS- (180 mg/ml) and S-IBU (11 mg/ml) and was seeded with BPE crystals (50 mg/ml) at  $T_H$ .

The resulting suspension from each method was held at  $T_H$  for a duration of  $t_H$  before it was linearly cooled down to  $T_L$  with a cooling rate  $R_c$ . The suspension was held at  $T_L$  for a duration of  $t_L$  before the solid phase was recovered by a glass filter preheated at 50°C in an oven. The crystalline product was then sent for purity and enantiopurity analysis by  $^1\text{H-NMR}$  and polarimeter. The operational condition  $R_c$ ,  $T_H$ ,  $t_H$ ,  $T_L$  and  $t_L$  were varied in order to investigate their effects on the enantiopurity of the final products (see Table 2).

**Seed Preparation.** The enantiopure co-crystal seeds of S-IBU:BPE were prepared by mixing equimolar of S-IBU (80 mg/ml) and BPE (73 mg/ml) with Heptane. The suspension was stirred at room temperature for 3 days before the solid phase was harvested by a glass filter. The recovered crystals were sent for analysis by XRPD and  $^1\text{H-NMR}$ .

**Table 2.** Operation Parameters used in the chiral resolution experiments:  $T_H$  is the maximum and starting temperature in the process;  $T_L$  is the minimum and final temperature in the process;  $t_H$  is the duration of holding at the maximum temperature before cooling;  $t_L$  is the duration of holding at the minimum temperature before harvesting the solid phase;  $R_c$  is the cooling rate from  $T_H$  to  $T_L$ ;  $c$  is the overall concentration of RS-IBU (RS), S-IBU (S) or BPE (B) in the suspension;  $V$  is the volume of the crystallization suspension.

Experiment Nr.	R <sub>1</sub>	R <sub>2</sub>	1	2	3	4	5	6	7	8	9
$T_H$ (°C)	53	50	58	58	58	58	58	58	58	58	58
$T_L$ (°C)	N.A.	N.A.	53	53	53	53	53	50	53	53	53
$t_H$ (hr)	24	24	0.2	4	3	4	4	4	4	1	4
$t_L$ (hr)	N.A.	N.A.	0.2	0	0	0.5	1	0.5	0.5	1	0
$R_c$ (°C/min)	N.A.	N.A.	0.1	0.1	0.1	0.1	0.1	0.1	1	0.1	0.1
$c_{RS}$ (mg/ml)	180	180	180	180	180	180	180	180	180	180	180
$c_S$ (mg/ml)	11	11	10*	11	11	11	11	11	11	11	11
$c_B$ (mg/ml)	50	50	50	50	50	50	50	50	50	50	50
$V$ (ml)	4	4	4	4	4	4	4	4	4	4	20
Seeding Method	N.A.	N.A.	A	B	C	B	B	B	B	B	B

\*The S-co-crystal seeds prepared in Exp. 1 were of *ca.* 95 wt% co-crystal purity.

Therefore, a slightly lower enantiomeric excess was initially present in the suspension.

### 3. RESULTS AND DISCUSSIONS

**Model System: IBU-BPE Conglomerate Co-crystals.** Ibuprofen (IBU) crystallizes as a racemic compound<sup>19</sup>, which prevents the effective application of crystallization-based chiral resolution. The formation of a conglomerate co-crystal has been reported between RS-IBU and the achiral co-former trans-1-(2-pyridyl)-2-(4-pyridyl)-ethylene (BPE)<sup>18</sup> (see detailed description of the IBU:BPE co-crystals in Chapter 3). The crystal structure of IBU:BPE has the space group P21 and contains one BPE and one IBU (either S- or R-enantiomer) molecule in the unit cell.

**The Design of a Preferential Crystallization Experiment for IBU:BPE Conglomerate Co-crystals.** In a typical preferential crystallization (PC) experiment of a pure component (non-co-crystal) system, the starting suspension, equilibrated at the starting temperature, is composed of a racemic solution phase and a solid phase containing enantiopure seed crystals from the desired enantiomer, via manual or auto-seeding. The suspension is cooled down, which creates supersaturation for both the desired and the undesired enantiomers. The solution phase is gradually enriched with the undesired enantiomer as the desired one keeps crystallizing via the growth and the secondary nucleation of the seed crystals. When the suspension reaches the end temperature, ideally the desired enantiomer reaches equilibrium and the undesired enantiomer has not yet crystallized. In this way, a maximum amount of enantiopure product is recovered. If the experiment would continue, the undesired enantiomer, which is in the metastable state, will eventually crystallize and bring the solution phase to its true racemic equilibrium in solution, while contaminating the crystalline product, a result that needs to be prevented.

The PC experiment of a conglomerate co-crystal system is slightly different from that of a pure component system, as one additional compound, the co-former, is involved. The solubility of the co-crystal is then not solely dependent on the concentration of the enantiomers but also on that of the co-former. In turn this co-former concentration decreases when the preferred co-crystal crystallizes out and therefore changes the concentration product of the counter enantiomer co-crystal. This complicates the design of the process, for instance the estimation of the maximum product that can be recovered from a PC experiment, as will be described in later paragraphs.

Nevertheless, for the design of a PC experiment for conglomerate co-crystals, the same prior information needs to be known as required for a pure component system: 1) the confirmation that the target system forms conglomerates; 2) the composition and temperature of the initial suspension; 3) the composition and temperature of the final equilibrium point, where crystals of both enantiomers are in equilibrium with the solution phase and 4) the composition of an ideal end point, where maximum product is recovered and no contamination from the undesired enantiomer takes place. In the following paragraphs, the prior information for the PC of IBU:BPE co-crystals is given and explained.

## Conglomerate Co-crystal Formation From RS-IBU and BPE

The IBU:BPE is confirmed as conglomerate co-crystals from previous studies (see Chapter 3). To understand the phase behavior in this system, a pseudo-binary phase diagram is constructed in this study. A pseudo-binary phase diagram describes the saturation temperature  $T_s$  change by varying the ratio between the two enantiomers, while keeping the molar fraction of Heptane and BPE, if applicable, constant. Three pseudo-binary phase diagrams (PD 1—3) are experimentally constructed and shown in Figure 2.

PD 1 is constructed with the concentration  $c_{IBU}$  of 180 mg/ml in absence of BPE. It can be clearly seen that PD 1 represents the racemic compound IBU system without the co-former, where two eutectic points are symmetrically located on the two sides of the racemic composition. The region between the eutectic points expresses the solubility of RS-IBU while the two sides show the solubilities of the enantiopure IBU crystals.

On the other hand, PD 2 and 3 represent the conglomerate co-crystal system IBU:BPE and have one eutectic point at the racemic composition. PD 2 uses the same  $c_{IBU}$ =180 mg/ml as PD1 but with a co-former BPE concentration  $c_B$  = 40 mg/ml. PD 3 is made with a slightly higher  $c_{IBU}$  (191 mg/ml) and  $c_B$  (50 mg/ml). In PD2 and PD3, each side of the phase diagrams indicates the solubility of the enantiopure co-crystals. The apparent difference between PD2 with and PD1 without BPE confirms that the IBU:BPE are indeed conglomerate co-crystals. Moreover, the solubility of the co-crystal is significantly lower than that of IBU, as the saturation temperatures  $T_s$  at the racemic composition of PD 2 and 3 are more than 18°C higher than that of PD1.

### Determination of the Starting Point 0

The second step is to determine the temperature and the composition of the starting suspension for which we used the pseudo-binary phase diagrams PD2 and PD3. The composition of the starting racemic solution is set to be 180 mg/ml RS-IBU and 40 mg/ml BPE. For this composition at equilibrium at 57.5°C, which is the saturation temperature  $T_s$  of the eutectic composition in PD 2, all the RS-IBU and BPE are dissolved. Afterwards, S-co-crystals are seeded, which contain around 11 mg/ml S-IBU and 10 mg/ml BPE (1:1 stoichiometric ratio of the two compounds). If the temperature keeps on increasing from 57.5°C, the S-co-crystal seeds start to dissolve, until 59.2°C, at which the entire solid phase is dissolved and the solution is corresponding to the circled point on PD3. In this case, no seeds are available for the PC experiment. In the present study, we select 58°C as the starting temperature  $T_H$  to ensure full dissolution of the R-co-crystals, while keeping enough S-co-crystal seeds available for the PC. The solution of the starting suspension is then slightly enriched with S-IBU but for simplicity, we assume the starting solution composition is still racemic (180 mg/ml RS-IBU and 40 mg/ml BPE). This solution composition of the starting suspension is named point 0 (Table 3).

## Determination of the Equilibrium Point 2

The end temperature  $T_L$  of the PC experiments is selected to be 53°C, which is significantly higher than the  $T_s$  of the RS-IBU, indicated by PD1, to prevent the crystallization of both RS-IBU and the R-co-crystals. The equilibrium composition of the solution phase at 53°C is determined via a reference experiment  $R_1$ , in which a Heptane suspension of 180 mg/ml RS-IBU, 11 mg/ml S-IBU and 50 mg/ml BPE was equilibrated at 53°C for 24 h.

In experiment  $R_1$  the IBU/BPE molar ratio of the solid phase, recovered from the equilibrated suspension at 53°C, was measured as  $p_{IB} = 1.13 \pm 0.02$ . This result indicates that the solid phase contains not only R- and S-co-crystals but also some pure RS-IBU crystals (*ca.* 6.3% wt), as pure co-crystals are expected to have a  $p_{IB} = 1$  as they have a 1:1 molar ratio of IBU/BPE. It is assumed that these RS-IBU crystals were the results of evaporation of the mother liquor between recovered crystals, in absence of a proper washing solvent during filtration. Therefore, in Figure 3 (left), only the molar distributions of the two enantiomers in co-crystals are displayed, since the RS-IBU was assumed to be fully dissolved during the experiments. This correction was performed for all the PC experiments as well.

Moreover, it was not possible to remove all crystalline product from the glass vials after the experiments. The same was also observed in all following PC experiments. In order to estimate the loss it was assumed that the solution phase in  $R_1$  has reached racemic equilibrium in the end of the experiment. If no crystals were lost during filtration, based on the amount and composition of the collected solid phase, the calculated solution composition in  $R_1$  is slightly enriched with S-IBU, which is contractor to the equilibrium assumption. By increasing the amount of solid phase by 4%, which is assumed to be lost during the filtration step, the calculated solution phase is then racemic. In Figure 3 (left), the amount of co-crystal phase from  $R_1$  are shown, corrected for the assumed 4% loss. The solution composition of the equilibrated suspension at  $T_L = 53^\circ\text{C}$ , named as point 2, is calculated based on the mass balance and displayed in Table 3.

Furthermore, in order to visualize the results of all PC experiments, we plot Figure 4 (left), in which the PC starting point 0 is the origin. For every point on this plot, the y-coordinate and the x-coordinate represent the amount of crystallized S- ( $\Delta_{CS-IBU:BPE}$ ) and R-co-crystals ( $\Delta_{CR-IBU:BPE}$ ), respectively. The equilibrium point 2 is also located in this plot. From Table 3, the solution composition of point 2 is 84.5 mg/ml S-IBU, 84.5 mg/ml R-IBU and 30.6 mg/ml BPE, which accounts for a difference of approximately 10.2 mg/ml S- and R-IBU:BPE co-crystals. Therefore, point 2 is located at (10.2,10.2) in Figure 4 (left). All the other points on the plot are located following the same principle.

## Determination of the Ideal End Point 1

The estimation of the maximum recovery of S-co-crystals from a PC experiment, requires the location of the ideal end point, named as point 1. To locate this point, two schematic process lines

originated from point 0, the solution composition at the start of the PC, and point 2, the final equilibrium composition, are used. The two lines are named process lines as they describe two sequential processes, which theoretically take place in a PC experiment. However, the actual PC process is likely deviated from the two lines, which is why they are only schematic. The first schematic process line, also indicated by a part of the y-axis in Figure 4 (left), starting from point 0, describes the solution composition change during the process where only S-IBU:BPE crystallizes and R-co-crystals remain dissolved. Along this line, the R-IBU concentration keeps constant but equimolar S-IBU and BPE are removed from the solution phase, since they crystallize as S-co-crystals.

The second schematic process line shows the solution composition for the process in which R-IBU:BPE crystallizes until the solution phase composition reaches the thermodynamically equilibrated point 2. Two equations are used to describe the solution composition change along the second line:

$$x_S * x_B = x_{S2} * x_{B2} \quad \text{Equation 4}$$

$$\frac{(c_S - c_{S2}) + (c_R - c_{R2})}{Mw_I} = \frac{c_B - c_{B2}}{Mw_B} \quad \text{Equation 5}$$

where  $c$ ,  $x$  and  $Mw$  stand for solution phase concentration, molar fraction and molecular weight. The subscriptions S, R, B and I refer to S-IBU, R-IBU, BPE and both IBU enantiomers. The subscription 2 stands for the composition at the equilibrium point at  $T_L$  (point 2).

At point 1, the S-co-crystals are in equilibrium with the solution phase and the R-co-crystals are supersaturated in the solution but not present in the solid phase. At point 2, both S- and R-co-crystals are present in the solid phase and both are in equilibrium with the solution phase. From 1 to 2, R-co-crystals crystallize, which decrease the concentration of both R-IBU and BPE in the solution phase. The decrease of BPE concentration also leads to the undersaturation of the S-co-crystal, as the solubility of co-crystals are represented by the product of the molar fractions of the co-formers involved<sup>11</sup>. Therefore, the S-co-crystals are partially dissolved to reach equilibrium with the solution phase, which is reflected by Equation 4. The crystallization of R-IBU and the dissolution of S-IBU are always accompanied by equimolar change of BPE, as the co-crystal has a 1:1 stoichiometry ratio, which are displayed in Equation 5. The second process line is indicated as the dashed line between point 1 and 2 in Figure 4 (left). It is noted that the construction of the second schematic process line actually starts from point 2, which is located via the reference experiment R<sub>1</sub>.

The intercept of the two schematic process lines gives the location of the ideal end point 1 and the maximum recovery of S-co-crystals in a PC experiment, which is given in Table 3. A lower  $T_L$  (50°C) is investigated in this study and its corresponding ideal end point 1' and equilibrium point 2' (see Table 3) are determined using the same procedure as for point 1 and 2, based on the result from the reference experiment R<sub>2</sub>.

Points 1, 1', 2 and 2' are all shown in Figure 4 (left). Additionally, the ideal end points of PC experiments if R-co-crystals are seeded is plotted in Figure 4 (left) as blue points 3 ( $T_L = 53^\circ\text{C}$ ) and 3' ( $T_L = 50^\circ\text{C}$ ), with corresponding schematic process lines connecting point 2 and 2', respectively.

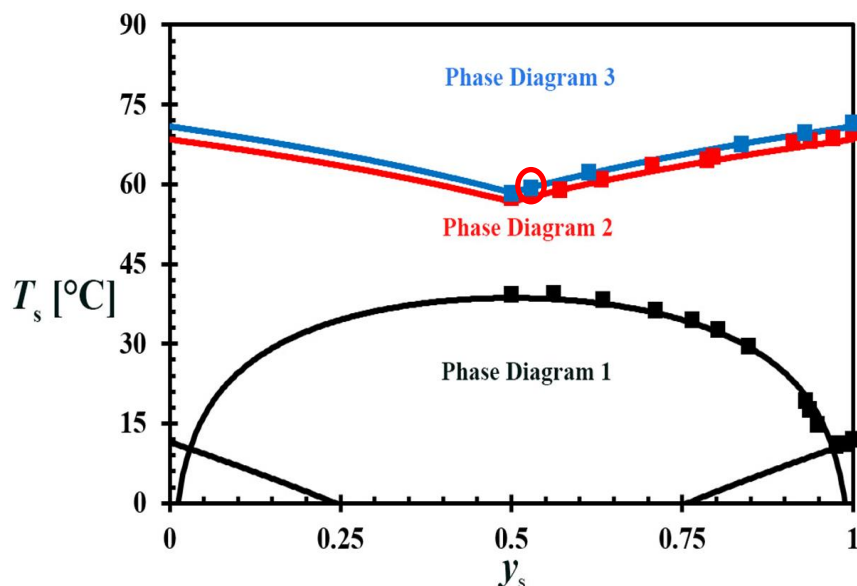


**Figure 2.** Pseudo-binary phase diagrams of IBU ( $c_{IBU} = 180 \text{ mg/ml}$ , 1) and IBU-BPE ( $c_{IBU} = 180 \text{ mg/ml}$  and  $c_{BPE} = 40 \text{ mg/ml}$ , 2, and  $c_{IBU} = 191 \text{ mg/ml}$  and  $c_{BPE} = 50 \text{ mg/ml}$ , 3) in Heptane showing the saturation temperature  $T_s$  as a function of  $y_s = x_s / (x_s + x_R)$ . The red and blue solid lines indicate the solubility of the enantiopure co-crystal R- or S-IBU:BPE, estimated from Equation 1. The black solid lines are guides to the eyes.

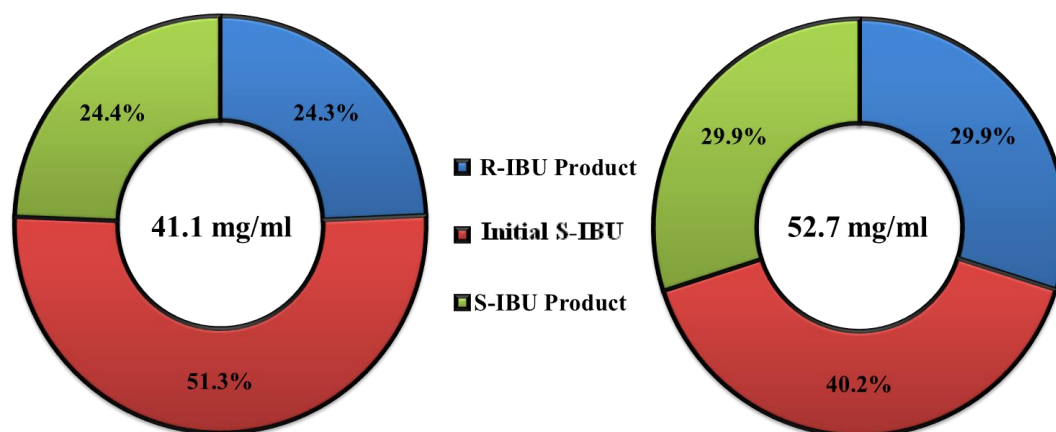


**Figure 3.** Left: Molar distribution of IBU over the co-crystalline phases obtained from the reference experiments  $R_1$  conducted at  $53^\circ\text{C}$ , assuming a solid phase loss of 4%. At  $53^\circ\text{C}$ , IBU existed in the solid phase as the R-co-crystals (blue part) and S-co-crystals (red + green parts). The red part is the amount of S-co-crystals formed from the initial S-IBU ( $c_s = 11 \text{ mg/ml}$ ), which were equivalent to the S-co-crystal seeds in all PC experiments. The green part is the

rest of the *S*-co-crystals, which are considered as the products. In addition, the masses of co-crystals recovered per unit volume of solvent are given. Right: Distribution of IBU over the co-crystalline phases obtained from the reference experiments  $R_2$  conducted at 50°C, assuming a solid phase loss of 3%. All parts have the same meaning as in  $R_1$ .

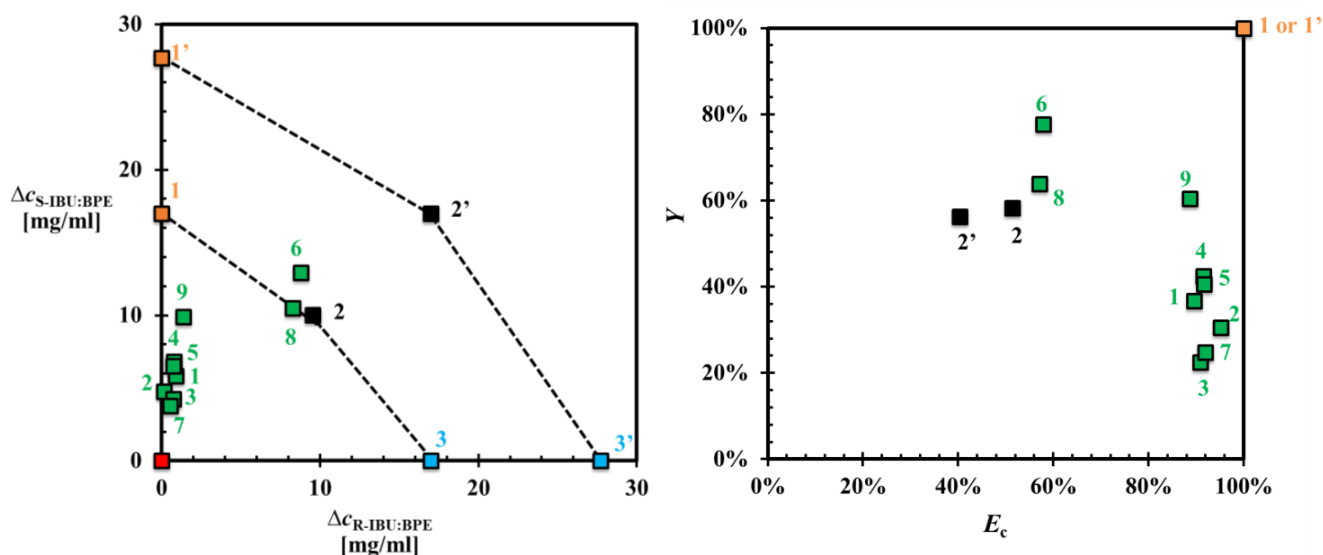


**Figure 4.** Left: Visualization of PC experiment results on a 2D plane, with the concentration of *S*- and *R*-IBU:BPE co-crystals as coordinates. The origin (red) represents the starting solution composition of a PC experiment. The orange points (1 and 1') represent the ideal end point of a PC experiment. The black points (2 and 2') show the equilibrium points of a PC experiment. The blue point displays the ideal end point if *R*-co-crystals, instead of their *S*-counterpart, are seeded in a PC experiment. The dashed lines are schematic process lines describing the crystallization of undesired co-crystals and dissolution of the desired ones. The blue points shows the ideal end points if *R*-IBU:BPE co-crystals are the desired product from a PC experiment. Right: Comparison of all PC experiments (green) by their co-crystal enantiomeric excess  $E_c$  and recovery yield  $Y$ . Point 1, 1' (orange), 2 and 2' (black) are also plotted as references.

**Table 3.** Solution concentrations of *S*-IBU ( $c_S$ ), *R*-IBU ( $c_R$ ), BPE ( $c_B$ ) and their saturation temperatures  $T_s$  of the chosen points 0—2 in Figure 4 (left).

	Overall Suspension	point 0	point 1 ( $T_L=53^\circ\text{C}$ )	$S^{**}$ ( $T_L=53^\circ\text{C}$ )	point 1' ( $T_L=50^\circ\text{C}$ )	$S$ ( $T_L=50^\circ\text{C}$ )	point 2 ( $T_L=53^\circ\text{C}$ )	point 2' ( $T_L=50^\circ\text{C}$ )
$c_S$ [mg/ml]	101	90	80.8	1	75.1	1	84.5	81.5
$c_R$ [mg/ml]	90	90	90	1.12	90	1.19	84.5	81.5
$c_B$ [mg/ml]	50	40	32.2	N.A.	27.2	N.A.	30.6	25.3
$T_s$ [ $^\circ\text{C}$ ]	59.2	57.5	N.A.*	N.A.	N.A.*	N.A.	53	50

\* $T_s$  of point 1 and 1' are not relevant in this study.

\*\* $S = (c_{B1} \cdot c_{R1}) / (c_{B2} \cdot c_{R2})$ , where the subscript 1 and 2 indicate point 1 or 1' and 2 or 2'.

**Table 4.** Comparison of characterization factors among Experiments 1—9.  $E_c$  (co-crystal Enantiomeric excess),  $\varphi$  (recovery ratio),  $Y$  (yield) and  $p_{SR}$  (ratio *S*-co-crystal products over *R*-co-crystal impurity).

Exp. Nr.	1	2	3	4	5	6	7	8	9
$E_c$ (%)	$89.6 \pm 1.3$	$95.2 \pm 1.4$	$90.9 \pm 1.4$	$91.5 \pm 1.4$	$91.7 \pm 1.4$	$57.8 \pm 0.9$	$92.0 \pm 1.4$	$57.2 \pm 0.9$	$88.7 \pm 1.3$
$Y$ (%)	$36.8 \pm 2.1$	$30.6 \pm 2.2$	$27.6 \pm 2.1$	$42.4 \pm 2.3$	$40.6 \pm 2.3$	$77.6 \pm 2.5$	$24.8 \pm 2.1$	$63.9 \pm 2.3$	$60.4 \pm 2.6$
$\varphi$ (%)	$33.7 \pm 1.9$	$24.9 \pm 1.8$	$22.5 \pm 1.7$	$34.5 \pm 1.9$	$33.0 \pm 1.9$	$63.2 \pm 2.1$	$20.2 \pm 1.7$	$52.0 \pm 1.9$	$50.2 \pm 2.1$
$p_{SR}$	$4.7 \pm 0.8$	$9.1 \pm 3.4$	$4.0 \pm 0.9$	$6.0 \pm 1.3$	$5.9 \pm 1.3$	$1.5 \pm 0.1$	$4.2 \pm 1.1$	$1.3 \pm 0.1$	$5.7 \pm 0.9$

**Preferential Crystallization.** Three experiments, Exp. 1—3, were conducted to verify that the desired enantiomer can be obtained via preferential co-crystallization with BPE, using seeding method A—C (Figure 5), respectively.

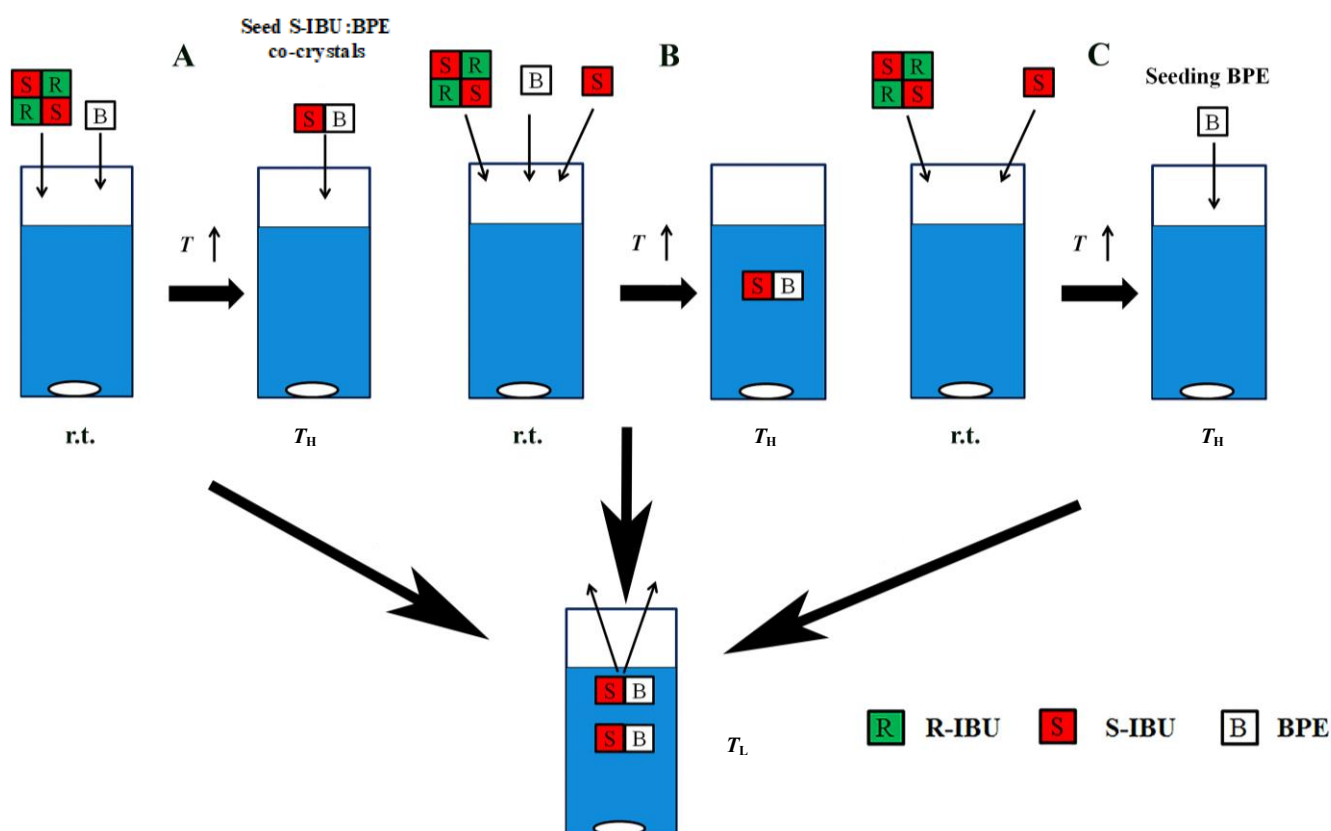


**Figure 5:** Schematic demonstration of the procedures of the 3 seeding methods used in the chiral resolution processes: A) RS-IBU and BPE were mixed with Heptane and fully dissolved at  $T_H$ , after which S-IBU:BPE co-crystals were seeded. B) S- and RS-IBU were mixed with BPE in Heptane and IBU:BPE co-crystals were formed. At equilibration at temperature  $T_H$ , only S-co-crystals remained in the suspension. C) Only S- and RS-IBU were mixed with Heptane and dissolved at  $T_H$ . Co-former BPE was subsequently seeded at  $T_H$  and S-IBU:BPE co-crystals were formed. The last step in all three processes was the same: the suspension was cooled down from  $T_H$  to  $T_L$  and the S-co-crystals grew and were subsequently recovered as products at  $T_L$ .

In Exp. 1, method A was used to seed S-IBU:BPE co-crystals into a saturated solution of RS-IBU and BPE at  $T_H$  ( $58^\circ\text{C}$ ) and the resulting suspension was linearly cooled down to  $T_L$  ( $53^\circ\text{C}$ ), during which the seed crystals were allowed to grow out. At  $T_L$  the crystalline phase was obtained and analyzed.

The purity of the obtained solid material product was captured in two ways. First, the co-crystal purity was quantified through the molar ratio of IBU to BPE which was determined to be  $p_{\text{IB}} = 1.093 \pm 0.017$ , indicating a small excess of IBU in the solids compared to a pure co-crystal with  $p_{\text{IB}} = 1$ . If we assume that the excess IBU is present as racemic compound, the co-crystal purity would be  $95.3 \pm$

0.7%. As in the case of the reference experiment R<sub>1</sub> and R<sub>2</sub>, these RS-IBU crystals are assumed to originate from the adhering mother liquor remaining between the recovered co-crystals. Therefore, they are not counted as products in calculating yields and enantiomeric excess. Alternatively the enantiomer purity was quantified through the enantiomeric excess of the co-crystals  $E_c$  (excluding RS-IBU), defined as  $E_c = (c_{S_c} - c_{R_c}) / (c_{S_c} + c_{R_c})$ , where  $c_{S_c}$  and  $c_{R_c}$  are the recovered S- and R-co-crystals. The  $E_c$  of Exp.1 is  $89.6 \pm 1.3\%$ , showing that a molar percentage of 5.2% of the IBU in the co-crystal material is the counter enantiomer, contaminating the product.

In addition to the purity of the product, other important factors to evaluate a PC experiment have been used such as the recovery ratio  $\varphi$ , yield  $Y$  and the ratio between S-co-crystal product and R-co-crystal impurity  $p_{SR}$ . The amount of S-co-crystal product  $c_P$  is defined as the total S-co-crystal recovered  $c_{S_c}$  minus the seeds  $c_0$ . In Exp. 1,  $c_{S_c}$  is  $25.2 \pm 0.4$  mg/ml,  $c_0$  is 18.8 mg/ml and  $c_P$  is  $6.3 \pm 0.4$  mg/ml. The amount of impurity R-IBU:BPE  $c_{R_c}$  is  $1.4 \pm 0.2$  mg/ml. The recovery ratio of Exp.1, defined as  $\varphi = c_P / c_0$ , is then  $33.7 \pm 1.9\%$ . This means that from the S-co-crystals seeded, around 1/3 additional S-IBU:BPE was recovered as the net product. The yield  $Y$  of Exp. 1, defined as the ratio between  $c_P$  and the maximum attainable S-co-crystals from point 1 (17 mg/ml), is then  $36.8 \pm 2.1\%$ . This result indicates that the potential of the PC experiment has yet to be achieved as around 2/3 attainable S-co-crystals have not been recovered. The last factor  $p_{SR}$  of Exp.1, defined as  $c_P / c_{R_c}$ , is  $4.7 \pm 0.8$ , confirming that the S-co-crystal is preferentially crystallized compared to its R-counterpart.

These characterization factors (e.g., purity and yield) enable us to visualize the experiments by plotting the yields versus the  $E_c$  as a green point in Figure 4 (right). The location of the Exp.1 is slightly deviated from the 100%  $E_c$  axis, reflecting the existence of a small amount of R-co-crystal impurity. It can also be seen that the point of Exp.1 has not reached point 1, indicating that maximum recovery has not been reached in the end of the experiment. This is in line with the relative low recovery ratio and yield from Exp.1. Moreover, the  $E_c$  and  $Y$  of Exp.1 are plotted in Figure 4 (right), as to compare its chiral resolution performance with other PC experiments.

The same analysis procedure is used for all the other PC experiments. Experiment 2 and 3 employed the seeding procedure B and C, respectively (see Figure 5). In Exp. 2, both S- and R-co-crystals crystallized in the suspension at room temperature and at  $T_H$  the R-IBU:BPE crystals were fully dissolved, leaving only S-IBU:BPE in the solid phase as seeds. In Exp. 3, nucleation of S-co-crystal was initiated via the seeding of BPE into an undersaturated IBU solution at  $T_H$ . After seeding, the remaining parts of Exp. 2 and 3 were the same as in Exp. 1. The crystalline products recovered at  $T_L$  were analyzed and the relevant characterization factors (e.g.,  $E_c$  and  $Y$ ) are compared with those from Exp.1 in Table 4. The two experiments are also visualized in Figure 4 (left) and compared in Figure 4 (right) for their yield and enantiomer purity. It can be seen from Table 4 that all three seeding methods can lead to similar chiral resolution, in the sense of achievable purity and amount of the products.

In all three experiments, significantly more S-co-crystal mass was recovered, compared with the amount of R-enantiomer, proving that the preferential crystallization experiments, regardless of the

seeding procedures, were successful in achieving enrichment. However, it can be seen from Figure 4 that the maximum amount of S-co-crystal product was not achieved from any of the three experiments, indicating that the yield and recovery ratio can be further improved. On the other hand, a small amount of R-co-crystal impurity contaminated the product already, suggesting that optimization of the current experiment procedure is needed in order to improve the yield without further reducing the enantiopurity of the products. Therefore, in the following sections, the effects of various operation parameters are investigated in order to optimize the PC process. Procedure B does not require a manual seeding step during the process, which makes it the experimentally most convenient method. Therefore, in the following section, method B was used as the standard case to investigate the effects of various operational parameters on the chiral resolution process.

**Effect of holding duration  $t_L$  at the end temperature  $T_L$**  Three experiments (2, 4 and 5) with different time periods  $t_L$  before the solid phases were harvested are compared in Figure 6 (left). The solid phases from Exp. 4 and 5 were not significantly different and neither were the solution compositions in both experiments (see Figure 4, left and Table 4). Furthermore, the comparison among these three solid phases (Figure 6, left) shows that no significant change in enantiopurity was observed if more time is given to the PC process, indicating that the significant crystallization of R-co-crystals is absent within 1 h after the system is cooled to 53°C. The R-co-crystal impurity in all three experiments might actually crystallize during the filtration step.

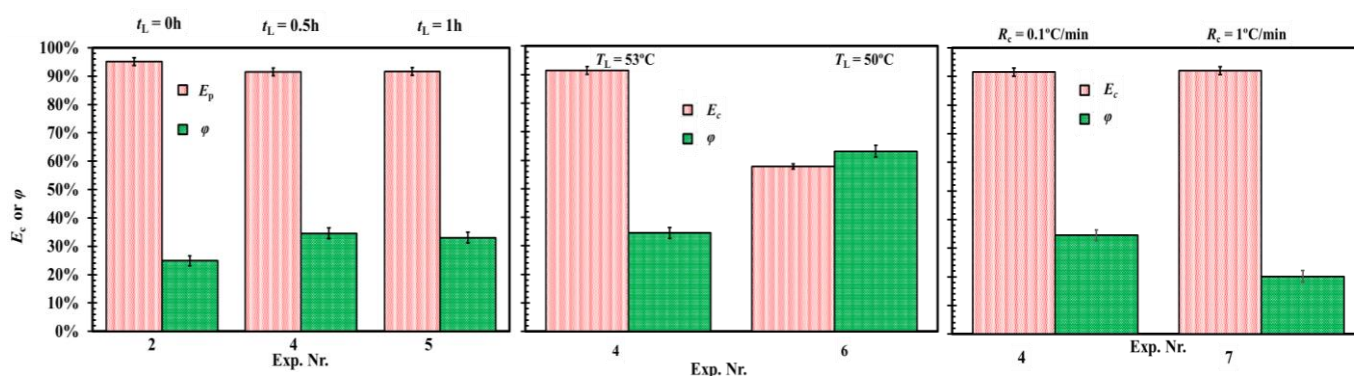


**Figure 6.** The comparison of co-crystal enantiomeric excess  $E_c$  and recovery ratio  $\phi$  among Exp. 2, 4 and 5, where the duration  $t_L$  at the end temperature  $T_L$  are different (left), between Exp. 4 and 6, where the end temperature  $T_L$  varies (middle), and between Exp. 4 and 7, where the latter employed a 10-times higher cooling rate than the former (right).

**Effect of  $T_L$**  The effect of the second operational parameter,  $T_L$ , was investigated by comparing the results from Exp. 4 and 6. In Exp. 6, the suspension was cooled down from 58°C to 50°C and held for 0.5 h before the solid phase was harvested (see Figure 6, middle and Table 4).

Around 20% of crystals recovered at 50°C were R-IBU:BPE co-crystals, which led to a significantly lower  $E_c$  compared to that of Exp. 4. The decrease in  $E_c$  was due to the primary nucleation

of R-co-crystals, at the higher supersaturation at the low  $T_L$  (see comparison of R-co-crystal supersaturation between  $T_L=53^\circ\text{C}$  and  $50^\circ\text{C}$  in Table 3). Additionally, a lower  $T_L$  led to a longer cooling period, which gave the R-co-crystals more time to crystallize.

**Effect of Cooling Rate  $R_c$ .** The effect of the rate of cooling was studied by comparing the results of Exp. 4 and Exp. 7, in which cooling rates of 0.1 and  $1^\circ\text{C}/\text{min}$  respectively were used. The comparison of  $E_c$  and  $\varphi$  from Exp. 4 and 7 is shown in Figure 6 (right) and Table 4. The enantiomeric excess of the two experiments were similar but less S-co-crystal products was recovered at the higher cooling rate. The solution phase in Exp.7 was less enriched in R-enantiomer compared to that in Exp. 4 (see Figure 6). However, in both experiments the crystal loss during filtration was observed and different amounts of crystals stuck or settled on the vial wall could lead to the differences in recovery ratio. Therefore, it cannot be concluded that a higher cooling rate absolutely leads to a lower recovery ratio.

**Effect of  $t_H$ .** Exp. 8, the suspension of which was held at  $58^\circ\text{C}$  for 1 h, was conducted to compare its results with Exp. 5 (see Figure 7, left), in which a longer  $t_H$  (4 h) was used. The recovered crystalline phase from Exp. 8 had an  $E_c$  of  $57.2 \pm 0.9\%$  and a  $p_{\text{IB}}$  of  $1.101 \pm 0.018$  ( $96.3 \pm 0.7\%$ ).

The comparison of results between Exp. 5 and 8 in Figure 7 (left) shows that the recovered crystals from the latter had a significantly lower  $E_c$ . On the other hand, the recovery ratio  $\varphi$  from Exp. 8 was much higher, compared with that of Exp. 5. Actually, it can be seen from Figure 4 (left) that Exp. 8 is at the process line, indicating that the S-co-crystals were in equilibrium at the end of the experiment. A likely reason for the results of Exp. 8 is as following: due to the short holding time at  $58^\circ\text{C}$ , part of the R-co-crystals, which were formed before the suspension reached  $T_H$ , did not fully dissolve. The remaining R-co-crystals in the suspension grew and nucleated during the cooling step and led to a lower  $E_c$  of the recovered solid phase. Similarly, there were some excess S-IBU:BPE not dissolved at  $T_H$  before the cooling step started. Therefore, the equilibrium for S-co-crystals were reached as there were more seeds in the beginning.

**Scale-up.** A 20 ml experiments (Exp. 9) was conducted to investigate the possibility and effect of scale-up. The results of Exp. 2 and 9 were compared, where the only difference was the volume of the suspension  $V$ . The recovered crystals from Exp. 9 had an  $E_c$  of  $88.7 \pm 1.3\%$  and an IBU/BPE ratio  $p_{\text{IB}}$  of  $1.122 \pm 0.018$  (co-crystal purity  $92.1 \pm 0.7\%$ ). The comparisons of  $E_c$  and recovery ratio  $\varphi$  between Exp. 2 and 9 are shown in Figure 7 (right).

When the volume of the suspension increased from 4 ml to 20 ml, a slight decrease in  $E_c$  of the recovered crystals was observed in Exp. 9. In order to cool down a larger volume of suspension (20 ml), a larger temperature difference between the bulk suspension and the cooling jacket was built up. Consequently, the region close to the vessel wall had a lower temperature in a 20 ml experiment than in a 4 ml one. Therefore, the primary nucleation of the R-co-crystals on the wall was more likely to take place in the case of 20 ml experiment. This led to a slightly decreased  $E_c$  of the recovered crystals.

On the other hand, the recovery ratio  $\varphi$  in a 20 ml experiment was significantly higher than that from a 4 ml experiment. It was noticed after the experiment that less product loss took place in Exp. 9 compared to any of the 4 ml scale experiment. This was probably due to a smaller surface/volume ratio when  $V$  increased.

The crystalline product from Exp. 9 was further purified to improve its enantiopurity by partially dissolving the product in Heptane to remove the R-co-crystals, along with some S-products (see details in the Appendix). The purified crystals had an  $E_c$  of  $97 \pm 2.2\%$  and an IBU/BPE ratio  $p_{IB}$  of  $0.965 \pm 0.015$ . Therefore, impurity and the chiral impurity contents of the products from Exp. 9 were decreased by approximately 3 and 7 times, respectively. The significant improvement of the purity and the enantiopurity of the crystalline product from Exp. 9 proves that a suitable downstream process can enhance the performance of the conglomerate-co-crystal-mediated chiral resolution.

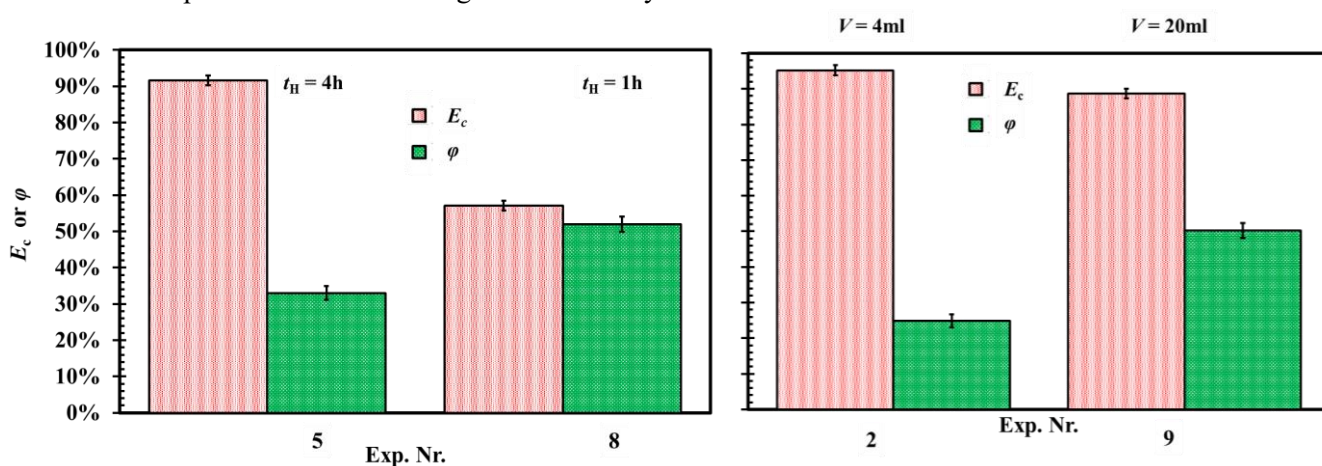


**Figure 7.** Comparison of enantiomeric excess  $E_c$  and recovery ratio  $\varphi$  between Exp. 5 and 8 (left) and between Exp. 2 and 9 (right).

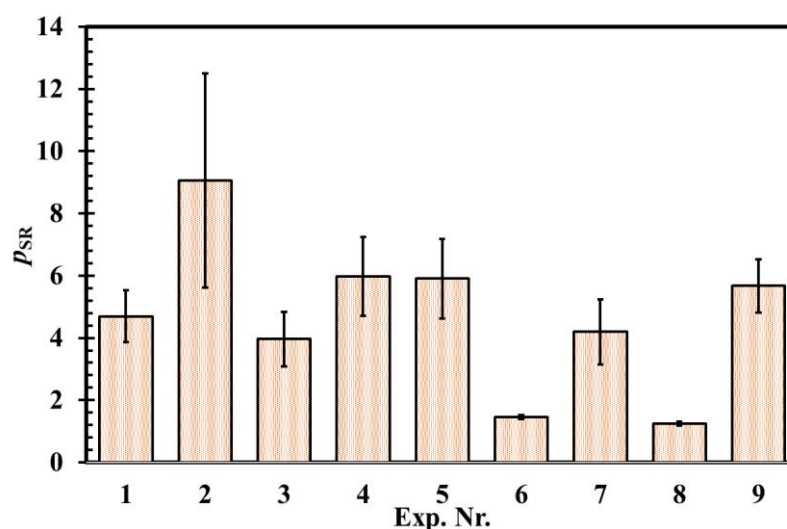


**Figure 8.** Summary of ratio  $p_{SR}$  of all PC experiments in Table 2.

## 4. DISCUSSIONS

In conventional preferential crystallization processes the seeding method A is commonly used, while the methods B and C are unique for the conglomerate co-crystal systems. Since primary nucleation of S-co-crystals seeds are involved in both method B and C, it is expected that the final products are of smaller sizes compared with those from method A. Moreover, in method A, products with a narrow crystal size distribution (CSD) can be recovered if the seeds are pretreated, for instance by sieving. Therefore, for industrial application in which also control over particle size needs to be achieved, the seeding method A is more suitable than the other two methods.

A summary of  $P_{SR}$  of all preferential crystallization experiments in Table 2 is displayed in Figure 8. In most of cases, except in Exp. 6 and 8, substantially more S-co-crystals are formed than R-co-crystals, with Exp. 2 having a  $P_{SR}$  ratio of almost 10, proving that the desired product is preferentially crystallized.

The recovery ratio  $\phi$  and recover yield  $Y$  of the co-crystal products from any of the PC experiment are relatively low. Generally in a preferential crystallization process, the amount of enantiopure product recovered is approximately equal to, if not more than, that of the added seeds<sup>4, 20</sup>. The relatively low  $\phi$  and  $Y$  can be partly attributed to the product loss during filtration. Part of the solid phase settled and then stuck on the vial wall when the suspension was poured on the glass filter. This loss can be minimized if the suspension is under mixing while being withdrawn from the crystallizer for filtration.

Another reason for the low yield and recovery ratio is that the PC experiments are likely finished before all the supersaturation for S-IBU:BPE is consumed. One way to increase the recovery yield is to increase the duration at the final temperature  $t_L$ , beyond the 1 h duration tested in this study. Alternatively, in order to increase the amount of S-products, the final temperature  $T_L$  can be lowered. In experiment 6, the suspension was cooled down to 50°C instead of 53°C. Significantly more S-co-crystal products were recovered compared to experiments performed at 53°C. However, the solid phase was contaminated by R-co-crystals, the amount of which was almost equal to the gained S-enantiomer products. In order to minimize such contamination, a faster cooling rate can be employed, which shortens the duration of the suspension staying at a lower temperature and reduces the chance of primary nucleation of the R-co-crystals. Additionally, chiral additives can be used to suppress the growth rate of the undesired enantiomer<sup>21</sup>, which leads to crystalline products of higher enantiopurity even when recovered at a lower temperature.

## 5. CONCLUSIONS

A chiral resolution of the racemic compound IBU is successfully performed by preferential crystallization, via the conglomerate co-crystal of IBU with the achiral co-former BPE. Three seeding methods have been developed and experimentally verified. Operation parameters such as the duration

at the final temperature  $t_L$  and cooling rate  $R_c$ , within their tested range in the present study, did not significantly affect the enantiopurity of the products while a shorter duration at the initial temperature ( $T_H$ )  $t_H$  and a lower final temperature  $T_L$  can lead to the primary nucleation of the undesired enantiomer impurities. Scale-up of the system can reduce the product loss during filtration while more investigation and design are needed to improve the net recovery ratio  $\varphi_n$ . This co-crystallization-mediated chiral resolution technique enables the recovery of desired enantiomer from racemic compounds, which are not suitable for any conventional chiral resolution methods before.

## REFERENCES

1. Lorenz, H.; Seidel-Morgenstern, A., Processes To Separate Enantiomers. *Angewandte Chemie International Edition* **2014**, *53* (5), 1218-1250.
2. Rouhi, A. M., Chirality at work. *Chem. Eng. News* **2003**, *81* (18), 56-61.
3. Ward, T. J.; Ward, K. D., Chiral Separations: A Review of Current Topics and Trends. *Analytical Chemistry* **2012**, *84* (2), 626-635.
4. Coquerel, G., Preferential Crystallization. In *Novel Optical Resolution Technologies*, Sakai, K.; Hirayama, N.; Tamura, R., Eds. Springer Berlin Heidelberg: Berlin, Heidelberg, 2007; pp 1-51.
5. Srisanga, S.; ter Horst, J. H., Racemic Compound, Conglomerate, or Solid Solution: Phase Diagram Screening of Chiral Compounds. *Crystal Growth & Design* **2010**, *10* (4), 1808-1812.
6. Noorduyn, W. L.; Kaptein, B.; Meekes, H.; van Enkevort, W. J. P.; Kellogg, R. M.; Vlieg, E., Fast Attrition-Enhanced Deracemization of Naproxen by a Gradual In Situ Feed. *Angewandte Chemie International Edition* **2009**, *48* (25), 4581-4583.
7. Li, W. W.; Spix, L.; de Reus, S. C. A.; Meekes, H.; Kramer, H. J. M.; Vlieg, E.; ter Horst, J. H., Deracemization of a Racemic Compound via Its Conglomerate-Forming Salt Using Temperature Cycling. *Crystal Growth & Design* **2016**, *16* (9), 5563-5570.
8. Spix, L.; Alfring, A.; Meekes, H.; van Enkevort, W. J. P.; Vlieg, E., Formation of a Salt Enables Complete Deracemization of a Racemic Compound through Viedma Ripening. *Crystal Growth & Design* **2014**, *14* (4), 1744-1748.
9. Wermester, N.; Aubin, E.; Pauchet, M.; Coste, S.; Coquerel, G., Preferential crystallization in an unusual case of conglomerate with partial solid solutions. *Tetrahedron: Asymmetry* **2007**, *18* (7), 821-831.
10. Würges, K.; Petruševska-Seebach, K.; Elsner, M. P.; Lütz, S., Enzyme-assisted physicochemical enantioseparation processes—Part III: Overcoming yield limitations by dynamic kinetic resolution of asparagine via preferential crystallization and enzymatic racemization. *Biotechnology and Bioengineering* **2009**, *104* (6), 1235-1239.

11. ter Horst, J. H.; Deij, M. A.; Cains, P. W., Discovering New Co-Crystals. *Crystal Growth & Design* **2009**, *9* (3), 1531-1537.
12. Schultheiss, N.; Newman, A., Pharmaceutical Cocrystals and Their Physicochemical Properties. *Crystal Growth & Design* **2009**, *9* (6), 2950-2967.
13. Grothe, E.; Meekes, H.; Vlieg, E.; ter Horst, J. H.; de Gelder, R., Solvates, Salts, and Cocrystals: A Proposal for a Feasible Classification System. *Crystal Growth & Design* **2016**, *16* (6), 3237-3243.
14. Springuel, G.; Leysens, T., Innovative Chiral Resolution Using Enantiospecific Co-Crystallization in Solution. *Crystal Growth & Design* **2012**, *12* (7), 3374-3378.
15. Neurohr, C.; Marchivie, M.; Lecomte, S.; Cartigny, Y.; Couvrat, N.; Sanselme, M.; Subra-Paternault, P., Naproxen–Nicotinamide Cocrystals: Racemic and Conglomerate Structures Generated by CO<sub>2</sub> Antisolvent Crystallization. *Crystal Growth & Design* **2015**, *15* (9), 4616-4626.
16. Chen, C. Y.; Chen, C. S., Stereoselective disposition of ibuprofen in patients with compromised renal haemodynamics. *British Journal of Clinical Pharmacology* **1995**, *40* (1), 67-72.
17. Wechter, W. J.; Bigornia, A. E.; Murray, E. D.; Levine, B. H.; Young, J. W., Rac-Flurbiprofen is more ulcerogenic than its (S)-enantiomer. *Chirality* **1993**, *5* (7), 492-494.
18. Elacqua, E. Supramolecular chemistry of molecular concepts:tautomers, chirality, protecting groups, trisubstituted olefins, cyclophanes, and their impact on the organic solid state. University of Iowa, 2012.
19. Shankland, N.; Florence, A. J.; Cox, P. J.; Sheen, D. B.; Love, S. W.; Stewart, N. S.; Wilson, C. C., Crystal morphology of ibuprofen predicted from single-crystal pulsed neutron diffraction data. *Chemical Communications* **1996**, (7), 855-856.
20. Levilain, G.; Coquerel, G., Pitfalls and rewards of preferential crystallization. *CrystEngComm* **2010**, *12* (7), 1983-1992.
21. Kongsamai, P.; Maneedaeng, A.; Flood, C.; ter Horst, J. H.; Flood, A. E., Effect of additives on the preferential crystallization of L-asparagine monohydrate. *The European Physical Journal Special Topics* **2017**, *226* (5), 823-835.

# Appendix Chapter 4

## Table of Contents

1. X-ray Powder Diffraction (XRPD) for crystalline phase (1)
2. Example for Proton nuclear magnetic resonance ( $H^1$ -NMR) for IBU/BPE measurement(2)
3. Downstream processing of products from Exp. 9 (3)

## X-ray Powder Diffraction (XRPD) for crystal composition identification

X-ray powder diffraction (XRPD) was carried out in a Bruker D2 Phaser (Bruker AXS GmbH, Karlsruhe, Germany). Data collection was carried out using monochromatic Cu K  $\alpha$ 1 radiation ( $\lambda = 0.154060$  nm) in the  $2\theta$  region between  $5^\circ$  and  $50^\circ$ , step size  $0.022^\circ 2\theta$ . Data evaluation was done with the Bruker program EVA.

The XRPD diffractograms of crystals collected from Experiment 1, 2, 9 and the seeds of Exp.1, along with the reference of S-IBU:BPE co-crystals are shown in Figure SI.

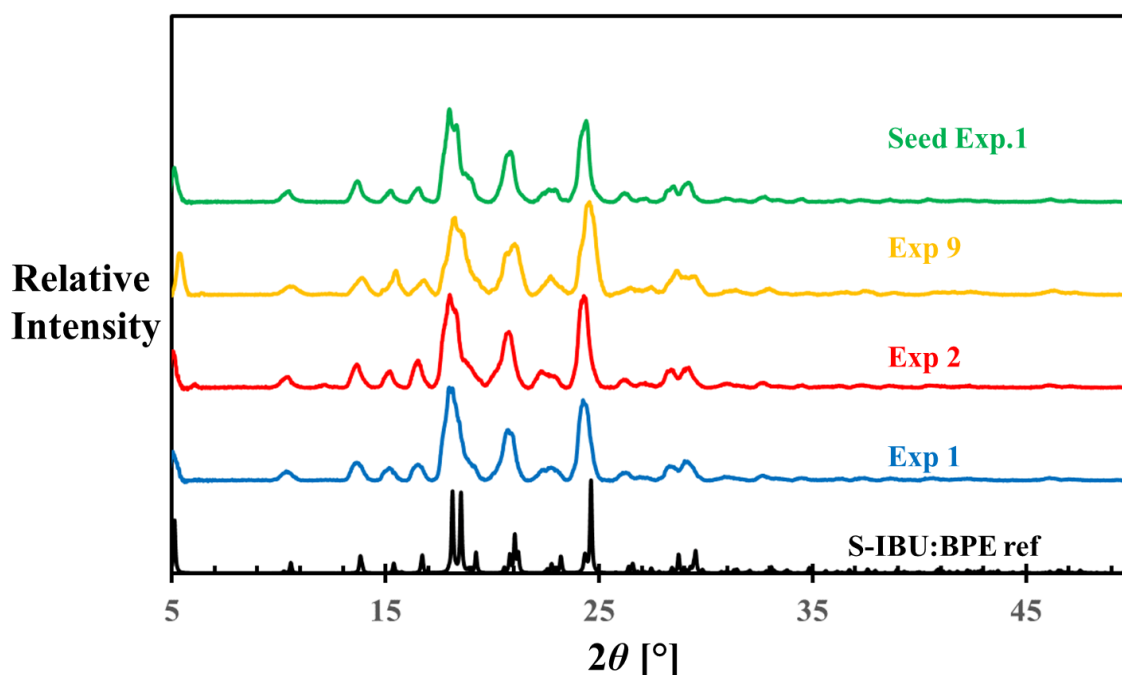


**Figure SI.** XRPD comparison between crystalline products from Exp. 1,2 and 9, seeds of Exp.1 and the reference S-IBU:BPE co-crystals (Chapter 3).

## Example for proton nuclear magnetic resonance ( $^1\text{H}$ -NMR) for crystal purity assessment

Figure SII shows the  $^1\text{H}$ -NMR spectrum of the product from Exp.1 as one example. The peaks between 7.32-9.04 represent 10 protons from BPE and the peak between 3.10-3.42 represents 1 proton from IBU. The ratio between IBU and BPE can also be calculated by taking into account all 18 protons from IBU, although the accuracy is not improved. Therefore, for simplicity, we use here only one peak of IBU for calculation.

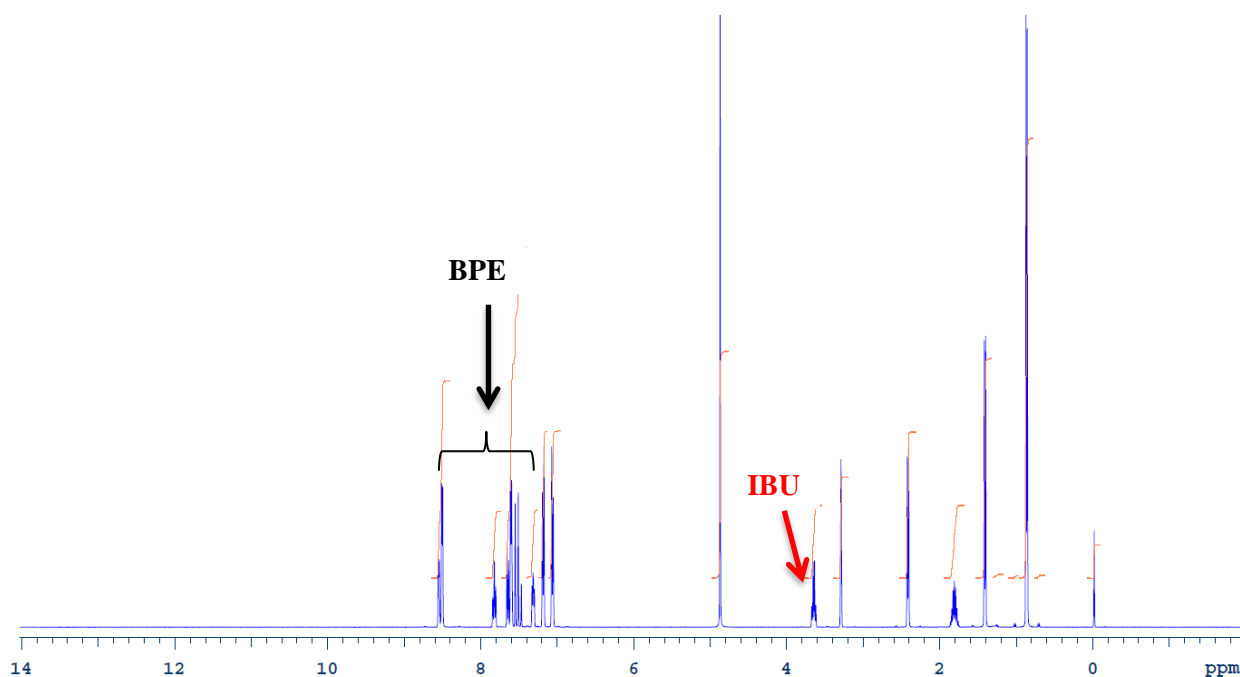


**Figure SII.**  $H^1$ -NMR measurement of crystalline product from Exp. 1.

### Downstream Process of Product from Exp. 9

200.2 mg crystalline product of the large scale experiment (Exp.9) was further purified by removing the impurities RS-IBU crystals (12.1 mg) and R-IBU:BPE co-crystals (12.4 mg). In Figure SIII, the downstream process is shown: the product from Exp. 9 was mixed with additional 10.7 mg BPE, which was equimolar to the RS-IBU crystals in the product. The mixed solid phase was then added in 2.36 ml Heptane and equilibrated at 45°C for two days. We measured beforehand that a saturated Heptane solution contains around 20.6 mg/ml co-crystals (1:1 molar ratio of IBU and BPE) at 45°C. Therefore, the amount of Heptane added here in the purification step was enough to dissolve all the impurities, along with S-IBU:BPE co-crystals equal to the amount of R-co-crystals. The undissolved solid phase, after equilibration, was recovered by a glass filter and sent for analysis.

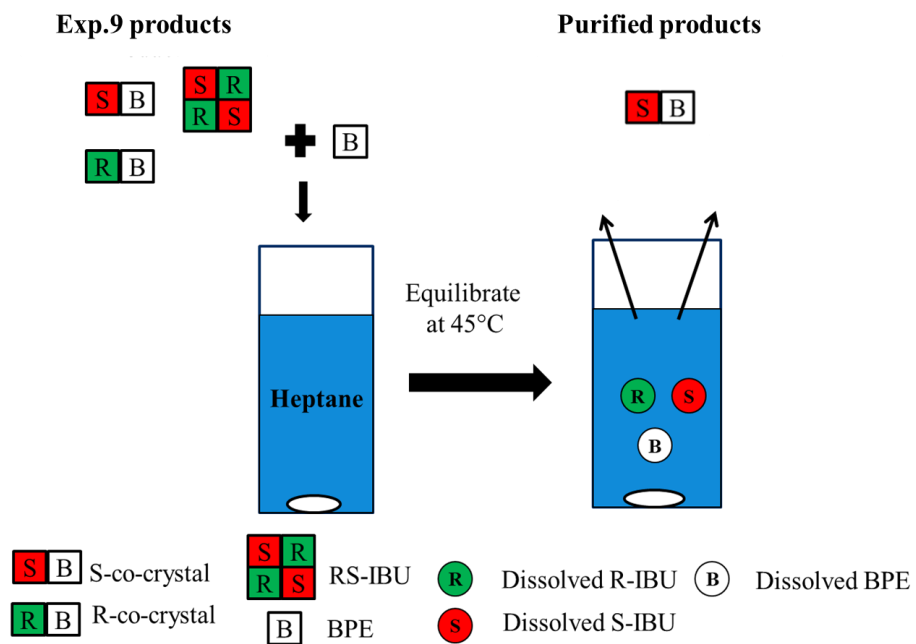


**Figure SIII:** Schematic demonstration of purification of the products from Exp.9: 200.2 mg of the products were mixed with additional 10.7 mg BPE, equimolar to the RS-IBU impurities. The mixture was added into 2.36 ml Heptane and the suspension was equilibrated at 45°C for two days. The solid phase from the equilibrated suspension was recovered and analyzed by H1-NMR and polarimeter



# Chapter 5. Deracemization of a Racemic Compound via Its Conglomerate-forming Salt Using Temperature Cycling

**Key words:** Deracemization, Temperature Cycling, Racemic Compound, Conglomerate-forming Salt, Process Optimization

**Abstract:** Salts of chiral molecules, which originally crystallize as racemic compounds, could form conglomerates. The utilization of such conglomerate salts, as intermediates for the deracemization of corresponding racemic compounds, expands the theoretical application range of Viedma Ripening by roughly 10 fold. In the present study, the use of temperature cycling on conglomerate forming salts as an alternative technique for Viedma ripening was studied. The racemic compound Phenylalanine (Phe) was successfully deracemized via its conglomerate-forming salt with 2,5-xylenesulfonic acid (XSA) by continuous heating-cooling cycles applied to its suspension in glacial acetic acid, coupled with a solution racemization reaction. In addition, the dependence of the deracemization rate on the operational parameters was studied. Enhanced racemization reaction kinetics, either by a larger amount of free amino acid or a higher concentration of catalyst, was shown to accelerate the deracemization process. It seems to indicate that a concentration difference between the two enantiomers, which could be diminished by a faster racemization rate, behaves as one of the major rate-limiting factors for the deracemization process. A larger mass fraction of solid dissolving and recrystallizing in the heating-cooling cycles, achieved by either a larger temperature swing or a smaller dry mass concentration, also leads to a faster deracemization. A change in cooling rate does not affect the deracemization rate significantly within the range tested, indicating a limited presence of secondary nucleation of the minor enantiomers. The results can be used as a preliminary foundation for process optimization as well as

mechanisms investigation. The advantages and disadvantages of temperature cycling and Viedma Ripening, as deracemization methods in an industrial setting are discussed.

## 1. INTRODUCTION

Viedma Ripening, the process in which an enantiopure solid phase is obtained from a racemic suspension of conglomerate crystals, under a near-equilibrium condition, by combining mechanical grinding and solute racemization, has shown to be a reliable method for acquiring the desired enantiomer by means of crystallization, in addition to preferential crystallization.<sup>1-5</sup> Following the success in obtaining enantiopure NaClO<sub>3</sub> crystals from an aqueous solution<sup>6,7</sup> and a conglomerate suspension<sup>8</sup> subjected to a temperature gradient, it was demonstrated that applying a combination of a racemization reaction in solution and heating-cooling cycles rather than grinding of a conglomerate suspension also resulted in full deracemization of the solid phase.<sup>6</sup> Although two major modelling studies have been reported to explain how the deracemization is achieved by the temperature cycles, only a few experimental studies have been conducted to deepen our understandings of the underlying mechanisms.<sup>7-8</sup>

Though being promising methods for deracemization, Viedma Ripening and the temperature cycling method have the intrinsic drawback of being only applicable to conglomerates, a racemic physical mixture of pure enantiomer crystals.<sup>9</sup> This constraint excludes the utilization of the deracemization methods for roughly 90% of the known chiral molecules since these compounds crystallize as racemic compounds, crystals consisting of both enantiomers.<sup>9</sup> One way around this restriction is by converting a racemic compound into a conglomerate salt: for a series of chiral compounds it has been shown that the probability of forming a conglomerate salt is 2 to 3 times larger than of forming a single component conglomerate.<sup>10</sup> Recently, Spix et al. managed to apply Viedma Ripening to racemic amino acid compounds, e.g. DL-Phenylalanine (Phe), via the formation of its conglomerate salt with 2,5-xylenesulfonic acid (XSA).<sup>11-12</sup> Their results showed, that using a conglomerate forming salt enables the utilization of Viedma Ripening to racemic compounds. This would expand the application range of Viedma ripening by roughly 10 times, if such conglomerate forming salts exist.

In this study, the model compound system Phe-XSA is used to verify whether deracemization through the temperature cycling method is also successful for a conglomerate salt of an intrinsically racemic compound. In addition, the effects of the operational parameters on the deracemization rate are studied, to achieve more experimental data as a preliminary foundation for process optimization and mechanism investigation. Finally, a qualitative comparison is made between the two deracemization methods.

## 2. EXPERIMENTAL

**Materials.** Solute and catalyst were purchased from Sigma Aldrich (DL-Phenylalanine (DL-Phe, 99%), D-Phenylalanine (D-Phe, 98%) and Salicylaldehyde (SAH, 98%)), Merck (L-Phenylalanine (L-Phe, 99%)) and Alfa Aesar (2,5-Xylenesulfonic acid hydrate (XSA·xH<sub>2</sub>O, 99%)). Glacial acetic acid was purchased from J. T. Baker (99-100%). MilliQ water and Acetonitrile (99%) from Sigma Aldrich were used as effluent for chiral HPLC analysis. Acetone (99%, Sigma Aldrich) was used as washing solvent during sampling.

Phenylalanine can be racemized in glacial acetic acid, catalysed by Salicylaldehyde. This reaction works optimally at a temperature of 100°C but one can still achieve sufficient racemization at lower temperature (e.g. 65°C). It is assumed that Phe was stable through the experiments since decomposition has only been observed in the cases of Tryptophan and Serine.<sup>16</sup> Only free amino acid can be racemized via the formation of a Schiff base.<sup>13</sup> Therefore, less 2,5-Xylenesulfonic acid was added so that the molar ratio between Phe and XSA in the system was between 1.30 and 1.45. The excess amount of Phe exists in the solution phase as free amino acid for the racemization reaction. The Phe:XSA molar ratio in each experiment is shown in Table.1. The molar ratio of Phe over XSA was calculated based on the molar weight of Phe (165 g/mol) and anhydrous XSA (186 g/mol). From TGA measurement, the purchased XSA·xH<sub>2</sub>O contains approximately 15% wt water. Therefore, the mass of anhydrous XSA was assumed to be 85% of the total XSA·xH<sub>2</sub>O used in preparing the suspensions.

The racemization reagent, SAH, was added in each experiment using a Pasteur pipette. In order to determine the amount of catalyst in the solution phase, 10 separate tests were performed in which the weight of 10 drops of SAH was measured. The average value, 13.2 mg/drop, was used to calculate the concentration of catalyst in each deracemization experiment. The standard deviation for the 10 separate tests was 4%.

**Solubility of DL-Phe-XSA in acetic acid.** The saturation temperature of DL-Phe-XSA was measured in acetic acid at various concentrations by adding a known amount of DL-Phe and XSA·xH<sub>2</sub>O and 1 ml of solvent to a 1.5 ml glass vial. The molar ratio Phe:XSA was always 1.31:1 to mimic the actual suspension composition in the deracemization experiment. The vials were placed in a Crystal16 (Technobis B.V.) and two temperature cycles were applied to all samples. Each cycle involved heating from 0°C to 80°C with a rate of 0.3°C/min, holding at 80°C for 100 min, cooling to 0° with a rate of 0.3°C/min and then holding at 0° for 100 min. The detected clear point was noted as the saturation temperature  $T_s$  of the corresponding concentration. Additional saturation temperatures were measured for which samples contained 13.2 mg/ml and 26.4 mg/ml catalyst, respectively. The concentrations  $c$  (mg/ml) vs. saturation temperature data  $T_s$  were fitted to the empirical function  $c = A \exp(BT_s)$  to interpolate the solubility at different temperatures.

**Verification experiments.** Three experiments were performed to determine whether deracemization can be achieved by using the temperature cycling method. In the standard experiment A1, 580 mg DL-Phe and 589 mg XSA·xH<sub>2</sub>O were mixed with 9 mL glacial acetic acid in a 25 mL round-bottom flask. In experiments A2 and A3, in addition, respectively 58 mg of D-Phe and 63 mg L-Phe were mixed with DL-Phe into the glacial acetic acid to prepare a scalemic suspension. The suspensions in all experiments were stirred by an oval PTFE-coated magnetic bar (L 20 mm, Ø 10 mm, 300 rpm) at 65°C for 1 hour. Then, two different temperature programs were applied to the suspensions, which are shown in Figure 1. The first temperature profile TP1, which was applied in experiments A1 and A2, consisted of four steps: holding at 65°C for 5 min, heating up to 70°C in 10 min with a linear profile, holding at 70°C for 5 min and finally cooling down to 65°C linearly with a cooling rate of 0.055°C/min. The other temperature profile TP2 was assigned to A3, and its only difference, compared with TP1, was a cooling rate of 0.11°C/min.

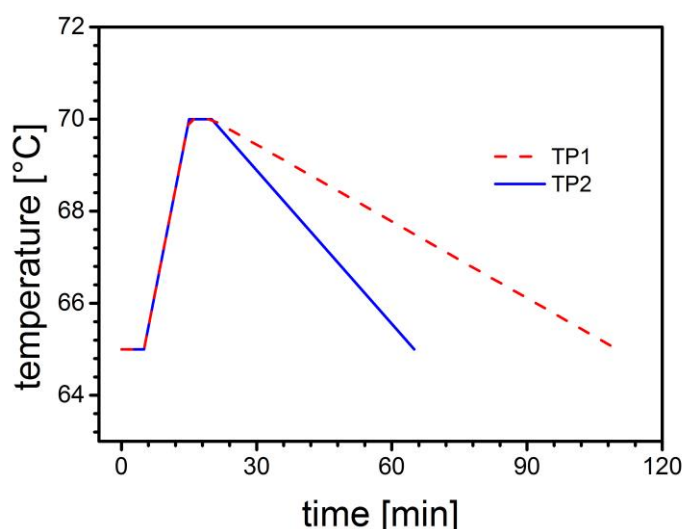


**Figure 1.** Temperature profiles for one temperature cycle applied in the verification experiments A1-A3. A1 and A2 used a cooling rate of 0.055°C/min (TP1), while that of A3 was 0.11°C/min (TP2).

The initial temperature cycles were applied to the suspension in the absence of the racemization catalyst SAH. The salt precipitation took place rapidly when Phe and XSA were mixed in the acetic acid, forming large agglomerates. Mixing was therefore not ideal in the initial suspension and a period of dissolution-growth cycles was needed to ensure that the suspension was homogeneous before deracemization experiments were started. After approximately 12 hours of these initial temperature cycles, a sample was taken at the end of the last cycle, at 65°C, the time of which was noted as  $t = 0$ , and then *ca.* 130 mg of SAH was added to the suspensions to start the racemization reaction. After that, samples were taken over time to measure the solid phase enantiomeric excess  $E$  using chiral HPLC. In each case the sample was taken at the end of a cycle.

**Operational Parameter Study.** The dependence of the deracemization rate on five operational parameters was studied: 1) total initial dry mass concentration  $c_t$ , which is the total mass of Phe and XSA·xH<sub>2</sub>O solids before being mixed into the acetic acid per unit of solvent volume; 2) catalyst concentration  $c_{cat}$ ; 3) excess enantiomer concentration  $\Delta c$  which is the additional mass of L- or D-Phe per unit volume of the solvent; 4) the rate of cooling from the highest to the lowest temperature  $R_c$  and 5) the temperature swing  $\Delta T$ , i.e. the difference between the lowest and the highest temperature in a temperature cycle. Four different temperature profiles (TP3-TP6) were used in order to study the effects of temperature swing and cooling rate.

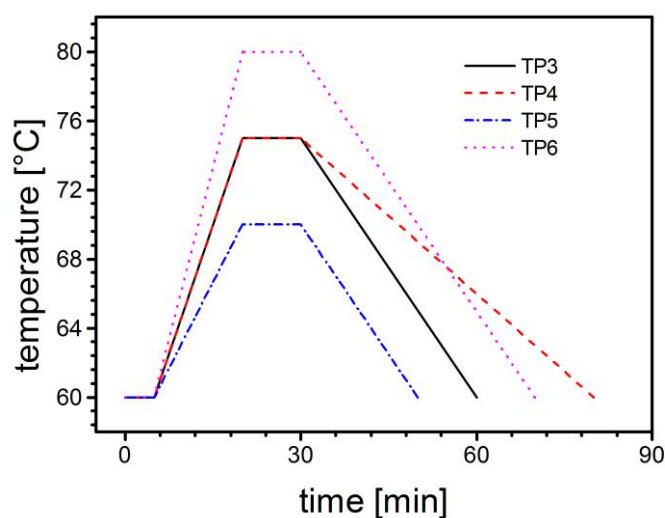


**Figure 2.** Temperature profiles for one temperature cycle applied in the parameter study to investigate the effect of temperature swing and cooling rate.

In this series, experiment B1 (see Table 1) was taken as a standard experiment, in which the 9 ml suspension contained 580 mg DL-Phe, 58 mg L-Phe and 589 mg XSA·xH<sub>2</sub>O. The procedure of B1 was the same as that of A1-A3, except that a different temperature profile, TP3, was applied. After B1, experiments B2-B7 were performed, where the value of one of the above-mentioned parameters was changed from that used in B1. Values of these parameters in all deracemization experiments are shown in Table 1, together with the molar weight ratio Phe:XSA, which was used as a measure for the amount of free amino acid in the solution and the mass fraction of solid involved in a cycle  $f_{\Delta T}$ , which was calculated as

$$f_{\Delta T} = \frac{c^*(T_{high}) - c^*(T_{low})}{c_t - c^*(T_{low})} \quad (1)$$

where  $c^*$  is the solubility of DL-Phe-XSA in the presence of a catalyst concentration of 13.2 mg/ml (except for B4, the  $f_{\Delta T}$  of which was calculated based on the Phe-XSA solubility with  $c_{cat}$  of 26.4

mg/ml). The mass fraction  $f_{\Delta T}$  can be controlled in two ways: through the dry mass concentration  $c_t$  and the temperature swing  $\Delta T$ .

**Sampling.** For sampling, including the initial sample, *ca.* 0.5 mL of the slurry was removed with a Pasteur pipette and vacuum filtered as fast as possible at room temperature on a P4 glass filter ( $\varnothing$  10 mm). The residue was washed with 2 mL of Acetone to remove the adhering racemic solution and dried.

**HPLC.** The enantiomeric excess  $E$  of the sample was measured using chiral HPLC. The analysis of Phe-XSA samples was as follows: 1 mg solid was dissolved in 1 mL Milli Q water; 2.5  $\mu$ L of the solution was injected in the HPLC column Chirobiotic T (250\*4.6 mm ID, 5  $\mu$ m, Astec); An eluent of acetonitrile/water (78/22 v/v) was used with a flow rate of 1 mL/min; The two enantiomers of Phe were detected at retention times of 8.9 min (L) and 9.9 min (D) at a wavelength of 220 nm. The concentrations of L and D enantiomers were determined by integrating the peaks at the two retention times. The enantiomeric excess was calculated as:

$$E = \frac{|A_L - A_D|}{A_L + A_D} \quad (2)$$

where  $A$  is the area of the peaks of L and D.

**Thermogravimetric Analysis (TGA).** The content of water in XSA was measured with a Perkin Elmer TGA 7 (Perkin Elmer). Samples of *ca.* 32 mg XSA were heated from 15°C – 620°C with a heating rate of 10°C/min, purged by a nitrogen flow of 40 ml/min.

### 3. RESULTS AND DISCUSSION

**Deracemization through Temperature cycling.** Figure 3 depicts the evolution of the solid phase enantiomeric excess  $E$  and its natural logarithm over time in all three verification experiments A1-A3 (for process conditions see Table 1).

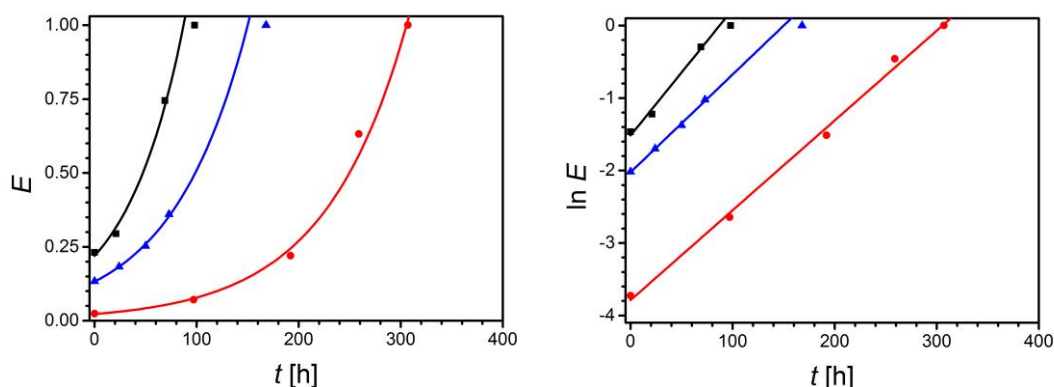


**Figure 3.** Left: Enantiomeric excess of the solids  $E$  as a function of time  $t$  in temperature cycling deracemization experiments of Phe-XSA A1 ( $\bullet$ ), A2 ( $\blacktriangle$ ) and A3 ( $\blacksquare$ ). The lines are best fits to

Equation 3. Right: the natural logarithm of the enantiomeric excess  $\ln E$  as a function of time  $t$ . Solid lines are linear fits of  $\ln(E)$  vs  $t$ . Process conditions for the experiments A1-A3 can be found in Table 1.

The verification experiment A1 started with a racemic suspension. In around 300 hours after adding the catalyst, a complete deracemization towards the L-enantiomer in the solid phase was achieved. The linear correlation between  $\ln E$  and  $t$  in Figure 3 (right) shows that the solid phase enantiomeric excess evolved exponentially during the majority of, if not the whole, deracemization experiment. The two experiments starting with a scalemic mixture, A2 and A3, led to a complete deracemization towards their initial enantiomer in excess, respectively in around 179 hours and 100 hours. These results validate that deracemization of Phe-XSA by programmed heating-cooling cycles can be achieved, as by Viedma ripening. The time needed for deracemization is largest for an initially racemic mixture, while the chiral outcome can be controlled by an initial solid phase enantiomeric excess of the preferred enantiomer.

To quantify the efficiency of the deracemization process Noorduin et al. derived an exponential equation as an approximation for the  $E$  evolution curves of Viedma ripening:

$$E(t) = E(0) \cdot \exp(kt) \quad (3)$$

which describes the enantiomeric excess  $0 \leq E \leq 1$  during Viedma ripening by two parameters:  $E(0)$ , the solid phase enantiomeric excess at  $t=0$  and the deracemization rate constant  $k$ .<sup>14</sup> Since all verification experiments displayed an exponential increase of  $E$  vs  $t$  for the major part of the process,  $k$ , estimated by fitting all experimental points with  $E$  below 1 into equation 3, was used as a measure for the deracemization efficiency. One should note however, that Viedma Ripening takes place at a fixed temperature leading to a consistent rate constant with time, while during temperature cycling deracemization occurs under varying temperatures and herewith the rate constant may also vary.<sup>8</sup> Therefore, the  $k$ -values obtained for temperature cycling deracemization represent an average over the whole experiment.

Moreover, any change to the used temperature cycle (temperature swing or cooling rate) changes the cycle time. When different temperature profiles are employed, a comparison of time-based rate constants  $k$  between experiments is clouded by the different cycle times. Therefore, it is necessary to investigate, in addition to the time-based deracemization rate constant, a cycle-number-based deracemization rate constant. For that equation 3 is modified to describe the evolution of the enantiomeric excess  $E_N$  at the end of each cycle, as a function of the number  $N$  of temperature cycles:

$$E_N(N) = E_N(0) \cdot \exp(k_N N) \quad (4)$$

This enables the study of the deracemization rate as a function of temperature cycle parameters such as temperature swing and cooling rate.

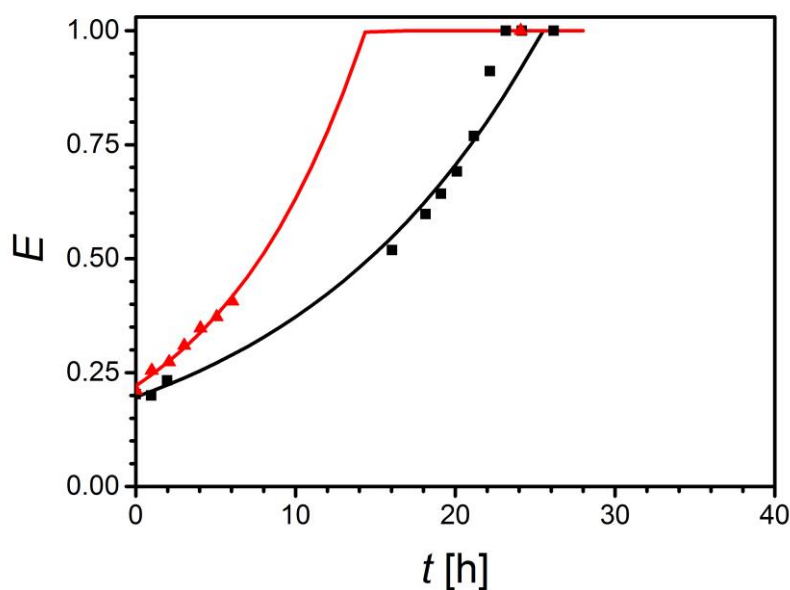
The values for both rate constants are displayed in Table 1 for all experiments. Errors in  $k$  and  $k_N$  values stem from two sources, the standard deviation from fitting experimental data to equations 3 and 4, and the deviation caused by the inaccuracy in catalyst concentration. The sum of these two deviations is shown in Table 1 as an overall error.

**Table 1.** Deracemization conditions and results: including excess enantiomer concentration  $\Delta c$ , molar ratio Phe: XSA, total dry mass concentration  $c_t$ , catalyst concentration  $c_{cat}$ , temperature swing  $\Delta T$ , cooling rate  $R_c$ , mass fraction of solid involved in a cycle  $f_{\Delta T}$ , temperature profile and the duration of a cycle. The results are represented by the deracemization rate constants  $k$  and  $k_N$ .

Experiment	$\Delta c$ (mg/ml)	Molar ratio Phe:XSA <sup>‡</sup>	$c_t$ [mg/ml]	$c_{cat}$ [mg/ml]	$\Delta T$ [°C]	$R_c$ [°C/min]	$f_{\Delta T}^*$	$T$ Profile	Cycle time [min]	$k$ [h <sup>-1</sup> ]
A1	0	1.31:1	130	14.7	5	0.055	0.05	TP1	110	0.012 ± 0.001
A2	6.4 (D)	1.44:1	135.6	14.7	5	0.055	0.048	TP1	110	0.013 ± 0.001
A3	7 (L)	1.45:1	137.8	14.7	5	0.11	0.047	TP2	65	0.017 ± 0.002
B1(ref)	6.4 (L)	1.44:1	136.7	14.7	15	0.5	0.14	TP3	60	0.064 ± 0.005
B2	6.4 (L)	1.44:1	95.6	14.7	15	0.5	0.222	TP3	60	0.105 ± 0.011
B3	6.4 (L)	1.44:1	136.7	7.4	15	0.5	0.14	TP3	60	0.044 ± 0.006
B4	6.4 (L)	1.44:1	136.7	29.4	15	0.5	0.14	TP3	60	0.160 ± 0.022
B5	0	1.31:1	130	14.7	15	0.5	0.148	TP3	60	0.039 ± 0.003
B6	6.4 (L)	1.44:1	136.7	14.7	15	0.3	0.14	TP4	80	0.056 ± 0.005
B7	6.4 (L)	1.44:1	136.7	14.7	10	0.5	0.082	TP5	50	0.028 ± 0.004
B8	6.4 (L)	1.44:1	136.7	14.7	20	0.5	0.212	TP6	70	0.117 ± 0.015

\* $f_{\Delta T}$  of all deracemization experiments were calculated based on the salt solubility in the presence of either a  $c_{cat}$  of 13.2 mg/ml or 26.4 mg/ml (B4). It is assumed that the difference between the  $c_{cat}$  used for  $f_{\Delta T}$  calculation and the actual values used in the deracemization experiments would not lead to a significant deviation in the corresponding  $f_{\Delta T}$ .

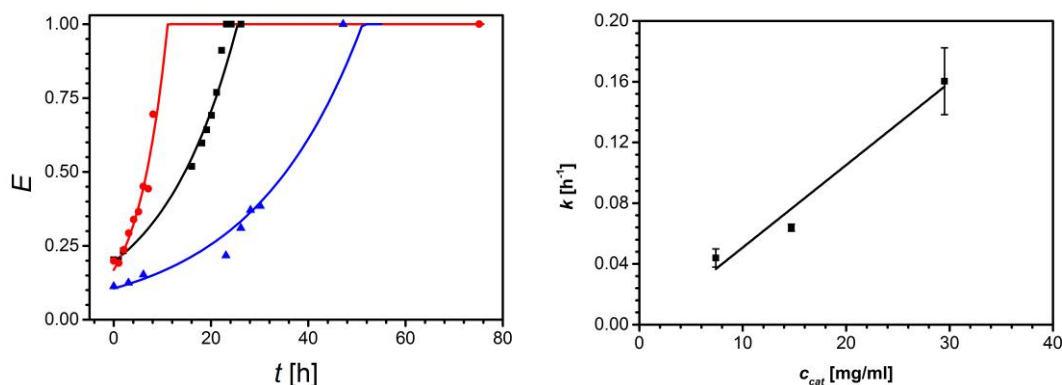
**Effects of the Initial Compositions on the deracemization rate constants.** First, the three operation parameters shared by both the temperature cycling method and Viedma Ripening were tested, the dry mass concentration  $c_t$ , the concentration  $c_{cat}$  of catalyst added and the excess enantiomer concentration  $\Delta c$ . Figure 4 shows that in the standard experiment B1 solid phase homochirality was achieved after approximately 23 hours with a deracemization rate constant  $k$  of  $0.066 \text{ h}^{-1}$  and a  $k_N$  value of also 0.066 per cycle because the cycle time was 1 h for that experiment.



**Figure 4.** Enantiomeric excess  $E$  as a function of time  $t$  with different dry mass concentration:  $c_t = 137.6 \text{ mg/ml}$  (■ standard experiment B1) and  $95.6 \text{ mg/ml}$  (▲ B2). The lines are best fits to equation 3.

The deracemization experiment B2 differs from B1 by having a roughly 40% lower dry mass concentration  $c_t$  of  $95.6 \text{ mg/ml}$  and is also shown in Figure 4. At a fixed temperature, a lower dry mass concentration  $c_t$  results in a lower suspension density, leading to a faster full deracemization, with a roughly 40% higher  $k$  of  $0.105 \text{ h}^{-1}$ . This faster deracemization rate at a lower suspension density was also found in both Viedma ripening and the temperature cycling method using other systems.<sup>6, 15</sup>

The next parameter tested was the catalyst concentration  $c_{cat}$  used for the solution phase racemization reaction. Two experiments, B3 and B4, were conducted in which, compared to B1, respectively a higher and a lower  $c_{cat}$  were used. The time development of  $E$  in all three experiments is shown in Figure 5.



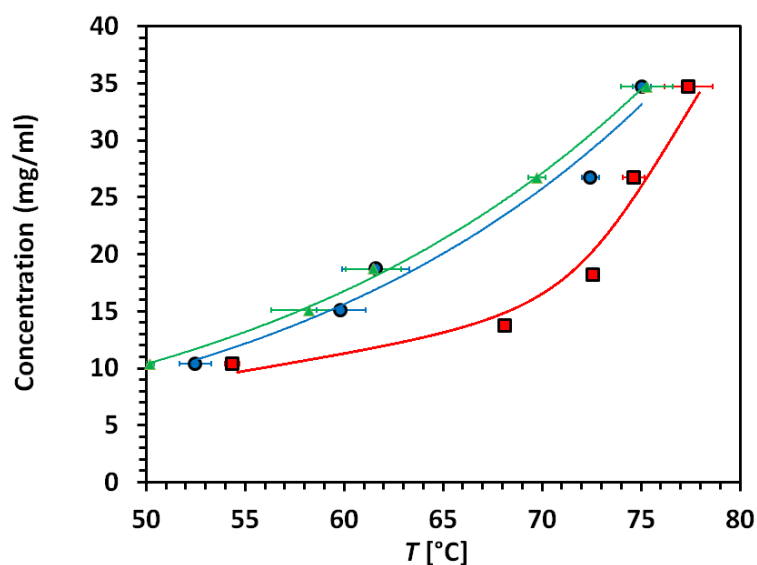
**Figure 5.** Left: Enantiomeric excess  $E$  as a function of time  $t$  with different catalyst concentration:  $c_{cat} = 29.4$  mg/ml ( $\bullet$  experiment B4), 14.7 mg/ml ( $\blacksquare$  standard experiment B1) and 7.4 mg/ml ( $\blacktriangle$  B3). The lines are best fits to equation 3. Right: Correlation between time-based deracemization rate constant  $k$  and catalyst concentration  $c_{cat}$  from experiment B1, B3 and B4. The solid line is a linear fit of the experimental points ( $\blacksquare$ ) and serves as a guide for the eye.

Figure 5 (left) shows that a higher catalyst concentration, such as in B4, increased the deracemization rate significantly. The experiment B3 with a lower catalyst concentration led to a slower deracemization. Figure 5 (right) indicates a roughly linear relationship between the deracemization rate constant  $k$  and the catalyst concentration  $c_{cat}$ , which has also been observed in Viedma Ripening of *N*-(2-methylbenzylidene)-phenylglycine amide by Noorduin et al.<sup>15</sup> This effect can be attributed to two factors: a faster racemization reaction and a changing solubility.

Yamada et al. tested the effect of catalyst concentration on the racemization kinetics of optical amino acids such as Alanine and Methionine and they found that a higher ratio of catalyst over amino acid led to a faster racemization reaction.<sup>13</sup> The faster racemization reaction in the solution phase might have resulted from the increased concentration of Schiff base formed by the additional catalyst and the amino acid. Spix et al. found that, starting with an enantiopure solution, the racemization reaction of Phe-XSA in acetic acid at 70°C took 1-2 hours to arrive at a racemic solution.<sup>11</sup> This duration is of the same order of magnitude as the cycle time applied in this study. Therefore, when there is an imbalance between the two enantiomers in the solution, it is likely that the relatively slow racemization reaction is not able to eliminate the concentration difference between the two enantiomers in time. A system with a faster racemization reaction would therefore have a smaller, if not negligible, difference in the concentration level of the two enantiomers and is expected to lead to a shorter deracemization time.

Another factor which could influence the deracemization rate constant through  $c_{cat}$  is the solubility change of Phe-XSA salt by the introduction of the catalyst. The presence of a higher concentration of catalyst might lead to an increase in the solubility of Phe-XSA in acetic acid. As has been observed from Figure 4, a higher racemization catalyst concentration facilitates the deracemization process. To verify the solubility dependence of the compound on the catalyst concentration the solubility of Phe-XSA in acetic acid with and without catalyst was measured and is shown in Figure 6. In the presence of a  $c_{cat}$  of 26.4 mg/ml, the saturation temperatures of Phe-XSA in acetic acid were reduced by approximately 2°C compared to those when  $c_{cat}$  was 13.2 mg/ml. This confirms that the solubility of the salt increases due to the presence of the catalyst, which subsequently speeds up the deracemization.

To summarize, when applying a higher  $c_{cat}$ , the combining effect of a faster solution phase racemization and lower solid phase suspension density could lead to a higher deracemization rate constant, as demonstrated in Figure 5. It is worth mentioning that the 4% standard deviation in catalyst amount added by Pasteur Pipette (see the experimental section), according to the correlation shown in Figure 5 (right), could lead to roughly an additional 5% error in  $k$ .



**Figure 6.** Solubility of DL-Phe-XSA salt (1.31:1 molar ratio) in acetic acid with catalyst ( $c_{cat} = 13.2$  mg/ml, ● and 26.4 mg/ml, ▲) and without catalyst (■). The lines are a guide to the eye.

The effect of excess enantiomer concentration  $\Delta c$  was investigated by comparing two pairs of experiments: A1 and A2 as pair one and B1 and B5 as pair two. A1 and B5 have  $\Delta c = 0$  mg/ml while for B1 and A2 additional L-Phe ( $\Delta c = 6.4$  mg/ml) respectively D-Phe ( $\Delta c = 6.4$  mg/ml), was present. Between the two pairs, different temperature profiles were used: TP1, which had a smaller temperature swing of 5°C and a cooling rate of 0.055°C/min, was applied to A1 and A2, while TP3 ( $\Delta T = 15^\circ\text{C}$  and  $R_c = 0.5^\circ\text{C}/\text{min}$ ) was used for B1 and B5.

The results for these two experiment sets are shown in Figure 7. As expected, a longer deracemization time was needed for B5 as compared to B1. On the other hand, in the first experiment pair, an  $E(0)$  of 0.144 in A2 was obtained while the evolution of  $E$  in A1 starting from 0 shows a similar deracemization rate constant ( $0.0124 \text{ h}^{-1}$  in A1 compared to  $0.0120 \text{ h}^{-1}$  in A2).

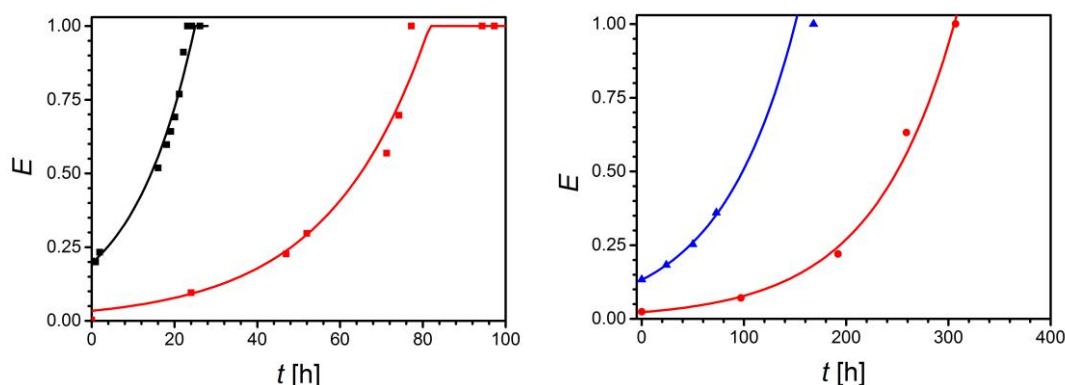


**Figure 7.** Enantiomeric excess  $E$  as a function of time  $t$  for different excess enantiomer concentrations:  $\Delta c = 0 \text{ mg/ml}$  ( $\blacksquare$  experiment B5, left and  $\bullet$  experiment A1, right),  $6.4 \text{ mg/ml}$  (L) ( $\blacksquare$  B1, left) and  $6.4 \text{ mg/ml}$  (D) ( $\blacktriangle$  A2, right). The lines in both figures are best fits to equation 3.

In experiments B1 and A2, the additional L-Phe or D-Phe had three effects on the overall suspension composition, a slightly higher dry mass concentration  $c_t$  which in turn raised the corresponding suspension density, a higher molar ratio Phe:XSA which led to more free amino acid for the solution racemization reaction (see Table 1) and an increased  $E(0)$  (see Figure 7).

Based on the observation from Figure 4, the slightly increased  $c_t$  in B1 and A2 should lead to a slower deracemization, which is opposite to what is observed for the pair of B1 and B5, while the pair of A1 and A2 does not show a change in deracemization rate. From equation 3,  $E(0)$  and  $k$  should be independent from each other, which would exclude an effect from the larger  $E(0)$ . Therefore, the most probable reason for the increased  $k$  in B1 compared to B5 lies in the second effect: an increased free amino acid by the additional L-enantiomer.

Spix et al. have reported that a higher amount of free amino acid in the solution phase increases the racemization reaction kinetics.<sup>11</sup> The racemization reaction was therefore faster in B1 than in B5. As has been discussed before, the solution could end up in more D-enantiomer enriched in B5 compared to B1 and the growth, agglomeration and secondary nucleation of the L-Phe-XSA crystals could be slowed down. As a consequence, the evolution of solid phase  $E$  was slower when no additional L-Phe was added in B5.

Based on the same reasoning, the racemization reaction was also faster in A2 than in A1. However, in the pair A1 and A2, a smaller  $\Delta T$  and cooling rate was used. The longer cooling period led to a smaller supersaturation of the minor solid phase enantiomer, in this case D-Phe-XSA, compared to

the supersaturation of the same enantiomer in B5. Therefore, a shorter, if not negligible, delay in the deracemization process was observed in the pair of A1 and A2.

#### **Effect of the temperature cycling conditions on the deracemization rate constants.**

The effects of two parameters related to the temperature profiles were investigated, i.e. the cooling rate  $R_c$  and the temperature swing  $\Delta T$ . Figure 8 shows that experiment B6 with  $R_c = 0.3^\circ\text{C}/\text{min}$  had a slightly smaller deracemization rate constant than the standard experiment B1 for which a higher cooling rate of  $0.5^\circ\text{C}/\text{min}$  was used. Interestingly, the cycle-based deracemization rate constant was slightly larger for B6 than for B1. However, if the errors in  $k$  and  $k_N$  in B1 and B6 are taken into account, the difference in the deracemization rate between these two experiments is negligible (See Table 1.). Therefore, it seems that within the range tested in this study, the cooling rate did not affect the deracemization rate significantly.

Suwannasang et al. found that the cooling rate did not influence the time needed to reach full deracemization, which indicates that in their case the deracemization process with a higher cooling rate needs more cycles to achieve solid phase homochirality. They attributed the less efficient deracemization per cycle to the increased secondary nucleation rate of the enantiomer of minor solid amount taking place during the cooling part of the temperature cycle. In their study, the lower efficiency in deracemization per cycle was exactly compensated by a shorter cycle time, which led to an unchanging deracemization time with increasing cooling rate.<sup>6</sup>

In the modelling study of Katsuno and Uwaha, a similar reduction in the enantiomeric excess evolution per cycle by faster cooling was obtained while the total time needed for full deracemization was not significantly influenced.<sup>8</sup>

In the present study, the cooling rate showed an impact on neither the time-based nor the cycle-based deracemization rate constants. The results suggest that the secondary nucleation of the minor enantiomer did not delay the deracemization per cycle to the same extent as it was in the literature. Therefore, in future investigations, even higher cooling rate  $R_c$  values can be tested to examine the possibility of speeding up the deracemization process by means of fast cooling.

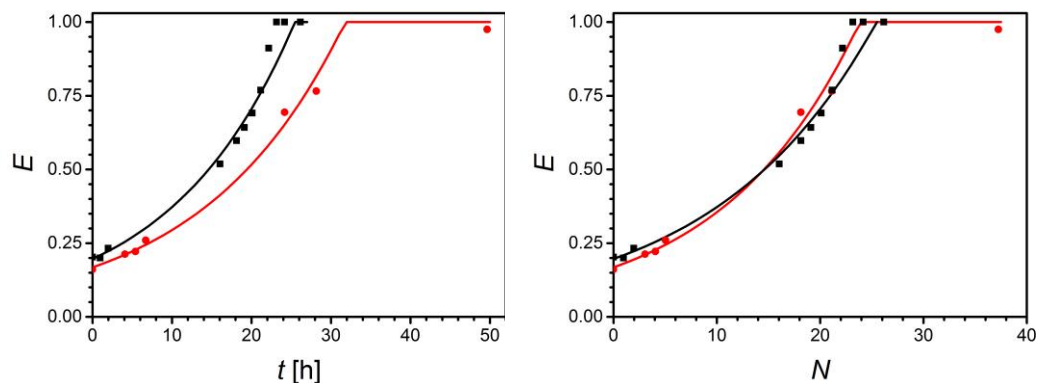


**Figure 8.** Enantiomeric excess  $E$  as a function of time  $t$  (left) and number  $N$  of temperature cycles (right) with different cooling rates:  $R_c = 0.3^\circ\text{C}/\text{min}$  ( $\bullet$  experiment B6) and  $0.5^\circ\text{C}/\text{min}$  ( $\blacksquare$  B1). The lines are best fits to equation 3 (left) and equation 4 (right).

The final parameter tested was the temperature swing  $\Delta T$ . In Figure 9, the results of experiment B1 with a temperature swing of  $15^\circ\text{C}$  is compared with those of B7 and B8, in which a smaller and a larger temperature swing of  $10^\circ\text{C}$  and  $20^\circ\text{C}$  were employed, respectively. It can be seen clearly that a faster full deracemization was achieved with a larger temperature swing  $\Delta T$  while less cycles were needed. Both the time-based and cycle-based deracemization rate constants increased with increasing temperature swing.

In their temperature cycling deracemizations, Suwannasang et al. observed a significant decrease in the time needed for full deracemization at lower suspension densities and in their following simulation work, in which the authors explored the possibility that the crystal growth kinetics are the cause of the deracemization, the same relation was found.<sup>6-7</sup> They explained this effect with the mass fraction  $f_{\Delta T}$  of solid involved in the dissolution-growth cycles.

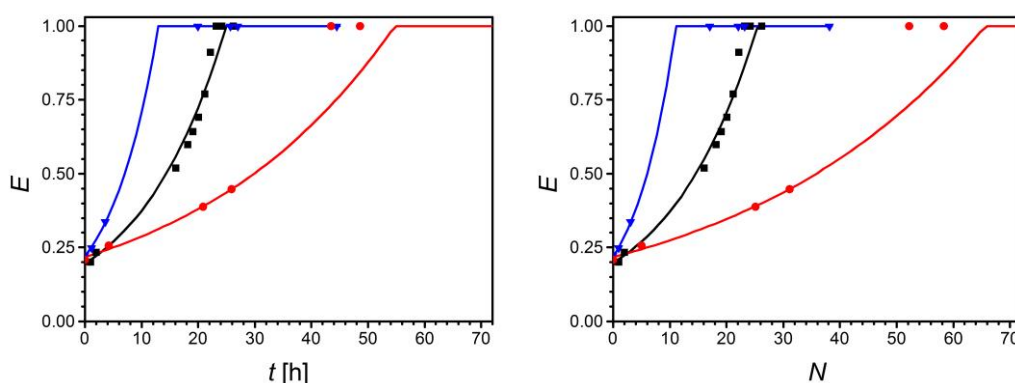


**Figure 9.** Enantiomeric excess  $E$  as a function of time  $t$  (left) and number  $N$  of temperature cycles (right) for different temperature swings:  $\Delta T = 10^\circ\text{C}$  ( $\bullet$  experiment B7),  $15^\circ\text{C}$  ( $\blacksquare$  B1) and  $20^\circ\text{C}$  ( $\blacktriangledown$  B8). The lines are best fits to equation 3 (left) and equation 4 (right).

Figure 10 shows the relationship between the temperature cycling-based deracemization rate constant  $k_N$  and the mass fraction  $f_{\Delta T}$  for all the experiments in this study. The cycle-based constant  $k_N$

was used to exclude the influence of the duration of each cycle when different  $\Delta T$  values were used. The four experiments exploiting the adjustment of  $f_{\Delta T}$  by  $\Delta T$  and  $c_i$ , namely B1, B2, B7 and B8, can be distinguished from the rest of the experiments in Figure 10 by their linear relationship as expressed by the line fitted through the four experimental points of these experiments indicated by the red points.

The other experiments, except B4 with a much higher catalyst concentration of 29.4 mg/ml, also seem to follow the linear trend of  $k_N$  versus  $f_{\Delta T}$ . From the parameter analysis above,  $k_N$  can be influenced by other factors such as  $\Delta c$  as well, however, the trend shown in Figure 10 indicates that among all the factors,  $f_{\Delta T}$  could be one of the most effective.

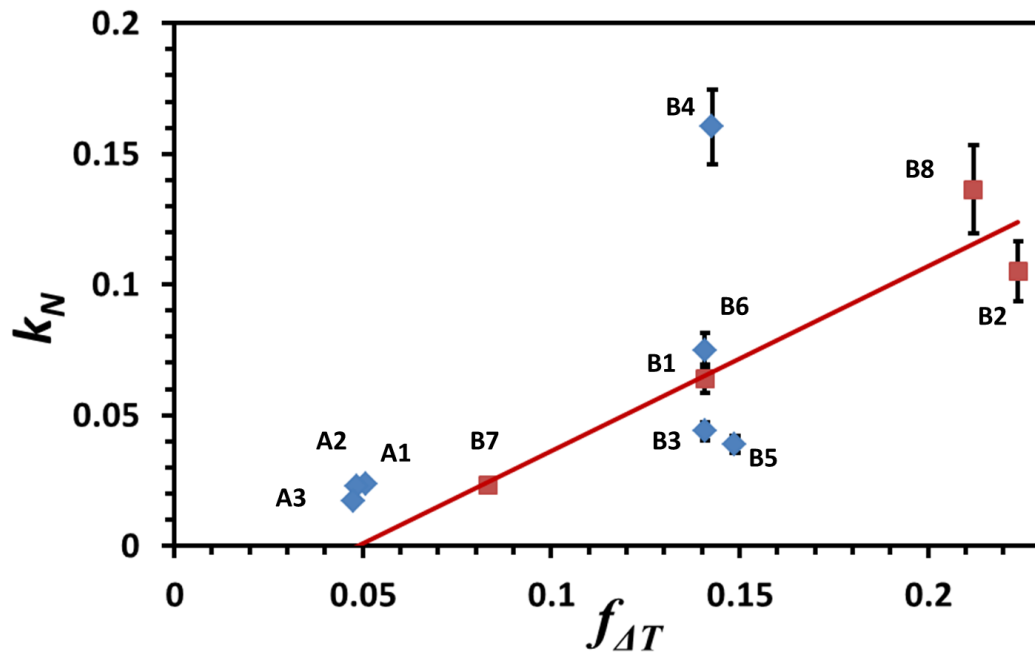


**Figure 10.** Cycle-number-based deracemization constant  $k_N$  vs mass fraction  $f_{\Delta T}$  of solid involved in the heating-cooling cycles. Experiments exploiting the effect of  $c_i$  and  $\Delta T$  are shown as ■ and other experiments in this study are shown as ♦. The solid line is a linear fit of the experimental points (■) and serves as a guide for the eye.

**Preliminary comparison between Temperature Cycling and Viedma Ripening.** The rate constants  $k$  of all the deracemization experiments performed are compiled in Figure 11. In addition, the rate constant  $k$  in the deracemization of the same salt system using Viedma ripening is included.<sup>11</sup> The rate constants in the verification experiments A1 to A3 are in the same range as the Viedma Ripening ones. By modifying some of the operational conditions, especially increasing the temperature swing, the deracemization rate is significantly increased. This comparison suggests that the temperature cycling method is a powerful alternative to Viedma Ripening.

Compared to Viedma Ripening, the industrial application of the temperature cycling method is likely to be more convenient: 1) It is easier to scale-up than Viedma Ripening. In order to achieve sufficient grinding, the total volume of glass beads and the slurry will require a significantly larger

crystallizer, which will increase the capital investment. Though recent studies have proved that glass beads can be replaced by ultrasound,<sup>16-17</sup> novel industrial crystallizers need to be developed to host the ultrasound generator. The crystallizers should be able to cope with technical issues such as the nonhomogeneity of the acoustic field in the suspension.<sup>18</sup> 2) The solid phase from a Viedma ripening process still needs additional steps to separate the crystals from the grinding beads, which might lead to product loss.

In any case, both the Viedma ripening and the temperature cycling method need to be further optimized in order to facilitate the deracemization efficiency. In the case of Viedma ripening, parameters such as the suspension density, the catalyst concentration and the intensity of grinding have been found influential to the deracemization efficiency.<sup>15</sup> While the temperature cycling method can be potentially tuned by these parameters, except the grinding intensity, it can also be further optimized by applying a larger temperature swing, which is proved in this study to be a major contributor for speeding up the deracemization process. Moreover, a change in  $\Delta T$  goes without penalty on the yield as is the case when adjusting the suspension composition. A larger temperature swing could even be counterbalanced by a faster cooling rate resulting in the same cycle time, provided that the cooling rate  $R_c$  is still small enough to avoid significant secondary nucleation of the enantiomer present in minority.

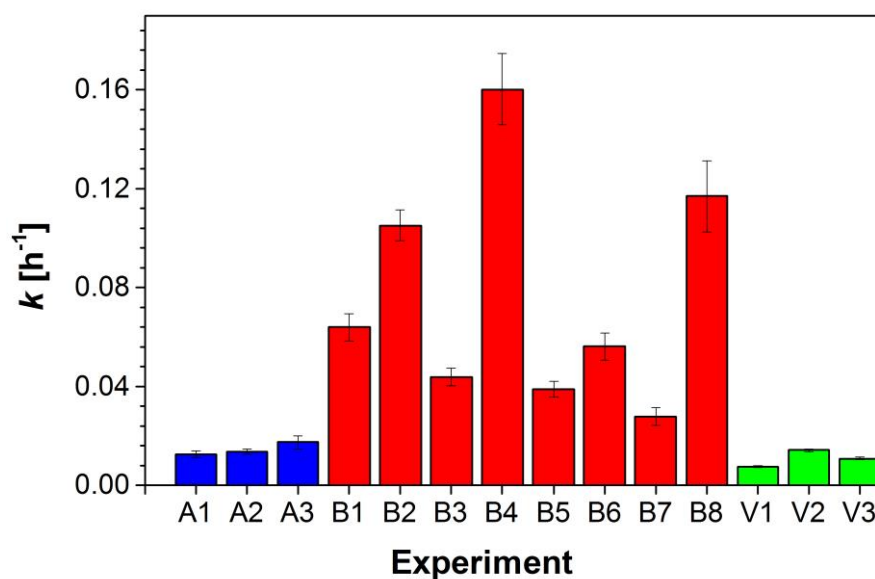


**Figure 11.** Time-based deracemization rate constant  $k$  of the temperature cycling method (A1-B8) and the grinding method (V1-V3).<sup>11</sup> Two different  $\Delta c$  were used in Viedma Ripening, 0 mg/ml (V1) and 6.4 mg/ml (L) (V2 and V3).

## 4. CONCLUSION

The successful deracemization of the racemic compound Phenylalanine by the temperature cycling method, via its conglomerate-forming salt, shows that the theoretical application range of this technique can be expanded likewise as was shown earlier for Viedma ripening. Moreover, the studied effects of operational parameters give insight in how to optimize the deracemization process. For the Phe-XSA system under investigation, the deracemization rate is mainly influenced by the kinetics of the solution racemization and the mass fraction  $f_{\Delta T}$  of solid involved in the temperature cycles. This information will benefit the design and optimization of an industrial application. A comparison of the deracemization rate using Viedma Ripening and the temperature cycling method indicates that the latter one is a powerful alternative tool for deracemization with additional parameters, such as the temperature swing  $\Delta T$ , to control and optimize the process.

## REFERENCES

1. Viedma, C., *Phys.Rev.Lett.* **2005**, *94*, 065504-1-4.
2. Pagni, R. M. C., R.N. , *Cryst. Growth Des.* **2002**, *2* (4), 249-253.
3. Noorduyn, W. L. I., T.; Milemaggi, A.; Leeman, M.; Meekes, H.; van Enkevort, W.J.P.; Kellogg, R.M.; Kaptein, B.; Vlieg, E.; Blackmond, D.G., *J. Am. Chem. Soc.* **2008**, *130*, 1158-1159.
4. Noorduyn, W. L. v. E., W.J.P.; Meekes, H.; Kaptein, B.; Kellogg, R.M.; Tully, J. C.; McBride, J.M.; Vlieg, E., *Angew. Chem. Int. Ed.* **2010**, *49*, 8435-8438.
5. Steendam, R. R. E. V., J.M.M.; van Benthem, T.J.B.; Meekes, H.; van Enkevort, W.J.P.; Raap, J.; Rutjes, F.P.J.T.; Vlieg, E., *Nat. Commun.* **2014**, *5*, 6543.
6. Suwannasang, K. F., A. E.; Rougeot, C.; Coquerel, G. , *Cryst. Growth Des.* **2013**, *13*, 3498-3504.
7. Suwannasang, K. C., G.; Rougeot, C.; Flood, A. E., *Chem. Eng. Technol.* **2014**, *37* (8), 1329-1339.
8. Katsuno, H. U., M., *Phys.Rev E Stat. Nonlin. Soft.* **2016**, *93*, 013002.
9. Srisanga, S. t. H., J. H. , *Cryst. Growth Des.* **2010**, *10* (4), 1808-1812.
10. Jean Jacques, M. L., Marie-Josephe Brienne, *Tetrahedron* **1981**, *37* (9), 1727-1733.
11. Spix, L. A., A.; Meekes, H.; van Enkevort, W. J. P.; Vlieg, E., *Cryst. Growth Des.* **2014**, *14*, 1744-1748.
12. Kimoto, H. S., K.; Ohashi, Y.; Hasegawa, M. , *Bull. Chem. Soc. Jpn.* **1989**, *62* (7), 2189-2198.
13. Yamada, S. H., C.; Yoshioka, R.; Chibata, I., *J. Org. Chem.* **1983**, *48* (6), 843-846.

14. Noorduin, W. L. M., H.; Bode, A. A. C.; van Enkevort, W. J. P.; Kaptein, B.; Kellogg, R. M.; Vlieg, E., *Cryst. Growth Des.* **2008**, *8* (5), 1675-1681.
15. Noorduin, W. L. M., H.; van Enkevort, W. J. P.; Millemaggi, A.; Leeman, M.; Kaptein, B.; Kellogg, R. M.; Vlieg, E., *Angew. Chem. Int. Ed.* **2008**, *47*, 6445-6447.
16. Rougeot, C. G., F.; Plaquevent, J.; Coquerel, G., *Cryst. Growth Des.* **2015**, *15* (5), 2151-2155.
17. Xiouras, C. v. A., J.; Panis, J.; ter Horst, J. H.; van Gerven, T.; Stefanidis, G. D., *Cryst. Growth Des.* **2015**, *15* (11), 5476-5484.
18. Ruecroft, G. H., D.; Ly, T.; Maxted, N.; Cain, P. W., *Org. Process Res. Dev.* **2005**, *9*, 923-932.

# Chapter 6. Concomitant Solid Separation through Electric Field Enhanced Crystallization

**Key words:** Crystal Engineering, Dielectrophoresis, Electrophoresis, Multi-component mixtures, Separation Technology

**Abstract:** When applied to a pure component suspension in an apolar solvent, a strong inhomogeneous electric field induces particle movement and the particles are collected at the surface of one of the two electrodes. This new phenomenon was used to separately isolate two organic crystalline compounds, phenazine and caffeine, from their suspension of 1,4-dioxane. First, the crystals of both compounds were collected at different electrodes under the influence of the electric field. Subsequent cooling crystallization allowed the immobilization and growth of the particles on the electrodes, which were separately collected after the experiment with purities higher than 91%. This method can be further developed into a technique for crystal separation and recovery in complex multicomponent suspensions of industrial processes.

## 1. INTRODUCTION

Crystallization is an effective and efficient separation technology that can, in a single process step, recover the desired compounds from solutions as high purity (>99%) crystalline solids<sup>1-4</sup>. However, such highly purified product is hard to obtain from a multi-component solution by direct crystallization, such as the product stream from a type-I Multicomponent Reaction (MCR),<sup>5-6</sup> or a racemic mixture of chiral pharmaceutical compounds,<sup>7</sup> since a mixed suspension is a likely result. Further purification of the solid phase usually requires additional steps (see Figure 1 (a) for instance), which will inevitably lead to the loss of valuable products. Alternatively, a single crystallization step coupled with simultaneous particle separation could diminish the product loss while effectively recovering desired solute from the mixed solution.

Particle manipulation and subsequent separation can be achieved by the application of electromagnetic fields: a magnetic field could separate polymorphs, crystalline solids with different solid-state structures, to prepare seeds for large-scale crystallization, provided that a suitable paramagnetic medium can be found<sup>8</sup>. Alternatively, an electric field has been used in the successful capturing or manipulation of desired nanoparticles<sup>9</sup> and the assembly of colloid particles for the production of, for instance, optically tunable micropatterns, biosensors, and biofuel cells.<sup>10-12</sup> In all of these cases, the liquid phases did not contain any dissolved particle materials. On the other hand, the electric field has been used to localize protein crystallization and control its nucleation rate from a clear solution, in absence of any seed crystals.<sup>13-14</sup> However, up till now, the combination of particle manipulation by an electric field with the crystallization process for the in-situ product separation and recovery has, to our knowledge, never been attempted. In the present study, the experimental proof is given for an electric field enhanced crystallization (EEC) process by which the two solutes from a multi-component solution are separately recovered, as schematically demonstrated in Figure 1 (b).

## 2. RESULTS

Subjected to an inhomogeneous electric field, particles in a suspension experience dielectrophoretic (DEP) and possibly electrophoretic (EP) forces: DEP originates from the difference in dielectric constants of the particles and the surrounding medium and drags the particles with larger dielectric constant towards the location of the electric field maxima,<sup>15-16</sup> while EP forces, which work only on charged particles, are directed towards the electrode with the counter charge.<sup>17</sup> To prevent electrochemical reactions, which would reduce the product yield, the current through a crystallizing suspension should be minimized. Meanwhile, the inhomogeneous field needs to be sufficiently strong and the dielectric constant of the solvent should be sufficiently small to ensure the effective manipulation of crystals by the DEP force. Therefore, the apolar and non-conductive solvent 1,4-dioxane was used in this study.

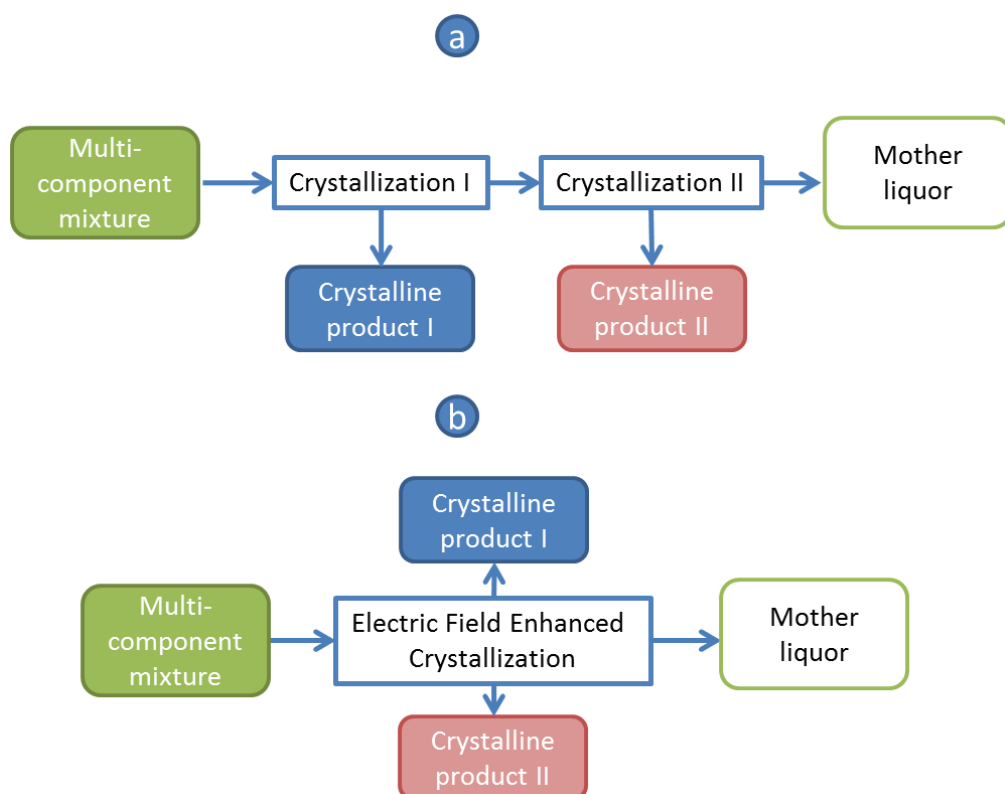


**Figure 1.** Schematic demonstrations of solutes separation from a multi-component solution by direct crystallization (a) and Electric Field Enhanced Crystallization (b).

We first applied an inhomogeneous electric field to a 6 mL isonicotinamide (INA) suspension in 1,4-dioxane (*ca.* 18 mg solid/ml solvent), generated by a Direct Current (DC) potential difference between two parallel rod-shape electrodes roughly 6 mm apart, which were immersed into the suspension. In the presence of a DC potential difference above approximately 2 kV, INA crystals started to move around the electrodes. More crystals participated in this circular movement with increasing potential difference. In addition, INA crystals gradually accumulated on the anode (Fig. 2). Above around 5 kV DC potential difference the amount of crystals collected at the anode was so large that a crystal bridge formed between the electrodes. Upon switching off the electric field, the collected crystals detached from the anode and settled back to the bottom. When a similar potential difference was applied to an INA solution in absence of crystals, the solution-air interface was only slightly vibrating. No movement of liquid could be observed in pure dioxane. This indicates that the motion of INA particles is, for a large part, related to the interaction of the crystals with the electric field. During the course of the experiments, no current larger than the detection limit of 0.01 mA was observed. No gas formation could be observed on either of the electrodes indicating that the solute does not undergo significant electrochemical reactions. Since the electric field was generated by a constant DC voltage and no

significant current was detected, it was assumed that there was an electrostatic field present in the suspension during the experiment.

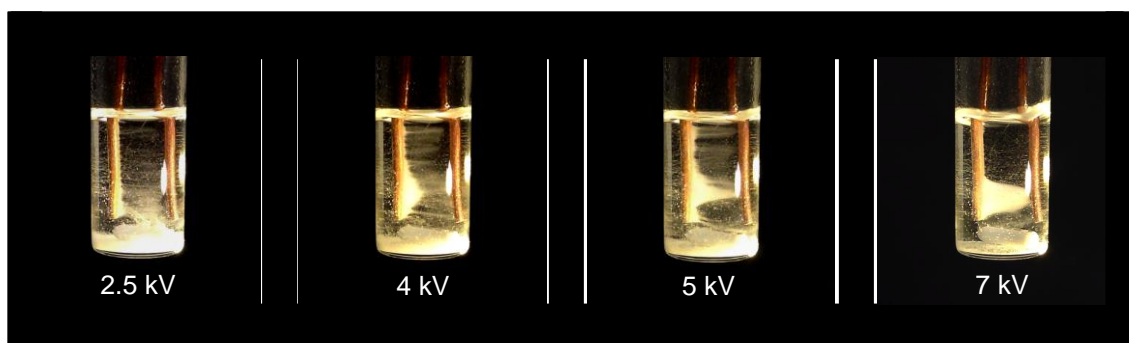


**Figure 2.** An inhomogeneous static electric field induced fluid and particle dynamics above a DC potential difference of 2 kV in a suspension of INA in dioxane. The INA crystals were collected at the anode and above around 5 kV DC potential difference a crystal bridge was formed between the electrodes. Although a magnetic stirrer bar was present in the vial, it was not used to stir the solution.

Equivalent experiments were conducted using the suspension of other organic compounds in 1,4-dioxane. Table 1 reveals an interesting result: particle motion was induced in all cases and crystals accumulated on either the anode or the cathode. When the polarity of the two electrodes was reversed by changing the potential difference from +7.5 kV to -7.5 kV, crystals that had accumulated on one electrode migrated to the other one, e.g. INA crystals moved from the old anode to the new one, instead of being attracted by both electrodes, which were symmetrically the two locations of field maxima.

**Table 1.** The electrodes at which the crystals accumulated for the experiments in which inhomogeneous electric fields of +7.5 and -7.5 kV were applied to the suspension of the organic compounds isonicotinamide (INA), niflumic acid (NIF), caffeine (CAF), phenazine (PHE) and 4-hydroxybenzoic acid (HBA) in the solvent 1,4-dioxane. When changing polarity the crystals accumulated on the electrochemically same electrode, i.e. when changing the polarity, INA crystals moved to the new anode.

Electrode	Crystalline compound		
Anode	INA	NIF	CAF
Cathode	PHE	HBA	

This selective accumulation of crystals on only one electrode indicates the involvement of both DEP and EP forces: the non-uniform electrostatic field exerts a positive DEP on the crystals in the suspension which triggers their motion towards the two electrodes. Even in apolar solvents, particle surfaces can be slightly charged<sup>18-20</sup> but the EP forces on the crystals becomes significant only in the vicinity of the electrodes. Crystals approaching the anode are further attracted until they settle on its

surface while crystals close to the cathode are repelled. The repelled crystals continue to circulate until they eventually are captured by the anode. Subsequently the entire crystalline mass accumulates on the surface of the anode. Since particulate materials differ in their electronic properties such as dielectric constant and surface charge, the combined effect of DEP and EP forces can lead to the accumulation of corresponding crystals on different electrodes, which enables the development of particle separation methods.<sup>21-23</sup>

However, in order to be collected from the solution, the accumulated crystals need to be immobilized on the electrode. This immobilization of crystals was realized by slowly cooling the suspension in the presence of the electric field. Upon cooling the solubility decreased and the accumulated particles could further grow on and attach to the electrode surface. Two separate experiments (see Figure 5 as Experiment 1A and 1B) were performed on the pure component suspensions of model compounds PHE and CAF.

In experiment 1A a suspension of PHE (*ca.* 26 mg solid/ml solvent) was prepared at 30°C. (see details in APPENDIX) A DC potential difference of -7.5 kV was then applied between the two electrodes and the PHE crystals accumulated at the cathode surface within 1 minute. In the presence of the electric field the suspension was slowly cooled down in an oil bath to 15°C in 3 hours and then kept at this temperature overnight to allow crystal growth to occur. After approximately 15 hours at 15°C, the electric field was turned off showing that most of the PHE crystals were attached to the cathode surface as is shown in Figure 3 (left) and could be directly removed from the solution by withdrawing the electrode. The same procedure was applied to a caffeine (CAF) suspension in experiment 1B and the corresponding crystals were collected from the anode (figure is not shown here).

Additionally, the existence of another solute in the solution phase (see Figure 5 and APPENDIX, Experiment 2A and 2B) did not influence the behavior of suspensions in the electric field. Similar to experiment 1B, CAF crystals in experiment 2A were collected from the anode, after cooling crystallization to 15°C under the electric field, from a solution mixture with additional PHE present below its saturation concentration (see Figure 3 (right)). The XRPD analysis of the crystalline product showed the presence of CAF crystals only (see APPENDIX). These experiments verify that the electric-field-induced particle capturing combined with cooling crystallization can be used as an in-situ recovery technique for a target system where only one compound is present in the solid phase.

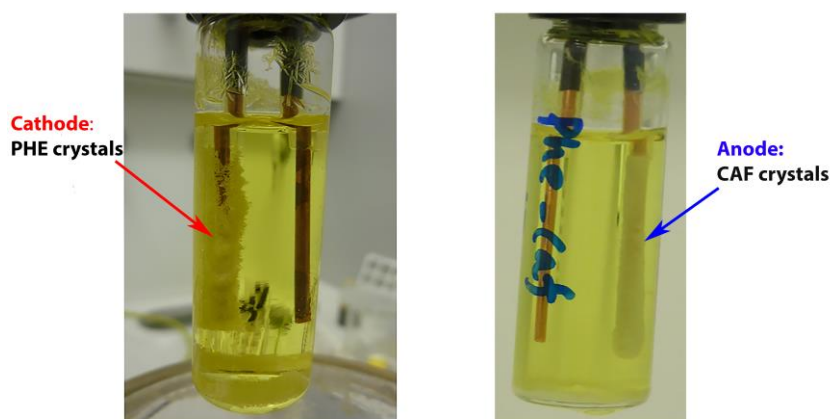


**Figure 3.** Left: PHE crystals accumulated and then attached on the **cathode** in a PHE suspension in dioxane after cooling in the presence of an electric field (Experiment 1A); Right: Suspended CAF crystals in a solution containing both CAF and PHE accumulated and then attached on the **anode** during seeded cooling crystallization controlled by an electric field (Experiment 2A).

Up until this stage, the EEC managed to collect crystals of PHE and CAF from their suspensions, with or without the presence of another solute in the liquid phase. The final step is to verify that the separation of PHE and CAF crystals during crystallization from their mixture can also be achieved by EEC. A 6 mL dioxane suspension containing both CAF (*ca.* 13 mg solid/ml solvent) and PHE (*ca.* 29 mg solid/ml solvent) crystals was prepared at 30°C (Experiment 3 in Figure 5, see details in APPENDIX). In the presence of a -7.5 kV DC potential difference crystals accumulated on the surfaces of both electrodes at 30°C (see Figure 4, left). The suspension was then linearly cooled down to 15°C in 3 hours and kept at this temperature overnight, during which time the electric field was constantly applied. Crystal layers of different shape and color were formed on both electrodes reflecting the appearance of PHE (cathode) and CAF (anode) crystalline phases (Figure 4, right).

The crystals from the two electrodes were removed from the bulk solution and separately weighed for yield estimation and then analyzed using XRPD and  $H^1$ -NMR for compositions. From the anode, 27 mg of crystalline material was recovered which consisted of  $91.4 \pm 2.2$  wt% of CAF. From the cathode, 177 mg of crystalline material was recovered which consisted of  $99.6 \pm 2.4$  wt% PHE (see Appendix). The yields of recovery of CAF and PHE were 20.9% and 53.5%, respectively (see summary in Figure 6). The same experiment was duplicated and lower yields but similar solid phase purities to those reported above were obtained. This result verified that the combination of the selective particle collection, induced by an inhomogeneous electric field, and cooling crystallization can indeed simultaneously separate two compounds from their mixture.

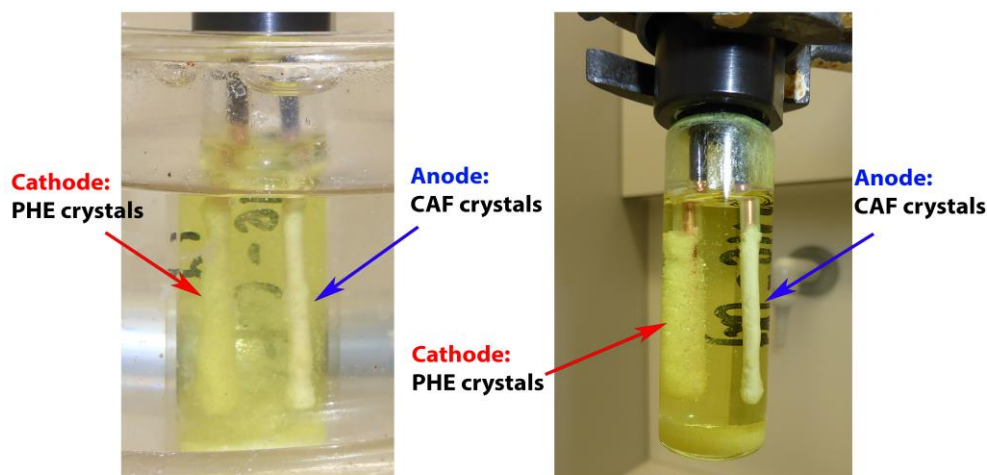


**Figure 4.** Crystals accumulated on both electrodes (left) upon applying an inhomogeneous electric field to a mixed suspension of CAF and PHE in dioxane at 30°C; After cooling in the presence of the electric field crystal layers of different colour, shape and thickness were collected from the two electrodes at 15°C. Some crystals still remained in the bottom of the vial (right).

### 3. CONCLUSIONS

In the present study, a novel separation technique, coupling particle manipulation by an inhomogeneous electrostatic field and cooling crystallization, here referred to as Electric Field Enhanced Crystallization (EEC), was developed. Experimental verification has been presented here that EEC can be employed to separate two solutes in crystalline form from their multi-component mixture. Although EEC is a promising technique, it still requires further development and optimization. An improved design of the cell will be able to improve the relative low yield of the collected particles caused by the setting of part of the crystals at the bottom of the vial despite the presence of the electric field (see Figure 4, right), or the loss of part of the crystalline material at the cathode that was scrubbed off into the solution due to the narrow vial mouth. The optimization of the electric field geometry and electrode design, based on deepened understanding of the combined effect of DEP and EP in an EEC process, are also bound to improve the yield. Impurities present in the crystalline phases may have been the result of adhering mother liquor between crystals during sampling, which subsequently crystallized out upon removing the solvent by drying the crystalline product. The interesting results lead to research questions concerning the effect of the electric field on crystallization kinetics, the variety of applicable solvents and crystallizing compounds, and electrochemical process engineering design and scale-up.

#### 4. EXPERIMENTAL SECTION

Phenazine (98%, Sigma), Caffeine (99%, Sigma), Isonicotinamide (99%, Sigma), Niflumic acid (99%, Sigma) and 4-Hydroxybenzoic acid (99%, Sigma) were used as received. The insulator solvent was chosen to be anhydrous 1,4-dioxane (99.8%, Sigma). All chemicals were used without further purification.

The yield ( $y$ ) of recovery was calculated based on the equation below:

$$y = \frac{m}{V \cdot (c_t - c^*)} \quad (1)$$

Here  $m$  (mg) is the mass of crystals A (either CAF or PHE) collected from either of the electrodes;  $c_t$  (mg/ml solvent) is the overall concentration of A in the mixed suspension;  $c^*$  (mg/ml solvent) is the solubility of A in the mixture solution at the temperature the crystals were collected;  $V$  (ml) is the volume of solvent.

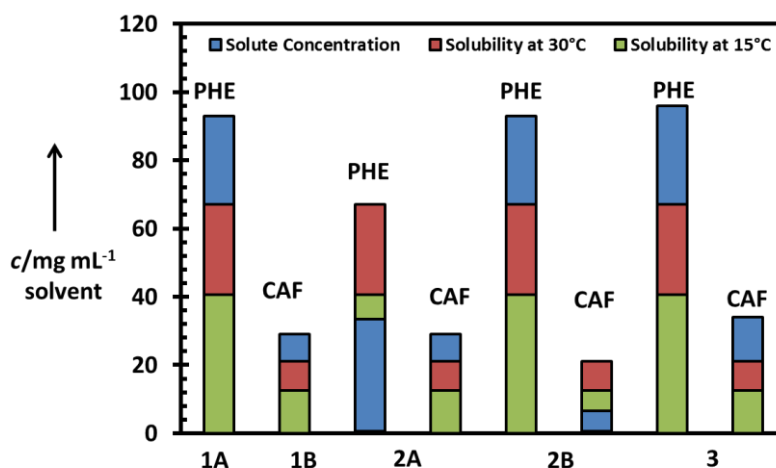


**Figure 5.** Concentrations and solubility at 15°C and 30°C of PHE and CAF in all experiments.

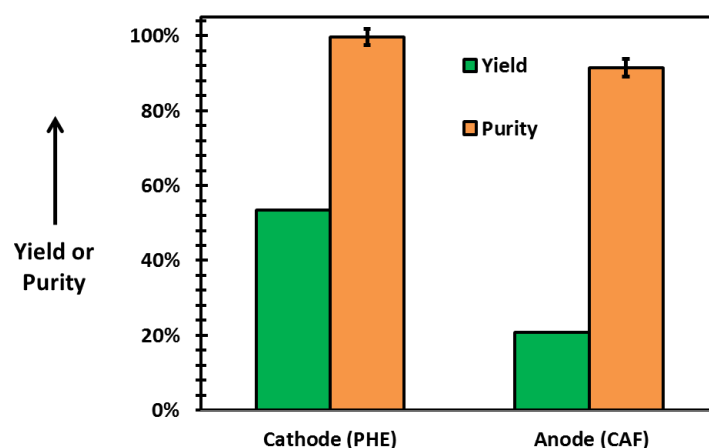


**Figure 6.** Yield and purity of PHE (cathode) and CAF (anode) in Experiment 3.

## REFERENCES

1. Garside, J., Industrial Crystallization from Solution. *Chemical Engineering Science* **1985**, *40* (1), 3-26.
2. Mullin, J. W., 1 - The crystalline state. In *Crystallization (Fourth Edition)*, Butterworth-Heinemann: Oxford, 2001; pp 1-31.
3. Myerson, A. S.; Ginde, R., 2 - Crystals, crystal growth, and nucleation. In *Handbook of Industrial Crystallization (Second Edition)*, Butterworth-Heinemann: Woburn, 2002; pp 33-65.
4. ter Horst, J. H.; Schmidt, C.; Ulrich, J., 32 - Fundamentals of Industrial Crystallization A2 - Rudolph, Peter. In *Handbook of Crystal Growth (Second Edition)*, Elsevier: Boston, 2015; pp 1317-1349.
5. Dömling, A.; Ugi, I., Multicomponent Reactions with Isocyanides. *Angewandte Chemie International Edition* **2000**, *39* (18), 3168-3210.
6. Shaaban, S.; Abdel-Wahab, B. F., Groebke–Blackburn–Bienaymé multicomponent reaction: emerging chemistry for drug discovery. *Molecular Diversity* **2016**, *20* (1), 233-254.
7. Lorenz, H.; Seidel-Morgenstern, A., Processes To Separate Enantiomers. *Angewandte Chemie International Edition* **2014**, *53* (5), 1218-1250.
8. Atkinson, M. B. J.; Bwambok, D. K.; Chen, J.; Chopade, P. D.; Thuo, M. M.; Mace, C. R.; Mirica, K. A.; Kumar, A. A.; Myerson, A. S.; Whitesides, G. M., Using Magnetic Levitation to Separate Mixtures of Crystal Polymorphs. *Angewandte Chemie International Edition* **2013**, *52* (39), 10208-10211.
9. Gascoyne, P. R. C.; Vykoukal, J., Particle separation by dielectrophoresis. *ELECTROPHORESIS* **2002**, *23* (13), 1973-1983.
10. Ammam, M.; Fransaer, J., AC-electrophoretic deposition of glucose oxidase. *Biosensors and Bioelectronics* **2009**, *25* (1), 191-197.
11. Ammam, M.; Fransaer, J., Alternating current electrophoretic deposition of *Saccharomyces cerevisiae* cells and the viability of the deposited biofilm in ethanol production. *Electrochimica Acta* **2010**, *55* (9), 3206-3212.
12. Hayward, R. C.; Saville, D. A.; Aksay, I. A., Electrophoretic assembly of colloidal crystals with optically tunable micropatterns. *Nature* **2000**, *404*, 56.
13. Hammadi, Z.; Veessler, S., New approaches on crystallization under electric fields. *Progress in Biophysics and Molecular Biology* **2009**, *101* (1), 38-44.
14. Koizumi, H.; Fujiwara, K.; Uda, S., Control of Nucleation Rate for Tetragonal Hen-Egg White Lysozyme Crystals by Application of an Electric Field with Variable Frequencies. *Crystal Growth & Design* **2009**, *9* (5), 2420-2424.
15. Pohl, H. A., *Dielectrophoresis: The Behavior of Neutral Matter in Nonuniform Electric Fields* Cambridge University Press: Cambridge, 1978.

16. Dash, S.; Mohanty, S.; Pradhan, S.; Mishra, B. K., CFD design of a microfluidic device for continuous dielectrophoretic separation of charged gold nanoparticles. *Journal of the Taiwan Institute of Chemical Engineers* **2016**, *58*, 39-48.
17. Paillat, T.; Touchard, G., Electrical charges and liquids motion. *Journal of Electrostatics* **2009**, *67* (2), 326-334.
18. Vissers, T.; Imhof, A.; Carrique, F.; Delgado, Á. V.; van Blaaderen, A., Electrophoresis of concentrated colloidal dispersions in low-polar solvents. *Journal of Colloid and Interface Science* **2011**, *361* (2), 443-455.
19. Vincett, P. S., High-field electrophoresis of insulating particles in insulating liquids. I. An electrical transient technique for studying particle mobility, charge, degree of aggregation, adhesive forces, and high-field charging mechanisms. *Journal of Colloid and Interface Science* **1980**, *76* (1), 83-94.
20. Vincett, P. S., High-field electrophoresis of insulating particles in insulating liquids. II. A study of the basic transport mechanisms, including a novel space charge limited conduction process. *Journal of Colloid and Interface Science* **1980**, *76* (1), 95-106.
21. Delgado, Á. V.; Carrique, F.; Roa, R.; Ruiz-Reina, E., Recent developments in electrokinetics of salt-free concentrated suspensions. *Current Opinion in Colloid & Interface Science* **2016**, *24*, 32-43.
22. Van Der Hoeven, P. C.; Lyklema, J., Electrostatic stabilization in non-aqueous media. *Advances in Colloid and Interface Science* **1992**, *42*, 205-277.
23. Morrison, I. D., Electrical charges in nonaqueous media. *Colloids and Surfaces A: Physicochemical and Engineering Aspects* **1993**, *71* (1), 1-37.

# Appendix Chapter 6

## Table of Contents

1. Electric field setup (2)
2. Details of Electric-field Enhanced Crystallization Experiments (2)
3. Verification that CAF and PHE do not co-crystallize (3)
4. X-ray Powder Diffraction (XRPD) for crystalline phase composition identification (3)
5. Proton nuclear magnetic resonance ( $H^1$ -NMR) for crystal purity assessment (4)

## Electric Field Setup

All experiments reported were conducted in the same setup consisting of two parallel rod-shaped copper electrodes, 6 mm apart from each other, in an 8 mL cylindrical glass vial (Figure SI). An electrostatic field can be generated by a DC potential difference, created by a HCN 140m-12500 high voltage power supply (F.U.G. Elektronik GmbH, Germany), between the two electrodes. At a potential difference of 7.5 kV the inhomogeneous field strength at a straight line between the electrodes, which is the peak value, would be  $1.25 \times 10^6 \text{ V m}^{-1}$ .

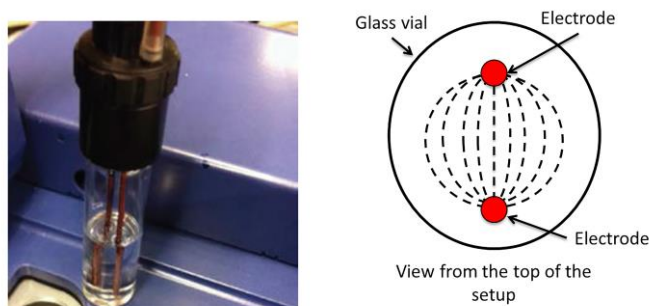


**Figure SI.** Left: The inhomogeneous field setup with the two rod-shaped copper electrodes connected to the high voltage DC power supply via a special PVC cap. The sample suspension is placed in the glass vial and the copper electrodes are emerged in the suspension and connected to the power supply to generate an inhomogeneous electrostatic field; Right: A simple schematic of the inhomogeneous electric field lines (dash lines) viewed from the top of the setup (right).

## Details of Electric-field Enhanced Crystallization Experiments

Experiment 1A: In experiment 1A a suspension of PHE was prepared (with the overall composition of 93 mg/ml solvent) at 30°C. Taken into account the solubility of PHE in dioxane at 30°C (67 mg/ml solvent), in total 26 mg/ml solvent PHE crystals were present in the suspension at this temperature.

Experiment 1B: In experiment 1B a suspension of CAF was prepared (with the overall composition of 29 mg/ml solvent) at 30°C. Taken into account the solubility of CAF in dioxane at 30°C (21 mg/ml solvent), in total 8 mg/ml solvent CAF crystals were present in the suspension at this temperature.

Experiment 2A: In experiment 2A a suspension of PHE and CAF was prepared (with the overall composition of PHE 33 mg/ml solvent and CAF 29 mg/ml solvent) at 30°C. In total approximately 8 mg/ml solvent CAF crystals and no PHE crystals were present in the suspension at this temperature.

Experiment 2B: In experiment 2B a suspension of PHE and CAF was prepared (with the overall composition of PHE 93 mg/ml solvent and CAF 10 mg/ml solvent) at 30°C. In total approximately 26 mg/ml solvent PHE crystals and no CAF crystals were present in the suspension at this temperature.

Experiment 3: A 6 mL dioxane suspension containing both CAF and PHE crystals was prepared at 30°C, which had an overall composition of CAF of 34 mg/ml solvent and PHE of 96 mg/ml solvent. If we assume the PHE and CAF solubilities were not influenced by their mutual presence in the solution, there were in total 13 mg/ml of CAF and 29 mg/ml of PHE crystals present in the suspension in the beginning of the experiment.

### Verification that CAF and PHE do not co-crystallize

The verification that Phenazine (PHE) and Caffeine (CAF) do not co-crystallize was done via the construction of a pseudo-binary phase diagram using the method from ter Horst, et al.<sup>[1]</sup> The solubility of PHE and CAF in 1,4-dioxane was measured in a Crystal16 (Technobis B.V.). Dioxane suspensions of either model compound were prepared and subjected to well-controlled heating and cooling cycles in a Crystal16 workstation. The temperature at which all crystals in a specific suspension were fully dissolved was noted as the saturation temperature  $T_s$  of the corresponding concentration. The solubility information of the model compounds can then be used to construct the corresponding Van 't Hoff plot (see Figure SII (left)) to extrapolate their solubility. The Van 't Hoff plot was constructed by a linearly fit of the data in the  $\ln x$  to  $1/T_s$  space, where  $x$  is molar fraction of the solute:

$$\ln x = -\frac{\Delta H}{R} \left( \frac{1}{T_s} - \frac{1}{T_0} \right)$$

A pseudo-binary phase diagram of PHE and CAF was constructed by measuring the  $T_s$  of various mixtures of the two solutes in dioxane. The compositions of each sample in the diagram are determined based on the following equation:

$$\frac{x_{CAF}}{x_{CAF}^*(T_{ref})} = 1 - \frac{x_{PHE}}{x_{PHE}^*(T_{ref})}$$

Here  $x_{PHE}$  and  $x_{CAF}$  are the molar fraction of respectively PHE and CAF in each sample while  $x_{PHE}^*$  and  $x_{CAF}^*$  are the molar solubilities at reference temperature  $T_{ref}$ . The saturation temperatures  $T_s$  of each sample were plotted against the solvent-excluded mole fraction  $y_{CAF} = x_{CAF}/(x_{CAF}+x_{PHE})$  (Figure SII, right).

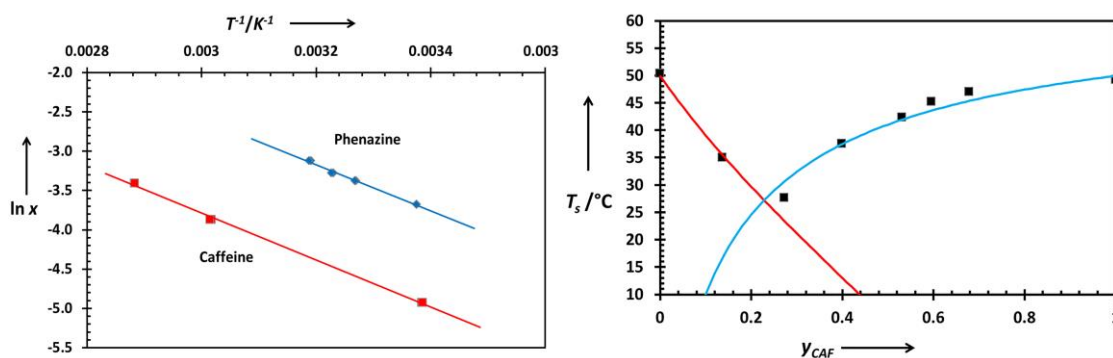


**Figure SII.** Left: Van't Hoff plot of PHE and CAF in 1,4-dioxane; Right: pseudo-binary phase diagram of PHE-CAF. The  $T_s$  of pure CAF and PHE predicted using Van't Hoff parameters are shown as red and blue solid lines, respectively.

Only one eutectic point (at  $y_{CAF} = 0.21$ ) can be found in the phase diagram (Figure SII (right)). The pseudo-binary phase diagram does not show any indications of co-crystal formation in 1,4-dioxane with the compositions tested. When a stable co-crystal is formed, there would be a region in the phase diagram with elevated  $T_s$  compared to those predicted using Van't Hoff parameters, shown as red and blue solid lines in Figure SII (right).

### X-ray Powder Diffraction (XRPD) for crystal composition identification

X-ray powder diffraction (XRPD) was carried out in a Bruker D2 Phaser (Bruker AXS GmbH, Karlsruhe, Germany). Data collection was carried out using monochromatic Cu K  $\alpha_1$  radiation ( $\alpha = 0.154060$  nm) in the  $2\theta$  region between  $8^\circ$  and  $50^\circ$ , step size  $0.022^\circ 2\theta$ . Data evaluation was done with the Bruker program EVA.

The XRPD patterns of crystals collected from Experiment 2A (left) and 2B (right) are shown in Figure SIII. Patterns of crystals from the anode (left) and the right (right) in Experiment 3 are shown in Figure SIV, compared with the references of PHE and CAF from CCDC.

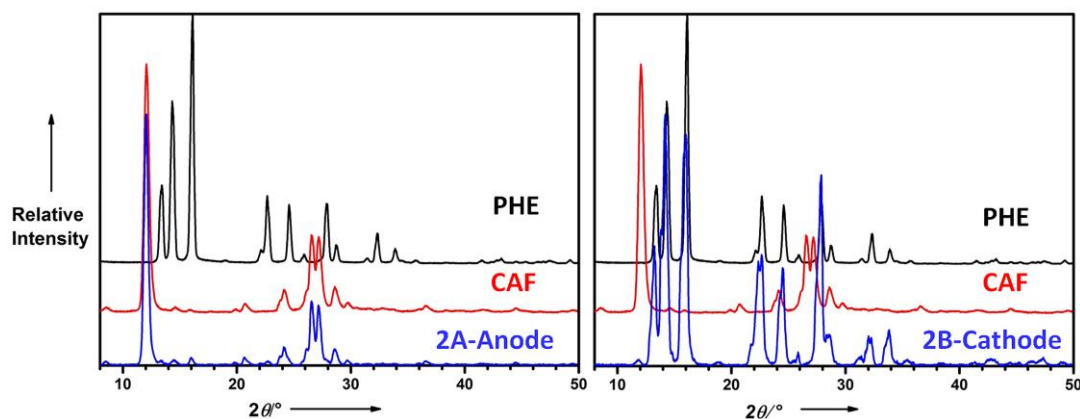


**Figure SIII.** XRPD comparison between crystals collected from the anode in experiment 2A (left) and from the cathode in experiment 2B (right) with source material PHE and CAF. The samples from experiment 2A contained almost all CAF and those from 2B contained only PHE.

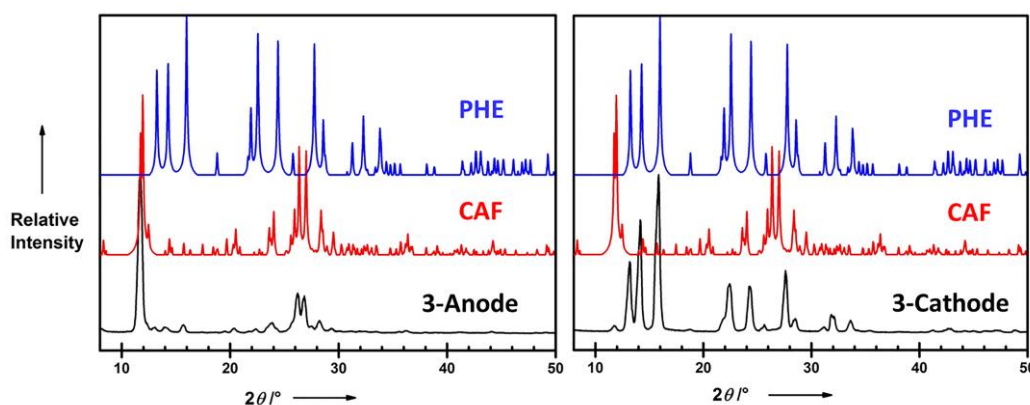


**Figure SIV.** XRPD comparison between crystals collected from the anode (left) and from the cathode (right) in experiment 3 with reference PHE (CCDC: GEPNOG) and CAF (CCDC: NIWFEE003). The samples from the anode mainly contained CAF while the samples from the cathode were mainly PHE.

### Proton nuclear magnetic resonance ( $^1\text{H}$ -NMR) for crystal purity assessment

Two crystalline products were separately collected from the cathode and the anode in experiment 3. Two sub-sample from each crystalline product, namely C1 and C2 as from the cathode and A1 and A2 as from the anode, was individually used to prepare in total four solution samples with the solvent  $\text{CDCl}_3$  (0.03% TMS, >99.96%, euriso-top) and the reference 1,2,4,5-tetramethylbenzene (durene,

Fluka Analytical, 99.83%). Each solution sample was evaluated by an Agilent 400 MHz NMR spectrometer and the mass fraction  $p_i$  of PHE and CAF in the corresponding sub-sample was calculated based on the obtained spectra, as in Equation (1).

$$\frac{\sum_1^{n_i} I_{ij}}{I_{ref}} = \left( \frac{p_i \cdot m_s \cdot \sum_j^{n_i} N_{ij}}{M_i} \right) / \left( \frac{p_{ref} \cdot m_{ref} \cdot N_{ref}}{M_{ref}} \right) \quad (1)$$

where  $I_{ij}$  (a.u.) is the integral of the  $j$ th identity peak of PHE or CAF in the NMR spectra where the integral of the reference peak  $I_{ref}$ , at 6.9 ppm, was set at 1000 a.u.;  $M$  (g/mol) is the molecular weight, which is 180 g/mol for PHE, 194 g/mol for CAF and 134 g/mol for the reference;  $m$  (mg) is the mass in the solution and  $N_{ij}$  is the number of protons to the  $j$ th identity peak of PHE or CAF.  $N_{ref} = 2$  for the reference peak.  $n_i$  is the number of identity peak of PHE or CAF. Subscript  $i$  stands for the two source materials PHE or CAF,  $ref$  is the reference durene and  $s$  is the sample. Values of parameters in Equation (1) of samples from experiment 3 can be found in Table SI, along with the mass fractions of PHE and CAF in each crystalline product.

**Table SI.** Summary of purity measurements of samples from experiment 3

Electrode	I.D. of sub-samples	$m_s$ (mg)	$m_{ref}$ (mg)	$I_{PHE,1}^1$ (a.u.)	$I_{PHE,2}^1$ (a.u.)	$I_{CAF,1}^2$ (a.u.)	$I_{CAF,2}^2$ (a.u.)	$I_{CAF,3}^2$ (a.u.)	$p_{PHE}^3$ (wt%)	$p_{CAF}^3$ (wt%)
Cathode	C1	13.1	12.5	1529.1	1559.3	17.9	17.2	18.3	98.8	1.5
	C2	13.6	12.8	1569.0	1613.6	17.8	18.0	18.4	100.4	1.5
Anode	A1	12.6	13.7	118.3	123.3	877.6	899.8	870.1	8.8	92.3
	A2	12.7	13.7	121.2	122.2	863.1	884.5	864.2	8.8	90.4

<sup>1</sup>The chemical shift of PHE identity peak is at 8.4 ppm (1<sup>st</sup>) and 7.9 ppm (2<sup>nd</sup>) and  $N_{PHE,1}=4$  and  $N_{PHE,2}=4$ ; <sup>2</sup>The chemical shift of CAF identity peak is at 3.9 ppm (1<sup>st</sup>), 3.5 ppm (2<sup>nd</sup>) and 3.3 ppm (3<sup>rd</sup>) and  $N_{CAF,j}=3$  for all three peaks. <sup>3</sup>The summation of  $p_{PHE}$  and  $p_{CAF}$  in some samples are slightly larger than 100%. The error is a combination of integration errors and weighing errors. The average of  $p_{PHE}$  (99.6±1.4 wt%) was used as the purity of the crystalline product from the cathode, while the average of  $p_{CAF}$  (91.4±1.0 wt%) was used for the crystalline product from the anode.

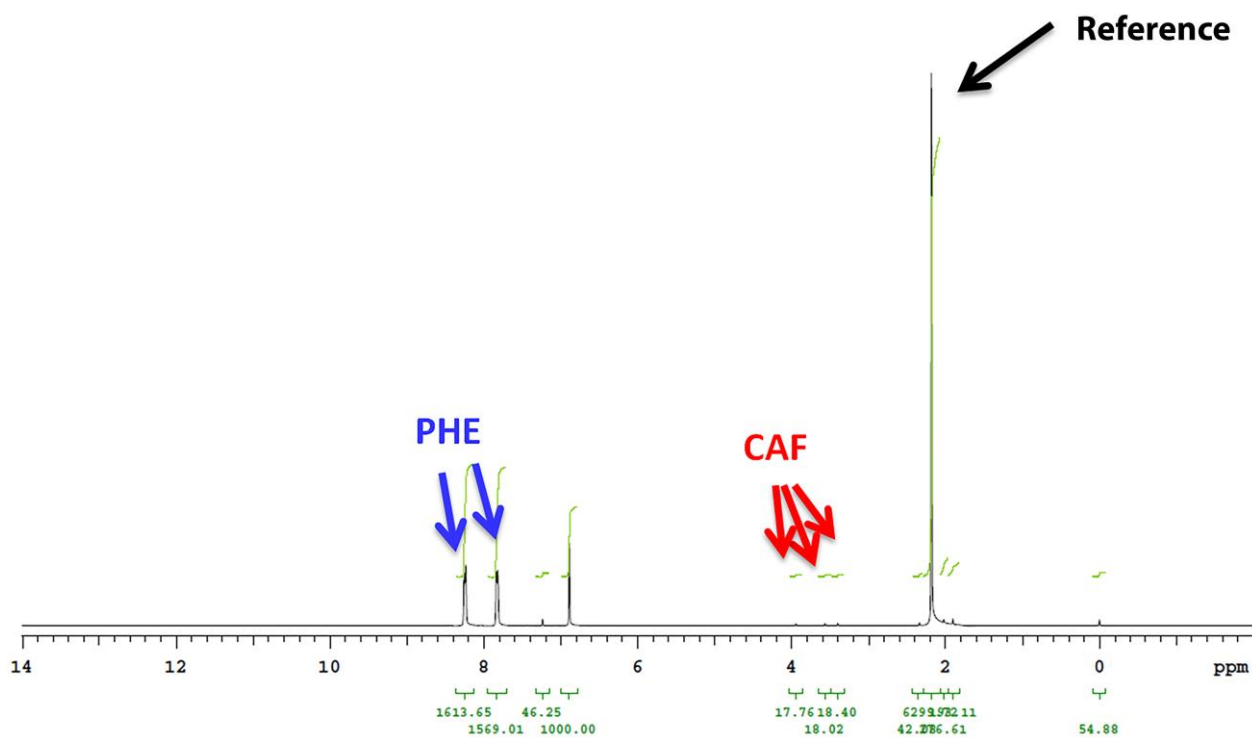
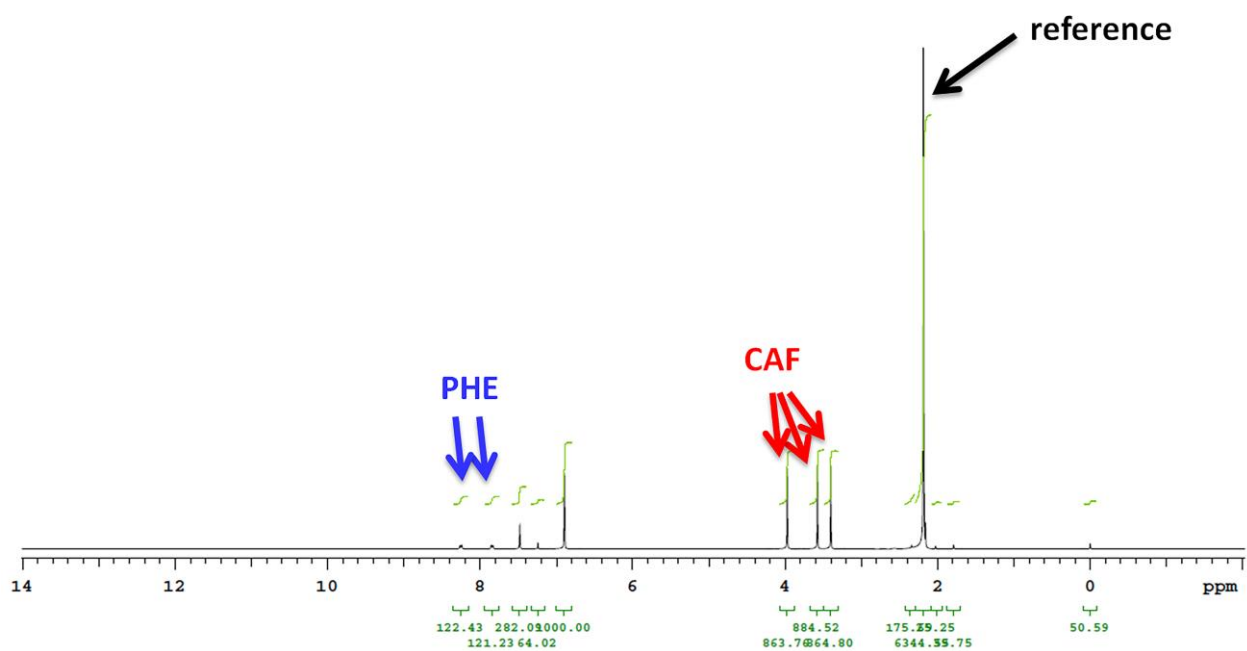


**Figure S5.**  $H^1$ -NMR measurement of crystals collected from the anode (up) and the cathode (down) in experiment 3.

## References

- [1] J. H. ter Horst, M. A. Deij, P. W. Cains, *Cryst. Growth Des.* **2009**, 9 (3), 1531 – 1537.



# Chapter 7. Solid Separation From a Multi-component Mixture by Electric-Field-Enhanced Crystallization

**Key words:** Electric-Field-Enhanced Crystallization, Multi-component mixtures, Separation Technology

**Abstract:** A two-step strategy has been developed to expand the application range of Electric-Field-Enhanced-Crystallization (EFEC) to multi-component mixtures where crystals of the two solutes are attracted by the same electrode, for instance the system of Caffeine (CAF) and Isonicotamide (INA). Via the new strategy, EFEC separately recovered CAF and INA from their 1,4-dioxane mixture, with purities higher than 95% and recovery yields up to 61.8%.

## 1. INTRODUCTION

Crystallization is an efficient and effective separation technology that can recover target compounds as highly purified (>99%) crystalline materials<sup>1-4</sup>. The advancement in chemical and biochemical processes presents crystallization technology with new challenges, one of which being the direct recovery of target product from multi-component mixtures. If crystallization is directly applied to such a multicomponent mixture, for instance a racemic mixture containing equal amount of both optical isomers<sup>5</sup>, the resulting mixed solid phase of pure isomer crystals requires additional steps to recover the purified product. These additional steps lead to inevitable product loss and cost increase. Therefore, a simultaneous process of solid separation and concomitant crystallization is beneficial for industries that treat multi-component mixtures on a daily basis.

Energy sources such as an electric field have been used to manipulate and separate target particles: Using an isolator solvent, an inhomogeneous electric field triggers motion of organic crystals in a suspension and the crystals accumulate on one of the two electrodes, probably due to a combined effect of electrophoresis and dielectrophoresis<sup>6-7</sup>. Based on this phenomenon, we have recently developed a novel technique, namely Electric-Field-Enhanced Crystallization (EFEC), which combines cooling crystallization with the particle manipulation ability of the electric field.<sup>8</sup>

In the model system of Phenazine (PHE) and Caffeine (CAF) in 1,4-dioxane, the crystals of PHE accumulated on the cathode while those of CAF accumulated on the anode. A paralleled cooling step led to the immobilization and growth of crystals on their corresponding electrodes. Eventually the crystals of PHE and CAF were separately recovered from the cathode and anode, respectively, thus achieving effective separation and recovery of the two compounds from their mixture.

EFEC separates two solutes from their mixture, provided that the crystals of the two compounds are attracted by different electrodes. The application area of EFEC can be greatly increased if compounds that are attracted to the same electrode can also be separated using EFEC. In the present study, we develop a new EFEC strategy that can be applied to any mixtures containing two solute compounds.

## 2. EXPERIMENT

**Materials.** Caffeine (99%, Sigma) and Isonicotinamide (99%, Sigma) were used as received. The insulator solvent was chosen to be anhydrous 1,4-dioxane (99.8%, Sigma). All chemicals were used without further purification.

**New Strategy for EFEC.** In dealing with mixture systems, for which the crystals of both solute compounds accumulate on the same electrode, EFEC requires a new two-step strategy. This strategy is schematically demonstrated in Figure 1 (top). In a solution of solutes A and B in dioxane, saturated for A and undersaturated for B, crystals of A are seeded at  $T_1$ . In the presence of a DC potential difference (e.g., +7.5 kV), the A crystal seeds accumulate on one of the electrodes (e.g., the anode) and the first

cooling step ( $T_1 \rightarrow T_2$ ) immobilizes the growing A crystals on the electrode. At  $T_2$ , compound B is saturated in the solution and its crystals are seeded into the mixture and the polarity of the potential difference is changed, i.e. the old anode and cathode become the new cathode and anode, respectively. Seeds of B accumulate on the empty electrode while the A crystals remain attached to the other electrode. The second cooling step from  $T_2$  to  $T_3$  enables the growth and immobilization of the B crystals and further growth of the A crystals separately on the electrodes. At  $T_3$  the crystals A and B are separately recovered from the two electrodes.

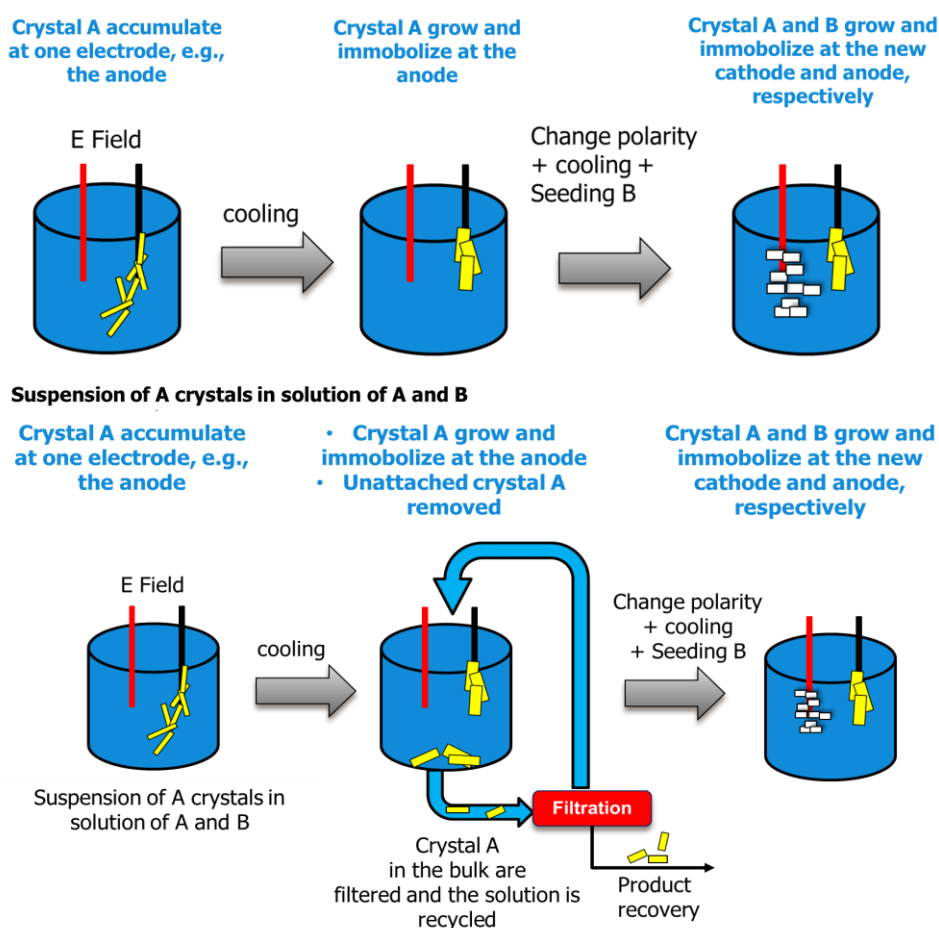


**Figure 1.** Top: Schematic demonstration of the new EFEC strategy to separate solute A and B for which crystals are attracted to the same electrode. In their corresponding pure component suspensions, crystals of A and B accumulate on the same electrode in the presence of an inhomogeneous electric field. In bottom, an additional slurry recycling step is introduced to the new EFEC strategy to minimize the contamination of crystal B products by A.

**Model System.** In order to verify the feasibility of the new strategy, the system of Caffeine (CAF) and Isonicotinamide (INA) in dioxane was selected as the model system. Details in the Appendix show that CAF and INA are no co-crystal formers and therefore that mixed suspensions of CAF and INA contain a mixture of pure component CAF and INA crystals. In the pure component suspensions and in the presence of an inhomogeneous DC electric field both CAF and INA crystals accumulate on

the anode. These two features make the system of CAF and INA in dioxane a suitable testing system for the new strategy.

### 3. RESULTS

**Crystal Growth with Reversed Electric Field.** One important question to examine is whether or not the immobilized crystals (e.g., INA) on the anode still grow after the electric field direction is reversed. If the crystals stop growing after reversing the field direction, the new strategy cannot be used to effectively recover the solute compound which is seeded first. Moreover, the supersaturation of this compound will be built up in the second cooling step and its primary nucleation can take place, inevitably contaminating the second seeded compound product.

In order to investigate the crystal growth after reversing the field, the two-step strategy in Figure 1 (top) was applied on a INA pure component suspension. The INA suspension had a concentration  $c_{INA}$  of 37 mg/ml solvent, which was corresponding to the solubility at 43°C. A DC voltage of +7.5 kV was applied on the suspension while it was cooling down from 40°C to 30°C. The system was held at 30°C overnight and the INA crystals were immobilized on the anode. Afterwards, the voltage was reversed to -7.5 kV and the temperature of the system decreased from 30°C to 20°C and stayed at this value overnight. INA crystals were still attached on the original anode (see Figure 2) and they were collected and weighed.

Approximately 15.8 mg/ml solvent INA crystals were recovered giving a yield of around 74.1%. In the first cooling step (40°C → 30°C), the theoretical amount based on the solubility difference between those temperatures was only 13.9 mg/ml crystals. Since the product collected after the polarity switch and second cooling step was considerably more, crystals still grow even with a reversed electric field direction, proving the effectiveness of the strategies in Figure 1.

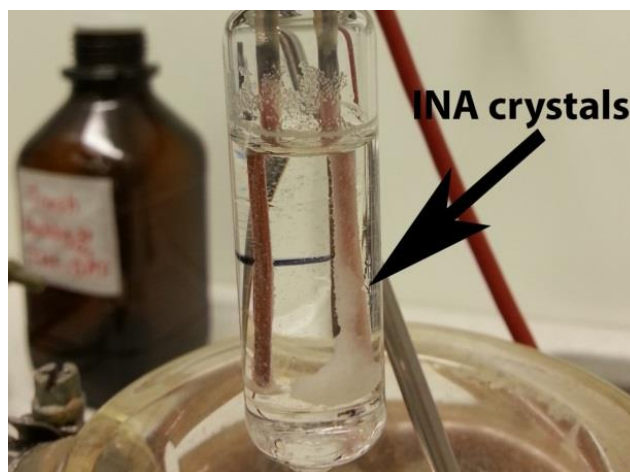


**Figure 2.** Grown INA crystals were still immobilized on the original anode after the suspension was cooled down in the presence of a reversed electric field.

**Verification Experiment A.** A 6 mL suspension of CAF (33.9 mg/ml solvent) and INA (23.4 mg/ml solvent) in dioxane was prepared at 40°C. The concentrations of CAF and INA corresponded to

their solubilities at 45°C and 30°C, respectively. Under these conditions, after equilibration, the solid phase contained only CAF crystals (*ca.* 4.8 mg/ml solvent, as the purple part of CAF column of experiment A in Figure 3) while INA was undersaturated in the solution. A DC potential difference of +7.5 kV was applied between two paralleled copper electrodes immersed in the suspension (See experiment setup in Appendix). In the presence of the inhomogeneous electric field, the CAF crystals started to circulate between the electrodes and gradually accumulated on the anode (the left electrode in Figure 4 (left)). Subsequently, the temperature of the suspension was linearly decreased to 30°C (0.17°C/min) and held at this value overnight (>15 h), during which the CAF crystals on the anode grew and were immobilized on the electrode. After switching off the electric field, the crystals remained collected at the electrode. Then, *ca.* 8.3 mg/ml INA crystals were seeded into the system and the electric field was switched on again with a reversed polarity of the DC field, i.e. the potential difference was changed to -7.5 kV. The newly added INA crystals started to accumulate on the new anode (the right electrode in Figure 4 (left)) while the CAF crystals on the original anode still remained immobilized. Subsequently, the temperature of the suspension was further decreased from 30°C to 15°C (0.17°C/min) and held at this value overnight (>15 h) which allowed the INA crystals to attach and grow on the new anode (see Figure 4 (left)). At the end of the experiment, after switching off the electric field, the crystals from both electrodes were separately collected and sent for analysis by XRPD and <sup>1</sup>H-NMR. A total of 9.2 mg/ml INA crystals, with a purity of 98.3%, were withdrawn from the new anode, which corresponds to a recovery yield of 49.5%. Similarly, 12.8 mg/ml CAF crystals with a purity of 95% were collected from the original anode, achieving a yield of 59.8% (see a summary of crystal yield and purity of experiment A in Figure 5 (left)). This result verified that, using the newly proposed strategy in Figure 1, EFEC can separate two solutes from each other in their mixture, even when the crystals of the solute compounds both accumulate on the same electrode under an inhomogeneous electric field.

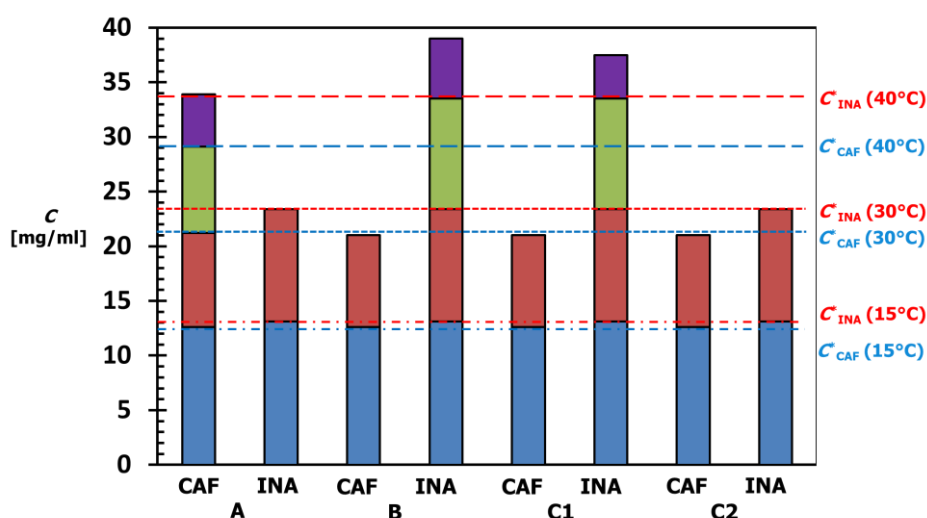


**Figure 3.** Overall concentrations of INA and CAF in all samples used in experiments A-C2. The solubility of the two solute compounds at 15°C, 30°C and 40°C are indicated by the horizontal lines. The concentrations are divided into four parts, represented by colors. The

*purple part stands for the crystals present in the initial suspension at 40°, the green the compound crystallized in the first cooling step (40°C → 30°C), the red the compound crystallized in the second cooling step (30°C → 15°C) and the blue compound remain in the solution phase at 15°C.*

In experiment A, it is observed that some of the seed crystals were not attached on the corresponding electrodes in the end of each cooling step, partly contributing to the relatively low recovery yield. In our previous study, unattached crystals have also been found in the system of PHE and CAF<sup>8</sup>. In the current system, the effect of the unattached crystals is not only on the recovery yield. After reversing the polarity of the electric field, the unattached crystal A can accumulate, together with the newly added crystal B, on the same unoccupied electrode, thus contaminating the product B. This effect has been observed in experiment B, where INA, instead of CAF as in A, was seeded first.

In experiment B, a 6 mL dioxane suspension of CAF and INA, with a different composition as that in experiment A, was prepared at 40°C. The overall concentrations of CAF (21 mg/ml solvent) and INA (39 mg/ml solvent) corresponded to their solubilities at 30° and 45°C, respectively. At 40°C, *ca.* 5.5 mg/ml solvent INA crystals presented in the solid phase (the purple part of column INA in experiment B in Figure 3) and CAF was undersaturated. A DC potential difference of +7.5 kV was applied in the suspension and the INA crystals started to move and accumulate on the anode. The temperature of the suspension was then linearly decreased to 30°C (0.17°C/min) and held at this value overnight (>15 h), during which the INA crystals on the anode grew and were immobilized on the electrode. Afterwards, *ca.* 8.3 mg/ml CAF crystals were seeded into the system and the polarity of potential difference was reversed to -7.5 kV. It was noticed that the newly added CAF crystals, together with some of the unattached INA crystals, accumulated on the new anode. The temperature of the system was then linearly decreased to 15°C with a cooling rate of 0.17°C/min. The system stayed at this temperature overnight and the grown crystals on both electrodes were collected separately and analyzed by XRPD, which showed that while the crystals from the original anode were mainly INA, those from the new anode composed of both INA and CAF crystals (see details in Appendix). Therefore, from experiment B, it can be seen that the new strategy of EFEC, in Figure 1 (top), needs to improve the purity of product B, by preventing the unattached crystal A from contaminating it. In the following

section, an adjustment in operating the new strategy is proposed and verified to enhance the purity of product B.

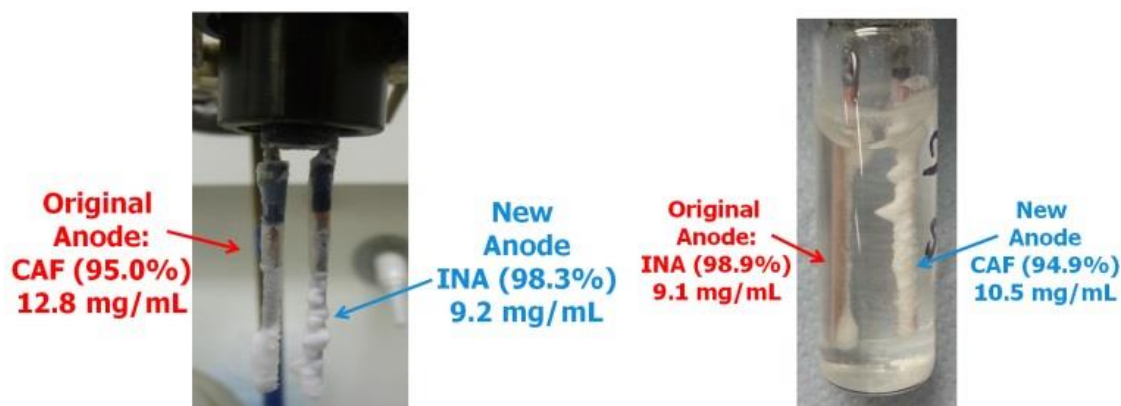


**Figure 4.** Using a two-step Electric-Field-Enhanced Crystallization technique (EFEC) without a suspension recycling step (left) and with a recycling step (right), Caffeine (CAF) and Isonicotinamide (INA) were separately collected on the two electrodes from their mixture in dioxane.

**Enhancing Purity of the New Strategy.** The contamination of the crystals in the new strategy can be diminished if the amount of seed crystals is carefully chosen so that the amount of un-immobilized crystals after the first cooling step is minimized. On the other hand, such contamination can also be removed by an adjusted operation of the strategy: before changing the DC voltage polarity and seeding the crystals of the second solute, the suspension is recycled through an external loop in which the remaining crystals are filtered and recovered as products. Afterwards, the seed crystals of the second compound are added to the clear solution and the procedure continues (see the schematic demonstration of the adjusted operation in Figure 1 (bottom)). In this way, the contamination observed in Experiment B can be minimized.

**Verification of the Adjusted Operation.** The feasibility of the proposed adjustment was tested in Experiment C. Since it was technically difficult to build an external recycling loop to the 8 mL glass vial used as the experiment setup, a procedure mimicking the suspension recycling step in the adjustment was established. Two 6 mL dioxane mixtures were prepared with different compositions: suspension C1 was prepared at 40°C and had a similar composition as that in Experiment B; Solution C2 was prepared at 30°C and its concentrations of CAF (21.2 mg/ml solvent) and INA (23.4 mg/ml solvent) were both corresponding to their solubility at 30°C (see composition details of both C1 and C2 in Figure 3).

Two paralleled copper electrodes were immersed in suspension C1 and a DC potential difference of +7.5 kV was applied between the electrodes. INA crystals accumulated on the anode and subsequently immobilized during the cooling step from 40°C to 30°C. The suspension was held at 30°C overnight and some INA crystals remained unattached. Subsequently, 8.3 mg/ml solvent CAF crystals were seeded in solution C2 at 30°C and the electrodes in C1 were transferred, with the attached INA crystals on the anode, to C2. The potential difference across the electrodes was then reversed to -7.5 kV and the seeded CAF crystals gradually accumulated on the new anode. A following cooling step from 30°C to 15°C immobilized the grown CAF crystals on the new anode while further growth of the INA crystals occurred (see Figure 4, right). The whole system was held at 15°C overnight and the crystals from the two electrodes were separately collected for analysis by XRPD and <sup>1</sup>H-NMR. Around 9.1 mg/ml solvent INA crystals, with a purity of 98.9%, were withdrawn from the original anode, which corresponded to a recovery yield of 37.5%. Similarly, approximately 10.5 mg/ml solvent CAF crystals (purity 94.9%) were collected from the new anode, achieving a yield of 61.8% (see a summary of crystal purity and yield in experiment C in Figure 5 (right)). No significant contamination of either CAF or INA, as in Experiment B, was observed, verifying the feasibility of the proposed adjustment in Figure 1 (bottom).

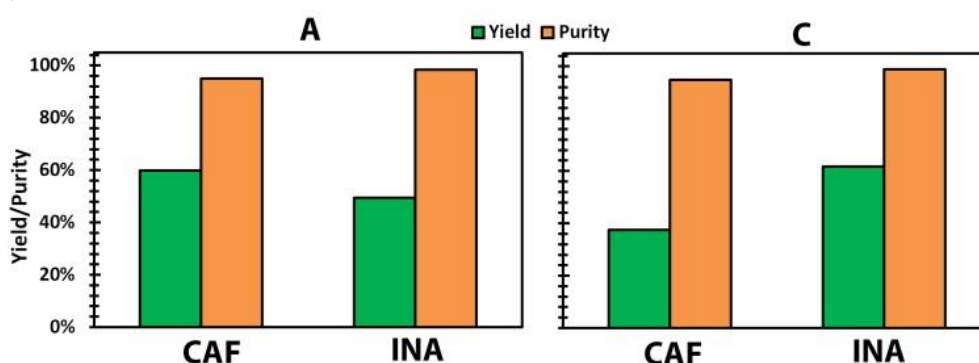


**Figure 5.** Yield (green) and purity (orange) of CAF and INA crystals collected from experiment A (left) and C (right).

#### 4. DISCUSSIONS

The newly proposed strategy and its adjustment enable the effective separation of INA and CAF from each other in their dioxane mixture. However, it can be still noticed that the recovery yields of both INA and CAF were relatively low, which has also been observed in our previous study of EFEC on the mixture system of Phenazine and Caffeine<sup>8</sup>. One reason for the relatively low yield is that part of the seed crystals are settled at the bottom of the glass vial rather than being attached on the electrode. This inefficiency could be minimized by an improved design of the electric field geometry and electrode, preferably based on simulation attempts on combining the effects of electrophoresis, the dielectrophoresis and the resulting fluid dynamics in the suspension. Furthermore, the reverse of electric field polarity does not stop the growth of the immobilized crystals on the electrode. This phenomenon indicates that there still exists supersaturation around the electrode, which is no longer the one attracting

crystals after the reversing of field polarity. The localization effect of an inhomogeneous electric field seems to be stronger on macroscopic crystals, compared to microscopic molecules in the solution phase.

## 5. CONCLUSIONS

A modified EFEC technique has been developed which separates two solute compounds from each other in their mixture. We extend the application of EFEC to systems where crystals of the two solute compounds both accumulate on the same electrode, under an inhomogeneous electric field. The successful separation of these two solutes by the two-step strategies has proven that EFEC can be utilized in dealing with any binary solute mixtures. Future investigation can further study the possibility of scaling up of the EFEC as well as the utilization of various solvent systems.

## REFERENCES

1. Garside, J., Industrial Crystallization from Solution. *Chemical Engineering Science* **1985**, *40* (1), 3-26.
2. Bennett, R. C., 5 - Crystallizer selection and design A2 - Myerson, Allan S. In *Handbook of Industrial Crystallization (Second Edition)*, Butterworth-Heinemann: Woburn, 2002; pp 115-140.
3. Mullin, J. W., 9 - Crystallizer design and operation. In *Crystallization (Fourth Edition)*, Butterworth-Heinemann: Oxford, 2001; pp 403-477.
4. Ter Horst, J. H.; Schmidt, C.; Ulrich, J., Fundamentals of industrial crystallization. In *Handbook of Crystal Growth*, 2015; Vol. II, pp 1317-1349.
5. Lorenz, H.; Seidel-Morgenstern, A., Processes To Separate Enantiomers. *Angewandte Chemie International Edition* **2014**, *53* (5), 1218-1250.
6. Mauro, A., Dielectrophoresis: The Behavior of Neutral Matter in Nonuniform Electric Fields. Herbert A. Pohl. *The Quarterly Review of Biology* **1980**, *55* (1), 68-69.
7. Paillat, T.; Touchard, G., Electrical charges and liquids motion. *Journal of Electrostatics* **2009**, *67* (2-3), 326-334.
8. Potticary, J.; Terry, L. R.; Bell, C.; Papanikolopoulos, A. N.; Christianen, P. C. M.; Engelkamp, H.; Collins, A. M.; Fontanesi, C.; Kociok-Kohn, G.; Crampin, S.; Da Como, E.; Hall, S. R., An unforeseen polymorph of coronene by the application of magnetic fields during crystal growth. *Nat Commun* **2016**, *7*.

# Appendix Chapter 7

## Table of Contents

1. Electric field setup (2)
2. Verification that CAF and INA do not co-crystallize (2)
3. X-ray Powder Diffraction (XRPD) for crystalline phase composition identification (3)
4. Proton nuclear magnetic resonance ( $H^1$ -NMR) for crystal purity assessment (4)

## Electric Field Setup

All experiments reported were conducted in the same setup consisting of two parallel rod-shaped copper electrodes, 6 mm apart from each other, in an 8 mL cylindrical glass vial (Figure SI). An electrostatic field can be generated by a DC potential difference between the two electrodes. At a potential difference of 7.5 kV the inhomogeneous field strength at a straight line between the electrodes, which is the peak value, would be  $1.25 \times 10^6 \text{ V m}^{-1}$ .

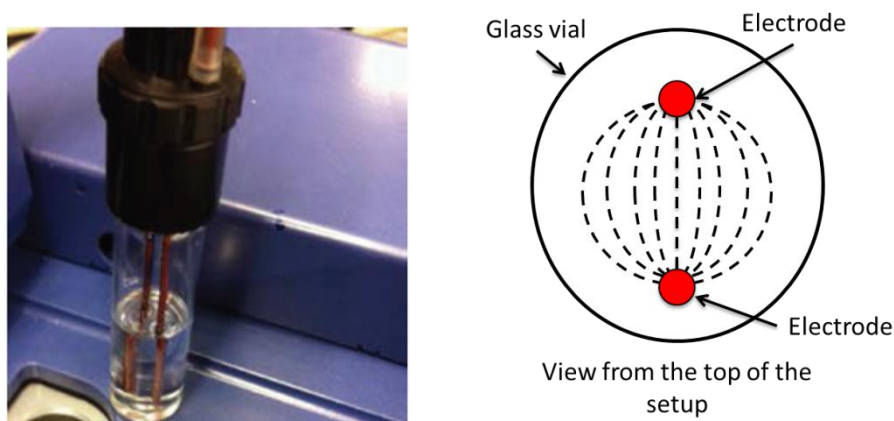


**Figure SI.** *Left: The inhomogeneous field setup with the two rod-shaped copper electrodes connected to the high voltage DC power supply via a special PVC cap. The sample suspension is placed in the glass vial and the copper electrodes are emerged in the suspension and connected to the power supply to generate an inhomogeneous electrostatic field; Right: A simple schematic of the inhomogeneous electric field lines (dash lines) viewed from the top of the setup (right).*

## Verification that CAF and INA do not co-crystallize

The verification that Isonicotinamide (INA) and Caffeine (CAF) do not co-crystallize was done via the construction of a pseudo-binary phase diagram using the method from ter Horst, et al.<sup>[1]</sup> The solubility of INA and CAF in 1,4-dioxane was measured in a Crystal16 (Technobis B.V.). Dioxane suspensions of either model compound were prepared and subjected to well-controlled heating and cooling cycles in a Crystal16 workstation. The temperature at which all crystals in a specific suspension were fully dissolved was noted as the saturation temperature  $T_s$  of the corresponding concentration. The solubility information of the model compounds can then be used to construct the corresponding Van 't Hoff plot

(see Figure SII (left)) to extrapolate their solubility. The Van 't Hoff plot was constructed by a linearly fit of the data in the  $\ln x$  to  $1/T_s$  space, where  $x$  is molar fraction of the solute:

$$\ln x = -\frac{\Delta H}{R} \left( \frac{1}{T_s} - \frac{1}{T_0} \right)$$

A pseudo-binary phase diagram of INA and CAF was constructed by measuring the  $T_s$  of various mixtures of the two solutes in dioxane. The compositions of each sample in the diagram are determined based on the following equation:

$$\frac{x_{CAF}}{x_{CAF}^*(T_{ref})} = 1 - \frac{x_{INA}}{x_{INA}^*(T_{ref})}$$

Here  $x_{INA}$  and  $x_{CAF}$  are the molar fraction of respectively INA and CAF in each sample while  $x_{INA}^*$  and  $x_{CAF}^*$  are the molar solubilities at reference temperature  $T_{ref}$ . The saturation temperatures  $T_s$  of each sample were plotted against the solvent-excluded mole fraction  $y_{CAF} = x_{CAF}/(x_{CAF}+x_{INA})$  (Figure SII, right).

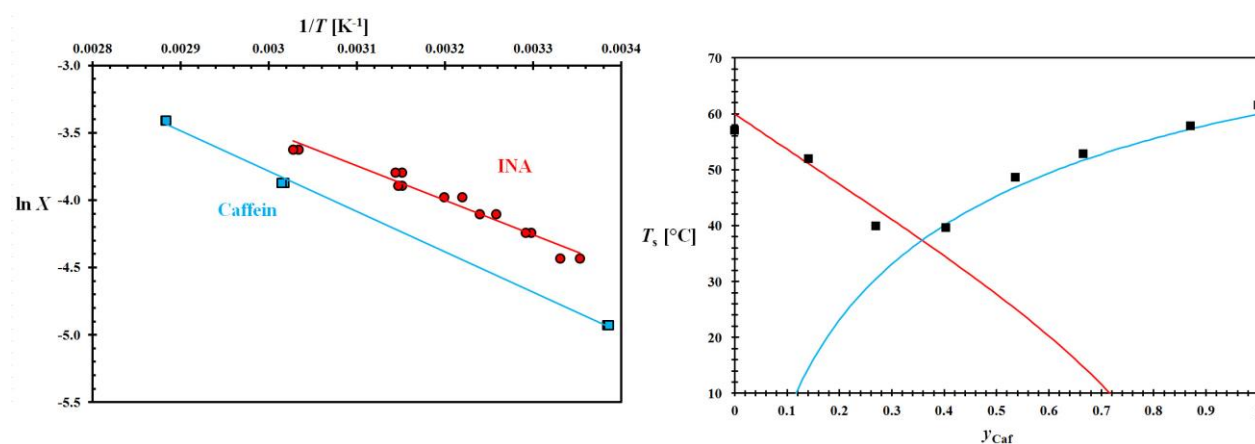


**Figure SII.** Left: Van't Hoff plot of INA and CAF in 1,4-dioxane; Right: pseudo-binary phase diagram of INA-CAF. The  $T_s$  of pure CAF and INA predicted using Van't Hoff parameters are shown as blue and red solid lines, respectively.

Only one eutectic point (at around  $y_{CAF} = 0.35$ ) can be found in the phase diagram (Figure SII (right)). The pseudo-binary phase diagram does not show any indications of co-crystal formation in 1,4-dioxane with the compositions tested. When a stable co-crystal is formed, there would be a region in the phase diagram with elevated  $T_s$  compared to those predicted using Van't Hoff parameters, shown as red and blue solid lines in Figure SII (right).

### X-ray Powder Diffraction (XRPD) for crystal composition identification

X-ray powder diffraction (XRPD) was carried out in a Bruker D2 Phaser (Bruker AXS GmbH, Karlsruhe, Germany). Data collection was carried out using monochromatic Cu K  $\alpha$ 1 radiation ( $\lambda = 0.154060$  nm) in the  $2\theta$  region between  $8^\circ$  and  $50^\circ$ , step size  $0.022^\circ 2\theta$ . Data evaluation was done with the Bruker program EVA.

The XRPD diffractograms of crystals collected from Experiment A, B and C are shown in Figure SIII, SIV and SV, respectively, compared with those from INA (Form I) and CAF.

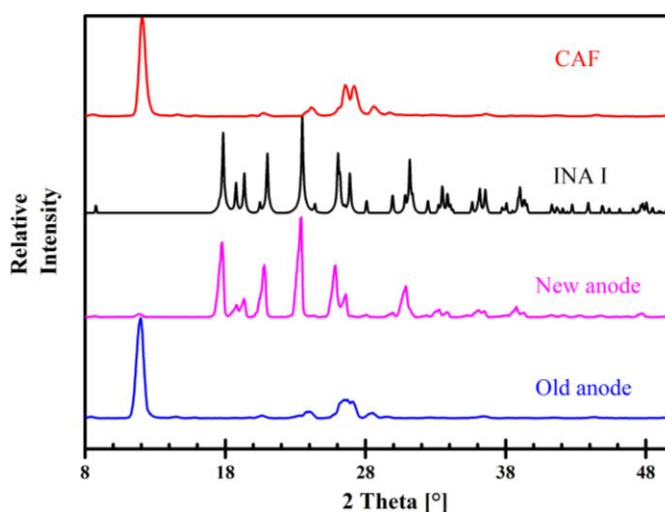


**Figure SIII.** XRPD comparison between crystals collected from the old and the new anode in experiment A with source material INA and CAF. The samples from the old anode contained almost all CAF and those from the new anode only INA (Form I).

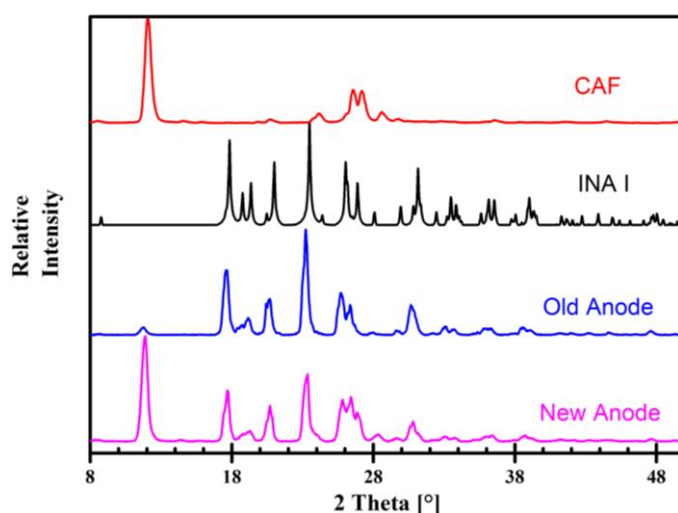


**Figure SIV.** XRPD comparison between crystals collected from the old and the new anode in experiment B with reference INA Form I (CCDC: EHOWIH01) and CAF. The sample from

the old anode mainly contained INA while the sample from the new anode was a mixture of both CAF and INA.

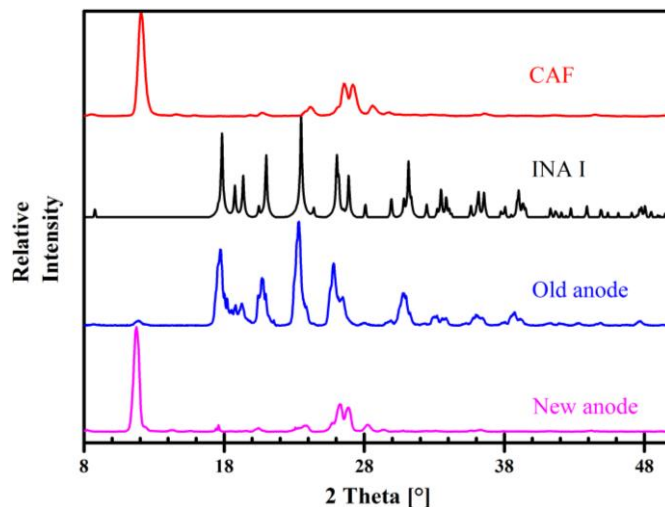


**Figure SV.** XRPD comparison between crystals collected from the old and the new anode in experiment C with reference INA Form I (CCDC: EHOWIH01) and CAF. The sample from the old anode mainly contained INA while the sample from the new anode was CAF.

### Proton nuclear magnetic resonance ( $^1\text{H}$ -NMR) for crystal purity assessment

Crystalline products were separately collected from the old and the new anode in both experiment A and C. The two samples from experiment A were named A1 (from the old anode) and A2 (the new anode) while the samples from C were named C1 (the old anode) and C2 (the new anode). *ca.* 25 mg each sample was dissolved at room temperature into 1 ml of solvent of 50/50 %v/v Chloroform (0.03% TMS, >99.96%, euriso-top)/Methanol- $d_4$  (>99.8%, euriso-top). Each solution sample was evaluated by an Agilent 400 MHz NMR spectrometer and the mass ratio  $p$  between INA and CAF in the corresponding sample was calculated based on the obtained spectra, as in Equation (1).

$$p = \frac{I_{\text{INA}}}{I_{\text{CAF}}} * \frac{N_{\text{CAF}}}{N_{\text{INA}}} * \frac{M_{\text{INA}}}{M_{\text{CAF}}} \quad (1)$$

where  $I_i$  (a.u.) is the integral of the identity peak of INA (at 8.7 ppm) or CAF (at 4.0 ppm) in the NMR spectra where the integral of the identity peak  $I_{\text{CAF}}$  was set at 100 a.u.;  $M$  (g/mol) is the molecular weight, which is 122 g/mol for INA and 194 g/mol;  $N_j$  is the number of protons to the identity peak of INA ( $N_{\text{INA}} = 2$ ) or CAF ( $N_{\text{CAF}} = 1$ ). Subscript  $i$  stands for the two source materials INA or CAF. Values of parameters in Equation (1) of samples from experiment A and C can be found in Table SI, along with the mass fractions of INA and CAF in each crystalline product. Assuming only CAF and INA existed in the crystalline samples, their purities  $w_i$  were calculated from  $p$ . As an example, the NMR spectra of the two samples from experiment A are shown in Figure SVI.

**Table SI.** Summary of purity measurements of samples from experiment A and C

Electrode	I.D. of samples	$I_{\text{INA}}$ (a.u.)	$P$	$w_{\text{CAF}}$ (wt%)	$w_{\text{INA}}$ (wt%)
Old Anode	A1	5.8	0.05	95	5
New Anode	A2	6226.7	58.67	1.68	98.3
	C2	5.9	0.05	94.9	5.1

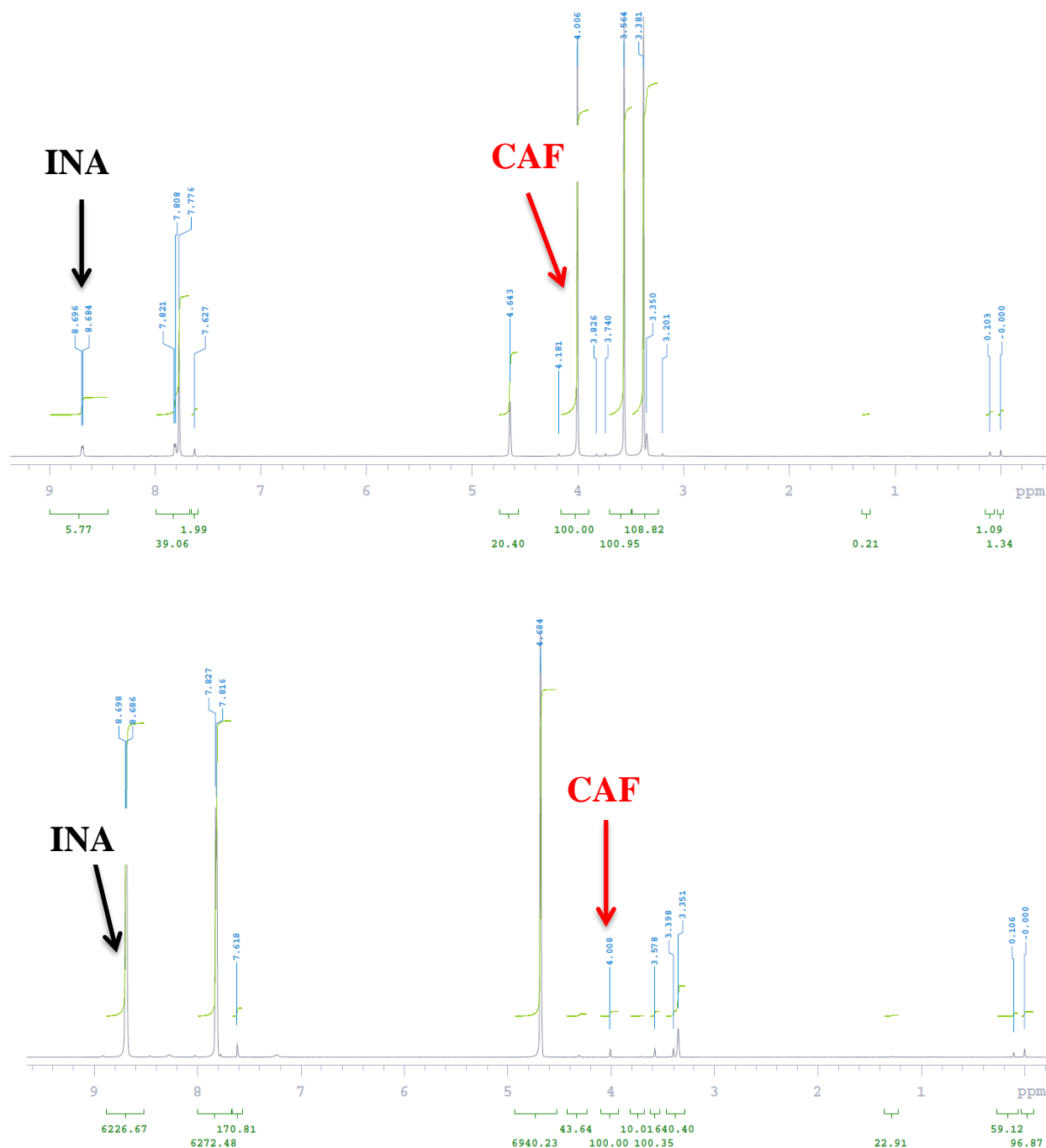


**Figure SVI.**  $^1\text{H-NMR}$  measurement of crystals collected from the old anode (up) and the new anode (down) in experiment A.

## References

- [1] J. H. ter Horst, M. A. Deij, P. W. Cains, *Cryst. Growth Des.* **2009**, 9 (3), 1531 – 1537.

## Chapter 8. Conclusions

(Bio-)chemical industries deal with multi-component systems on a daily basis, fermentation broth, crude oil and milk, to name a few. The separation and purification of the target compounds, which are often delicate, chiral and temperature sensitive, from a multi-component mixture impose a challenge for the industries. Especially chiral systems, from which the components are chemically identical but can possess completely different biochemical properties are notoriously difficult to purify in their enantiopure form. This is partly due to the fact that only 10 % of these compounds crystallize as conglomerates, which are accessible for crystallization based chiral resolution techniques. On the other hand, multi-component crystalline materials bring modification of the physical properties, such as solubility, of the target compound, which can be beneficial for the desired application. Therefore, in this thesis, we explore to:

1. **Expand the application range of chiral resolution techniques to racemic compounds by converting them into conglomerate multi-component crystals.**

and:

2. **Crystallize and separate a target product from impurities in a multi-component solution, using the forces of an electric field on solid particles.**

**Multi-component Crystallization as an intermediate for Chiral Resolution of Racemic Compounds:** In Chapter 2 the development of a method is described for the quick screening of co-crystal systems of the Cambridge Crystallography Data Center (CCDC) and the quick verification whether these co-crystals are in the form of conglomerates or racemic compounds. It is demonstrated that the condition to form an enantiopure co-crystal from an enantiomer and a co-former can be used as a starting point for the formation of stable co-crystals from the corresponding racemic mixture and the co-former. This quick experimental method can be used to screen the list of potential conglomerate co-crystals, also generated from this study. All the co-crystals identified in this study are valuable for future study to investigate the principle behind the formation of co-crystals from chiral compounds. Unfortunately the data of the CCDC combined with our experimental screening showed that the 10% rule, which states that around 10% of chiral compounds crystallize as conglomerates, is unlikely to be

valid for co-crystals from chiral compounds. This indicates the technical difficulties in the conversion of racemic compounds into conglomerate co-crystals for the application of chiral resolution.

Chapter 3, we developed a systematic procedure, which is based on two types of pseudo-binary phase diagram, to identify the types of co-crystals formed from a target racemic compound and a co-former. Three model systems, diastereomeric co-crystals Phenylalanine-Valine, Racemic Compound co-crystals Ibuprofen-1,2-Bis(4-pyridyl)ethane and Conglomerate co-crystals Ibuprofen-trans-1-(2-pyridyl)-2-(4-pyridyl)-ethylene, have been successfully identified by their corresponding Type-II pseudo-binary phase diagrams. Moreover, the liquid-solid equilibrium information in the co-crystal systems demonstrated by the phase diagrams provides guideline for conceptual design of suitable chiral separation processes for the target compounds.

Chapter 4 describes the successful recovery of enantiopure S-Ibuprofen (IBU), a commonly used medicine, in the form of its conglomerate co-crystal with trans-1-(2-pyridyl)-2-(4-pyridyl)-ethylene (BPE) from a racemic solution of Heptane. We demonstrated that three different seeding procedures all managed to recover S-IBU:BPE as products. The highest amount of co-crystal product was up to 50% of the original seeds added and the enantiomeric excess  $E$  of all the recovered products was as high as 95%. The success in recovering enantiopure S-IBU as co-crystals expands the application of chiral resolution technique to many racemic compounds, which conventionally cannot be resolved.

In Chapter 5, another way of converting racemic compounds into conglomerates, by forming salt with suitable counter-ions is demonstrated. The target racemic compound Phenylalanine is successfully deracemized by the temperature cycling method via its conglomerate salt with 2,5-xylenesulfonic acid, with a solution racemization reaction in Acetic acid. Furthermore, we identified that the deracemization rate of the model system is mainly influenced by the kinetic rate of the racemization reaction as well as the mass fraction of solid phase involved in the dissolution-recrystallization cycles in the process. The results of this study verifies the application of deracemization on racemic compound via conglomerate salt formation as well as provides preliminary information for the design and operation of suitable deracemization processes for the target compounds.

In conclusion, our study demonstrates the validity of using conglomerate multi-component crystals (e.g., co-crystals and salts) as intermediates to apply chiral resolution on racemic-compounds-forming systems. Moreover, we provide a quick method to screen a list of systems, which potentially contain conglomerate co-crystals. We also developed a phase-diagram-based method to determine the identities of co-crystals formed from racemic compounds, while providing design guidelines for a suitable chiral resolution process.

**Electric-Field-Enhanced-Crystallization for Solutes Separation from Multi-component Mixtures:** Another objective of this dissertation is to develop a novel separation technique, utilizing the particle manipulation ability of a DC electric field. In this study, we discovered that, in an inhomogeneous DC electric field, generated by two electrodes, crystals in an insulator suspension (e.g., in Dioxane) are mobilized and attracted to one of the electrodes. This phenomenon, probable a joint effect of dielectrophoresis and electrophoresis, has been combined with cooling crystallization into a novel separation technique, namely electric-field enhanced crystallization (EFEC).

In Chapter 6, we demonstrated the first application of the EFEC: in a mixed Dioxane suspension of Phenazine (PHE) and Caffeine (CAF), EFEC triggered motion of both crystals and attracted them on different electrodes, PHE on the cathode and CAF on the anode. A subsequent cooling crystallization immobilized the crystals and enabled separate recovery of the two types of crystals. The crystalline products contained more than 90% of the corresponding compounds.

Chapter 7 gives another different application of EFEC: in another model system, Isonicotinamide (INA) and CAF, a different strategy of EFEC was utilized: the Dioxane suspension of INA and CAF contained only one of the two crystals and the solid phase was immobilized on the anode by EFEC. Afterwards, the other crystals were seeded into the system and the polarity of the field was reversed, which led the accumulation of the seeds on the new anode. A subsequent cooling step immobilized both crystals on different electrodes and were separately recovered in the end of the process. INA and CAF crystals of higher than 95% purities were recovered as products from the two electrodes.

In conclusion, our study of the two model systems proves that EFEC is a potential tool to effectively separate and recover target products from their multi-component mixtures, such as the desired enantiomer from its racemic mixture, which can potentially increase the productivity of a batch preferential crystallization process. Future investigation can be focused on improving the recovery yields of this technique, e.g., via the innovative design of the electric field geometry. Moreover, studies should be conducted to clarify the underlining mechanisms behind EFEC, so that the technique can be further developed into an optimized and robust tool.



# Curriculum Vitae

Weiwei Li was born on the 26<sup>th</sup> November, 1985, in Shanghai, China. After finishing his Bachelor degree of Bio-engineering in Shanghai Jiaotong University (2004-2008), Weiwei moved to Delft, the Netherlands, to further proceed his education. Weiwei obtained his MSc degree in Biochemical Engineering from the Faculty of Applied Science in Delft University of Technology in 2011. During his master, Weiwei focused on the downstream process, especially chromatography technology, in the field of sustainable resources production from biomass. After his Master, Weiwei continued his study, in the same faculty, as a trainee of Professional Doctorate of Engineering (PDeng) in the field of Bioprocess Engineering (2011—2013). During his PDeng period, Weiwei continued exploring the process design and evaluation of renewable energy production, especially biodiesel from solar light and CO<sub>2</sub>, using algae as cell factories.



From September 2013, after obtaining his PDeng degree, Weiwei started a PhD, in the department of Process and Energy, with Prof. dr. ir. Andrzej Stankiewicz and Prof. dr. ir. Joop H. ter Horst as promoters and Dr. ir. Herman Kramer as co-promotor. As his PhD project, Weiwei researched the application of using various novel crystallization techniques (e.g., Electric-field-enhanced-crystallization) in the separation of target compounds from complex multi-component systems. The results of these studies have eventually been crystallized in the form of this dissertation.

At present, Weiwei is working as a research specialist in the Corporate R&D in FrieslandCampina B.V. His work involves the development of various separation techniques, including crystallization, in the manufacturing of new nutritional products from milk.



# Publications

## Journal publications

1. Li, W. W.; Radasci, N.; Kramer, H. J. M. ; Van der Heijden, A. E. D. M.; Ter Horst J. H., Solid Separation from a Mixed Suspension through Electric - Field - Enhanced Crystallization. *Angewandte Chemie International Edition* **2016**, *55* (52), 16088-16091.
2. Li, W. W.; Spix, L.; De Reus, S. C. A. ; Meekes, H. ; Kramer, H. J. M.; Vlieg, E.; ter Horst, J. H., Deracemization of a Racemic Compound via Its Conglomerate-forming Salt Using Temperature Cycling. *Crystal Growth and Design* **2016**, *16* (9), 5563-5570.
3. Li, W. W.; Grothe, E.; Kramer, H. J. M.; Meekes, H.; De Gelder, R.; Ter Horst, J. H., Is 10% rule valid for Co-crystals from Racemic Compounds? (in preparation)
4. Li, W. W.; De Groen, M.; Kramer, H. J. M.; De Gelder, R.; Tinnemans, P.; Meekes, H.; Ter Horst, J. H., A Screening Approach for Resolution Opportunities in Complex Multicomponent Chiral Systems (in preparation)
5. Li, W. W.; Kramer, H. J. M.; Ter Horst, J. H., Chiral Resolution of a Racemic Compound via its Conglomerate Co-crystal (in preparation)
6. Li, W. W.; Kramer, H. J. M.; Van der Heijden, A. E. D. M.; Ter Horst, J. H., Solid Separation From a Multi-component Mixture by Electric-Field-Enhanced Crystallization (in preparation)

## Conferences

1. Li, W. W.; Radacsi N.; ter Horst J. H., *Application of Strong Electrostatic Fields during the Crystallization of Active Pharmaceutical Ingredients (APIs)*, European Young Engineer Conference (EYEC), Warsaw, Poland, May 2014.
2. Li, W. W.; Radacsi N.; ter Horst J. H., *Crystallization of Active Pharmaceutical Ingredients in a Strong Electrostatic Field*, International Workshop on Industrial Crystallization (BIWIC), Rouen, France, September 2014.
3. Li, W. W.; Radacsi N.; ter Horst J. H., *Application of Strong Electrostatic Fields during the Crystallization of Active Pharmaceutical Ingredients (APIs)*, International Symposium on Industrial Crystallization (ISIC), Toulouse, France, September 2014.
4. Li, W. W.; Kramer, H. J. M.; Meekes, H.; ter Horst, J. H., *Understanding the Phase Diagram of Multicomponent Solids of Chiral Compounds*, The Netherlands Process Technology Symposium (NPS), Utrecht, the Netherlands, November 2014.
5. Li, W. W.; Kramer, H. J. M.; Spix, L.; Meekes, H.; Vlieg, E.; ter Horst, J. H., *Using Temperature Cycling to Deracemize the Conglomerate-forming Salt of a Racemic Compound*, British Association of Crystal Growth (BACG), London, June 2015.
6. Li, W. W.; Kramer, H. J. M.; ter Horst, J. H., *Chiral Separation of a Racemic Compound via its Conglomerate Co-crystal*, International Symposium on Industrial Crystallization (ISIC), Dublin, Ireland, September 2017.

7. Leon, C. M.; Li, W. W.; Kramer, H. J. M.; ter Horst, J. H., *Electric-Field-Enhanced Crystallization in Multi-component Mixtures*, International Symposium on Industrial Crystallization (ISIC), Dublin, Ireland, September 2017.

## Acknowledgement

So.

4 years of sweat, laughter and tear all crystallize into this book. Some say that this is an achievement of your hard-work. I consider it more as a certificate verifying a long journey I have been through. Indeed this was a long journey, but luckily I never had to walk alone. Therefore, this chapter is devoted to you all, my dear companions on the road.

The first people I want to thank are my promotors.

Joop, thank you for hiring me and warning me how difficult this project would be. You successfully stimulated my stubbornness so that I never thought about quitting during my PhD, even during the most stressful period. You are almost always right, which irritated me so much during our argument about my project and forced me to find more evidence to fight back. Consequently, our argument could always give me more insight about my work and more understanding of the topic. I really appreciate that. I am sorry that I don't drink alcohol...when you learned about this, I could see your regret of hiring me. Well, at least I got you once 😊. Good luck in your future work, Joop. I sincerely hope our paths will cross again.

Andrzej, thank you for your support and guidance all through the project, especially when Joop left Delft and I was lost in concern about my future. I learned a lot from your desire and ability to bring people together and make cooperation into possibilities (e.g., DPTI).

To Herman, where can I start expressing my gratitude to you? Maybe from the moment when you join the supervision of me with Joop when he left Delft, although my project is not related to you in the first place? Or maybe from the weekend drinks you treated me when I was struggling with completing my thesis while working for FrieslandCampina? There are so many moments that I am so grateful about. Herman, you are a brilliant and renowned scientist but this is not why I am grateful you are my supervisor. I don't care about what the regulation says, in my heart, you are also my promotor. Herman, enjoy your retirement and please keep yourself from getting injured 😊.

I also would like to thank my graduation committee: Prof. de Jong, Prof. van Esch, Prof. Seidel-Morgenstern, Prof. Maes and Prof. Kellogg. Thank you for accepting my invitation. I am looking forwards to our intensive discussion during my defense.

Over the years, I have had the privilege to work temporarily in two prestigious institutes and with many brilliant and kind colleagues. Firstly, I would like to thank my colleagues in Radboud University of Nijmegen, where I spent 1 month working in the group of Prof. Elias Vlieg. Elias, thank you so much

for hosting me in your group and I really enjoyed my stay there, where I have learned so much. Hugo, I have never seen a messier office than yours but you also have one of the most outstanding brains I have ever known. Rene, thank you so much for your patience in explaining to me over and over again about the crystallography meanings of any co-crystals I have formed. Special thanks to Erik, who is always there when I need help with equipment. You even travelled all the way to Delft to help me trouble-shooting my own HPLC machine. Paul, we haven't talked too much but I know I can always rely on your knowledge in crystallography, which is essential for the paper we are working on together. To my project partner Eline: first of all, Eline, congratulations to your new life achievement. I still remember the first time we met during the STW progress meeting. You just came back from your honeymoon from the most North part of human civilization. From that moment on, I have not only found a new colleague, but also a good friend. Thank you for accompanying me in our joint project and I hope to see you in the near future. Laura, our joint paper is the first publication from me and will always mean special to me. I enjoyed every conversation we had, especially the one time you visited me in Delft. I wish you all the luck in your career and your life. To my other colleagues in Nijmegen, Ellie, Wester, Ton and Elizabeth, thank you for welcoming me to your group and including me in all kinds of activities.

During my PhD, I was lucky to spend 4 months working in CMAC in Glasgow, a great city I unfortunately visited during the worst season of the year (November—February). Nevertheless, I enjoyed every minute of my stay there. I had the pleasure to know and work with many young talented scientists: Andrew, great knowing you and thank you so much for introducing me to the deep-fried pizza. This was the first time in my life I could not finish a meal; Maria, I am sorry that our potential business plan did not go through 😞 but I have enjoyed our short-lived enthusiasm about an international travelling cooperation; Vaclav, thank you for enlightening me how to play Monster Hunter and Europa Universalis IV. To Raaz, Stephanie, Sara, Hector, Inka, I would never understand how you guys can afford buying lunch from the restaurant every day on a pathetic UK PhD salary but I appreciated that you also never commented on my pathetic Dutch lunch 😊. Thank you for accompanying me during the dark and cold Glasgow winter.

There are two colleagues I want to specially thank here. Rene Steendam, who I met in Nijmegen but also worked together in Glasgow. Rene, I couldn't wish for a better colleague to chat over some terrible instant coffee in CMAC. Thank you for also becoming my friend and also sharing with me one of your happiest moments. Both Wenli and I wish you good luck in Limerick and future career. To Carlos, who has visited me in Delft for several months: I couldn't be happier when you took over the electric-field-enhanced-crystallization work, as I know you will turn it into a promising topic. Don't worry about your progress. Everyone has been through up and down in their PhD. It will come around eventually.

My project is sponsored by STW and I would like to acknowledge my user committee members: To Danny and Carmen: thank you for helping us with the Crystal 16 and Crystalline systems. Your machines rock! I enjoyed our casual chat as well; To Jan, we go all the way back to my PDeng years and you have not changed a bit ever since then. I really appreciated your sharp questions, which can always get me thinking deeper about my work; To Rolf, thank you for introducing me to Prof. Eppink. Although the cooperation did not go through eventually, I still learned a lot from him, which benefitted me profoundly during the final phase of my project; To Dick, thank you for giving all kinds suggestions during our progress meeting, some of which are tremendously helpful; To Bernard, thank you for your advices on the chemistry of our compounds; To Alex, thank you for our interesting chat in Zurich about life, science and beer 😊.

Now back to Delft and there are a lot of people I am deeply in debt with.

First, my two paranymphs: Marloes and Karsten. Thank you guys for supporting and ‘defending’ me in one of my most important moments in my life. Marloes, you are caring and mean in the same time to me and I cannot wish for a better office mate. I hope they will keep the ‘door of truth’ forever, which is one of the most important legacies from us. Please get better soon and we miss you in your super hype and slightly drunk version 😊. Karsten, you are caring and mean as well with a twist of stubbornness and a German sense of humor. I cannot be happier for you when you found a job back home but also sad that you are leaving. I promised you that I will try this time to keep in touch and I intend to keep my promise. Until next time, my dear friend. A third person I want to address is my photographer Tim. Tim, I enjoyed our dinner and chat every time, since you came to Delft. You can complain about almost everything but you will always find a way around. I wish you good luck with your job hunting and personal life. Hope you will stay in the Netherlands so you don’t have to start over again. Thank you guys, all three of you, for visiting me in Glasgow when the Northern wind was blowing there. You brought, ironically, the warmth from the Netherlands to me.

And how can I go through my PhD without my friends and colleagues from P&E? To my colleagues from IRS (no, not the tax office in US, my friends have souls): Antoine (thank you for everything), Burak, Johan, Leslie (oh Leslie, what was I going to do without you in my PhD?), Fatima, Fatma, Maryam, Rumen, Sergio, Farnaz, Javier, Rohit, Lalit, George, Barry, Daniel, Hakan, Guido, Vikrant, Sathish, my life here would have been much tougher without your company. To Metin, thanks for the road trip to Luxemburg and so many dinners we had. You have shared with us so many beautiful culture of your homeland; To Jurrian, thank you for always coming up with interesting facts about China and politics. Moreover, thank you for sharing similar opinion about sports with me 😊. To my other colleagues Meng, Xuan, Jie, Noura, Dion, Remco, Seyed, Ahmadreza, Hasan, Mahinder, Sebastian, Mariette, Vilborg, Mohammed, Niko, Vincent, Gustavo, Uttiya, Johan and Wim, I really appreciate our time during the football practice, lunch talk, department drink/BBQ and many other activities. Special

thanks to Helma, Rob, Michel, Aard and Jaap: because of your help, my work in P&E was so smooth. I also want to thank my students: Debby, Oscar and Moj. You guys perhaps have taught me more than I taught you. Each one of you has made a career that you should be proud of. Thank you for attending my ceremony. Maybe in the future we will work together again 😊.

I also want to thank my new colleagues in FrieslandCampina for supporting me during my last phase of thesis writing. Thanks to my colleagues from the process technology department to come to Delft and support me during my defense. To my manager, Ed, thank you for hiring me to this wonderful company and caring about my struggle during my thesis writing. Special thanks to my double-colleague Ali: since you joined us, commuting became a fun 😊. To all my colleagues in FC, I cannot hope for a better first job in the industry than here. Each one of you makes me feel like home in Wageningen.

I also owe my PhD to my colleagues and friends from the past. To Jan and Marcel, my former supervisors during PDeng, thank you for teaching me so much. I look up to your career and personality. To my friends: Susanna, Mar, Xavi, Andrea, Yasmin, Reza, Phuong, Emma, Ana Maria, Jorge, Diana, Jon, Noa, Bert, Iona, Paschalis, Emma, Rafaela, David, Jelle, Hugo and many more, thank you for being there. We don't meet too often any more but the thoughts that you guys still are around make me feel happy and energized. I treasure every moment spending with you and thank you all for blessing me with my thesis writing. As one of my graduation resolution, I promise I will be more active in reaching out. After all, you guys are like my family here in a new country I call home now.

There are two people I want to thank. I have never met them and they are both dead. Nevertheless, without them, my thesis writing during working in FC would have been more difficult. The first one is Robert Jordan, the author of my favorite book series 'the Wheel of time'. Thank you for bringing me into a world of sword and magic, where I can forget about my struggle of thesis. The second one is Anthony Bourdain, the TV chef who brought me to every corner of the world from my living room. Thank you Tony, for showing me the future I can look forwards to, once I have finished my thesis. Rest in peace to both of you.

Now to my actual family from China. To my dad Mingzhi and my mom Ming, I love you guys and I couldn't have hoped for better parents. You encouraged me to study abroad and supported me both financially and mentally. Without you, I would not be here. Special thanks to my cousin, Weiyin. You are the closest thing I have to a sister. I am so happy that you are here supporting me. Thank you for being in my life.

Of course you all know who I will thank the last, because she is the one I owe the most of my gratitude to. To my beautiful wife Wenli: you brought meaning into my life and a reason to fight every day. Thank you for always encouraging and sometimes bullying me to stop complaining and mustering up my strength to finish my thesis. Thank you for forcing me to stop writing and to go on a short trip just

to forget about everything. Without your love, I might not make it through. So Wenli, this book is for you.





